Pablo Almaraz

Diversity, variability and persistence: elements for a non-equilibrium theory of eco-evolutionary dynamics

Tesis Doctoral
Programa de Doctorado en Ciencias y Tecnologías Marinas
Universidad de Cádiz

LaTeX template modified from: https://github.com/CRIStAL-Sigma/phd-thesis-template

First printing, December 2022

Diversidad, variabilidad y persistencia: elementos para una teoría de no-equilibrio de dinámicas eco-evolutivas

Tesis Doctoral presentada por

Pablo Almaraz García

para optar al grado de
Doctor en Ciencias y Tecnologías Marinas
por la
Universidad de Cádiz

Directores:

Dr. Javier T. Ruiz Segura

Dr. Oscar Godoy del Olmo

"Reality is not perceived, it is conceived"

C. S Holling, 1983

Para Amelia, por los besos y los días

Agradecimientos

La elaboración de esta tesis doctoral fue posible gracias a una Ayuda Pre-doctoral para la Formación del Profesorado Universitario del Ministerio de Universidades (FPU16/00626). El centro de adscripción durante el disfrute de la Ayuda fue el Instituto de Ciencias Marinas de Andalucía, de la Agencia Estatal Consejo Superior de Investigaciones Científicas (ICMAN-CSIC). La participación en varios congresos durante el periodo doctoral fue financiada por el proyecto FarFish (H2020-SFS-21-2016-2. Project no. 727891), cuyo investigador principal fue el Dr. Javier T. Ruiz Segura, director de esta tesis doctoral. Durante mi estancia de 7 años en el ICMAN, estuve contratado en el año 2016 por el proyecto "Detección de medusas en el mar balear y su relación con las condiciones ambientales: hacia el desarrollo de un sistema de predicción pre-operacional", financiado por la Conselleria d'Agricultura, MediAmbient i Territori (Gobierno Balear), ICTS SOCIB, y CSIC, y con la Dra. Laura Prieto como investigadora principal. Posteriormente, en 2017 estuve contratado por el proyecto "PERMEAD: Efecto de la permeabilización de las marismas del Parque Nacional de Doñana sobre la estructura trófica de sus ecosistemas acuáticos", financiado por el Ministerio de Transición Ecológica y Reto Demográfico, y con la Dra. Emma Huertas como investigadora principal. Estoy muy agradecido a Laura y a Emma por su apoyo en esos momentos, y en general a todo el personal, científico y no científico, del ICMAN, que hace muy fácil trabajar allí. Siempre tuve total libertad para desarrollar mi trabajo al ritmo que yo quisiera. También le estoy muy agradecido al Dr. Gabriel Navarro por su ayuda de múltiples formas, por aportarme su visión de las ciencias marinas, y de la ciencia en general, y por introducirme inicialmente en el ICMAN.

Javier Ruiz, como director de esta tesis, y como responsable del grupo de Oceanografía de Ecosistemas en el ICMAN, me brindó su ayuda de múltiples formas: con los muchos intercambios y discusiones sobre ecología, matemáticas y filosofía de la ciencia. Pero también con su visión y destreza únicas en el manejo de las cuestiones de política y gestión científicas, que fueron de importancia crítica en muchos momentos. En este sentido, y desde la Universidad de Cádiz, el profesor Dr. Fidel Echevarría, tutor de esta tesis, fue determinante a la hora de resolver las numerosas cuestiones administrativas que surgen de una tesis doctoral que se desarrolla con el concurso de tres administraciones distintas. También en la Universidad de Cádiz, las múltiples conversaciones con el Dr. Oscar Godoy, co-director de esta tesis, el Dr. Andrés Cózar, la Dra. Ana Bartual y el Dr. Fernando Ojeda fueron muy enriquecedoras a la hora de intentar orientar el devenir de mi trabajo

en estos últimos años. La incisiva visión de Fernando Ojeda sobre la ecología y sobre la política científica fue especialmente estimulante en muchos momentos. La energía, pasión y positividad de Oscar Godoy son, afortunadamente, contagiosas.

Durante el desarrollo del doctorado realicé una estancia de tres meses en el Instituto Federal Suizo de Ciencias y Tecnologías Acuáticas (Eawag) en Dübendorf, Suiza. Esta estancia fue posible gracias a la generosa ayuda de Luis J. Gilarranz, investigador en el Eawag, y a Oscar Godoy. Sin la ayuda económica de ambos hubiera sido imposible realizar ninguna estancia durante el periodo pre-doctoral, y les estoy profundamente agradecido. El Ministerio de Universidades concedió la ayuda parcial para realizar la estancia breve un año después de realizarse. En Suiza, fue muy importante el apoyo constante de Luis J. Gilarranz, fundamentalmente en un periodo tan difícil como una pandemia. Luisjo es una persona especialmente noble en un mundo, el de la ciencia, donde en muchas ocasiones la nobleza se penaliza. Las conversaciones suizas con Luis J. Gilarranz, Carlos Melián y Jordi Bascompte fueron muy enriquecedoras, y contribuyeron a aclarar muchas de las ideas reflejadas en esta tesis. Jordi Bascompte fue muy generoso y estimulante en las muchas reuniones informales que tuvimos en el comedor de la Universidad de Zurich.

Durante el último año de desarrollo de esta tesis doctoral, disfruté de un contrato de investigador en el Departamento de Ecuaciones Diferenciales y Análisis Numérico de la Universidad de Sevilla, enmarcado en el proyecto "Complejidad y sistemas dinámicos: teoría matemática y aplicaciones a ecología y a la neurociencia de la consciencia", financiado por el FEDER, Consejería de Economía, Conocimiento, Empresas y Universidad de la Junta de Andalucía, FEDER 2014-2020, referencia P20-00592. Este contrato fue posible gracias al profesor Dr. José A. Langa Rosado, investigador principal, y fue continuado por el profesor Dr. Fernando Soler-Toscano. Agradezco profundamente su ayuda en este momento, al igual que al resto de representantes del grupo de investigación: Antonio Suárez, Jose R. Portillo y Piotr Kalita. Durante todo este año ellos me han dado toda la libertad para poder dedicarme a la redacción final de la tesis en momentos complicados, por lo que les agradezco sinceramente su generosidad y comprensión. Además, la visión y los conocimientos que me ha aportado, y me sigue aportando, este excelente grupo con el que tengo el privilegio de trabajar, me ha descubierto todo un mundo nuevo en la intersección entre las matemáticas y la naturaleza. Esta visión, especialmente liderada por José A. Langa, está contribuyendo a cambiar la forma en la que me aproximo al análisis y la comprensión de la realidad.

Amelia sabe muchas cosas sobre lo que siento por ella, pero aquí tiene que saber, sobre todo, ésto: sin su existencia, no tengo ninguna duda de que ni el grado en ciencias del mar, ni el máster en matemáticas ni, por supuesto, esta tesis, hubieran visto la luz.

Contents

List of Figures

List of Tables

0.1 English abstract

Natural ecosystems persist in variable environments by virtue of a suite of traits that span from the individual to the community, and from the ecological to the evolutionary scenarios. How these internal characteristics operate to allow living beings to cope with the uncertainty present in their environments is the subject matter of quantitative theoretical ecology. Under the framework of structural realism, the present dissertation project has advocated for the strategy of mathematical modeling as a strategy of abstraction. The goal is to explore if a range of natural ecosystems display the features of complex systems, and evaluate whether these features provide insights into how they persist in their current environments, and how might they cope with changing environments in the future. A suite of inverse, linear and non-linear dynamical mathematical models, including non-equilibrium catastrophe models, and structured demographic approaches is applied to five case studies of natural systems fluctuating in the long-term in diverse scenarios: phytoplankton in the global ocean, a mixotrophic plankton food web in a marine coastal environment, a wintering waterfowl community in a major Mediterranean biodiversity hot-spot, a breeding colony of a keystone avian scavenger in a mountainous environment and the shorebird community inhabiting the coast of UK. In all case studies, there is strong evidence that ecosystems are able to closely track their common environment through several strategies. For example, in global phytoplankton communities, a latitudinal gradient in the positive impact of functional diversity on community stability counteracts the increasing environmental variability with latitude. Mixotrophy, by linking several feeding strategies in a food web, internally drives community dynamics to the edge of instability while maximizing network complexity. In contrast, an externally generated major perturbation, operating through planetary climatic disruptions, induce an abrupt regime shift between alternative stable states in the wintering waterfowl community. Overall, the natural systems studied are shown to posses features of complex systems: connectivity, autonomy, emergence, non-equilibrium, non-linearity, self-organization and coevolution. In rapidly changing environments, these features are hypothesized to allow natural system to robustly respond to stress and disturbances to a large extent. At the same time, future scenarios will be probably characterized by conditions never experienced before by the studied systems. How will they respond to them, is an open question. Based on the results of this dissertation, future research directions in theoretical quantitative ecology will likely benefit from non-autonomous dynamical system approaches, where model parameters are a function of time, and from the deeper exploration of global attractors and the non-equilibriumness of dynamical systems.

0.2 Resumen en español

Los ecosistemas naturales persisten en ambientes variables en virtud de un conjunto de rasgos que van desde el individuo hasta la comunidad, y desde el escenario ecológico hasta el evolutivo. Cómo operan estas características internas para permitir a los seres vivos hacer frente a la incertidumbre presente en sus entornos es el objetivo de la ecología teórica cuantitativa. Bajo el marco del realismo estructural, la presente tesis doctoral se ha basado en la estrategia de modelado matemático como una estrategia de abstracción. El objetivo es explorar si una variedad de ecosistemas naturales muestran las características de sistemas complejos y evaluar si estas características brindan información sobre cómo persisten en sus entornos actuales y cómo podrían hacer frente a entornos cambiantes en el futuro. Se ha aplicado un conjunto de modelos dinámicos inversos, lineales y no lineales, incluidos modelos de catástrofe de no-equilibrio y enfoques demográficos estructurados, a cinco casos de estudio de sistemas naturales que fluctúan a largo plazo en diversos escenarios: fitoplancton en el océano global, una red trófica de plancton mixotrófico en un entorno costero marino, una comunidad de aves acuáticas invernantes en un importante punto caliente de biodiversidad del Mediterráneo, una colonia de reproducción de un carroñero clave en un entorno montañoso y la comunidad de aves limícolas que habitan el hábitat costero del Reino Unido. En todos los casos, se evidencia que los ecosistemas pueden reaccionar íntimamente a su ambiente a través de varias estrategias. Por ejemplo, en las comunidades globales de fitoplancton, un gradiente latitudinal en el impacto positivo de la diversidad funcional sobre la estabilidad de la comunidad contrarresta la creciente variabilidad ambiental con la latitud. La mixotrofia, al vincular varias estrategias en una red alimentaria, lleva internamente la dinámica de la comunidad al borde de la inestabilidad a través de la maximización de la complejidad en la red de interacción. Por el contrario, una gran perturbación generada externamente, que opera a través de alteraciones climáticas planetarias, induce un cambio de régimen abrupto entre estados estables alternativos en la comunidad de aves acuáticas invernantes. En general, se muestra que los sistemas naturales estudiados poseen las características de los sistemas complejos: conectividad, autonomía, emergencia, no-equilibrio, no-linealidad, auto-organización y coevolución. En entornos que cambian rápidamente, se sugiere que estas características permiten que el sistema natural responda de manera sólida al estrés y las perturbaciones. Al mismo tiempo, los escenarios futuros probablemente estarán caracterizados por condiciones nunca antes experimentadas por los sistemas estudiados. Cómo estos sistemas responderán a ellos, es una pregunta abierta. Con base en los resultados de esta tesis, las futuras direcciones de investigación en ecología cuantitativa teórica probablemente se beneficiarán de los enfoques de sistemas dinámicos no autónomos, donde los parámetros del modelo son una función del tiempo, y de la exploración más profunda de los atractores globales y el no-equilibrio de la dinámica de los sistemas.

Introduction 1

"How can you predict the result when you can't predict what you will be measuring?"

P. W. Anderson, 1997

1.1 The status of theory in ecology

In a recent synthesis of community ecology as a discipline, Mark Vellend, 2016 proposes a reorganization of theoretical ecology analogous to the field of population genetics. With the aim of characterizing ecological mechanisms and patterns, four high-level processes can be identified: *Ecological drift*, expressing the probabilistic nature of the demographic characteristics of ecological systems, from genes to life-history traits; *Selection*, a consequence of the deterministic fitness differences among individuals of different species in a community, expressed at the demographic component or the intrinsic, per-capita growth rate; *Dispersal*, including the (directed or not) movements in a landscape of differing habitat suitability which feedbacks to selection; and *Speciation*, which is the macroevolutionary consequence of the operation of ecological drift, selection and dispersal. However, in this reorganization of an **emergent** ecological theory, a suite of at least 24 pre-existing **fundamental** theories and/or models are put forward (Table 5.1 in Vellend, 2016).

The figure provided by Vellend, 2016 might fall short: in a review on the status of theory in ecology, Marquet et al., 2014 identify at least 78 ecological theories used by ecologists since 1945. The obvious proposal was to call for a synthesis. Again, another recent synthesis (Pásztor et al., 2016), calls for a reformulation of theoretical ecology under (yet again) a Darwinian approach. The bottom line of these contributions is the same: ecology, as a science, seems under a never-ending loop of theory production and reorganization, in particular in comparison with other disciplines (Reiners et al., 2017; Reiners and Lockwood, 2009). What is special, if any, about ecology?

A prevailing view among the more philosophically-inclined ecologists is that the fundamental problem of ecological systems is the **medium number of particles** curse (Allen and Starr, 2017; see Figure 1.1). Systems with a small number of particles, such as planetary systems, and systems with a large number of particles, such as a

"I am personally of the opinion that really good scientists are basically amateurs, operating as their pleasure dictates and quite immune to philosophical advice" (Fretwell, 1972)

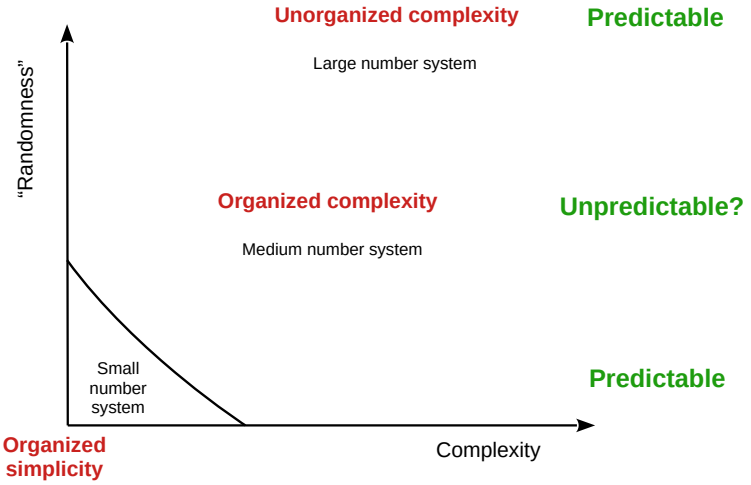

Figure 1.1: The organization of systems in a randomness-complexity trade-off (Allen and Starr, 2017). Systems with a small number of particles, such as planetary systems, bear an organized simplicity: they are highly predictable. In the other extreme, systems with a large number of particles, such as a water mass is accessible to statistical mechanics and its behavior is thus predictable. The problem lies in medium number systems: their organized complexity renders their predictability limited.

water mass, are equally and successfully predictable: while their *perceived* randomness might greatly differ, both the **organized simplicity** in the deterministic behaviour of the small number system, and the **unorganized complexity** in the statistical-mechanical behaviour of large number systems, allow for a large degree of predictability (Allen and Starr, 2017). The problem is with medium number systems: too much *particles* to make the system neatly deterministic and simply organized; but too few particles to allow for a statistical-mechanical description of the system. This is where ecology lies. Purely deterministic and purely stochastic approaches have consistently fail in providing much insight on the behaviour and predictability of ecological systems. Indeed, the deterministic view was abandoned very soon (May, 1973), and the statistical-mechanical never went too far (Kerner, 1959, 1962). Even if most ecologists might be unaware of this system-view (Fig 1.1), the explanation to the *mess* in which ecology as a scientific discipline seems stuck (Lawton, 1999) is usually the same: ecological systems are ***complex***.

"With apologies to practicing biologists, especially ecologists who labor firsthand with perhaps the hardest observational material in all science, I am going to trespass a bit in difficult and unfamiliar terrain and venture some ideas at secondhand" (Kerner, 1962)

1.2 *Complexology* IN ECOLOGY

Complexity is a concept with a long scientific tradition (Horgan, 1995). In an attempt to unify different definitions of complexity across disciplines, Lloyd, 2001 identified more than 35 alternative meanings. This lead to the creation of yet a new term: *complexology*, the sciences of complexity (Horgan, 1995). While this term has been used with a negative connotation, complexity should be rigorously defined if ecology aspire to an adequate explanation and predictability of ecological systems. In this dissertation, I will use the **complexity criteria** of Rzevski and Skobelev, 2014, and explore in subsequent chapters some

elements for a non-equilibrium theory of ecological dynamics. According to this view, a system can be distinguished from purely deterministic and purely random systems, and hence be regarded as a complex system, if the following seven criteria are fulfilled:

1. **Connectivity**. A complex system is made of a (large) number of richly interconnected agents. A network approach regards *agents* as nodes, and interconnections as vertices among nodes. As in medium number systems (Fig. 1.1), connectivity should be intermediate: a null connectivity makes the system a no-system (agents are independent); full connectivity also makes the system a no-system: dynamically, there is only one agent (Margalef, 1968). In ecology, agents can be genes, species, communities, etc., but also the equilibria and local attractors of models used to understand real systems.

Connectivity in nature: The *network approach* to ecological interactions is revealing a highly structured, far from random, pattern in how the network architectures found in nature beget stability and maximize biodiversity (e.g., Bascompte, Jordano, and Olesen, 2006; Kéfi et al., 2016; Guimarães, 2020)

2. **Autonomy**. In a complex system, there is not a well-defined centralized, top-down control: agents have a *degree of autonomy*. In ecology, this means that interactions among agents are *localized*: they typically interact with a limited set of neighboring agents, even though the resulting dynamics is expressed and understood at a global, not local, level (Solé and Bascompte, 2006).

Autonomy in nature: Either in spatial dispersal networks (Ranta, Fowler, and Kaitala, 2008), food webs (Montoya and Solé, 2002) or mutualistic networks (Bascompte and Ferrera, 2020), *small-world* and nested patterns are typically the norm.

3. **Emergence**. Although interactions among agents are local, the rules governing the system as a whole are not *codified* in the local interactions: interaction among local agents are *fundamental*, but system dynamics is *emergent*. The key feature of emergent behaviour is the *feedback* between the agents and the system: both are constrained by the behaviour of each other (Casti, 1979).

Emergence in nature: The *feedbacks* between individual behavioral decisions in social species and population dynamical patterns in variable environments are a clear example of emergence in evolutionary ecology (see Oro, 2020).

4. **Non-equilibrium**. Natural systems are perturbed by external shocks at temporal and spatial rates orders of magnitude smaller than their characteristic fluctuation rate: most systems are not able to return to the *stable equilibrium* between two consecutive disturbances. Therefore, the global behaviour of a complex system is typically *far from equilibrium*, and the equilibria influencing their dynamics in general will be *unstable* (Prigogine, 1978).

Non-equilibrium in nature: The fluctuating pattern of a large ensemble of natural populations suggest that non-equilibrium conditions are ubiquitous (Benincà et al., 2008; Clark and Luis, 2020; Cenci and Saavedra, 2019)

5. **Non-linearity**. Interactions among agents in a system are driven by positive feedbacks, autocatalytic processes, and amplification of external and internal perturbations. The magnitude of individual perturbations might be independent of the magnitude of system response: in the global dynamical behavior of a system, qualitatively different responses emerge for the same perturbation conditions. The accumulation of small disturbances might give rise to *catastrophic* responses at tipping points (Casti, 1979; Scheffer, 2009).

Non-linearity in nature: The catastrophic collapse of fish populations under increasing fishing pressure in variable environments (Sguotti et al., 2019), and laboratory experiments testing for tipping points in slowly shifting conditions (Dai et al., 2012) are good examples of non-linear behavior in real systems.

6. **Self-organization**. Both the emergent and the fundamental components of a complex system show *evolvability*: in response to internal and external perturbations, agents may shift their interactions and change the global connectivity, *adapting* to external shocks and increasing the *resilience* to repel future perturbations (Solé and Bascompte, 2006).

Self-organization in nature: The presence of traveling waves in the spatio-temporal patterns of many natural populations is a salient example of a self-organizing pattern (Bjørnstad et al., 2002; Ranta, Lundberg, and Kaitala, 2006; Solé and Bascompte, 2006).

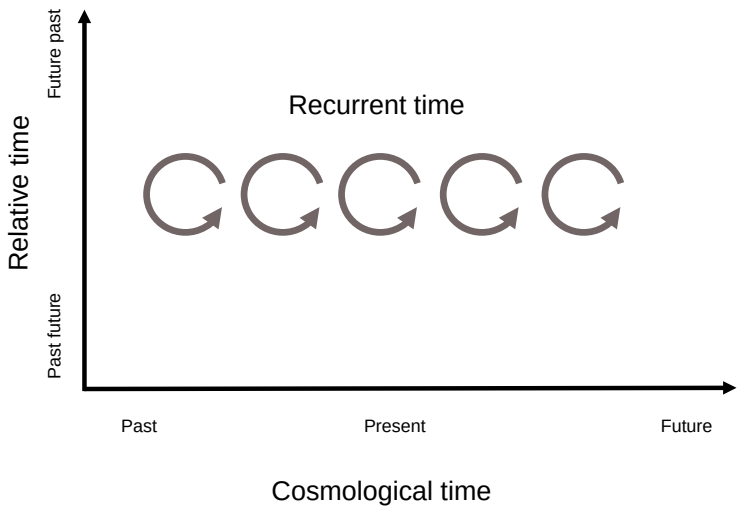

Figure 1.2: Three types of time in ecology (Post, 2019): cosmological, relative and recurrent. Ecological events taking place in a *recurrent* scheme, repeat themselves along an unidirectional *cosmological* time, thus inducing a *relative* time for populations and communities living in seasonal environments: "future" and "past" shift recurrently across the life cycle of an organism.

7. **Coevolution**. Complex systems are *open*: they continually modify their environment, and these changes feed back on the system in a permanent *co-evolutionary* pathway: this process is *irreversible*, since the particular random sequence of perturbations leave a structural and dynamical fingerprint in the form of an *arrow of time* (Lewontin, 1966b; Blum, 1968; Prigogine, 1980).

Coevolution in nature: Coevolution as a consequence of interactions between species, and among species and their environments, is one of the major sources of phenotypic and dynamic changes at all time and spatial scales in nature (Thompson, 2013; Sultan, 2015)

1.3 Time in ecology

In the criteria for complexity given above, and indeed in all the theoretical approaches to ecology and evolution reviewed (Vellend, 2016; Marquet et al., 2014; Pásztor et al., 2016), there is a common running theme: **time**. Ecological systems, with their permanent flow of matter and energy, can only be understood through a temporal dimension. As evolvable systems in which the arrow of time is prominent, information contained in natural systems makes it possible a partial reconstruction of the past (Lewontin, 1966b; Margalef, 1968; Gould, 1970). And, as *historical documents* (Williams, 1992), only the limited information contained in the present can be used by natural systems to persist under future changing conditions. This is the role of *historicity*, which makes no sense in the time-reversible theories in physics (Lamb and Roberts, 1998), but are prominent in biology (Blum, 1968; Van Valen, 1976, 2003). This makes the study of time in ecology not only interesting, but also unavoidable.

Time is a resource, for example for migrating species in which phenology is of paramount importance, or in ecosystems with a strong seasonal component. But it is also a **dimension** in which the relevant ecological and evolutionary mechanisms, patterns and processes take place. Recently, Post, 2019 proposed an integrated framework for addressing the study of time in ecology (see Fig. 1.2). Under this framework, the *temporal dimension* experienced by every organism has three components:

1. **A cosmological time**. This is the *relativistic* time dimension and, in practice, is the same for all organisms. It only flows forward. A biological manifestation of the impact of cosmological time is senescence (Ratikainen and Kokko, 2019).

2. **A recurrent time**. For species living in seasonal environments, the conditions across the annual cycle are recurrent across years. This makes recurrent events *predictable*, and hence adaptability to seasonal environments is common in many species (Bernhardt et al., 2020).

"If the moving element is everywhere along the Time length at once, it is not moving." (Dunne, 1927)

3. **A relative time**. The very existence of a recurrent time, makes *relative* time a third temporal dimension for long-lived species. Given that the seasonal environment recur over cosmological time, not only every present condition was *experienced* in the past, but also every future condition has already been experienced in the past. Again, the role of history in ecology is prominent (Gould, 1970; Williams, 1992).

1.3.1 *Goals of the dissertation project*

Following this framework, in this dissertation the recurring theme across all chapters (see below) will be the **mechanics of the temporal fluctuation of natural populations and communities in variable environments**: from single species dynamics to functionally diverse communities; from linear approaches, to non-linear, out-of-equilibrium viewpoints; and from ecological to evolutionary approaches. In all this case studies, the emergent questions will be:

1. **How are the different temporal scales of ecological interactions and environmental perturbations, relative to the life history of the focal organisms, contributing to the complexity of the modeled dynamics?**

2. **How may the organizational level and functional resolution of species and communities inform on the feedbacks between diversity, life-history traits and demographic rates of contemporary dynamics?**

3. **To what extent the major patterns emerging from the analysis of disparate case studies of natural ecological systems fluctuating in variable environments relate to the notion of complexity?**

4. **Which elements of the current theoretical and quantitative ecology toolbox, as used in the present dissertation, may help in fostering advances towards a non-equilibrium theory of complex ecological systems living in non-stationary environments?**

Before providing a detailed outline of the present dissertation, I will lay out my philosophical approach to tackle these problems.

1.4 Philosophical approach of the dissertation project

Ecologists have been traditionally skeptical on the usefulness and even the possibility of openly discussing the philosophical underpinnings and implications of the way ecology is done, and the kinds of entities ecologists consider as existing. Notable exceptions include the work of classical theoreticians, such as Richard Lewontin (Lewontin, 1966b, 1969), Leigh Van Valen (Van Valen, 1973a, 1973b, 1975, 1976), Richard Levins (Levins, 1968; Levins and Lewontin, 1987), Ramón Margalef (Margalef, 1968) or Stephen D. Fretwell (Fretwell, 1972). Recently, however, some authors are addressing these issues with more or less depth (Reiners and Lockwood, 2009; Justus, 2021).

"Philosophy can be ignored but not escaped, and those who most ignore least escape." David Hawkins (in Rosen, 2012)

The philosophical framework of the present dissertation project is that of **structural realism** (Ladyman, 1998) and **constrained perspectivism** (Giere, 2006). Structural realism posits that the most precise way to understand reality is through scientific constructs based on empirical observations of entities and their relationships: under this perspective, reality is in the mathematical structure of a theory, and not in a particular formulation of that theory (see Cartwright, 1983 for a provocative discussion). Indeed, under structural realism the concept of reality is purely epistemological, and has no bearing with the ontological nature of the entities themselves (Ladyman, 1998). As a refinement of structural realism, constrained perspectivism acknowledges that different realities arising from particular scientific constructs (mathematical structures) illuminate different aspects of a problem: knowledge, and indeed reality, are *contingent* (Giere, 2006).

"Things are different: this makes science necessary. Things are similar: this makes science possible." (Levins and Lewontin, 1987)

The reason for this philosophical position is that the strategy followed in this dissertation is that of **mathematical modelling as a strategy of abstraction** (Levins, 1966, 2007; Wimsatt, 2007; Almaraz, 2014). This is a strategy with a long and fruitful tradition in population ecology (Kingsland, 1995; Cushing et al., 2003). The process of understanding and explaining phenomena in the real world begins with theoretical concepts, which are then translated into mathematical models that can be tested and refined. If the model accurately reflects the behavior of real-world objects, it can be used to develop phenomenological laws that describe this behavior. These laws may be true of the objects in reality, but the fundamental laws that govern the behavior of the objects in the model may not necessarily hold true in the real world (Cartwright, 1983). That is, the strategy of model

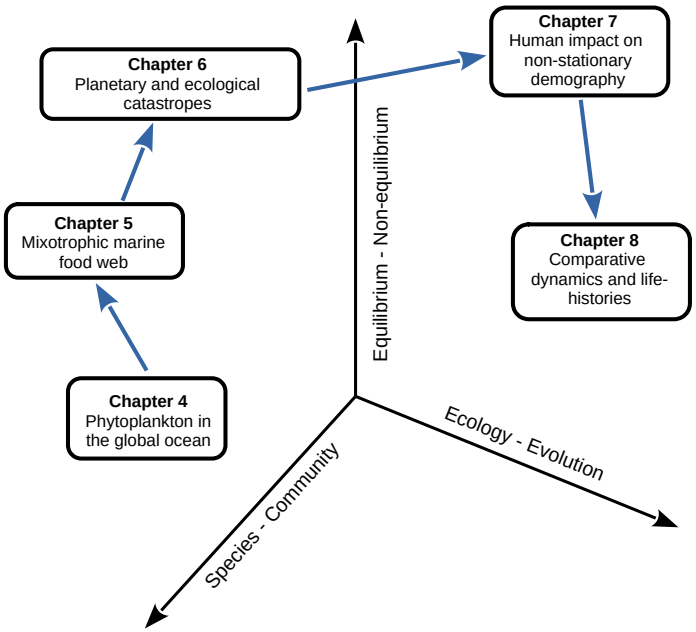

Figure 1.3: Conceptual flow in the chapters of the dissertation project. Each one is located in a specific position along three axes: from the species to the community, from equilibrium to non-equilibrium dynamics and from ecological to evolutionary perspectives. The chapters of the dissertation are thus presented in a clockwise direction (see the outline).

construction in ecology is that of abstraction: particular models, as constrained perspectives, illuminate particular aspects of the world. Only when different perspectives, each one constrained by their assumptions, make similar predictions of the behaviour of objects in the real world, we can say there is evidence that a *locus* of truth, in the structurally realistic sense, is located in the intersection. To a degree, this departs from the anti-realist position of Cartwright, 1983, and regards scientific model construction as a search for **robust models** (Levins, 1966; Orzack and Sober, 1993; Levins, 1993), or **structurally stable models** (DeBaggis, 1953; Thom, 1975): a family of mathematical constructions different enough to be regarded as alternative abstractions, but whose predictions intersect to some extent. This is similar to the Ying-Yang problem in the classification of dynamical systems (Stewart, 1988), and is the position held in this dissertation.

"Our truth is the intersection of independent lies." (Levins, 1966)

"For physical systems to perform certain operations they must, if they are to be useful, possess a certain degree of stability: small perturbations should not affect the essential features of the system." (DeBaggis, 1953)

1.5 General outline of the dissertation project

The general conceptual flow of the following chapters in this dissertation is presented in Figure 1.3. The major theme of the dissertation project, as explained above, evolve around three themes, that can be represented as different axes. The description of each chapter, and the justification for the position of each one within these axes is given in the following:

The manuscript is divided into nine chapters.

Chapter 2 **Mathematical stability in dynamical systems.** This chapter is a technical introduction to the different mathematical

concepts of stability of autonomous dynamical systems that will be used throughout the dissertation project.

CHAPTER 3 **Stability in real systems** This chapter introduces the mathematical concepts of stability as currently used in dynamical models applied to real ecological systems, in continuous and discrete time.

CHAPTER 4 **Temporal coexistence mechanisms stabilize the planetary dynamics of marine phytoplankton** This first case study explores the relationship between the functional diversity and the dynamical and structural stability of marine phytoplankton communities in the Longhurst provinces of the global ocean. The mathematical approach used is a multivariate autoregressive model, a linear first-order approach. This model is an equilibrium approach, so this chapter is located in the lower left part of Figure 1.3.

CHAPTER 5 **Mixotrophic interactions drive a complex marine food web to the edge of instability** This second case study explores the role of ecological interactions and environmental variability in weekly biomass fluctuations of a planktonic food web in a temperate coastal region during a 9-year period. The studied food web include several mixotrophic funnctional types, and the dynamical model used is a non-linear Lotka-Volterra-Ricker state-space model. This chapter is placed one step above the preceding chapter in Figure 1.3: a more diverse communtiy, and a non-linear dynamics to the edge of instability.

CHAPTER 6 **Alternative Stable States in the Dynamics of a Bird Community Triggered by a Planetary-Scale Environmental Catastrophe** This case study explores the regime shift between two alternative stable states in the multi-decadal dynamics of a major wintering waterfowl community, induced by a catastrophic geological event with transient global perturbations of climatic patterns. A highly non-linear, stochastic cusp catastrophe model is used to capture the non-equilibrium pattern. This chapter is thus placed in the highest place in Fig. 1.3. It is an ecological community with a clearly non-equilibrium dynamics.

CHAPTER 7 **Long-term demographic dynamics of a keystone scavenger disrupted by human-induced shifts in food availability** This chapter was published in ***Ecological Applications* (2022), 32 (6), e2579**. (Almaraz et al., 2022). This contribution explores the impact of shifts in the abundance and availability of food resources, modulated by human activities, on the highly non-stationary but plastic demography and life-history of the largest world breeding population of a long-lived keystone terrestrial scavenger. This chapter is thus placed on the upper right region of Fig.1.3: a single species, with a non-equilibrium dynamics, but closer to the evolutionary axis.

CHAPTER 8 **Covariation among life history traits, demographic rates, and population dynamics in a globally threatened taxa** The last case study is a comparative population dynamics approach with several species of shorebirds: it explores the covariation among several life-history traits and demographic rates, as an evolutionary legacy, and the population dynamics and stability using both structured and unstructured approaches. The focus was on single species dynamics and mainly linear models, so the chapter is placed in the lower right region of Fig.1.3.

CHAPTER 9 **Discussion** This chapter provides a general discussion of the patterns emerging from the case studies analyzed, in the light of the main goal of the dissertation project.

CHAPTER 10 **Conclusions** Some final concluding remarks on the implications of the results and directions for future work.

2 Mathematical stability in dynamical systems

Before introducing the different notions of stability that will be used throughout this dissertation, several useful definitions and results related to dynamical systems theory will be outlined. In this dissertation we will focus on autonomous systems (unless otherwise specified), that is,

$$\frac{d\boldsymbol{x}}{dt} = \mathbf{F}(\boldsymbol{x}), \quad t \geq t_0 \tag{2.0.1}$$

where $\mathbf{F} \in \mathcal{C}(\mathbb{R}^N; \mathbb{R}^N)$. We will write $\boldsymbol{x}_t$ instead of $\boldsymbol{x}(t)$, and assume the existence of a global solution for $t \geq t_0$, whatever the initial data imposed $x_{t_0} = x_0$.

"Each definition is a piece of secret ripped from Nature by the human spirit."

Nikolai Nikolaievick Luzin

2.0.1 *Definitions*

Definition 2.0.1 (State space)**.** *The set of possible states $\{\boldsymbol{x}_t, t \geq t_0\} \subset \mathbb{R}^N$ of the dynamical system (2.0.1) is called **state space** and is denoted by **E**. They are also called **phase spaces**.*

Definition 2.0.2 (Equilibrium point in autonomous systems)**.** *Let $x^* \in \mathbb{R}^N$ be a point such that $x_t = x^*$ is a constant **solution** of the system. It is then said that the point $x^* \in \mathbb{R}^N$ is an **equilibrium point** of the system.*

It is immediate that the equilibrium points are solutions of the equation $\mathbf{F}(x^*) = 0$, and vice versa. Thus, the equilibrium points of (2.0.1) are the stationary solutions of the system.

Definition 2.0.3 (Equilibrium point in maps of autonomous systems)**.** *Let $\boldsymbol{f} \in \mathcal{C}(\mathbb{R}^N; \mathbb{R}^N)$ and be the autonomous system of **difference equations**, or iterated map*

$$x_{\mu+1} = f(x_\mu), \quad \mu \in \mathbb{N}, \tag{2.0.2}$$

*and let $x^* \in \mathbb{R}^N$ be a fixed point of f. It is then said that x^* is a **equilibrium point** of (2.0.2).*

Definition 2.0.4 (Attractor)**.** *Let $\boldsymbol{A}$ be a closed subset of the state space $\boldsymbol{E}$ of a dynamical system governed by a state vector $\boldsymbol{x}_t$. For any choice of initial states $\boldsymbol{x}_0$, the subset $\boldsymbol{A}$ is an **attractor set** of the system if all trajectories evolve towards it, that is,*

$$\lim_{t \to \infty} \operatorname{dist}(\boldsymbol{x}_t, \boldsymbol{A}) = 0.$$

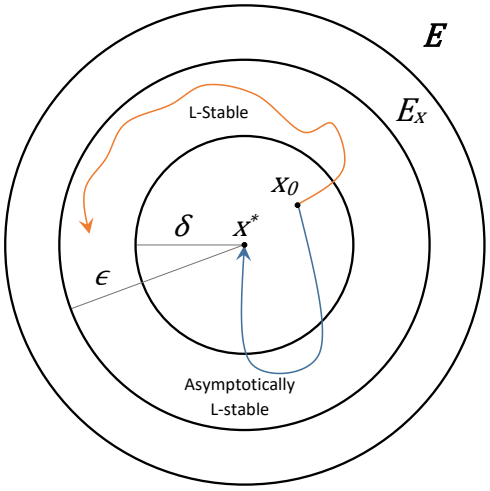

Figure 2.1: Graphical representation of the criterion of local dynamical stability in Lyapunov's sense. The equilibrium point point x^* is L-stable if, for each ϵ-region centered in x^*, it is possible to find a δ-smaller region, centered at x^*, such that, if the system is disturbed by an infinitesimal magnitude $|x_0 - x^*|$ within the δ-region, never leaves the ϵ-region. If the system remains in the ϵ-region is said to be L-stable (orange path), if it returns asymptotically to equilibrium x^* is said to be asymptotically L-stable (blue trajectory).

In continuous flows and maps, the simplest attractors are the equilibrium points of the system, $x^* \in \mathbb{R}^N$.

Definition 2.0.5 (Jacobian)**.** *Be the autonomous system*

$$\frac{d\boldsymbol{x}}{dt} = \boldsymbol{F}(\boldsymbol{x}, \Gamma), \tag{2.0.3}$$

*where Γ is a set of parameters that define the dynamics of the system. The **Jacobian matrix** of F evaluated at the equilibrium point x^* is given by*

$$J = \left.\frac{\partial \boldsymbol{F}(\boldsymbol{x}, \Gamma)}{\partial x}\right|_{x=x^*} \tag{2.0.4}$$

2.0.2 *Stability in Lyapunov's sense*

The most widely used notion of dynamical stability in mathematical applications to real problems is that of Lyapunov (LYAPUNOV, 1992; Hirsch, Smale, and Devaney, 2013). One of the the advantages of this method is that it is applicable to any system defined by equations with continuous and/or continuously differentiable functions, which universally represent real systems (Hirsch, Smale, and Devaney, 2013).

Lyapunov's indirect method

Definition 2.0.6. *Let the autonomous system be 2.0.1. Let $\boldsymbol{E}$ be the phase space of the system, and let x^* be a point of equilibrium. Let E_x be a subspace of $\boldsymbol{E}$ that contains a x^*, $x^* \in E_x \subseteq \boldsymbol{E}$. Let $|\cdot|$ be the Euclidean norm on $\boldsymbol{E}$. Then, if will say that x^* is:*

1. ***Stable in Lyapunov's sense (L-stable)** if:*

$$(\forall \epsilon > 0)(\exists \delta > 0)(|x_0 - x^*| < \delta \Rightarrow (\forall t \geq t_0)(|x_t - x^*| < \epsilon)), \epsilon > \delta. \tag{2.0.5}$$

2. ***Asymptotically stable*** *if, in addition to fulfilling the condition above, it is possible to choose a* $\delta > 0$ *such that*

$$\lim_{t\to\infty} |x_t - x^*| = 0. \tag{2.0.6}$$

The figure 2.1 shows a graphical representation of the concepts of L-stability and asymptotic stability. The indirect method assumes that it is possible to **linearize** the dynamical system around the equilibrium x^*. That is, it is possible to evaluate the Jacobian J in x^*. The stability criterion is established based on the eigenvalues of J, λ_i. It can be proved (LYAPUNOV, 1992) that a dynamical system represented by a differential system is **asymptotically L-stable** if the real part of the ith eigenvalue of the Jacobian J is strictly negative:

$$Re\lambda_i(J) < 0, \quad \forall i \tag{2.0.7}$$

The dominant eigenvalue of this set determines the maximum rate of return to equilibrium, so it is often called the **asymptotic resilience** (R_∞) of a system to infinitesimal displacements of equilibrium (Arnoldi, Loreau, and Haegeman, 2016):

$$\mathrm{R}_\infty = \frac{1}{\max[Re\lambda_i(J)]} \tag{2.0.8}$$

In systems described by difference equations, the criterion of local asymptotic L-stability is restricted to cases where all eigenvalues of the Jacobian lie within the **unit circle** in the complex plane (Hirsch, Smale, and Devaney, 2013).

Since J is evaluated at the equilibrium point x^*, the stability criterion by the indirect method of Lyapunov refers to **infinitesimal** neighborhoods of equilibrium, so it is a criterion of **local stability** (Figure 2.1).

Lyapunov's direct method

Theorem 2.0.7. *Let be a system of ordinary differential equations (Eqn. 2.0.1) that describe the dynamics of the vector of states* $\boldsymbol{x}_t$. *Let* $L : \Omega \to \mathbb{R}$ *be a differentiable function defined on an open set* Ω *containing the equilibrium point* x^* *of the system. Suppose that:*

1. *The function is positive definite:* $L(x^*) = 0$ *y* $L(\boldsymbol{x}_t) > 0$ *if* $x^* \neq x_t$.

2. $\frac{d}{dt}L(\boldsymbol{x}_t) \leq 0$ *in* $\Omega - \{x^*\}$.

So x^* *is stable, and any function that satisfies 1) and 2) is called a* ***Lyapunov function*** *for* x^*. *If, in addition, the function satisfies*

3. *The time derivative is strictly negative:* $\frac{d}{dt}L(\boldsymbol{x}_t) < 0$ *in* $\Omega - \{x^*\}$.

Then x^* *is* ***asymptotically stable*** *and* L *is a* ***strict Lyapunov function*** *(Malisoff and Mazenc, 2009; Hirsch, Smale, and Devaney, 2013).*

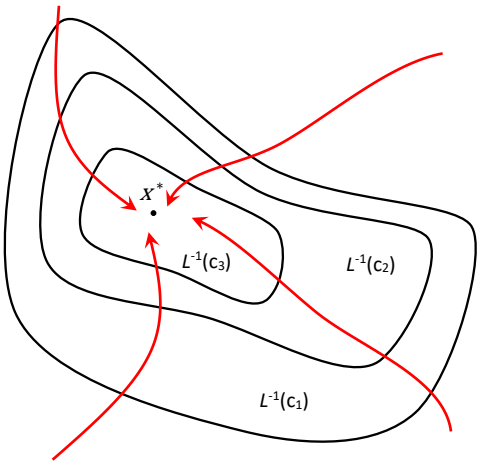

Figure 2.2: Graphical representation of the trajectories of a strict Lyapunov function. The trajectories (in red) are successively decreasing through smaller and smaller regions ($L^{-1}(c_1) \rightarrow L^{-1}(c_2) \rightarrow L^{-1}(c_3)$). According to Lyapunov's Theorem, the condition $\frac{d}{dt}L(\mathbf{x}_t) < 0$ guarantees that when a solution crosses the level $L^{-1}(c)$ it moves towards the set where $L \leq c$ and does not come out again (Based on Hirsch, Smale, and Devaney, 2013).

Proof. Let $\delta > 0$ be sufficiently small, so that the closed ball $B_\delta(x^*)$ around the equilibrium point x^* of radius δ is within Ω. Let α be the minimum value of L on the boundary of $B_\delta(x^*)$, that is, on the sphere $S_\delta(x^*)$ of radius δ centered at x^*. By definition, $\alpha > 0$. Let $\mathcal{U} = \{x \in B_\delta(x^*) | L(x) < \alpha\}$. So, no solution starting at $\mathcal{U}$ can reach $S_\delta(x^*)$, since L is not increasing on the solution curves. Therefore, no solution starting at $\mathcal{U}$ can leave $B_\delta(x^*)$. This proves that x^* is stable (Hirsch, Smale, and Devaney, 2013). Suppose that assumption 3) above is fulfilled, such that the function L is strictly decreasing over the solutions in $\mathcal{U} - \{x^*\}$. Let x_t be a solution starting at $\mathcal{U} - \{x^*\}$ and suppose $x_{t_n} \rightarrow Z_0 \in B_\delta(x^*)$ for some sequence $t_n \rightarrow \infty$. So, $Z_0 = x^*$. To see this, note that $L(x_t) > L(Z_0) \forall t \geq 0$, because $L(x_t)$ decreases and $L(x_{t_n}) \rightarrow L(Z_0)$ by continuity of L. If $Z_0 \neq x^*$, let Z_t be the solution which starts at Z_0. For any $s > 0$, we have $L(Z_s) < L(z0)$. Therefore, for any solution that starts sufficiently near Z_0 we have $L(Y_s) < L(Z_0)$. If we make $Y(0) = X_{t_n}$ for sufficiently large values of n, we arrive at the contradiction:

$$L(x_{t_n+s}) < L(Z_0)$$

Therefore, $Z_0 = x^*$. This proves that x^* is the only possible limit point of the set $\{x_t | t \geq 0\}$ and this completes the proof of the Lyapunov's Theorem (e.g., Hirsch, Smale, and Devaney, 2013).

■

Figure 2.2 shows a graphical representation of the strict Lyapunov function. As in the indirect method, the direct method it assumes that the disturbance on the state variable is infinitesimal. Note, However, that the stability in this case is **global**: every strict Lyapunov function is a positive scalar function, whose time derivative is negative except at the equilibrium point, where it vanishes. The existence of a Lyapunov function guarantees that the infinitesimal analysis characterizes the global equilibrium. However, there is no general analytical method

for finding a candidate Lyapunov function, although some ODE systems do have known and well-studied Lyapunov functions (MacArthur, 1970; May, 1973; Gilpin, 1974; Goh, 1977; Takeuchi, 1996)

2.0.3 *Transient stability in Lyapunov's sense: reactivity*

Stability in Lyapunov's sense, either as a local or global description, is understood asymptotically: a system is L-stable when $t \to \infty$. This description may be adequate on many physical systems. For example, the Hamiltonian function of mechanical systems is a Lyapunov function of such systems, so the fundamental understanding is achieved asymptotically. In other systems, such as biological ones, the asymptotic global description can be less relevant than the transitory description (Justus, 2008; Hastings, 2004). The paradigm is that of an ecological community of several competitive, predator-prey, or mutualistic populations (Svirezhev and Logofet, 1983). This is essentially a evolution problem, not just in the mathematical sense but also in the biological sense: the rate of evolution of the phenotypic characteristics of natural populations is of the same order of magnitude as the demographic rate of change (DeLong et al., 2016). The consequence of this equivalence is that the stability of ecological systems behaves like a moving equilibrium (Chesson, 2017), so it is necessary to introduce transient dynamical stability measures. Here, I will introduce **reactivity** (Neubert and Caswell, 1997; Caswell, 2007) as a measure of stability in Lyapunov's sense for transient dynamics.

Definition 2.0.8 (Reactivity)**.** *Be the following ODE system:*

$$\frac{d\boldsymbol{x}}{dt} = \boldsymbol{A}\boldsymbol{x}. \tag{2.0.9}$$

where $\boldsymbol{A}$ *is the square matrix that defines the dynamics of the system. Let* $\|\cdot\|$ *be the norm operator, and let* $\|x_0\|$ *be a perturbation of the asymptotic equilibrium of the system.* ***Reactivity*** *is defined as the reciprocal of initial resilience,* $-R_0$*, and is calculated as the maximum instantaneous of amplification rate, immediately after the disturbance, over a range of initial disturbances:*

$$-R_0 = \max_{\|x_0\| \neq 0} \left| \frac{1}{\|\boldsymbol{x}\|} \frac{d\|\boldsymbol{x}\|}{dt} \right|_{t=0} \tag{2.0.10}$$

Regardless of the asymptotic behavior of the equilibrium solutions, a system with $-R_0 > 0$ *has* ***reactive transitory stability*** *in Lyapunov's sense (Neubert and Caswell, 1997; Caswell and Neubert, 2005).*

The expression 2.0.10 implies evaluating the initial amplification for every possible disturbance. However, one can derive a formula that allows calculation of reactivity regardless of initial conditions (Wolkowicz and Styan, 1980; Neubert and Caswell, 1997; Caswell and Neubert,

2005):

Lemma 2.0.9. *The instantaneous growth rate of the infinitesimal perturbations of the equilibrium of an ODE system as defined in Eq. 2.0.9 can be written as:*

$$\frac{d\|\boldsymbol{x}\|}{dt} = \frac{d\sqrt{\boldsymbol{x}^T\boldsymbol{x}}}{dt} = \frac{\boldsymbol{x}^T(\boldsymbol{A}+\boldsymbol{A}^T)}{2\|\boldsymbol{x}\|} \tag{2.0.11}$$

The matrix $(\boldsymbol{A}+\boldsymbol{A}^T)/2$ *is the symmetric or Hermitian part of* $\boldsymbol{A}$*,* $H(\boldsymbol{A})$ *Wolkowicz and Styan, 1980. Therefore,*

$$\frac{1}{\|\boldsymbol{x}\|}\frac{d\|\boldsymbol{x}\|}{dt} = \frac{\boldsymbol{x}^T H(\boldsymbol{A})\boldsymbol{x}}{\boldsymbol{x}^T\boldsymbol{x}} \tag{2.0.12}$$

and, evaluated at equilibrium,

$$\left|\tfrac{1}{\|\boldsymbol{x}\|}\tfrac{d\|\boldsymbol{x}\|}{dt}\right|_{t=0} = \frac{\boldsymbol{x}_0^T H(\boldsymbol{A})\boldsymbol{x}_0}{\boldsymbol{x}_0^T\boldsymbol{x}_0} \tag{2.0.13}$$

The right hand side of the equation 2.0.13 is called the Rayleigh ratio (Wolkowicz and Styan, 1980; Neubert and Caswell, 1997). The maximum of this quotient over all perturbations $\boldsymbol{x}_0$ *is the reactivity as defined in the equation 2.0.10. Since the matrix* $H(\boldsymbol{A})$ *is symmetric and real, its eigenvalues are real and the associated eigenvectors are orthogonal. The Rayleigh ratio is maximized by the eigenvector corresponding to the dominant eigenvalue of* $H(\boldsymbol{A})$ *which is, in fact, the maximum value of the quotient. Therefore, if* λ_1 *is the dominant eigenvalue,*

$$-R_0 = \lambda_1 H(\boldsymbol{A}) = \frac{1}{2}(\boldsymbol{A}+\boldsymbol{A}^T) \tag{2.0.14}$$

So, we have the following:

1. *If a system is* ***asymptotically unstable****, it is necessarily* ***reactive****:*

$$\Re\lambda_1(J) > 0 \quad \Rightarrow \quad \lambda_1 H(\boldsymbol{A}) > 0 \tag{2.0.15}$$

2. *If a system is* ***asymptotically stable****, it could be* ***reactive*** *or* ***non-reactive****.*

The reactivity of a system measures the behavior of solutions when $t \to 0$. Analogously to asymptotic resilience, **initial resilience** can be defined as the reciprocal of reactivity, R_0. The figure 2.3 graphically shows the complementarity between asymptotic L-stability and reactivity.

2.0.4 *Stability in Lagrange's sense*

Lemma 2.0.10. *Consider a non-autonomous system*

$$\frac{d\boldsymbol{y}}{dt} = \boldsymbol{M}(\boldsymbol{y}, t) \tag{2.0.16}$$

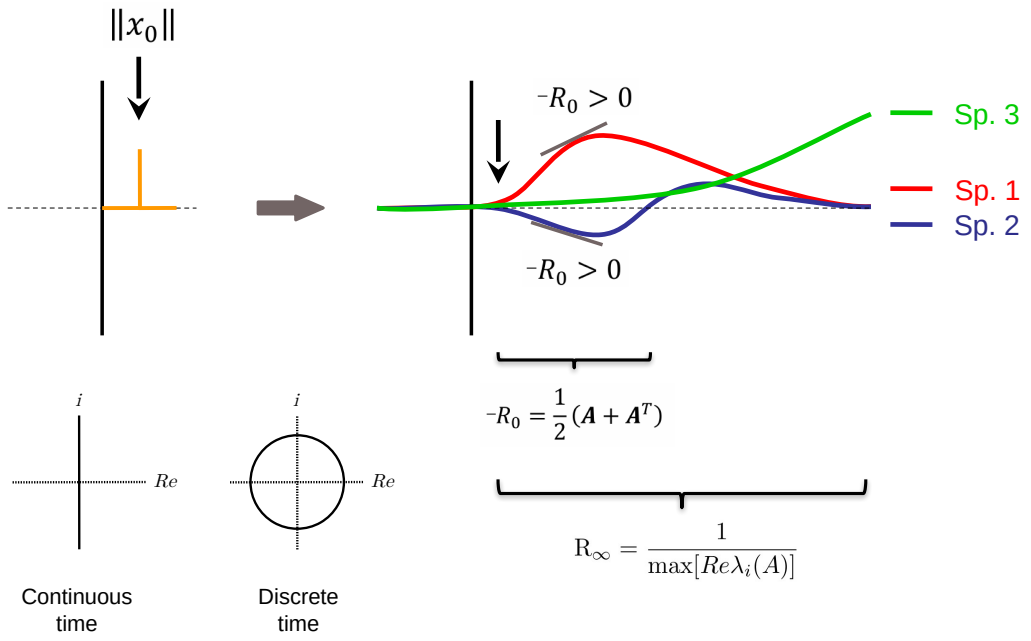

Figure 2.3: Graphical representation of the immediate and asymptotic response of different idealized systems to an infinitesimal disturbance (orange pulse, $\|x_0\|$). An asymptotically stable system (R_∞ <0) can either be reactive ($-R_0$ >0, path in red) or non-reactive ($-R_0 < 0$, trajectory in blue). The reactivity of each system is represented as the tangent to the curve of the state variable immediately after the disturbance. An asymptotically unstable system ($R_\infty > 0$, green path) is equally reactive ($-R_0 > 0$).

where $\boldsymbol{M}$ *is is a nonlinear function of time and* $y_1, y_2 ... y_n$*, are the state variables that make up the state vector* $\boldsymbol{y}$*. Let* $\boldsymbol{y}(0,t) = 0$ *be the initial position. Let* t_0*, be an initial moment,* $\boldsymbol{y}(t_0) = \boldsymbol{y}_0$ *an initial state, and* T *a finite time. Let* $t_0 < T < \infty$*, such that the solution of the 2.0.16 system is:*

$$\|\boldsymbol{y}(t, y_0, t_0)\| \to \infty \tag{2.0.17}$$

when $t \to T$*. Then, the solution of the system is said to has* ***finite escape time*** *(Thornton and Mulholland, 1974). The system is* ***unstable as a whole****.*

Lemma 2.0.11. *Let* $\beta > 0$ *be a strictly positive constant, a function of the initial conditions,* $\beta = \beta(\boldsymbol{y}_0, t_0)$*, such that the solution*

$$\|\boldsymbol{y}(t, y_0, t_0)\| < \beta \quad \forall t > t_0 \tag{2.0.18}$$

Then,

1. *If* β *exists for any initial condition, then we say that the system is* ***stable in Lagrange's sense****.*
2. *If* β *is independent of time,* $\beta = \beta(\boldsymbol{y}_0)$*, then the system is* ***uni-***

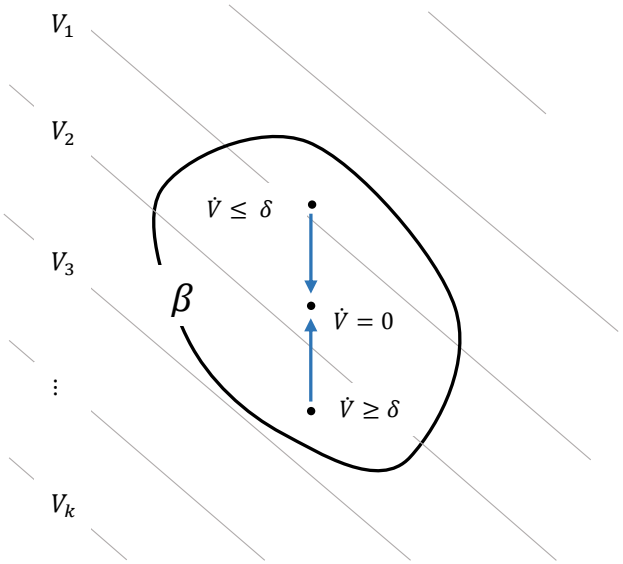

Figure 2.4: Graphical representation of stability in Lagrange's sense. Shown is the rate of change of a Lyapunov function $V = \{V_1, V_2, ..., V_k\}$ subjected to a disturbance gradient. Interpreted in terms of energy, the time derivative of $V, \dot{V}$, reaches a minimum at $\dot{V} = 0$, which represents the steady state. The bounded region β comprises the space within which the system displays stability in Lagrange's sense. Those disturbances of magnitude $\delta > 0$ that increase the energy of the system, will decrease with time and the system will eventually be in the state of minimum energy, $\dot{V} \leq \delta < 0$. Similarly, disturbances that decrease the energy of the system will be asymptotically attenuated, $\dot{V} \geq \delta > 0$. (Based on Thornton and Mulholland, 1974).

***formly stable in Lagrange's sense**. The solutions of the system are **uniformly bounded**.*

*In both cases, the system is **stable as a whole**: for all compact K there exists a compact $\tilde{K} \supset K$ such that any path starting at K remains at $\tilde{K}$ when $t \to \infty$ (Hammouri and Othman, 1992).*

Figure 2.4 shows a graphical representation of stability in Lagrange's sense. In the linear case, the stability in Lyapunov's sense implies stability in Lagrange's sense, but this this is not the case in the non-linear case (Bacciotti and Rosier, 2005; Hammouri and Othman, 1992). From the point of view of applications to the dynamics of real systems, and unlike the stability in Lyapunov's sense, the most important aspect of the stability in Lagrange's sense is that it refers to the **stability of the system as a whole**, and not to the stability of the equilibrium points. In fact, it is possible to prove (Kahane, 1972; Hammouri and Othman, 1992) that the dynamics of systems with a diagonal-dominant matrix have **bounded** solution sets: positive initial conditions lead to positive solutions. Since populations in natural ecosystems can only take strictly positive values, this property of stability in Lagrange's sense is very important to understand the logic of stability in the ecological sense (Thornton and Mulholland, 1974; Svirezhev and Logofet, 1983).

2.0.5 *Intrinsic stochastic invariability*

In this section, a recently developed dynamical stability class will be defined, called intrinsic stochastic invariability (Arnoldi, Loreau, and Haegeman, 2016). This approach to equilibrium provides a intermediate notion between resilience and reactivity, and measures the inverse of the dominant stationary response of a dynamical system to random (white noise) disturbances.

Definition 2.0.12 (Brownian motion and white noise)**.** *Consider a series of infinitesimal time steps of length δt:*

$$t_k = k\delta t \rightarrow t_{k+1} = (k+1)\delta t \tag{2.0.19}$$

At each step t_k a walk is drawn randomly from a Gaussian distribution with mean 0 and variance δt. At the limit in continuous time, $\delta t \rightarrow 0$, this process defines a ***Brownian motion*** *W_t. Define the derivative ξ_t as the stochastic signal that satisfies*

$$W_t = \int_0^t \xi_s ds \tag{2.0.20}$$

If we write $dW_t = \xi(t)dt$, the signal $\xi(t)$ is called ***white noise*** *(Arnoldi, Loreau, and Haegeman, 2016).*

Definition 2.0.13 (intrinsic stochastic invariability)**.** *Let an ODE system be*

$$\frac{d\boldsymbol{x}}{dt} = \boldsymbol{A}\boldsymbol{x} \tag{2.0.21}$$

where $\boldsymbol{x}$ is a vector with n state variables, x_i, and A is a square matrix. Let $r = 1, 2, ..., R$ be exogenous factors, modeled as independent white noise signals, $dW_r(t)$, which impact the system. The effect of the factor r on the variable of state x_i is denoted by T_{ir}. Then, the system described by the equation 2.0.21 is rewritten as a stochastic differential equation ()

$$d\boldsymbol{X} = A\boldsymbol{X}dt + T d\boldsymbol{W}(t) \tag{2.0.22}$$

where $\boldsymbol{W} = (W_1, ..., W_r)^T$ is a set of Brownians walks (Wiener processes, Arnoldi and Haegeman, 2016). The second moments of the equation 2.0.22 are represented by the stationary covariance of the system, $C_* = \mathbb{E}\boldsymbol{X}_t\boldsymbol{X}_t^T$. According to the theory of EDEs (Arnold, 1974), these matrices follow the equation $C_* = \hat{A}C_t + \Sigma$, where $\hat{A}C = AC + CA^T$ is a lifted operator (Arnoldi, Loreau, and Haegeman, 2016) and $\Sigma = TT^T$ is a positive semi-definite matrix containing the correlations of the white noise exogenous variables. Then, the stationary covariance matrix can be write as

$$C_* = -\hat{A}^{-1}(\Sigma) \tag{2.0.23}$$

The covariance matrix of the disturbances (Σ) maximizes the norm of the covariance matrix of responses (C_t). Applying the Frobenius norm, $\|\Sigma\| = \sqrt{Tr(\Sigma^T\Sigma)}$, it is possible to define the ***variability matrix****, $\mathcal{V}_s$*

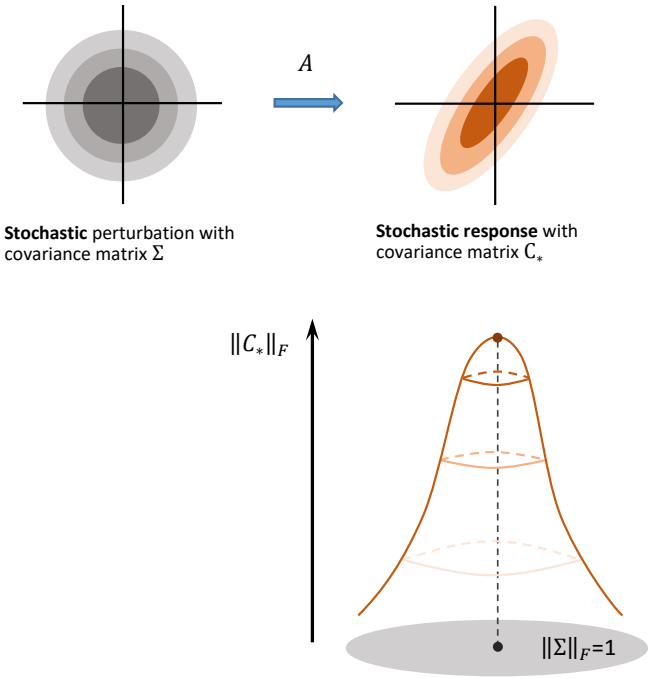

Figure 2.5: Graphical representation of stochastic variability ($\mathcal{V}_s$) for a system with two state variables. A Gaussian stochastic multivariate disturbance (white noise), distributed continuously in time with covariance matrix Σ, generates a Gaussian stochastic multivariate response with covariance matrix $C_* = -\hat{A}^{-1}(\Sigma)$. The variability in this response is measured by the Frobenius norm of this matrix, $\|C_*\|_F$, on the set of normalized disturbances, $\|\Sigma\|_F = 1$. For obtaining an intrinsic measure, the worst-case scenario is examined, generated by the perturbation matrix Σ that causes the maximum variability. The intrinsic stochastic invariability is the simply measured as $\mathcal{I}_s = \frac{1}{2\mathcal{V}_s}$. Based on Arnoldi, Loreau, and Haegeman, 2016.

as the largest ***stationary covariance matrix*** *defined over the set of normalized disturbances. Relaxing the assumption that* Σ *is necessarily a covariance matrix, we get:*

$$\mathcal{V}_s = \sup_{\|\Sigma\|_F=1} \left\| -\hat{A}^{-1}(\Sigma) \right\|_F = \left\| \hat{A}^{-1} \right\| \tag{2.0.24}$$

where $\|\hat{A}^{-1}\|$ *is the spectral norm of the space of linear operators that can be written as an extended array,* $A \otimes \mathbb{I} + \mathbb{I} \otimes A$*, where* $\mathbb{I}$ *is the identity matrix and* $\otimes$ *is the tensor (Kronecker) product (Arnoldi, Loreau, and Haegeman, 2016). The worst-case scenario is that generated by the perturbation matrix* Σ *that induces the maximum variability. Then, the* ***intrinsic stochastic invariability****,* $\mathcal{I}_s$*, is defined as the inverse of stochastic variability:*

$$\mathcal{I}_s = \frac{1}{2} \left\| -(A \otimes \mathbb{I} + \mathbb{I} \otimes A)^{-1} \right\|^{-1} \tag{2.0.25}$$

Figure 2.5 shows a graphical representation of the stochastic variability of a dynamical system. Arnoldi et al. (Arnoldi, Loreau, and Haegeman, 2016) show that white noise is a limit case of a largest class of uncorrelated disturbances. This is especially important in the application of intrinsic stochastic invariability to real systems. In particulat, stochastic variability can be interpreted in an equivalent way as the maximum response (worst-case response) to two alternatives scenarios:

1. A persistent sequence of disturbances of **infinitesimal intensity** and of **continuous** distribution in time.

2. A persistent sequence of disturbances of **finite intensity** and of **discrete** and random distribution in time.

The introduction of finite disturbances in this new approach to dynamical stability qualitatively differentiates intrinsic stochastic variability from stability in Lyapunov's sense and in Lagrange's sense.

2.0.6 *Ordering of dynamical stability measures*

The intrinsic nature of the dynamical stability measures proposed in this work implies that the response of a system does not depend on the direction or intensity of the applied disturbance, but on the internal dynamics of the system itself (Arnoldi, Loreau, and Haegeman, 2016; Arnoldi and Haegeman, 2016). This makes it possible to compare and order the different measures (Arnoldi, Loreau, and Haegeman, 2016):

$$R_0 \leq \mathcal{I}_s \leq R_\infty \tag{2.0.26}$$

This means that, for any dynamical system, the initial resilience always produces the lowest degree of stability, while asymptotic resilience always provides the highest (see Arnoldi, Loreau, and Haegeman, 2016 for a proof).

2.1 Structural stability

As we have seen, the analysis of the dynamical stability of a system is refered to the study of the consequences of disturbances on the state variable(s) of the dynamical system (perturbations on the initial conditions), either when $t \to \infty$ (Resilience), when $t \to 0$ (Reactivity) or when the system continuously responds to persistent disturbances over time (stochastic variability). Equally, dynamical stability can refer to the local or global stability of non-trivial equilibrium points of a system (stability in Lyapunov's sense) or to the stability of the system as a whole (stability in Lagrange's sense).

The notion of structural stability, or robust systems (Andronov and Pontryagin, 1937), was initially conceived as a way to address qualitative stability of a system against disturbances in the vector of parameters. The qualitative analysis of an ODE system is based on the geometric description of the space of their orbits. The analysis of structural stability pursues, basically, to establish equivalence relations that capture the geometrical structure of a system before and after being perturbed (Arnold, 1988; Palis and Melo, 1982). In essence, if a set is equipped with a topology and with an equivalence relation, then its structurally stable elements are those that are internal to the equivalence relation (Arnold, 1988; Palis and Melo, 1982; Peixoto, 1959; Smale, 1967). As such, it is an approach qualitatively different from

that of dynamical stability (although see Arnoldi, Loreau, and Haegeman, 2016). In this section, a definition of structural stability for low-dimensional systems will be proposed, along with methods to estimate it.

2.1.1 *Definitions*

Definition 2.1.1 (Diffeomorphism)**.** *Let $\mathcal{A}$ and $\mathcal{B}$ be two differentiable varieties, and let $f : \mathcal{A} \to \mathcal{B}$ be a differentiable mapping. Then the map f is a* ***diffeomorphism*** *if it is* ***bijective*** *and if its inverse, $f^{-1} : \mathcal{B} \to \mathcal{A}$, is also differentiable. If the function f is continuous and differentiable with order p, then it is said to be a* $\boldsymbol{C^p - diffeomorphism}$*.*

Definition 2.1.2 (Diffeomorphic systems)**.** *Let $\boldsymbol{M}$ be a differentiable manifold, and let $\boldsymbol{v}$ be a vectors field over $\boldsymbol{M}$. Let $(\boldsymbol{M}_1, \boldsymbol{v}_1)$ and $(\boldsymbol{M}_2, \boldsymbol{v}_2)$ be two dynamical systems. We will say that both systems are* ***diffeomorphic*** *if there exists a diffeomorphism $f : \boldsymbol{M}_1 \longrightarrow \boldsymbol{M}_2$ which converts the vector field $\boldsymbol{v}_1$ into the vector field $\boldsymbol{v}_2$.*

Definition 2.1.3 (Topological Equivalence)**.** *The* ***phase flow*** *of a vector field $\boldsymbol{v}$ over $\boldsymbol{M}$ is denoted by the transformations $g^t : \boldsymbol{M} \longrightarrow \boldsymbol{M}$ which, at time 0, converts each initial condition x_0 of the system*

$$\frac{dx}{dt} = \boldsymbol{v}(x) \tag{2.1.1}$$

in the $g^t x_0$ value of the solution at time t. Given that $g^{t+s} = g^t g^s$ and $g^0 = 1$, and assuming that the manifold $\boldsymbol{M}$ is ***compact****, the transformations $g^t x$ are defined for all $t \in \mathbb{R}$ and $x \in \boldsymbol{M}$. If there is a* ***homeomorphism*** *from the phase space of a system to the phase space of the second, this implies the conversion of the* ***phase flow*** *of the first to the phase flow of the second:*

$$f(g_1^t x) \; equiv g_2^t(fx) \tag{2.1.2}$$

Under these conditions, the two systems are said to be ***topologically equivalents*** *(topologically conjugate). Which is equivalent to saying that the following diagram*

$$\begin{array}{ccc} M_1 & \xrightarrow{g_1} & M_1 \\ \Big\downarrow f & & \Big\downarrow f \\ M_2 & \xrightarrow{g_2} & M2 \end{array}$$

is ***commutative****. From the point of view of differentiable manifolds, diffeomorphic systems are indistinguishable from each other (they are* ***topologically equivalent****; Arnold, 1988; Robinson, 1974).*

Definition 2.1.4 (Orbital topological equivalence)**.** *Let there be two dynamical systems* $(\boldsymbol{M}_1, \boldsymbol{v}_1)$ *and* $(\boldsymbol{M}_2, \boldsymbol{v}_2)$*. If there exists a homeomorphism of the phase space of the first system into the phase space of the second such that the* ***oriented phase curves*** *of the first system are converted to oriented phase curves of the second, then systems* $(\boldsymbol{M}_1, \boldsymbol{v}_1)$ *and* $(\boldsymbol{M}_2, \boldsymbol{v}_2)$ *are said to be* ***orbitally topologically equivalent*** *(Arnold, 1988).*

2.1.2 *Stability in Andronov-Pontryagin's sense*

For historical reasons, the first definition of structurally stable systems is included here. Originally named **robust systems** by Soviet mathematicians Aleksandr Andronov and Lev Pontryagin (Andronov and Pontryagin, 1937), we will follow the development of DeBaggis (DeBaggis, 1953), Smale (Smale, 1969) and Peixoto (Peixoto, 1959).

Definition 2.1.5 (Robust systems)**.** *Consider the following ODE system, with two state variables,* x, y*:*

$$\frac{dx}{dy} = P(x,y) \quad \frac{dy}{dt} = Q(x,y) \tag{2.1.3}$$

defined in the domain $\mathcal{D}$ *of the* xy *plane. It is assumed that the functions* P, Q *are continuously differentiable in* $\mathcal{D}$*, or of class* C^1*. The vector field* (P, Q) *enters transversely into the boundary domain,* $\partial\mathcal{D}$*. The Fundamental theorem of existence of ODE says that for initial conditions* (x_0, y_0) *in* $\mathcal{D}$ *it is possible to find a small enough real* t *in absolute value,* $|t| < \epsilon$*, such that the functions* $f(x_0, y_0, t), \quad g(x_0, y_0, t)$ *satisfy the initial conditions* $f(x_0, y_0, 0) = x_0, \quad g(x_0, y_0, 0) = y_0$ *and the ODE system*

$$\begin{aligned} \frac{df(x_0,y_0,t)}{dy} &= P(f(x_0,y_0,t), g(x_0,y_0,t)) \\ \frac{dg(x_0,y_0,t)}{dt} &= Q(f(x_0,y_0,t), g(x_0,y_0,t)) \end{aligned} \tag{2.1.4}$$

So, there exists a ϵ*-homeomorphism* $f : \mathcal{D} \longrightarrow \mathcal{D}$ *(*f *moves each point by* $\mathcal{D}$ *by amount* $< \epsilon$*) which transforms the trajectories of the original system into trajectories of the perturbed system, and the system is said to be* ***robust*** *(****structurally stable****, Andronov and Chaikin, 1949; DeBaggis, 1953).*

2.1.3 *Local structural stability*

Definition 2.1.6 (Local structural stability)**.** *Let* $\boldsymbol{M}$ *be a compact manifold of class* C^{r-1} $(r \geq 1)$*. Let* $\boldsymbol{v}$ *be a vector field of class* C^r *over* $\boldsymbol{M}$*. It is assumed that* $\boldsymbol{v}$ *is not tangent to the boundary of* $\boldsymbol{M}$*,* $\partial\boldsymbol{M}$*, if it exists. The system* $(\boldsymbol{M}, \boldsymbol{v})$ *is* ***structurally stable*** *if there exists a neighborhood of* $\boldsymbol{v}$ *in space* C^1 *such that, every vector field in this*

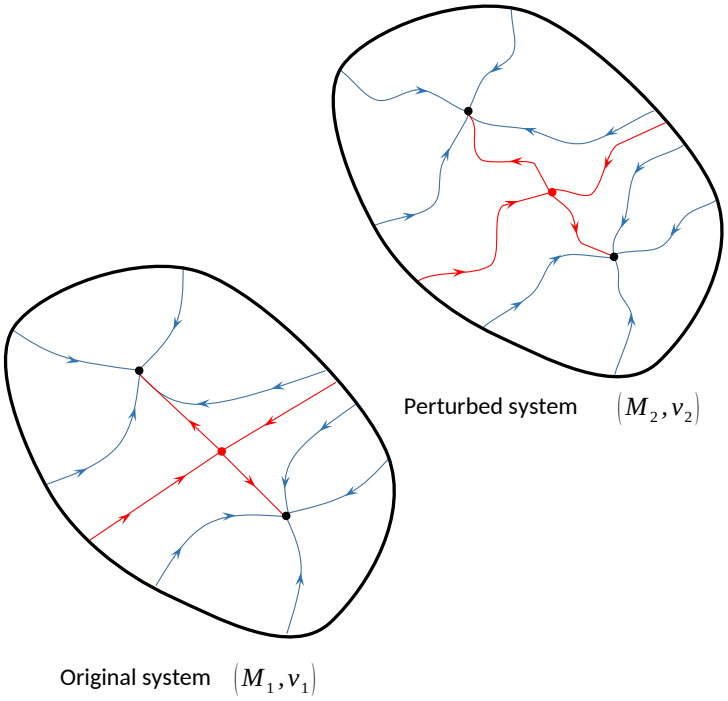

Figure 2.6: Graphic representation of the notion of local structural stability. The original dynamical system (M_1, v_1) is characterized by two stable nodes (in black, solution orbits in blue) and a saddle point (in red, solution orbits in red). When subjected to a perturbation $< \epsilon$, the perturbed system (M_2, v_2) shows a homeomorphism with the original system: the phase portrait is orbitally topologically equivalent.

neighborhood defines an orbitally topologically equivalent system to the original (Arnold, 1988).

Figure 2.6 shows an example of a structurally stable system subjected to an ϵ-perturbation. That is, a small disturbance, of type C^1 (Arnold, 1988), that causes a qualitative change in the orbits of the original system in such a way that the perturbed system is orbitally topologically equivalent to the original system: the qualitative dynamics does not change with the disturbance.

Smale proved (Smale, 1966) that the compact differentiable manifolds of dimension greater than 4 with vector fields equipped with a C^r topology, $(r > 0)$ are not dense. Subsequently, Peixoto and Pugh (Peixoto and Pugh, 1968) demonstrated that, when the manifold is open and its vector fields are equipped with the same topology, systems are never dense when the dimension is greater than 2. This suggests that for high-dimensional systems, the probability of finding structurally stable elements decreases rapidly (Arnold, 1988).

2.1.4 *Stochastic structural stability*

Definition 2.1.7. *Be an autonomous ODE system*

$$\frac{d\boldsymbol{x}}{dt} = A\boldsymbol{x} \tag{2.1.5}$$

and let J be the Jacobian matrix of the system. The coefficients of matrix J fluctuate in time (are subject to process error). Let P_k be a series of real matrices describing the internal fluctuations of the matrix A and its correlations. Let σ^2 be the independent variance of the fluctuations and let $\boldsymbol{e}_i$ be the standard orthonormal basis of the phase space. So $P_k = \sigma \boldsymbol{e}_i \boldsymbol{e}_j^T$. Let W_t^k a series of independent Wiener processes (Itô interpretation). Then, the perturbed system is represented as a linear homogeneous SDE:

$$d\boldsymbol{X}_t = \left(\mathrm{A}dt + \sum_k P_k dW_t^k \right) \boldsymbol{X}_t \tag{2.1.6}$$

Define $\mathcal{P}$ from an arbitrary sequence of real matrices P_k, $\mathcal{P}(C) = \sum_k P_k C P_k^T$. Let $\dot{C}_t$ be a lifted operator of the previous SDE, such that

$$\dot{C}_t = (\hat{A} + \mathcal{P}) C_t \tag{2.1.7}$$

Let $\|\mathcal{P}\|$ be the spectral norm of $\mathcal{P}$, a measure of the intensity of internal shocks. If the fluctuations of the elements in A are independent, $\|\mathcal{P}\| = n^2\sigma^2$, where n is the dimension of the system. Let $\alpha(\hat{A}+\mathcal{P})$ be the spectral abscissa that separates the region of stability (< 0) from that of instability (≥ 0). Then, it is possible to define the ***stochastic structural stability*** *as:*

$$\mathcal{S}_{\mathrm{STR}}^W = \inf\{\|\mathcal{P}\| | \alpha(\hat{A} + \mathcal{P}) > 0\} \tag{2.1.8}$$

where the infimum is calculated over the perturbations $\mathcal{P}$ (Arnoldi and Haegeman, 2016).

According to this definition, structural stability in stochastic systems is represented as the magnitude of the internal random disturbances (white noise type) necessary to destabilize the stationary variance of the system Arnoldi and Haegeman, 2016. In other words, the response of a dynamical linear system to external random disturbances reflects the intensity of internal fluctuations that the system can accommodate before becoming stochastically unstable. The magnitude of these disturbances are reflected in the spectral abscissa, $\alpha(\hat{A} + \mathcal{P})$.

2.2 Unification of dynamic and structural stability

In this section we will present the theorem that relates the intrinsic stochastic invariability of a system with its stochastic structural stability (Arnoldi and Haegeman, 2016). This provides a fundamental bridge between both approximations of great relevance in mathematical applications.

Theorem 2.2.1 (Unification of dynamical stability and structural stability)**.** *In real linear dynamical systems, the measures of dynamical*

stability and structural stability coincide, $\mathcal{S}^W_{\text{STR}} = \mathcal{I}_s$; namely:

$$\frac{1}{2}\left\|-(A\otimes\mathbb{I}+\mathbb{I}\otimes A)^{-1}\right\|^{-1} = \inf\{\|\mathcal{P}\||\alpha(\hat{A}+\mathcal{P})>0\}. \tag{2.2.1}$$

Proof. Let A be a stable Jacobian matrix, and let $\mathcal{I}_s = \frac{1}{v}$. This implies (Eq. 2.0.24) the existence of two normalized positive arrays: the correlation matrix in the noise (Σ) and the matrix of system response, $\mathit{\Pi}$, such that:

$$-\hat{A}^{-1}\Sigma = v\mathit{\Pi} \quad \Leftrightarrow \quad \hat{A}\mathit{\Pi} + v^{-1}\Sigma = 0 \tag{2.2.2}$$

Let $\mathcal{P}$ be an operator of the form $\sum_k P_k \cdot P_k^T$, for a set of real P_k. The spectral decomposition of positive semi-definite matrices Σ and $\mathit{\Pi}$ is,

$$\Sigma = \sum_{i=1}^{n} \lambda_i \mathbf{u}_i \mathbf{u}_i^T, \quad \mathit{\Pi} = \sum_{i=1}^{n} \mu_i \mathbf{v}_i \mathbf{v}_i^T \tag{2.2.3}$$

Let n^2 be internal disturbances independent of the matrix A, and let $P_k = \sqrt{\frac{\lambda_i \mu_j}{v \mathbf{u}_i \mathbf{v}_j^T}}$. Then,

$$\begin{aligned}\mathcal{P}(C) &= \sum_k P_k C P_k^T \\ &= v^{-1} \sum_{i=1}^{n} \lambda_i \mathbf{u}_i \mathbf{u}_i^T \sum_{j=1}^{n} \mu_j \langle \mathbf{v}_j, C\mathbf{v}_j \rangle \\ &= v^{-1} \text{Tr}(\mathit{\Pi} C)\Sigma\end{aligned} \tag{2.2.4}$$

Applying the Hilbert-Schmidt inner product (Trefethen and Embree, 2005) $\langle X, \mathcal{Y} \rangle = \text{Tr}(X^* \mathcal{Y})$, from which the Frobenius norm is derived, it is seen that $\mathcal{P}$ takes the compact form $\mathcal{P} = v^{-1}\langle \mathit{\Pi}, \cdot \rangle \Sigma$. This means that $\mathcal{P}(\mathit{\Pi}) = v^{-1}\Sigma$ y $\|\mathcal{P}\| = v^{-1}$. Then,

$$(\hat{A} + \mathcal{P})\mathit{\Pi} \geq 0. \tag{2.2.5}$$

Therefore, $\mathcal{P}$ corresponds to the internal noise intensity $\|\mathcal{P}\| = v^{-1}$, and we get that:

$$\mathcal{S}^W_{\text{STR}} \leq \mathcal{I}_s \tag{2.2.6}$$

Now, suppose $\mathcal{S}^W_{\text{STR}}(A) = p$. There is a operator $\mathcal{P}$, such that $\|\mathcal{P}\| = p$ and $\hat{A} + \mathcal{P}$ is unstable. This means that there is a dominant eigenvalue that is located on the imaginary axis, but there is also a dominant eigenvalue at 0. Thus, for any matrix X with $\|X\|_F = 1$ we have:

$$(\hat{A} + \mathcal{P})X = 0 \quad \Leftrightarrow \quad X = -\hat{A}^{-1}(\mathcal{Y}), \tag{2.2.7}$$

where $\mathcal{Y} = \mathcal{P}(X)$. Given that $\|\mathcal{Y}\|_F \leq p$, we have that $\|\hat{A}^{-1}\| \geq p$. Considering the form of $\mathcal{I}_s$ (Equation 2.0.25):

$$\mathcal{S}^W_{\text{STR}} \geq \mathcal{I}_s \tag{2.2.8}$$

which completes the proof (Arnoldi and Haegeman, 2016).

■

Stability in real systems

3

Starting with the seminal work by Lewontin, 1969, the concept of stability as applied to ecological systems is still an active research area (e.g., Logofet, 1993; Donohue et al., 2016). The dynamical system approach represented by the generalized Lotka-Volterra scheme is one of the most studied models in the field of dynamical systems, either in their direct applications to the analysis of real ecosystems and as in mathematical analysis (eg. Takeuchi, 1996; Logofet, 1993, 2005; Svirezhev and Logofet, 1983; Capone, De Luca, and Rionero, 2013; Mierczynski and Schreiber, 2002). The analysis of this model has allowed us to derive stability measures specifically designed for real systems, that is, those systems restricted to the case where the phase space is strictly positive (Svirezhev and Logofet, 1983).

This section will introduce the Lotka-Volterra model, both in continuous and discrete time versions, as well as a simplified formulation of the original model oriented to high-dimensional inverse problems. These models will be used throughout this dissertation project. In the discrete-time case, I will introduce reformulations of the stability measures. Finally, several additional stability definitions will be introduced, specifically oriented to the analysis of the permanence and persistence of ecological systems (Takeuchi, 1996).

3.1 Lotka-Volterra model of inter-specific interaction

The Lotka-Volterra model in continuous time has the form:

$$\frac{dN_i}{dt} = N_i \left(r_i - \sum_{j=1}^{k} \alpha_{ij} N_j \right), i = 1, 2, ..., k \tag{3.1.1}$$

where N_i represents the population density (or size) of a species i in an ecosystem with k species, and the parameter $r_i > 0$ represents the intrinsic growth rate of the species i. The coefficient α_{ij} measures the quantitative effect (the interaction) of the species j on the species i, for the set of k species of the ecosystem. The square matrix containing the coefficients a_{ij} is represented by $\mathbf{A} = \{a_{ij}\} \in \mathbb{R}^{k \times k}$, and is called the **interaction matrix** (Levins, 1968; Novak et al., 2016). Depending on the sign of the entries in the matrix, we can talk about competition $(-,-)$, mutualism $(+,+)$ and predation $(-,+)$, among other types of interactions (Takeuchi, 1996; Hofbauer and Sigmund, 1998). Finally, the term in parentheses is called **per capita growth rate** of the species i, $(r_i - \sum_{j=1}^{k} \alpha_{ij} N_j)$.

From the point of view of real systems, the state space of the equation 3.1.1 is represented by the **positive ortant**

$$\mathbb{R}^k_+ = \{n = (n_1, n_2, ..., n_k) \in \mathbb{R}^k | n_i \geq 0, \quad \text{for} \quad i = 1, 2, ..., k\} \quad (3.1.2)$$

The ortant $\mathbb{R}^k_+$ is **invariant**: any solution that is in $\mathbb{R}^k_+$ remains in $\mathbb{R}^k_+$ for any time the solution is defined (Takeuchi, 1996). That is, this restriction of ecological systems implies defining the necessary conditions for the system to be stable in Lagrange's sense. Specifically, the positive ortant is defined by those values of the vector $\mathbf{r}_i = \{r_1, ..., r_k\}^T$ and of the matrix $\mathbf{A}$ that make the equilibrium points of the Lotka-Volterra system **feasible**:

Definition 3.1.1 (**Feasible equilibrium Points**). *Let N_i^* be a stable equilibrium point of the equation 3.1.1. Be the set of linear equations*

$$r_i = \sum_{j=1}^{k} \alpha_{ij} N_j^* \quad (3.1.3)$$

*If there exists a set of points $N_i^* > 0$ that are solutions of the equation 3.1.3, then the point N_i^* is said to be **feasible** (Svirezhev and Logofet, 1983; Logofet, 1993; Hofbauer and Sigmund, 1998). The Jacobian matrix of the Lotka-Volterra system (Equation 3.1.1) is then written as:*

$$J = \text{diag}\{\boldsymbol{N}^*\}(\boldsymbol{A}) \quad (3.1.4)$$

The Lotka-Volterra model, despite its simplicity, is capable of exhibiting complex dynamic behaviors, from globally stable point equilibria to multiple locally stable or unstable equilibria, limit cycles and chaos (Takeuchi, 1996; Hofbauer and Sigmund, 1998). In the following sections, a series of definitions related to the quantitative and qualitative stability of the ecological systems represented by the general Lotka-Volterra model will be given.

3.1.1 *dynamical stability beyond Lyapunov*

Dimitrii Logofet (Logofet, 2005, 2016) has proposed a series of extensions of the concept of dynamical stability in the Lyapunov sense inspired by the type of interactions between species represented in the Lotka-Volterra model. Due to their applied importance, some of these notions will be examined here.

Definition 3.1.2 (**D-stability**). *Let J be the Jacobian matrix of the Lotka-Volterra model. Let D be a positive square diagonal matrix, $D = \text{diag}\{d_1, ..., d_n\}$ of dimension $k \times k$. Let $\boldsymbol{D}_n$ be the multiplicative group of positive definite diagonal matrices. The matrix J is called **D-stable**, $J \in \boldsymbol{DS}_n$ if DJ is stable for any positive diagonal D :*

$$DJ \in \boldsymbol{S}_n \quad \forall D \in \boldsymbol{D}_n. \quad (3.1.5)$$

The eigenvalues of any Jacobian matrix J are a function of the particular values of the equilibrium point. That is, for the same matrix $\mathbf{A}$ it is possible to simultaneously find both stable and unstable feasible equilibrium points. In this case, the concept of D-stability guarantees the local stability of every feasible point (Logofet, 2005).

Definition 3.1.3 (**Volterra-dissipative matrix**). *The matrix A is **Volterra-dissipative**, or Volterra-Lyapunov, $A \in \boldsymbol{DiS}_n$, if there exists a diagonal matrix $D \in \boldsymbol{D}_n$ such that the matrix DA generates a negative definite quadratic form (DAx, x). Equivalently, the matrix $DA + A^T D$ is positive definite.*

Unlike the D-stability, the Volterra-dissipativity of a matrix constitutes a sufficient condition to guarantee the global stability of an equilibrium. In fact, a Volterra-dissipative matrix is necessarily D-stable. Logofet (Logofet, 1993, 2005) has shown that if the community matrix $\mathbf{A}$ is Volterra-dissipative, then every feasible equilibrium is also globally stable.

3.1.2 *Qualitative stability: permanence, persistence and coexistence*

Definition 3.1.4 (**Permanence**). *A system is **permanent** if there exists a compact in the interior of the phase space such that all orbits that start at inner points go asymptotically to the compact (Schuster, Sigmund, and Wolff, 1979). Since the state space is $\mathbb{R}^k_+$, permanence implies the survival of all initially existing species (Takeuchi, 1996; Hofbauer and Sigmund, 1998; Schreiber, 2000).*

Definition 3.1.5 (**Strong persistence**). *A system is **strongly persistent** (Freedman and Waltman, 1977) if*

$$\lim_{t \to +\infty} \inf N_i(t) > 0 \quad \forall i. \tag{3.1.6}$$

Definition 3.1.6 (**Persistence**). *A system is **persistent** if*

$$\lim_{t \to +\infty} \sup N_i(t) > 0 \quad \forall i. \tag{3.1.7}$$

Definition 3.1.7 (**Stable coexistence**). *If an equilibrium point is **feasible** and **globally stable**, then **coexistence** is said to be stable (Svirezhev and Logofet, 1983; Logofet, 1993; Saavedra et al., 2017). This is equivalent to saying that the system is **strongly persistent**.*

Note that the definition of permanence is equivalent to saying (Takeuchi, 1996) that there exists a $k > 0$ independent of the ini-

tial conditions such that, for any $N_i(t) > 0$ in $t = 0$ and $\forall i$, the $\liminf_{t\to+\infty} N_i(t) > k$ and the $\limsup_{t\to+\infty} N_i(t) < 1/k$. That is, in the latter case the orbits are uniformly bounded. Therefore, permanence implies stability in Lagrange's sense (Svirezhev and Logofet, 1983) and the feasibility of any equilibrium point. Furthermore, if the equilibrium point is feasible, then the system described by the Lotka-Volterra model is necessarily permanent and by definition strongly persistent. Note that, furthermore, strong persistence implies persistence. However, it is possible for an equilibrium point to be feasible but unstable, which makes feasibility a necessary but not sufficient condition for stable coexistence: it is also necessary for the equilibrium to be globally stable (Goh, 1977). Since, in general, it is difficult to prove the global stability condition (Logofet, 1993), in real applications it is necessary to focus on feasibility and local structural stability (Saavedra et al., 2017).

3.1.3 *Feasibility, structural stability and stable coexistence*

As seen before, the feasibility condition of an equilibrium is determined simultaneously by the vector of intrinsic growth rates, $\mathbf{r}$, and by the magnitude of the community matrix, $\mathbf{A}$. Then, it is possible to define the domain and the feasibility condition as necessary (although not sufficient) conditions for stable coexistence and structural stability:

Definition 3.1.8 (**Feasibility Domain**). *Let $\boldsymbol{A}^{-1}\boldsymbol{r} > 0$ be the necessary condition for an equilibrium point of the Lotka-Volterra system to be feasible ($\boldsymbol{N}^* > 0$). Then, the **feasibility domain**, $\boldsymbol{D}_F(\boldsymbol{A})$, is defined as:*

$$\boldsymbol{D}_F(\boldsymbol{A}) = \{\boldsymbol{r} \in \mathbb{R}_+^k | \boldsymbol{A}^{-1}\boldsymbol{r} > 0\} \tag{3.1.8}$$

Writing the elements of A as column vectors, we get:

$$\boldsymbol{A} = \begin{pmatrix} \alpha_{11} & \cdots & \alpha_{1k} \\ \vdots & \ddots & \vdots \\ \alpha_{k1} & \cdots & \alpha_{kk} \end{pmatrix} = \begin{pmatrix} \vdots & \vdots & \vdots \\ \boldsymbol{v}_1 & \boldsymbol{v}_2 & \boldsymbol{v}_k \\ \vdots & \vdots & \vdots \end{pmatrix} \tag{3.1.9}$$

The elements of the feasibility domain are given explicitly by all possible linear combinations of the column vectors $\boldsymbol{v}_i$. Then, one can write:

$$\boldsymbol{D}_F(\boldsymbol{A}) = \{\boldsymbol{r} = N_1^*\boldsymbol{v}1 + N_2^*\boldsymbol{v}2 + ... + N_k^*\boldsymbol{v}k | (N_1^*, .., N_k^*) > 0\} \tag{3.1.10}$$

The domain of feasibility is therefore the conic hull, or the **algebraic cone** spanned by the vectors $\mathbf{v}_1, \mathbf{v}_2, ..., \mathbf{v}_k$. The notion of **feasibility condition** is introduced here:

Definition 3.1.9 (**Feasibility condition**). *Let Ω be the **solid angle** of the algebraic cone of the feasibility domain. Let $\Omega = 1$ be the normalized solid angle in the case that the coefficients of interactions between species are 0, $\alpha_{ij} = 0, \forall i \neq j$. Ribando (Ribando, 2006) shows*

that the solid angle of such a cone can be computed for any arbitrary dimension as

$$\Omega(\boldsymbol{A}) = \frac{2^n|\det(\boldsymbol{A})|}{\pi^{n/2}} \int \cdots \int_{R^k_{\geq 0}} e^{-x^T \alpha^T \alpha x} d\boldsymbol{x} \tag{3.1.11}$$

If we write $\alpha^T\alpha = \frac{1}{2}\Sigma^{-1}$*, integration becomes*

$$\Omega(\boldsymbol{A}) = \frac{2^n}{(2\pi)^{n/2}\sqrt{|\det(\boldsymbol{A})|}} = \int \cdots \int_{\mathbb{R}^k_{\geq 0}} e^{-x^T \frac{1}{2}\Sigma^{-1} x} d\boldsymbol{x} \tag{3.1.12}$$

Up to a multiplicative factor of 2^n*, the solid angle* Ω *is the cumulative distribution of a multivariate normal centered at 0 and variance-covariance matrix* Σ *(Ribando, 2006).*

Figure 3.1 shows a geometric representation of the solid angle for a theoretical ecological community. As defined, the solid angle of the algebraic cone generated by the feasibility domain is uniquely determined by the combination of interaction coefficients of the community matrix **A**. Given the proper normalization, this angle can be interpreted as the probability of randomly sampling a vector of intrinsic growth rates that are inside the cone and that give rise to feasible equilibrium points (Svirezhev and Logofet, 1983; Logofet, 1993; Rohr, Saavedra, and Bascompte, 2014; Saavedra et al., 2017). That is, the solid angle Ω represents the **feasibility probability**, or the **ecological persistence probability**, and is directly related to the notion of **structural stability**: the greater the value of Ω, the greater the probability of finding a combination of intrinsic growth rates, r_i, and interaction coefficients, α_{ij}, that are compatible with feasible ecosystems.

3.2 Discrete-time stochastic dynamical systems with Lotka-Volterra type interactions

In practical applications of dynamic systems analysis to inverse evolution problems, the general strategy consists in the use of discrete-time models (Durbin and Koopman, 2001; Lande, Engen, and Saether, 2003; King et al., 2010). The discrete-time version of the Lotka-Volterra model is written as

$$N_{i,t+\Delta t} = N_{i,t} + N_{i,t}\left(r_i - \sum_{j=1}^{k} \alpha_{ij} N_{j,t}\right), i = 1, 2, ..., k \tag{3.2.1}$$

where, as in the continuous-time model (Equation 3.1.1), $N_{i,t}$ is the abundance of the population of the species i at time t, and the parameters r_i represent the intrinsic growth rates of each species i in an ecosystem with k species. The coefficients α_{ij} represent the magnitude of the effect of the population of the species j on the population of the species i. Normally, the time step Δt is set to one unit, $\Delta t = 1$.

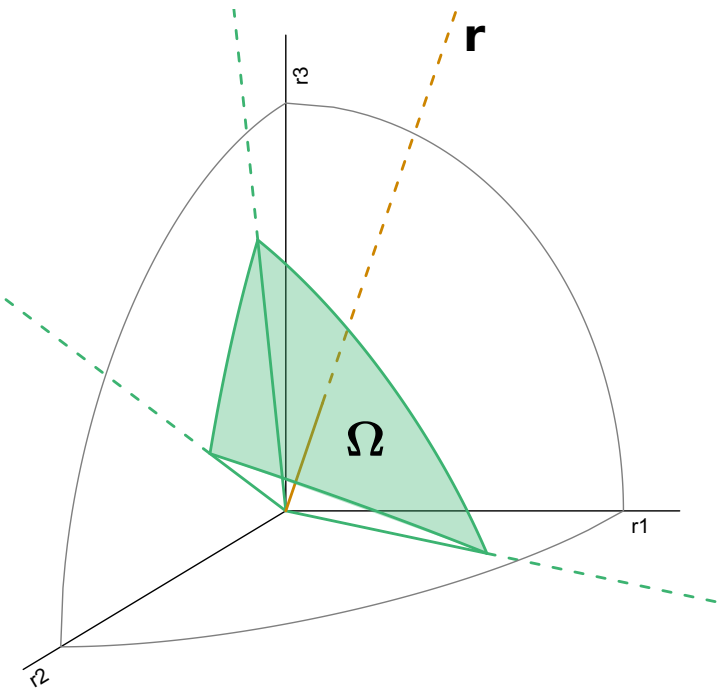

Figure 3.1: Graphical illustration of the feasibility domain of a theoretical ecological community, represented by a community matrix **A** of three species. The coordinates in the figure represent the parameter space of intrinsic growth rates, r_i, whose resultant vector **r** is represented by the orange line. The solid angle (Ω) of the feasibility cone is represented by the green shaded region, and is bounded by the column vectors of the community matrix **A**. Within this region the community is **structurally stable**, since it contains feasible and stable solutions (Based on Saavedra et al., 2017).

Although the stability properties of the model in its discrete-time version are similar to those of continuous time, there are some differences that will be detailed later. On the other hand, the introduction of stochastic disturbances, as will be seen, will force us to reformulate some approaches to dynamical stability. The probability of finding qualitatively more complex dynamics, such as limit cycles and chaotic attractors, is also higher in models formulated in discrete time (Hirsch, Smale, and Devaney, 2013). For these reasons, and despite the apparent simplicity of the Lotka-Volterra model (Equations 3.1.1 and 3.2.1), in practical applications a simplified but equivalent model with Lotka-Volterra type interactions in stochastic environments is used (for example, Ives et al., 2003; Hampton et al., 2013; Ovaskainen et al., 2017). This model is then introduced for ecological scenarios, and the dynamic and structural stability properties are established in the next section.

Definition 3.2.1 (**Multivariate Autoregressive Model**). *Let* $\boldsymbol{n}_t$ *be the* $k \times 1$ *vector of the population abundances of* k *species at time* t, $\boldsymbol{n}_t = \{n_{1,t}, n_{2,t}, ..., n_{k,t}\}^T$. *Let* $\boldsymbol{C}$ *be a* $k \times 1$ *vector of real constants. Let* $\boldsymbol{A}$ *be the matrix of the system, analogous to the community matrix of the Lotka-Volterra system (Equation 3.2.1), and of dimension* $k \times k$,

containing the interaction coefficients $alpha_{ij}$*:*

$$\boldsymbol{A} = \begin{pmatrix} \alpha_{11} & \cdots & \alpha_{1k} \\ \vdots & \ddots & \vdots \\ \alpha_{k1} & \cdots & \alpha_{kk} \end{pmatrix} \tag{3.2.2}$$

that quantify the per capita effect of each population on itself (intra-specific interaction, α_{ii}*, main diagonal) and of the population of the species* j *on the species* i *(inter-specific interaction ,* α_{ij}*, off-diagonal). Finally, let* $\boldsymbol{E}_t$ *be a vector of process errors with a multivariate normal distribution of mean* $\boldsymbol{0}$ *and positive variance-covariance semi-definite matrix* Σ*. Then, a discrete-time* ***Multivariate Autoregressive Model*** *(MAR from now on) can be defined as:*

$$\boldsymbol{n}_{t+1} = \boldsymbol{C} + \boldsymbol{A}\boldsymbol{n}_t + \boldsymbol{E}_t \tag{3.2.3}$$

The vector $\boldsymbol{E}_t$ *represents the operation of an arbitrary number of stochastic factors that impact on the abundance of the different populations. These factors are assumed to be temporally uncorrelated, but they can covary between species through the off-diagonal terms of the* Σ *matrix. Note that, in this case, the Jacobian matrix coincides with the community matrix.*

Lemma 3.2.2 (**The MAR model as an approximation to stochastic nonlinear systems**)**.** *Let* $\boldsymbol{f}$ *be a non-linear function and be the following discrete-time stochastic process:*

$$\boldsymbol{n}_{t+1} = \boldsymbol{f}(\boldsymbol{n}_t, \boldsymbol{R}_t) \tag{3.2.4}$$

where $\boldsymbol{R}_t$ *is a random variable, in the form of a vector* $k \times 1$ *with mean* $\boldsymbol{0}$*, representing the operation of a set of* k *stochastic processes that impact on the growth rate of each population. Let* $\boldsymbol{n}_\infty$ *be the stationary distribution of the stochastic process. So, it is possible to approximate the equation 3.2.4 by a first-order Taylor expansion around* $\boldsymbol{n} = \boldsymbol{n}_\infty$ *and* $\boldsymbol{R} = 0$ *:*

$$\boldsymbol{n}_{t+1} \approx \boldsymbol{f}(\boldsymbol{n}_\infty, 0) + \frac{\partial \boldsymbol{f}}{\partial\, \boldsymbol{n}}(\boldsymbol{n}_\infty, 0)[\boldsymbol{n}_t - \boldsymbol{n}_\infty] + \frac{\partial \boldsymbol{f}}{\partial \boldsymbol{R}}(\boldsymbol{n}_\infty, 0)\boldsymbol{R}_{t+1} \tag{3.2.5}$$

Let $\boldsymbol{A} = \frac{\partial \boldsymbol{f}}{\partial \boldsymbol{n}}(\boldsymbol{n}_\infty, 0)$*,* $\boldsymbol{C} = \boldsymbol{f}(\boldsymbol{n}_\infty, 0) - \boldsymbol{A}\boldsymbol{n}_\infty$ *y* $\boldsymbol{E}_t = \frac{\partial \boldsymbol{f}}{\partial \boldsymbol{R}}(\boldsymbol{n}_\infty, 0)\boldsymbol{R}_{t+1}$*. Then, the MAR model is a first-order approximation to nonlinear stochastic autoregressive models with stationary variance (Ives et al., 2003).*

The MAR model is a simplification of ecological reality, characterized by high non-linearity and high dimensionality (Ives et al., 2003; Clark et al., 2007). However, as a first-order approximation to non-linear stochastic processes, and due to its simplicity, it is the most widely used model in inverse evolution problems (e.g., Ovaskainen et al., 2017). Parameter estimation in inverse evolution problems constitutes the main challenge in high-dimensional ecological problems (for

example, Clark, 2007; King et al., 2010). Therefore, the simplicity of the MAR and its equivalence with the Lotka-Volterra model allows to approach the analysis of dynamic and structural stability in an optimal way from the computational point of view.

3.2.1 *Dynamic and structural stability in discrete-time stochastic dynamical systems*

In this section the necessary reformulations are introduced to address the study of stability in discrete-time stochastic dynamic systems. The equilibrium of a system subjected to stochastic disturbances is characterized by the stationary probability distribution of the state vector, which is reached from a transient distribution.

Definition 3.2.3 (**Stationary distribution**). *Be $\boldsymbol{E}_t$ a multivariate normal process error impacting on the state vector of a MAR model. Then, the **stationary distribution** has mean $\boldsymbol{\mu}_\infty$ and covariance matrix $\boldsymbol{V}_\infty$, and is written as (Ives et al., 2003):*

$$\begin{aligned} \boldsymbol{\mu}_\infty &= (\boldsymbol{I} - \boldsymbol{A})^{-1}\boldsymbol{C} \\ \boldsymbol{V}_\infty &= \boldsymbol{A}\,\boldsymbol{V}_\infty\boldsymbol{A}^{'} + \Sigma \end{aligned} \tag{3.2.6}$$

*where $\boldsymbol{A}^{'}$ is the transpose matrix. Applying the operator **Vec** (Horn and Johnson, 2013) to both sides of the covariance equation ($\boldsymbol{V}_\infty$) yields*

$$\boldsymbol{Vec}(\boldsymbol{V}_\infty) = (\boldsymbol{I} - \boldsymbol{A} \otimes \boldsymbol{A})^{-1}\,\boldsymbol{Vec}(\Sigma) \tag{3.2.7}$$

Definition 3.2.4 (**Transient distribution**). *Conditional on an initial state $\boldsymbol{x}_0$, the **transient distribution** of vector $\boldsymbol{X}_t$ is a multivariate normal distribution with mean vector $\boldsymbol{\mu}_t$ and covariance matrix $\boldsymbol{V}_t$:*

$$\begin{aligned} \boldsymbol{\mu}_t &= \boldsymbol{\mu}_\infty + \boldsymbol{A}^t(\boldsymbol{x}_0 - \boldsymbol{\mu}_\infty) \\ \mathbf{Vec}(\boldsymbol{V}_t) &= [\boldsymbol{I} - (\boldsymbol{A} \otimes \boldsymbol{A})^t][\boldsymbol{I} - \boldsymbol{A} \otimes \boldsymbol{A}]^{-1}\mathbf{Vec}(\Sigma) \end{aligned} \tag{3.2.8}$$

Since the eigenvalues of $\boldsymbol{A} \otimes \boldsymbol{A}$ are equal to the product of all pairs of eigenvalues of $\boldsymbol{A}$, if $\boldsymbol{A}^t \to 0$, then $(\boldsymbol{A} \otimes \boldsymbol{A})^t \to 0$ and, consequently, $\boldsymbol{\mu}_t \to \boldsymbol{\mu}_\infty$ and $\boldsymbol{V}_t \to \boldsymbol{V}_\infty$ when $t \to \infty$.

- **Stability in the sense of Lyapunov**

  1. **Asymptotic resilience**. If all the eigenvalues of the matrix **A** of the dynamical system defined by the equation 3.2.3 are inside the unit circle in the complex plane, then the system is asymptotically stable in the Lyapunov sense (when $t \to \infty$). This is equivalent to the condition that the spectral radius of the matrix is less than 1 ($\rho(\mathbf{A} < 1)$. Also, in this case the variance of

the process N_t is stationary (Ives et al., 2003). The **asymptotic resilience** (R_∞) is then measured as the rate of return from the transient distribution to the stationary distribution (Ives et al., 2003), which is determined by the inverse of the absolute value of the real part of the dominant eigenvalue of the Jacobian of the MAR model,

$$R_\infty = \frac{1}{|\max[\mathrm{Re}(\lambda(\mathbf{J}))]|} \tag{3.2.9}$$

2. **Reactivity and initial resilience**. Let $\|E_{\varepsilon_t}[\Delta\mathbf{n}_{t+1}|\Delta\mathbf{n}_t]\|$ be the squared Euclidean distance of the expectation of $\Delta\mathbf{n}_{t+1}$ given $\Delta\mathbf{n}_t$ and assuming the stationary distribution of mean μ_∞. The expectation of the change in distance from μ_∞ between consecutive times is $\|E_{\varepsilon_t}[\Delta\mathbf{n}_{t+1}|\Delta\ textbf{n}_t]\|^2 - \|\mathbf{n}_t\|^2$. Since $\mathbf{n}_t$ is a random variable, the reactivity depends on the expectation of the distribution of $\mathbf{n}_t$. To obtain an estimate of the long-term averaged reactivity it can be assumed that the distribution of $\mathbf{n}_t = \mathbf{n}_\infty$. So, an estimate of **worst case reactivity** in stochastic systems can be written as (Ives et al., 2003):

$$\frac{E_{\mathbf{x}_\infty}[\|E_{\varepsilon_t}[\Delta\mathbf{n}_{t+1}|\Delta\mathbf{n}_t]\|^2] - E_{\mathbf{x}_\infty}[\|\Delta\mathbf{n}_t\|^2]}{E_{\mathbf{x}_\infty}[\|\Delta\mathbf{n}_t\|^2]} = \max[\Re\lambda(J^{'}J)] - 1. \tag{3.2.10}$$

In a stochastic system whose stationary distribution is subjected to an infinitesimal perturbation, the worst-case reactivity expresses the maximum response along the vector of state variables $\mathbf{n}_t$ that can be expected from a system when $t \to 0$. That is, the instantaneous deviation of the transient distribution with respect to the stationary distribution. In a complementary way, the reciprocal of reactivity measures the **initial resilience** of the system, R_0 (Arnoldi, Loreau, and Haegeman, 2016).

- **Intrinsic stochastic invariance and stochastic structural stability**. The theorem that allows unifying dynamical stability and structural stability (Equation 2.2.1) is directly applicable to discrete-time dynamic systems (Arnoldi and Haegeman, 2016). In this case, the intrinsic stochastic invariability and stochastic structural stability are defined as

$$\mathcal{I}_s = \mathcal{S}^W_{\mathrm{STR}} = -\frac{1}{\Delta t}\log\left(1 - \frac{1}{\|(\mathbb{I} - \mathcal{A})^{-1}\|}\right), \tag{3.2.11}$$

where the lifted operator $\mathcal{A}$ acts on the covariance matrix (Equation 2.0.23) as $\mathcal{A} = \mathbf{A}C\mathbf{A}^T$, and is identified with the tensor (Kronecker) product of the community matrix over itself, $\mathbf{A} \otimes \mathbf{A}$.

Both the domain and the stability condition introduced above (Eqns. 3.1.8 and 3.1.12) have the same form in the case of discrete-

time systems (Saavedra et al., 2017).

4 Temporal coexistence mechanisms stabilize the planetary dynamics of marine phytoplankton

Pablo Almaraz[1,2], Andrés Cózar[3],Gabriel Navarro[2]

1. Departamento de Ecuaciones Diferenciales y Análisis Numérico, Facultad de Matemáticas, Universidad de Sevilla, Sevilla, Spain.

2. Grupo de Oceanografía Operacional, Instituto de Ciencias Marinas de Andalucía, CSIC, Puerto Real, Spain.

3. Departamento de Biología, Universidad de Cadiz, Puerto Real, Spain

Abstract

Species within ecosystems are more likely to coexist if they segregate the use of shared resources. In a variable environment, coexistence can be mediated through the opportunities created by temporal and spatial heterogeneities: spatial and temporal fluctuations allow different species to use resources without overlapping each other. In fluctuating environments, the 'insurance hypothesis' predicts that environmental asynchrony between competing species should trigger a positive link between diversity and ecosystem stability through temporal and spatial niche segregation. This prediction has been supported by small-scale experimental approaches, but tests of the positive diversity-stability relationship at large spatio-temporal scales are lacking. Using satellite-derived abundance estimates, we model the multi-annual community dynamics and stability of the four major phytoplankton functional types in the 48 biogeochemical non-polar provinces of the world oceans. A pervasive latitudinal gradient in community stability, biotic interactions and environmental forcing suggest a larger resilience of high-latitude communities resulting from a stronger impact of competitive interactions. In contrast, low-latitude communities are more strongly affected by environmental fluctuations and display a larger temporal variability. Species environmental synchrony declined sharply with latitude, and was negatively correlated with stability across biogeographical provinces. In-situ measurements from hundreds of world oceanographic cruises point to a latitudinal increase in phytoplankton functional diversity variability linked to a decrease in environmental synchrony, which provides the mechanistic link between diversity and stability through temporal niche segregation. An ordering in the stability metrics of global marine phytoplankton communities,

point to the increase in reactive dynamics as an early-warning signal of the loss of structural stability and ultimately of asymptotic resilience. Overall, our results highlight the centrality of functional diversity as a stabilizing agent of marine phytoplankton communities at a global scale, thus providing a macroecological support to the insurance hypothesis.

KEYWORDS biodiversity, environmental synchrony, functional diversity, insurance hypothesis, niche segregation, ocean color, storage effect.

4.1 INTRODUCTION

The current rate of planetary biodiversity loss is unprecedented in the geological record (Barnosky et al., 2011; Cowie, Bouchet, and Fontaine, 2022). This has raised concerns about the impact of biodiversity on ecosystem function and ecological stability (Loreau, 2010b). The impact of diversity on the dynamics and functioning of ecosystems is one of the founding ideas of modern ecology (May, 1973; Pimm, 1984; McCann, 2000). The emerging consensus today regards biodiversity as the main determinant of ecosystem functioning and stability (Loreau, 2010b; Hooper et al., 2012; Tilman, Reich, and Isbell, 2012). In this sense, the current rate of species loss at a global level, unparalleled in the geological record (Dirzo and Raven, 2003), is promoting the use of theoretical and empirical approaches to understand the impact of diversity on ecological stability (McCann, 2000; Ives and Carpenter, 2007). The essential question that these approaches seek to answer is: Are the most diverse ecosystems capable of resisting greater disturbances without losing functionality? The answer to this question has changed over the last few decades (Pimm, 1984). The pioneering work of May, 1972, which used models of arbitrarily large synthetic ecosystems where species were randomly connected, suggested that an increase in the diversity and strength of interactions of an ecosystem was linked to a decreased stability.

This perspective, based on the analysis of mathematical models, prevailed during the following two decades despite being severely criticized due to empirical evidence pointing to a positive effect of diversity on stability in both synthetic (Roberts, 1974) real ecosystems (e.g., McNaughton, 1977). Likewise, the analysis of mathematical models of natural ecosystems, in which a non-random pattern of interactions between species was specified, suggested that the expected effect of diversity on aggregate stability (that is, on the sum of the abundance of all species) was positive, not negative (Yodzis, 1980). Today, both theoretical and empirical perspectives suggest that the pattern of interspecific interactions, as well as their relative magnitude, are fundamental in explaining the stabilizing effect of diversity on the aggregate dynamics of ecosystems (Ives and Carpenter, 2007; Loreau, 2010b; McCann, 2010; Rohr, Saavedra, and Bascompte, 2014; Barabás, J. Michalska-Smith, and Allesina, 2016). The stabilizing effect of diversity may

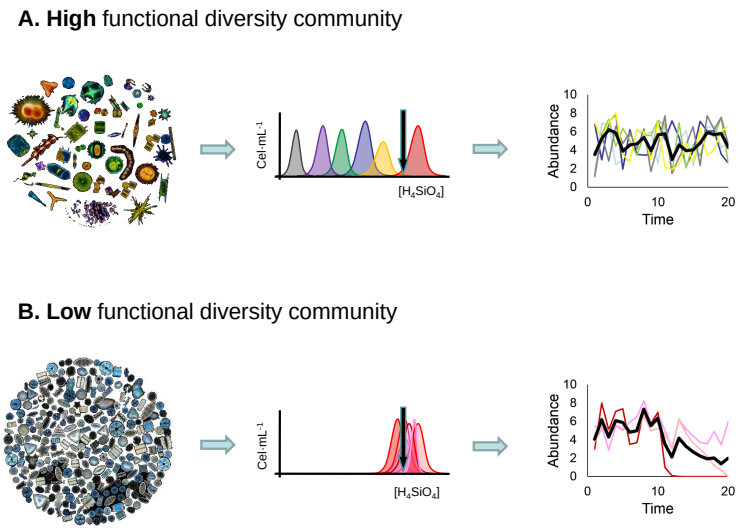

Figure 4.1: The insurance hypothesis in ecology. In **A**, the equilibrium abundance distribution (in the middle) for a community with a high functional diversity is shown along a single niche axis (the concentration of Silica, $[H_4SiO_4]$). As niche overlap is very low, in an environment with temporal fluctuations in Silica, represented by a reduction of Silica concentration below the black arrow, the extinction of a single functional type (red abundance distribution) does not affect average community abundance (black thick time series). In **B**, the equilibrium abundance distributions of a community with low functional diversity are strongly packed; in this case, temporal fluctuations in Silica prompt the extinction os several species, and the average community abundance is severely impacted.

be determined by various temporal mechanisms (Lehman and Tilman, 2000). One of the main mechanisms, inspired by the field of financial economics, is formalized in the so-called "*insurance hypothesis*" (Yachi and Loreau, 1999).

4.1.1 *Impact of functional diversity on ecological stability: the insurance hypothesis*

In classical financial theory, a diversified investment portfolio shows smaller fluctuations in overall returns due to temporal asynchrony in individual asset fluctuations (Markowitz, 1952). In the same way, the ecological insurance hypothesis suggests that an increase in the functional types of species in an ecosystem will have a damping effect on aggregate stability (Fig. 4.1): since each of them occupies different ecological niches, the stabilizing mechanism lays in the asynchrony in the response of different functional types to environmental fluctuations (e.g., Ives, Klug, and Gross, 2000; Lehman and Tilman, 2000; Schindler, Armstrong, and Reed, 2015). In other words, biodiversity would provide insurance against the mismatch in the level of resource use and the decline in the stability of the ecosystem because a high functional diversity increases the probability that some of the species present will be efficient in maintaining ecosystem functionality (eg, primary production) during periods of environmental disturbance (Naeem and Li, 1997; Yachi and Loreau, 1999).

A fundamental element in this hypothesis is the concept of functional diversity (Tilman, 2001). According to this idea, phenotypically equivalent species can be grouped into homogeneous functional types because the role these species play in an ecosystem is similar. This perspective allows us to speak of biodiversity as synonymous with variability in the functional types of species, and introduces the con-

cept of redundancy as a high species richness within each functional type (Tilman, 2001; Hillebrand and Matthiessen, 2009). Therefore, the buffering effect of diversity on stability lies in high functional redundancy between species, rather than high species richness (Naeem and Li, 1997; Yachi and Loreau, 1999).

The insurance hypothesis has been validated through laboratory (Naeem and Li, 1997; Steiner et al., 2005) and field experiments (Tilman, Reich, and Knops, 2006). All experiments suggest an increase in the temporal stability of certain ecosystem properties, such as biomass and productivity, as the number of species within each functional type increases. In marine ecosystems, Danovaro et al., 2008 and Zeppilli et al., 2016 have revealed the positive effect of biodiversity on the functioning of benthic ecosystems in different oceans of the planet, although these studies do not entail a validation of the insurance hypothesis as they do not consider the aggregate temporal stability of the communities studied. Phytoplankton, responsible for 50% of the primary production of the biosphere (Falkowski, Barber, and Smetacek, 1998), is fundamentally involved in the functioning of planetary biogeochemical cycles (Siegel et al., 2013) and in the dynamics of networks of pelagic trophic zones of the global ocean (Chassot et al., 2010). However, today there are virtually no studies that evaluate the impact of functional diversity on the stability of marine phytoplankton communities, despite the importance that this evidence could have for understanding and, eventually, predicting the functioning of marine ecosystems in global change scenarios (Acevedo-Trejos et al., 2014; Behrenfeld et al., 2016). Furthermore, despite the accelerating global loss of biodiversity, to date the insurance hypothesis has not been validated on a planetary scale.

Marine phytoplankton communities are competitive-type horizontal communities (Loreau, 2010a). In this scenario, the prediction derived from the insurance hypothesis is that a positive relationship should be established between the functional diversity of phytoplankton communities and their aggregate temporal stability, mediated by an increase in environmental synchrony between the different functional types that make it up (Yachi and Loreau, 1999; Ives and Hughes, 2002). The goal of the present work is to validate of the insurance hypothesis on a planetary scale using data from communities of primary producers. The general strategy will be based on the analysis of global, independent and freely accessible databases on the diversity and temporal dynamics of marine phytoplankton. A mathematical and statistical modeling approach will be used through the use of intensive computational techniques. These approaches are based on several recent developments provided by the mathematical analysis of the different dimensions of ecological stability (Ives et al., 2003; Logofet, 2016; Arnoldi and Haegeman, 2016; Arnoldi, Loreau, and Haegeman, 2016).

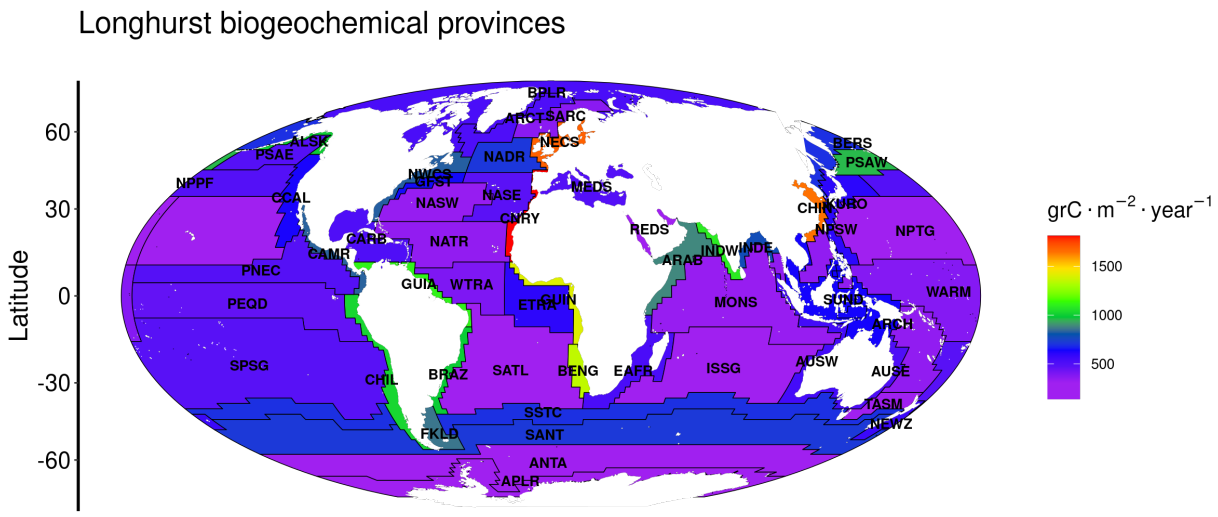

Figure 4.2: Global map showing the 54 biogeochemical provinces defined by (Longhurst, 2007) for the pelagic ecosystem, which constitute the spatial sampling units of this work; see Table S1 in the Supplementary Material for the description of the acronyms and the characteristics of each area. The color gradient refers to the average productivity (grC·m^{-2}·year^{-1}) obtained for each area using the VGPN model (Behrenfeld and Falkowski, 1997) applied to satellite remote sensing data from the SeaWiFS mission of the NASA (1997-2010; see main text for details).

4.2 Material and methods

This study covers all the pelagic region of the global ocean (Fig. 4.2). The structure of this region can be defined on the basis of seasonal cycles of production and consumption. According to these cycles, it is possible to establish four large biomes characterized, among other factors, by the general structure of the mixed layer (Longhurst, 2007): 1) Polar Biome, which includes regions located above 60° latitude and which are defined by a mixed layer of brackish water that forms at the beginning of each spring in the marginal sector of the ice; 2) Westerly wind biomes, comprising regions located between 30° and 60° latitude, and where the the mixed layer depth is forced by local winds and variation in irradiance; 3) Trade wind biomes, which include large areas located between the equator and 30° latitude. In these areas the depth of the mixed layer is determined by large-scale geostrophic forcing; and 4) Coastal biomes, distributed throughout all latitudes, where the depth of the mixed layer is subject to local phenomena such as upwellings, runoff, tidal mixing, etc. They are therefore particularly productive (Fig. 4.2).

Based on the physical, biological, geological, and chemical processes operating in each of the large pelagic biomes, it is possible to define 54 global regions known as Longhurst biogeochemical provinces (Longhurst, 2007). Each of these provinces, shown in Fig. 4.2, constitutes an optimal partition of pelagic space within which environmental conditions are unique on a global and inter-annual scale (Reygondeau et al., 2013). In the present work, the 48 non-polar biogeochemical Longhurst provinces will be considered as the sampling units that will allow the analysis of latitudinal gradients in the diversity and stability of global phytoplankton communities. The PHYSAT algorithm, which relies on a passive remote sensor, cannot provide data for the Polar regions during the winter seasons. This is the reason why these areas were excluded from the study (see also Feng et al., 2015). The Flanders Marine Institute of Belgium (VLIZ) has standardized the spatial co-

ordinates of each Longhurst province in a freely accessible Geographic Information System (GIS) profile file (VLIZ, 2009), which will be used in this work.

4.2.1 *Global estimates of functional diversity*

Data Recent studies have focused on the analysis of global patterns of richness and species diversity of microplankton, which includes those species of primary producers whose equivalent spherical diameter (ESD) is between 20 and 200 μm (Irigoien, Huisman, and Harris, 2004; Chust et al., 2013; Rodríguez-Ramos, Marañón, and Cermeño, 2015). This global database (Sal et al., 2013) includes abundance (cells/mL) and biovolume (μm/cell) data for 1311 species from various microplankton kingdoms (chromista, plantae, protista, and protozoa) detected in 788 sampling stations distributed throughout all global latitudes, and including samples from the surface up to 160 m. Although this global database has the advantage of being standardized (Sal et al., 2013), it does not contain data on picoplankton abundance (DEE: 0.2-2 μm). This size class is clearly dominant in large regions of the global pelagic ocean, mainly at low latitudes where it can account for more than 90% of the total abundance of primary producers (Moran et al., 2015; Flombaum et al., 2013). A second large open access database focusing on phytoplankton in this size class (Buitenhuis et al., 2012; Flombaum et al., 2020) contains the abundance (cells/mL) of cyanobacteria of the genera *Prochlorococcus* and *Synechococcus*, and picoeukaryotes, estimated by flow cytometry at 40946 sampling stations spread over all oceans from the surface to depths of 3000 m. The biovolume for each of these functional types was estimated using the standard equations available in the literature (Hillebrand et al., 1999) and assuming an approximately spherical geometry.

In total, the taxonomic database compiled for this work includes 41734 samples taken in 48 oceanographic surveys spread over all the oceans and in which 1314 species/functional types of phytoplankton are represented. Sampling dates comprise all months on multiple dates from 1980 to 2002. Figure 4.3 shows the spatial location of each sampling station contained in the global micro- and picophytoplankton database.

Species Distribution Modeling Since the microplankton abundance database contains fewer sampling points than the picoplankton one, it was necessary to generate an aggregate database where each of the 788 microplankton abundance sampling points included the picoplankton abundance predictions obtained from from the 40946 sampling points of the latter. To do this, Species Distribution Modeling (SDM) tools were used, which allow estimations (predictions) of abundance of one or several species at different points in space from a previous database with georeferenced abundance data for each species (Flombaum et al., 2013; Flombaum et al., 2020; Flombaum and Martiny, 2021). Gener-

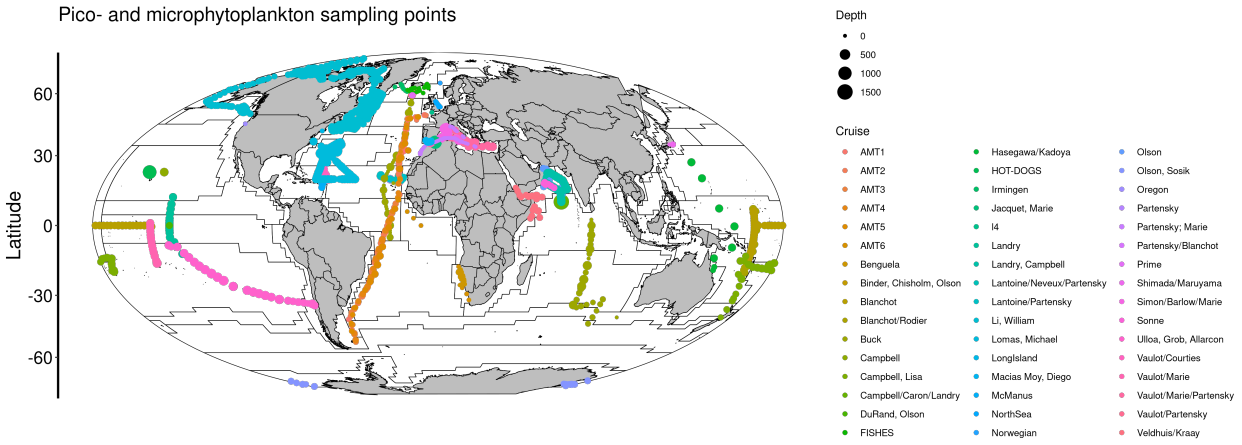

Figure 4.3: Sampling points of pico- (Buitenhuis et al., 2012) and microphytoplankton (Sal et al., 2013) collected monthly from 1980 to 2002 by 48 oceanographic cruises in the global pelagic region. In total 41734 samples are represented, from the surface to 3000 m. deep. Note that many sample points therefore appear vertically overlapping. Similarly, several cruises went to take samples for both size classes, so some sampling points also appear overlapping.

alized Additive Models (GAMs) were used for their ability to generate predictions with the same level of accuracy as other more complex approaches (Leathwick, Elith, and Hastie, 2006). The R mgcv package was used to fit the GAMs to the abundance data; this package allows estimation of regression splines where the smoothing parameter is selected by generalized cross-validation (Wood, 2006). Using this method, a database was finally obtained where each of the 788 final sampling points contain abundance data for both pico- and microplankton at different depths. This database will be referred to as the aggregate database from now on.

Cell size is considered a meta-trait (Barton et al., 2013) that explains a large part of the diversity in the phenotypic, physiological and ecological attributes of phytoplankton (Marañón, 2015), such as the efficiency in nutrient uptake, the sinking rate, light absorption, herbivory rate, mobility, etc. Therefore, the variance in size or biovolume is considered a good estimator of functional diversity in phytoplankton (Acevedo-Trejos et al., 2015; Smith, Vallina, and Merico, 2016). For each sampling point and for each depth of the aggregated database, an empirical estimate of functional diversity was derived as the abundance-weighted variance in biovolume (σ_w^2):

$$\sigma_w^2 = \sum_{i=1}^{k} \left(w_i \left[B_i - \overline{B_w} \right] \right)^2 \tag{4.2.1}$$

where w_i is the proportion of the abundance of species i with respect to the total of k species; B_i is the biovolume of species i, and $\overline{B_w}$ is the weighted average biovolume of the sample. Once the functional diversity estimate was obtained for each sampling point of the aggregated database, SDMs were used through GAMs to estimate the functional diversity in each of the 54 Longhurst areas, averaged over time and with depth. The centroids of each area were used as spatial prediction points (See Figure 4.3 and Table S1).

4.2.2 *Community dynamics modeling*

Data The launch in 1997 of NASA's Sea-viewing Wide Field-of-view Sensor (SeaWiFS) ocean color mission (McClain, 2009; Siegel et al., 2013) has allowed the development of algorithms capable of discriminating phytoplankton functional types from satellite data (IOCCG, 2009). In this work, the open access database generated by the PHYSAT algorithm (Alvain et al., 2005; Alvain et al., 2008) has been used to model the dynamics and stability of marine phytoplankton communities in each of the 48 non-polar Longhurst biogeochemical provinces represented (Figure 4.2).

The PHYSAT algorithm (`http://log.univ-littoral.fr/Physat`) is a bio-optical model capable of discriminating several functional types of dominant phytoplankton in the images provided by ocean color sensors that estimate different reflectances of the ocean surface (Alvain et al., 2005; Alvain et al., 2008; Alvain, Loisel, and Dessailly, 2012; Navarro et al., 2017). The identification of the functional group is based on assigning to each one of them spectral characteristics of the reflectance to each spectral band, once the contribution of chlorophyll in each one has been eliminated (normalized reflectance). To establish the relationship between normalized reflectance and phytoplankton types, data from photosynthetic pigments that are markers of different phytoplankton species have been used (Alvain et al., 2005). Therefore, by normalizing the color data collected by bio-optical sensors, it is possible to establish the contribution of various functional types of phytoplankton to the total light reflected at each pixel of a given resolution, which in this case is of 9 km. The PHYSAT algorithm has been successfully applied to data from SeaWiFS missions (Alvain et al., 2005; Alvain, Loisel, and Dessailly, 2012; IOCCG, 2020).

The data provided by the PHYSAT algorithm have been produced by the French CNRS Oceanography and Geosciences Laboratory, and are publicly accessible (`http://mren3.univ-littoral.fr/~david/PHYSAT/PHYSAT_GlobalMapOfMonthlyDominantsGroups_1997-2010.tar.gz`; data downloaded 1 Jan 2016, and updated up to 2012 in 2018). The database contains monthly averaged maps of the dominant phytoplankton functional types at each pixel in all pelagic regions of the planet, at a spatial resolution of 9 km, from October 1997 to December 2010. The current version of the PHYSAT algorithm is able to discriminate six functional types of phytoplankton: Nanoeukaryotes, Diatoms, *Synechococcus*, *Prochlorococcus*, *Phaeocystis* and Cocolithophorids. The dominance data for the first four types have been validated with those obtained by in-situ sampling in several oceanographic cruises (Alvain, Loisel, and Dessailly, 2012). Due to optical interference problems with suspended solids, the data for Cocolithophorids will not be considered in this work.

Once the data had been processed, the dominance time series of

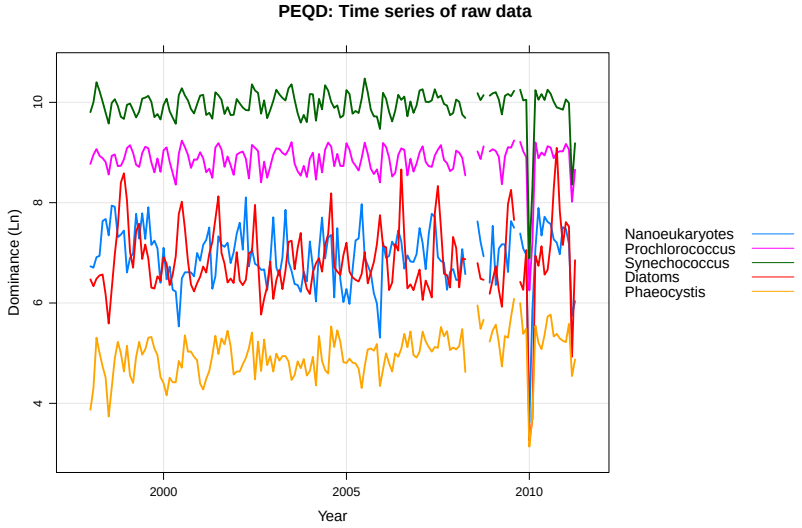

Figure 4.4: Mean monthly dominance time series of the five functional types of phytoplankton produced by the PHYSAT algorithm from 1998 to 2012 for the Pacific Equatorial Divergence region, Longhurst PEQD biogeochemical province. Data transformed with natural logarithms (Ln) are shown. Note that some months lack data, due to problems with the processing of information from the SeaWiFS mission, the constant presence of cloud cover, etc.

each functional type were segregated for each of the 48 non-polar Longhurst biogeochemical provinces shown in Figure 4.2. Therefore, a new database with four series was obtained for each area. temporal dominance averaged monthly (Nanoeukaryotes, Diatoms, *Synechococcus* and *Prochlorococcus*); each series has a time dimension of 156 months (13 years). These 48 sets of community dominance time series will serve as the databases on which the properties of temporal stability and environmental synchrony will be estimated. Recent approaches (Litchman and Klausmeier, 2008; Mutshinda et al., 2016) have shown that the different species belonging to the same functional type show equivalent behavior from a dynamic point of view. This suggests the convenience of grouping them by functional types, as the PHYSAT algorithm does. As an example, Figure 4.4 shows the dominance time series generated by the PHYSAT algorithm for each functional type of phytoplankton in the Mediterranean community.

State-space modeling of community dynamics A critical assumption of the present work is that the estimations of relative dominance of the functional types of phytoplankton obtained by means of the PHYSAT algorithm are equivalent to the numerical abundance of each type. Since this algorithm has been validated with in-situ abundance data (Alvain, Loisel, and Dessailly, 2012), it is possible to use the quantitative estimate of the validation error as an empirical estimate of the observation error in a state space model (King et al., 2010; Almaraz et al., 2012). This type of approach allows the simultaneous modeling of two equations: 1) A process equation, which expresses the relationships between the variables and parameters of interest, such as population density, interspecific interactions, environmental effects, etc.; and 2) An observation equation, where the process variables, which are not directly observed (they are latent), are associated with the empirical observations through a measurement model that explicitly includes the variance or the sampling error.

Let $\hat{\mathbf{n}}_{t+1,p}$ and $\mathbf{y}_{t,p}$ be the vectors of the prediction of latent abundances ($\mathbf{n}_{t+1,p}$) and dominances generated by the PHYSAT algorithm, respectively, corresponding to the five ($k = 5$) functional types of phytoplankton in the province of Longhurst p and in the months t and $t+1$. Let the vector $\mathbf{l}_{r,p}$ represent the effect of the multi-year trend on the dynamics of community abundance over the 13 years, $r = \{1, 2, ..., 13\}$, specified by the ordinal categorical variable l_r. Be $\mathbf{B}_p$ a matrix of size $\mathbb{R}^{k \times m}$ for each province p encapsulating the impacts of m environmental variables c on the population growth rate of each functional type k. We considered sea-surface temperature and productivity as the environmental covariates forcing the long-term dynamics of the five phytoplankton functional types. These are the environmental covariates that more strongly determine the distribution and abundance of phytoplankton (Reynolds, 2006; Longhurst, 2007). Finally, be $\mathbf{A}_p \in \mathbb{R}^{k \times k}$ the square community matrix containing the intra- and inter-specific interaction coefficients, α_{ij}:

$$\mathbf{A}_p = \begin{pmatrix} \alpha_{11} & \cdots & \alpha_{1k} \\ \vdots & \ddots & \vdots \\ \alpha_{k1} & \cdots & \alpha_{kk} \end{pmatrix} \tag{4.2.2}$$

Note: this matrix is not necessarily symmetric! Interactions among pairs of species can differ both quantitatively (magnitude) or qualitatively (sign).

Finally, be $\mathbf{\Sigma}_p$ a symmetric, positive semi-definite variance-covariance matrix containing the stochastic (within-specific) residual variance terms on the main diagonal and the (inter-specific) residual covariance terms in the off the diagonal:

$$\mathbf{\Sigma}_p = \begin{pmatrix} \sigma_{11} & \cdots & \text{cov}_{1k} \\ \vdots & \ddots & \vdots \\ \text{cov}_{k1} & \cdots & \sigma_{kk} \end{pmatrix} \tag{4.2.3}$$

Note: this matrix is, by definition, symmetric.

Let $\mathbf{\Phi}$ be a column vector with independent, uncorrelated and identically distributed observation errors, (τ_i) of each functional type k $\mathbf{\Phi} = \{\tau_1, .., \tau_k\}^T$. The empirical values of the observation errors were obtained from the percentage agreement of the in-situ validation of the PHYSAT (Alvain, Loisel, and Dessailly, 2012) algorithm. Then, the extended Bayesian Multivariate Autoregressive State Space (MARSS) model is written as:

$$\begin{aligned} \hat{\mathbf{n}}_{t+1,p} | \mathbf{n}_{t,p} &\sim NMV\left(\mathbf{n}_{t,p} + \mathbf{A}_p \mathbf{n}_{t,p} + \mathbf{l}_{r,p}[y_r] + \mathbf{B}_p \mathbf{c}_{t,p}, \mathbf{\Sigma}_p\right) \\ \mathbf{y}_{t,p} | \mathbf{n}_{t,p} &\sim N\left(\mathbf{n}_{t,p}, \mathbf{\Phi}\right) \\ \mathbf{n}_{0,p} &\sim N\left(\boldsymbol{\mu}_{0,p}, \mathbf{\Phi}_0\right) \end{aligned} \tag{4.2.4}$$

for $t = \{1, 2, ..., 156\}$, $p = \{1, 2, .., 48\}$ and $m = \{1, 2\}$.

The first equation in 4.2.4 is called the **process equation** (Clark

and Bjørnstad, 2004) and specifies the evolution of the abundance of the phytoplankton community as a latent vector in the state space, distributed as a multivariate normal. The vector of abundances is conditioned on a vector of surface dominance observations through a normal distribution, and this conditioning is specified in the second equation of 4.2.4, called the **observation equation**. Finally, the initial state, $\mathbf{n}_{0,p}$ of the vector of latent states is specified in the third equation of 4.2.4 as a normal distribution with mean $\boldsymbol{\mu}_{0,p}$ and variance $\boldsymbol{\Phi}_0$, and will serve as a prior distribution model for the vector $\mathbf{n}_{1,p}$ (for example, West and Harrison, 1997). The MARSS is thus a completely stochastic model, since it is able to separate the variability of the process from the observation error (Durbin and Koopman, 2001). In Bayesian language, these types of models are commonly called dynamic linear models or latent Bayesian networks (West and Harrison, 1997; Clark and Bjørnstad, 2004).

Estimation of environmental synchrony and community stability The information contained in the matrices $\boldsymbol{\Sigma}_p$ and $\mathbf{A}_p$ is sufficient to define the properties of environmental synchrony and community stability, respectively. The environmental synchrony, $\overline{\rho_s}$ can be estimated as the mean of the correlations in the response to environmental fluctuations between all pairs of functional types:

$$\rho_s = \frac{1}{n} \sum_{i \neq j}^{n} \frac{cov(i,j)}{\sigma_i \sigma_j} \tag{4.2.5}$$

where $n = [S(S-1)]/2$, is the maximum possible number of pairs of correlations between the S functional types, $i \neq j$. The environmental synchrony index ($\overline{\rho_s}$) is distributed between -1 and 1. Positive values denote a synchronized response to environmental fluctuations between the functional types of the community, which would indicate a niche overlap (Lehman and Tilman, 2000; Loreau, 2010a). On the contrary, negative values are representative of communities with niche segregation between functional types, with perfect segregation when ρ_s = -1. When $\rho_s = 0$, the fluctuations in the responses to the environment between the different functional types are independent of each other. In the case of competitive communities like the ones examined in this work, the environmental synchrony is expected to take only positive values ($0 \leq \rho_s \leq 1$).

The concept of stability of an ecological community can take several complementary meanings (Pimm, 1984; Ives and Carpenter, 2007; Donohue et al., 2013; Donohue et al., 2016). The most widely used is resilience, which measures the asymptotic rate of return to equilibrium of a community that is displaced from it by an infinitesimal disturbance (May, 1973; Ives et al., 2003). In systems of difference equations, resilience is measured as the modulus of the dominant eigenvalue of the Jacobian matrix, $\mid \lambda_1 \mid$, which is obtained by linearizing the system around an equilibrium point (Elaydi, 2005). Denoting an equilibrium point as n^*, the Jacobian matrix of the system represented by Eqn.

4.2.4 is simply:

$$J_p = \left.\frac{\partial f}{\partial n}\right|_{\boldsymbol{n}=\boldsymbol{n}^*} = \mathbb{I} - \mathbf{A}_p. \tag{4.2.6}$$

where the Jacobian of the phytoplankton community in each Longhurst area (J_p) is the matrix of partial derivatives of the function represented in Eqn. 4.2.4 with respect to the state variables in the vector $\boldsymbol{n}$ evaluated at the equilibrium point $\boldsymbol{n}^*$; $\mathbb{I}$ is the identity matrix. The magnitude of $\mid \lambda_1 \mid$ is, therefore, a measure of the local dynamic stability of a system, or Lyapunov stability, since it evaluates the response to an infinitesimal perturbation of the initial condition . If $\mid \lambda_1 \mid < 1$, the system defined by Eqn. 4.2.4 is locally stable (see **??**). We also calculated the reactivity, or initial resilience of each community (see 3.2.10), also called the worst-case reactivity (Ives et al., 2003); and the stochastic invariability of each community as a measure of structural stability (Arnoldi and Haegeman, 2016; see 3.2.11). All these measure are introduced in section 3.2.1 of the present Thesis. Finally, we tested for the empirical ordering of the different stability measures according to the theoretical expectations of Arnoldi, Loreau, and Haegeman, 2016; Arnoldi and Haegeman, 2016.

4.2.3 *Likelihood, parameter model, and joint posterior probability*

The likelihood model expresses the probability of obtaining the total sets, from $t = 1$ to T, of the latent ($\mathbf{N}$) and observed ($\mathbf{Y}$) vectors conditioned on a set of parameters. In the case of the MARSS model specified in a Bayesian scheme, and omitting the p subscripts of each Longhurst area, the likelihood has the following form:

$$\begin{aligned} p(\mathbf{N}, \mathbf{Y} | \mathbf{A}, \mathbf{L}, \mathbf{B}, \Sigma, \boldsymbol{\Phi}, \boldsymbol{\mu}_0, \boldsymbol{\Phi}_0) = \\ \overbrace{p_h(\mathbf{n}_0 | \boldsymbol{\mu}_0, \boldsymbol{\Phi}_0)}^{\text{Initial latent state}} \\ \times \overbrace{\prod_{t=1}^{T-1} p_h(\mathbf{n}_{t+1} | \mathbf{n}_t, \mathbf{A}, \mathbf{L}, \mathbf{B}, \Sigma)}^{\text{Process equation}} \\ \times \overbrace{\prod_{t=1}^{T-1} p_0(\mathbf{y}_t | \mathbf{n}_t, \boldsymbol{\Phi})}^{\text{Observation equation}} \end{aligned} \tag{4.2.7}$$

where p_h and p_o are the probability densities of the latent process and the observation process, respectively;$\mathbf{L}$ is the parameter vector of the multi-year trend from $r = 1$ to $R = 13$, and $\mathbf{B}$ is the matrix for environmental effects (see above). The product of the initial state equation and the process equation expresses the joint probability of the latent states. Likewise, the observation equation specifies the probability of sampling the observations from the latent states. The specification of the Bayesian model, however, requires writing the posterior probabilities of the vector of states and of the parameters conditional on the observations (Clark, 2007; Gelman et al., 2020). This is achieved by

the product of the likelihood model specified above (Equation 4.2.7) and a model of previous values of the parameters. Therefore, it is necessary to build the previous model. In this work, conjugate prior distributions will be specified for the location parameters and for the scale parameters, and in all cases vague (Gelman et al., 2020) distributions will be used. This allows the likelihood model to dominate over the parameter model during subsequent simulation. Again omitting the subscripts p:

- The intra- and inter-specific interaction coefficients (entries of the matrix $\mathbf{A}$) were modeled as prior normal distributions with mean $\mu_\alpha = 0$ and variance $\sigma_\alpha 2 = 10^3$,

$$\alpha_{ij} \sim N(\mu_\alpha, \sigma_\alpha^2), \quad \forall i, j = 1, .., k. \tag{4.2.8}$$

- The parameters that model the effect of the multi-year trend, $\mathbf{l}_r$, were specified as prior normal distributions with mean $\mu_l = 0$ and variance $\sigma_l^2 = 10^3$,

$$lr, i \sim N(\mu_l, \sigma_l^2), \quad \text{for } n = 1, .., 12, \quad i = 1, .., 4. \tag{4.2.9}$$

  As before, a zero-sum constraint was specified for the vector $\mathbf{l}_{r,i}$, that is, $l_{1,i} = -\sum_{r=2}^{R} \sum_{i=1}^{k} l_{r,i}$.

- The real random variables of the matrix $\mathbf{B}$, encapsulating the effects of temperature and productivity, were modeled as prior normal distributions with mean $\mu_B = 0$ and variance $\sigma_B^2 = 1$,

$$b_i \sim N(\mu_B, \sigma_B^2), \quad i = 1, .., k. \tag{4.2.10}$$

- The variance-covariance matrix Σ was specified as an scaled Wishart distribution, which is the Huang-Wand approximation conjugate distribution of the multivariate normal (Huang and Wand, 2013): $\Sigma \sim W(\omega, S)$, where ω is the scale matrix and S is the number of degrees of freedom. In this distribution the standard deviation and correlation parameters are marginally non-informative (see Almaraz et al., 2022 for an example).

- Finally, the vector of initial latent states, $\mathbf{n}_0$ was specified as a distribution normal with mean the dominance generated by the PHYSAT algorithm, $\mathbf{Y}_0$ and variance the vector of observation errors, $\mathbf{\Phi}$.

Once the parameter model has been built, the joint posterior probability of the Bayesian MARSS model can be specified. Omitting,

again, the subscript p, this probability has the form:

$$\begin{aligned} p(\mathbf{A},\mathbf{L},\mathbf{B},\Sigma,\mathbf{\Phi},\mathbf{N}|\mathbf{Y},\cdots) \propto \\ N(\mathbf{n}_0|\mathbf{y}_0,\mathbf{\Phi}) \\ \times \prod_{t=1}^{T-1} MVN(\mathbf{n}_{t+1}|\mathbf{A}\mathbf{n}_t + \mathbf{l}_r[y_r] + \mathbf{B}\mathbf{c}_t, \mathbf{\Sigma}) \\ \times \prod_{t=1}^{T-1} N(\mathbf{y}_t|\mathbf{n}_t,\mathbf{\Phi}) \\ \times N(\mathbf{A}|\boldsymbol{\mu}_\alpha, \boldsymbol{\sigma}_\alpha^2) \\ \times N(\mathbf{l}_r|\boldsymbol{\mu}_l, \boldsymbol{\sigma}_l^2) \times N(\mathbf{B}|\boldsymbol{\mu}_b, \boldsymbol{\sigma}_{\boldsymbol{B}}^2) \times SW(\Sigma|\omega, S) \end{aligned} \tag{4.2.11}$$

where "$\cdots$" represents the set of previous parameters. Note the proportionality of the joint posterior probability: this is because the normalization constant, which involves integration over the entire parameter space Clark, 2007; Gelman et al., 2020, has been omitted. This normalization constant, however, will be the one that will be marginalized during the numerical simulation scheme that will be used to estimate the posterior probability of the parameters and states.

4.2.4 *Posterior estimation and model validation*

The high dimension of the Bayesian MARSS model, and the presence of missing data in the observation equation, make it necessary to use numerical simulation methods specifically designed for this type of computationally complex scenarios. In this work, Markov Monte Carlo (MCMC) chain techniques have been used through the Gibbs sampling algorithm (Gelfand and Smith, 1990; Gelman et al., 2020) to solve the factorization of the joint posterior probability shown in the equation 4.2.11. This method is widely used in approaches to inverse evolution problems in state space (Geweke and Tanizaki, 2001), particularly in the field of ecology (Clark, 2007). The Gibbs algorithm is able to handle very high-dimensional models by factoring a multivariate posterior density into a set of low-dimensional densities that can be sequentially sampled (Gelfand and Smith, 1990). This strategy exploits the fact that a set of conditional distributions uniquely determines their joint distribution (Gelman et al., 2020). Thus, the Gibbs algorithm alternately samples from the conditional distribution of each parameter and latency, or block of parameters and states, updating each value before proceeding to the next.

Although it is easy to analytically derive conditional posterior distributions for each parameter and state of the equation 4.2.11, in this work we have used open source computational approaches capable of automatically factoring any arbitrarily complex model into its conditional probabilities, and estimating the probability later using the Gibbs algorithm. The Bayesian MARSS model was written in the BUGS language and the JAGS program (Plummer, 2003) from the R

environment (RCoreTeam, 2021) was used to find the posterior probability of parameters and vector of states, from which the properties of dynamic and structural stability. The JAGS program, being written in C++, is capable of efficiently constructing posterior probabilities for very high-dimensional problems, such as the one proposed in this work.

For each of the 48 Longhurst provinces of the global ocean, the MARSS model was fitted using 3 independent Markov chains, with random initial values for the parameter vector and the state vector. Prior to simulation, the dominance time series produced by the PHYSAT algorithm were log-transformed and standardized. The chains were extended for 60.000 iterations, and the first 30.000 were discarded as adaptation period. After this point, the Gibbs algorithm seemed to be effectively sampling from the posterior distribution. The remaining 30.000 iterations were thinned every 30 values in order to reduce the autocorrelation of the Markov chains. The posterior distribution of the community matrix **A** was used to derive estimates of each measure of dynamic and structural stability. Post-predictive calibration (Gelman et al., 2020) was used to verify the ability of the Bayesian MARSS model to recover the simulated dynamics from a previous model. To do this, during each MCMC iteration a synthetic database was generated from the posterior distribution of the model. At the end of the simulation, the simulated (synthetic) series were compared with the observed ones. Standard verification methods (for example, (Gelman et al., 2020)) were also used to verify that the simulation optimally explored the back parameter space.

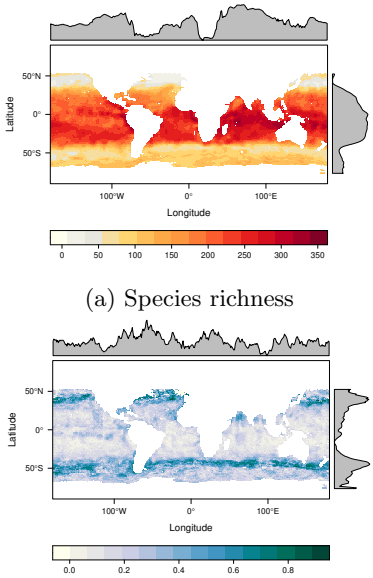

(a) Species richness

(b) Species turnover.

Figure 4.5: Seasonally-averaged latitudinal variation in species richness (**a**) and turnover (**b**) of global marine phytoplankton (data from Righetti et al., 2019). Margin plots are the smoothed frequency distributions of species richness and turnover across latitudes and longitudes, with 1° steps.

4.3 Validation of the insurance hypothesis

Physical factors, such as temperature and photoperiod, vary systematically with latitude. This generates a gradient in seasonality from the equatorial zone, where there is no significant seasonal variation, to the polar latitudes, where seasonality is very marked. These thermodynamic conditions determine the abundance and temporal distribution of phytoplankton on a planetary scale (Alvain et al., 2008; Demarcq et al., 2012; Vallina et al., 2014). In this way, physical forcing represents a control mechanism for the temporal stability of phytoplankton communities causally independent of the effect of functional diversity.

In order to statistically separate the effects of both types of factors, a spatial simultaneously autoregressive Structural Equation Model (SARSEM) was built to represent the plausible relationship structure between functional diversity, environmental synchrony and structural stability, taking into account the effect of the factors physical forcing on each of these variables. The SARSEM approach allows estimating the individual direct and indirect causal effects of different variables in an arbitrarily complex correlation structure (Grace and Irvine, 2020). The correlation matrix thus generated can be statistically contrasted

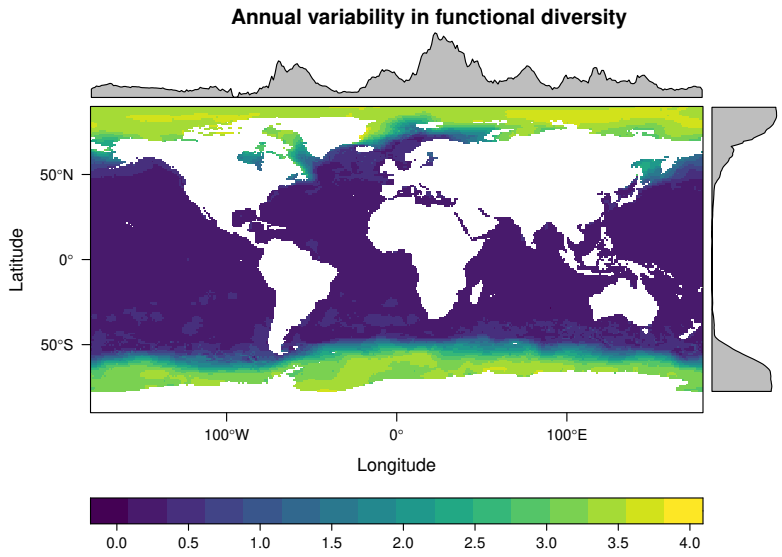

Figure 4.6: Annual variability in functional diversity of marine pyhtoplankton, represented by the seasonally-averaged variance in the weighted biovolume of *Prochlorococcus*, *Synechococcus*, Picoeukariotes, nanoeukariotes and Microeukariotes at a resolution of 1^{o} across the global ocean. Results from quantitative niche modelling of abundance data (Sal et al., 2013; Buitenhuis et al., 2013; Visintini, Martiny, and Flombaum, 2021.

with the expected correlation structure if the proposed causal relationship were plausible. Regardless of the effect of functional diversity on structural stability predicted by the insurance hypothesis, in this paper the following hypotheses of structural relationships between the variables have been considered: 1) Functional diversity is directly controlled by temperature and productivity (Morán et al., 2017; Thomas et al., 2012); 2) Environmental synchrony is controlled by productivity and seasonality, since greater seasonality determines greater temporal segregation of niches (Chesson, Pacala, and Neuhauser, 2001); and 3) Structural stability is controlled by the competitive ratio (Logofet, 2016), which in turn may be partially controlled by environmental synchrony: an increase in niche segregation reduces the magnitude of inter-specific competition (Loreau, 2010a). A positive and statistically significant effect of functional diversity on structural stability mediated by environmental synchrony, independently of the individual effects of temperature, seasonality and the competitive ratio, would imply a statistical validation of the prediction of the insurance hypothesis in the marine phytoplankton.

Seasonality was quantified for each Longhurst biogeochemical province as the proportion of the aggregate temporal variance explained by the MARSS seasonal parameter, while the competitive ratio was quantified as the aggregate temporal variance explained by the intra-specific interactions in relation to the variance explained by the inter-specific ones. The piecewiseSEM R package was used to construct and fit the spatial SARSEM to the results obtained after fitting MARSS to community dynamics data from each Longhurst biogeochemical province. The Maximum Likelihood method was used to find the parameters of the correlation matrix and to estimate the discrepancy with the expected matrix.

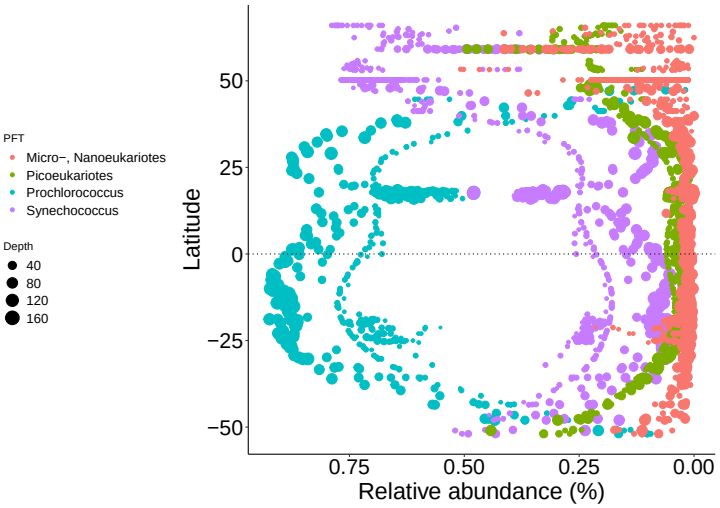

Figure 4.7: Latitudinal variation in the proportional abundance of *Prochlorococcus*, *Synechococcus*, Picoeukariotes, nanoeukariotes and Microeukariotes across the global ocean. Results from quantitative niche modelling of abundance data (Sal et al., 2013; Buitenhuis et al., 2013; Visintini, Martiny, and Flombaum, 2021.)

4.4 Results

4.4.1 *Global patterns of functional diversity, species richness and species turnover*

The output of the quantitative niche modeling from the aggregated database of in-situ abundance sampling suggests a robust latitudinal pattern in functional diversity variation (Fig. 4.6): Diversity, as measured through the variance in abundance-weighted biovolume, is relatively low at latitudes near the equator, particularly in the tropics, and rises gradually at temperate latitudes. The increase in functional diversity accelerates exponentially above 50° latitude in both hemispheres.

This pattern is inversely related to the modeled global relative abundance for *Prochlorococcus*, which shows a high dominance (>75%) at tropical and equatorial latitudes (Figure 4.7). In contrast, *Synechococcus* dominates at mid-latitudes (50°), while picoeukariotes and Microplankton dominates at high latitudes (> 50°).

The pattern of species richness is opposite to the increase of functional diversity with latitude (Figure 4.5a): The largest seasonally-averaged values for species richness are found in equatorial and tropical regions. In contrast, the latitudinal pattern of species turnover reproduces the pattern found for functional diversity (Figure 4.5b), with peak turnover values found at high latitudes and minimum values near the equator.

4.4.2 *Global patterns in community dynamics and stability properties*

The Bayesian scheme designed to fit the MARSS model to the phytoplankton community dynamics time series converged correctly for all Longhurst biogeochemical provinces: no evidence of non-convergence was found for the three posterior Markov chains, which showed ade-

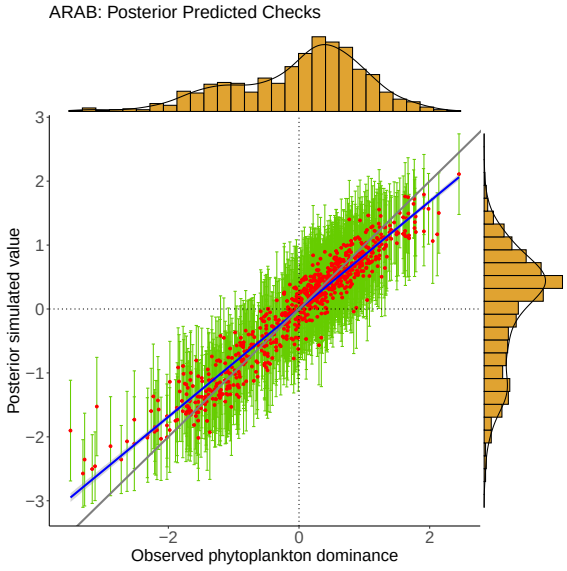

Figure 4.8: Example of posterior predicted checking (PPC) for the Northwest Arabian Sea upwelling Loghurst province (ARAB). Red dots show the average of 1000 posterior simulated MCMC values for all monthly observed phytoplankton dominance data, generated with the parameterized community dynamics (MARSS) model; vertical green lines show the 68% credible interval for each mean value. The gray line is the Y=X regression line, and the blue line is the Maximum Likelihood adjusted regression line. The margin plots show the distribution of simulated (vertical) and observed (horizontal) data.

quate mixing after the period of adaptation during the MCMC. The posterior cross-correlation between model parameters and latent states was < 0.4 in all cases. Posterior predictive simulation analyses suggest that the MARSS is able of reproducing the observed dynamics with a high degree of accuracy for all provinces (see Figure 4.8 for an example).

All phytoplankton communities met the local linear stability condition (spectral radius < 1; Figure 4.9). However, no pattern was detected in the latitudinal gradient of dynamic stability (GAM: R^2 = 7%, edf = 2.378, p = 0.208), although high values close to 1 were observed in some provinces of the tropical gyres, such as the North Pacific Tropical Gyre (NPTG) and the Indian Subtropical Gyre (ISSG), as well as the South Subtropical Convergence (SSTC) (see Figure 4.10).

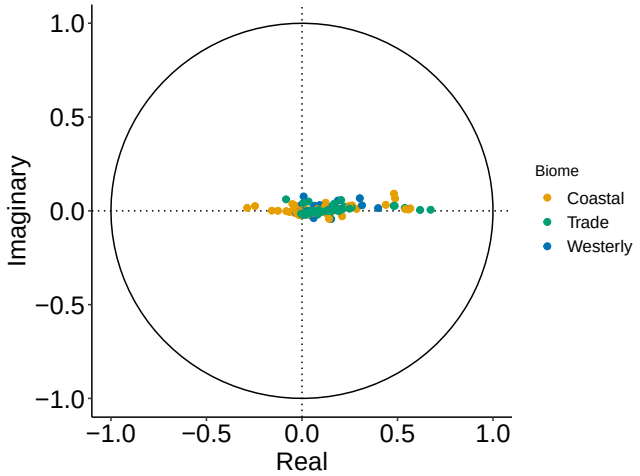

Figure 4.9: Location in the complex plane of the estimated posterior eigenvalues of the community matrices (A_p) of the 48 Longhurst provinces. The colors indicate three main biomes of the pelagic region of the global ocean. For clarity, posterior credibility intervals are omitted.

The latitudinal gradient in environmental synchrony was significantly nonlinear (Figure 4.11: GAM: R^2 = 40.5%, edf = 3.364, p

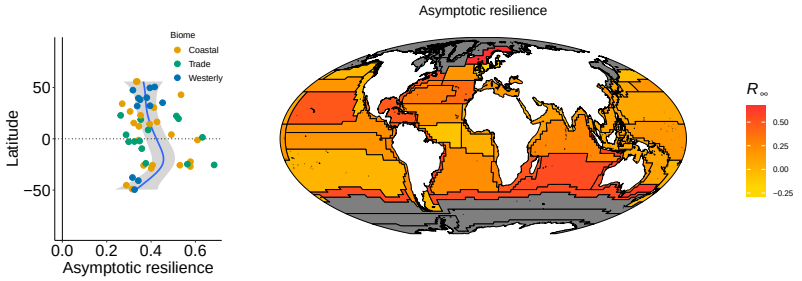

Figure 4.10: Latitudinal variation of the asymptotic resilience (R_∞; see Eqn. 3.2.9) for each Longhurst province of the planet. In the left, the blue line is the function of a GAM fitted to the data, with the 90% confidence interval as a shaded region. On the right, the global distribution map of asymptotic resilience.

< 0.001). All environmental synchrony values were positive. Low-latitude provinces showed relatively high average synchrony values ($0.4 < \rho_s < 0.7$), higher in tropical provinces than in those located around the geographic equator. The provinces at high latitudes showed low degrees of synchrony, fundamentally those located in polar biomes, whose values were close to 0 (Figure 4.11).

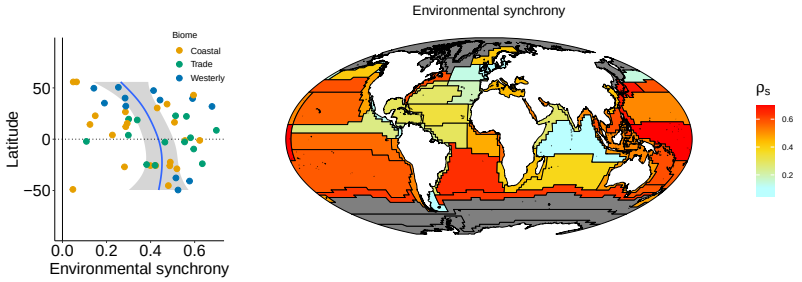

Figure 4.11: Latitudinal variation of environmental synchrony (See Eqn. 4.2.5) for each Longhurst province of the planet. In the left, the blue line is the function of a GAM fitted to the data, with the 90% confidence interval as a shaded region. On the right, the global distribution map of environmental synchrony.

In contrast to the pattern of asymptotic stability, the distribution of the estimated posterior values of initial resilience (reactivity) suggests that most of the provinces of the global ocean are not reactive (Figure 4.12). Transient instability was modeled only in some low-latitude provinces. However, the credibility intervals constructed for the posterior estimates (omitted for visual clarity) overlap 0 in all cases. The latitudinal distribution pattern of the reactivity values is similar to that of the asymptotic resilience: the provinces of tropical latitudes show a greater reactivity, mainly in the large oligotrophic gyres.

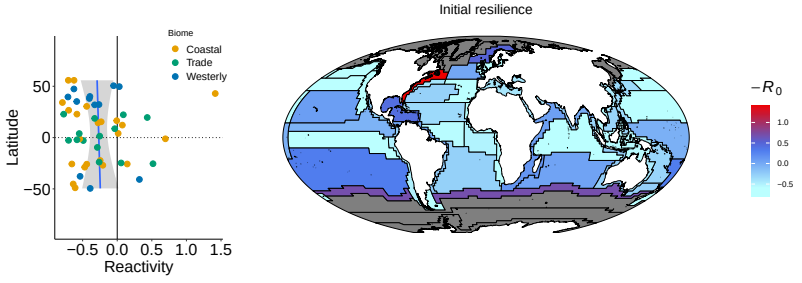

Figure 4.12: Latitudinal variation in initial resilience, or reactivity ($-R_0$; see Eqn. 3.2.10) for each Longhurst province of the planet. In the left, the blue line is the function of a GAM fitted to the data, with the 90% confidence interval as a shaded region. On the right, the global distribution map of reactivity.

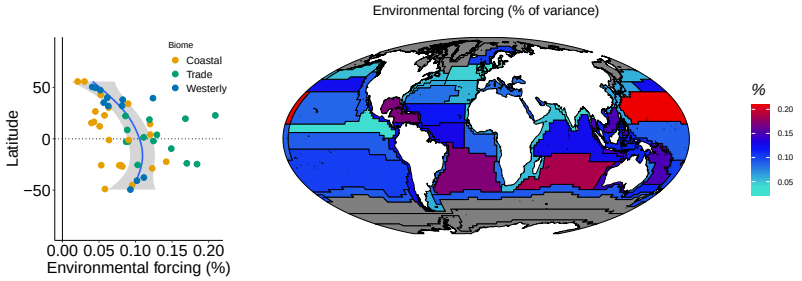

Figure 4.13: Latitudinal variation in the relative impact of environmental forcing, including temperature and productivity effects, for each Longhurst province of the planet. shown is the % of community temporal variance explained. In the left, the blue line is the function of a GAM fitted to the data, with the 90% confidence interval as a shaded region. On the right, the global distribution map of environmental forcing.

This global pattern of reactivity is similar to the pattern in the impact of environmental forcing (temperature plus productivity effects) on global phytoplankton communities. The latitudinal gradient of stochastic structural stability (stochastic invariance, 3.2.11) was significantly nonlinear (Figure 4.14: GAM: $R^2 = 29.6\%$, edf $= 2.981$, p $<$ 0.001). The provinces located in the large oligotrophic gyres are generally characterized by relatively low stochastic structural stability. In contrast, provinces located at high latitudes are structurally more stable, particularly those in the Northern Hemisphere (Boreal Polar, BPLR, and Arctic Polar, ARCT; Figure). This gradient is similar to the pattern in the competitive ratio (Figure 4.18), which increases significantly from the equator towards higher latitudes. This increase is due to an increase in the proportion of the aggregate variance explained by intra-specific competition with latitude, and secondarily to a decrease in the variance explained by inter-specific competition (Figure 4.18).

Finally, figure 4.15 shows the latitudinal gradient of the probability pf feasibility. The latitudinal variation was weakly nonlinear (GAM: $R^2 = 29\%$, edf $= 6.199$, p $= 0.044$), and suggest a trend to increasing values of feasibility with latitude.

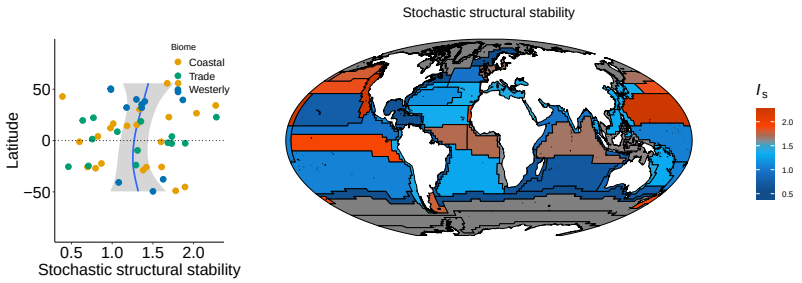

Figure 4.14: Latitudinal variation in stochastic structural stability, or stochastic invariance (I_s; see Eqn. 3.2.11) for each Longhurst province of the planet. In the left, the blue line is the function of a GAM fitted to the data, with the 90% confidence interval as a shaded region. On the right, the global distribution map of stochastic structural stability.

4.4.3 *Relationship among stability measures*

Figure 4.16 shows the correlation among the four community stability metrics. While the relationship between asymptotic resilience and the rest of metrics is generally weak, reactivity (initial resilience) is strongly and negatively correlated with both measures of structural stability: an increase in reactivity for a given Longhurst province is

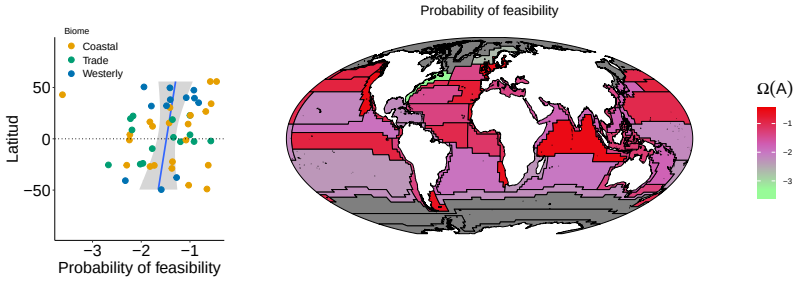

Figure 4.15: Latitudinal variation in the probability of feasibility, a measure of structural stability ($\Omega(\mathbf{A})$; see Eqn. 3.1.12) for each Longhurst province of the planet. In the left, the blue line is the function of a GAM fitted to the data, with the 90% confidence interval as a shaded region. On the right, the global distribution map of the probability of feasibility.

indicative of a loss of structural stability, both through a decrease stochastic invariance and a drop in the probability of feasibility. Indeed, both measures of structural stability are strongly positively correlated. Finally, Figure 4.17 depicts the ordering of the magnitudes of initial resilience (R_0), stochastic structural stability (I_S) and asymptotic resilience (R_∞).

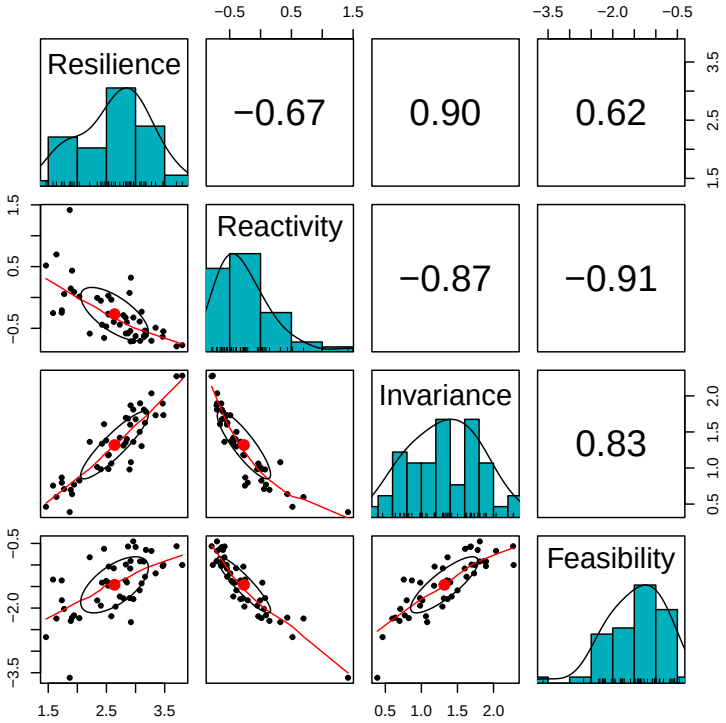

Figure 4.16: Correlation matrix among the four stability metrics. Bivariate scatter plots are shown below the diagonal, histograms on the diagonal, and the Pearson correlation above the diagonal. The robust regression fittings through LOESS smoothed regressions are shown in red, while the correlation ellipses are shown in black with the centroid in red.

4.4.4 *Validation of the insurance hypothesis*

Figure 4.19 shows the final spatial simultaneous auto-regressive structural equation model (SARSEM) designed to statistically validate the prediction of the insurance hypothesis. The covariance matrix estimated by Maximum Likelihood does not differ significantly from that expected if the proposed relationships were compatible with the ob-

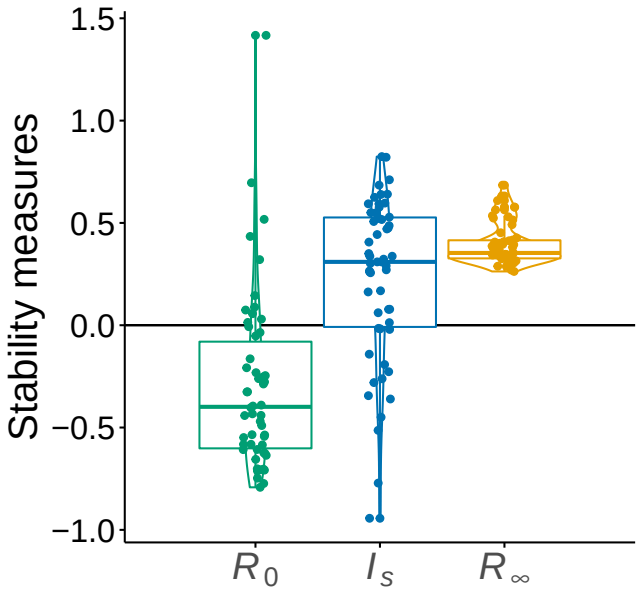

Figure 4.17: Ordering of the magnitude of initial resilience (R_0), stochastic structural stability (I_S) and asymptotic resilience (R_∞) according to the theoretical prediction of Arnoldi, Loreau, and Haegeman, 2016. Stochastic structural stability is calculated in the log-scale. Violin plots shows the density of the distributions of points for each measure, while boxes represent the 75% interquartile range.

servations (Fisher's C = 19.795, degrees of freedom = 81, p = 0.344). The proposed SARSEM thus adequately explains the data.

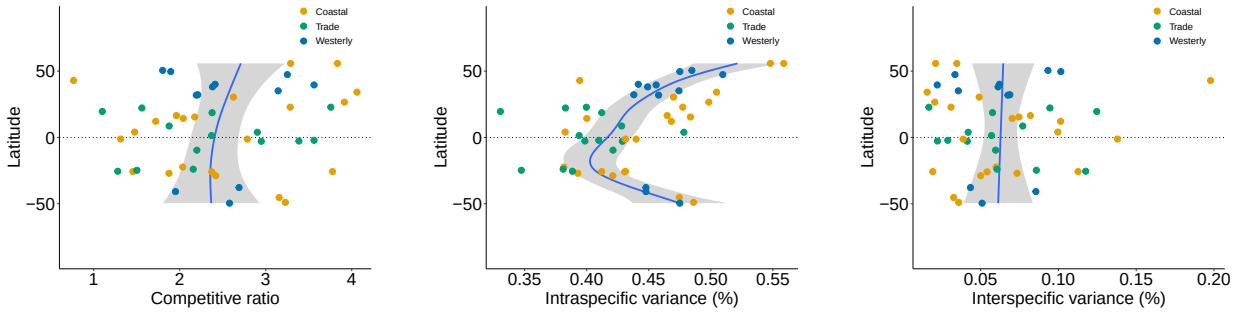

(a) Competition ratio of intra- to interspecific interactions.

(b) Variance explained by intraspecific interactions.

(c) Variance explained by interspecific interactions.

Figure 4.18: In (**a**), the competition ratio shows the impact of intraspecific interactions relative to interspecific interactions. In (**b**), the proportion of community temporal variability explained by intraspecific interactions, and in (**c**), the proportion of community temporal variability explained by interspecific interactions.

Across the global ocean, both sea surface temperature and the seasonal variability of productivity, which are negatively correlated, are the external variables driving the dynamics and stability of marine phytoplankton (Figure 4.19). In particular, the variability of productivity jointly exerted a positive effect on the seasonal variability of functional diversity, the competition ratio and reactivity, while impacting negatively on environmental synchrony. A larger seasonal variability of functional diversity, in turn, decreased the competition ratio which in turn increased the magnitude of stochastic structural stability and reduced the strength of reactivity. Environmental synchrony, which was only weakly linked to seasonal variability of functional diversity, increased the magnitude of reactivity. After accounting for these effects, the spatial autoregressive parameters of the system of equations in the spatial SARSEM were all non-significant (parameters ρ in Figure

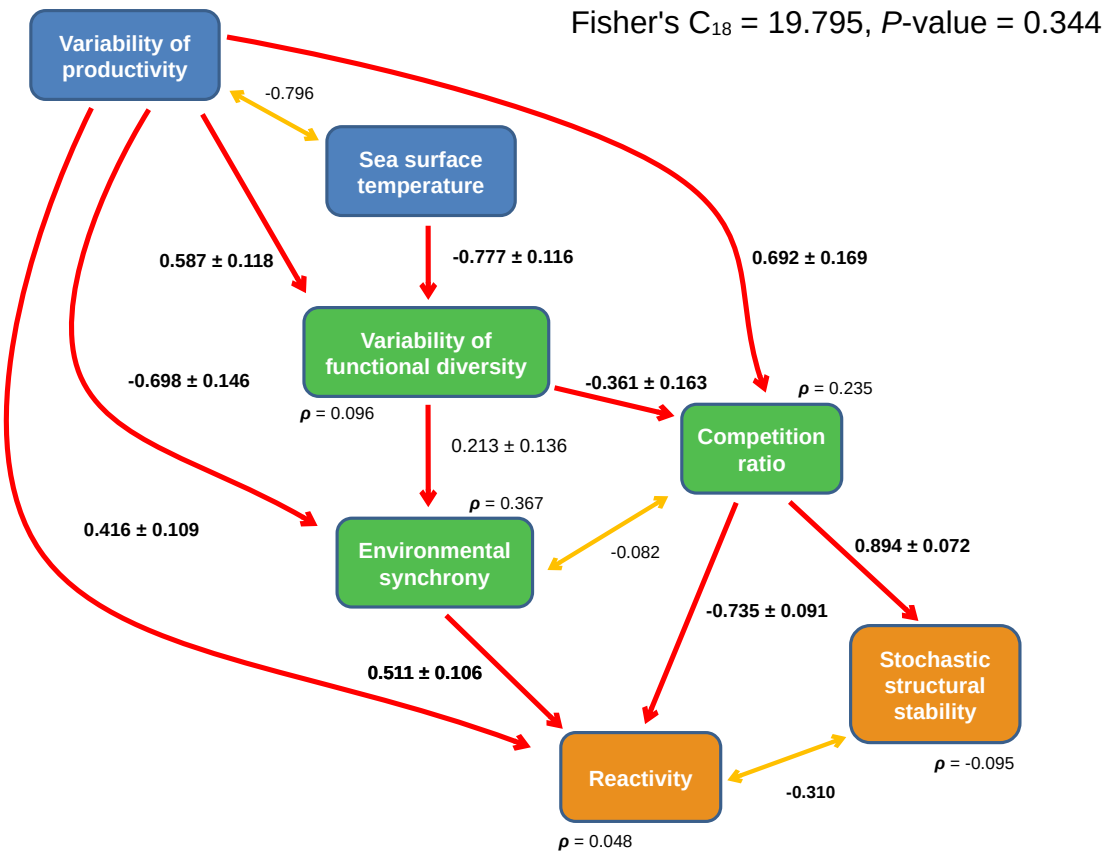

Figure 4.19: Final model constructed using Spatial Auto-Regressive Structural Equation Modeling (SARSEM). This approach models the structural relationships among a set of environmental variables (blue boxes), diversity-related variables (green boxes) and the metrics of community stability (orange boxes). The values besides the red arrows denote the path coefficient (± SE), and the values beside the yellow arrow the residual correlation. The parameter ρ is the spatial autoregression coefficient for each external variable. The Fisher's C value test the hypothesis that the proposed model is causally compatible with the observed data.

4.19).

4.5 Discussion

Recent studies have characterized the global patterns of phytoplankton diversity in terms of richness, turnover and specific diversity (Chust et al., 2013; Vallina et al., 2014; Rodríguez-Ramos, Marañón, and Cermeño, 2015; Righetti et al., 2019). Some authors consider temperature to be the main mechanism for controlling the diversity, functional redundancy and richness of phytoplankton (Thomas et al., 2012; López-Urrutia and Morán, 2015; Righetti et al., 2019; Sommeria-Klein et al., 2021; Zhong et al., 2020), which coincides with the results of this study. Species richness is positively correlated with sea-surface temperature at a global scale (Righetti et al., 2019), while species turnover is negatively correlated. Likewise, hydrodynamic forcing factors, such as meso- and sub-meso-scale fronts, are some of the main physical mechanisms that control phytoplankton abundance and diversity on a global scale (Clayton et al., 2013; Lévy et al., 2015). Despite this, some of the evidence currently available suggests the absence of patterns in the richness and diversity of marine phytoplankton related to latitude, temperature or productivity (Cermeño et al., 2008; Cermeño et al., 2013; Rodríguez-Ramos, Marañón, and Cermeño, 2015), although

global analyses of phytoplankton functional diversity patterns based on size variance do suggest the existence of latitudinal patterns similar to those found in the present study (Acevedo-Trejos et al., 2014; Acevedo-Trejos et al., 2015). Moreover, the analysis of expanded datasets suggest that tmeperature is teh main structuring enviornmental factor of phytoplancton richness and diversity at a global scale (Righetti et al., 2019; Righetti et al., 2020). Even at geological time scales, there is a negative relationship between functional diversity and temperature (Womack et al., 2021).

In phytoplankton, cell size explains a large part of the diversity in the ecological functioning of marine ecosystems (Barton et al., 2013; Marañón, 2015; Casey et al., 2022; Sommeria-Klein et al., 2021). Following (Acevedo-Trejos et al., 2015; Smith, Vallina, and Merico, 2016) we used the variance in phytoplankton biovolume as a measure of functional diversity across the global ocean. Functional diversity followed a latitudinal gradient similar to species turnover and opposite to species richness (Righetti et al., 2019). First, this suggest that there is not necessarily a direct relationship between specific diversity and functional diversity in phytoplankton (Weithoff, 2003). Second, recent studies suggest a latitudinal tension between two complementary mechanisms of community control, namely niche assembly and dispersal limitation (Chust et al., 2013). Global analysis of the variation in the immigration rate suggests a greater importance of niche segregation in marine phytoplankton, although the immigration rate is higher at high latitudes (Chust et al., 2013). On the contrary, the large tropical oligotrophic gyres present lower immigration rates, which could be related to the lower functional diversity revealed by the present study in the tropical provinces. The results show that the low functional diversity of these provinces is determined by the dominance of cyanobacteria of the genus *Prochlorococcus* in the oligotrophic regions of the planet, as other studies also suggest (Moran et al., 2015; Flombaum et al., 2013; Visintini, Martiny, and Flombaum, 2021; Visintini and Flombaum, 2022). Therefore, the cause of the apparent conflict in the empirical latitudinal gradients of marine phytoplankton richness, turnover and diversity is probably due to the fact that some approaches do not take into account the picophytoplankton fraction. This size fraction is particularly relevant in phytoplankton communities, as some biotic and abiotic factors can strongly limit their abundance and distribution in present and futures scenarios (Zhong et al., 2020; Flombaum et al., 2013; Follett et al., 2022), and hence functional diversity and community stability.

Ecological communities that reside in strongly seasonal environments are subject to a greater temporal segregation of niches, which determines less environmental synchrony regardless of the effect of functional diversity (Chesson, 2000; Chesson, Pacala, and Neuhauser, 2001). The results of this study suggest, in fact, a strong impact of seasonality on the environmental synchrony of phytoplankton func-

tional types at a global scale, which is greater at high latitudes, probably due to the increase in the diversity of temporal niches provided by a fluctuating environment (Chesson, Pacala, and Neuhauser, 2001; Righetti et al., 2019). Moreover, seed banking of many phytoplankton taxa as a response to harsh environmental conditions (Ellegaard and Ribeiro, 2018) may provide a specific mechanism for the storage effect. The SARSEM suggests that a highly variable productive environment increases the magnitude of both intraspecific interactions and initial resilience, and increased the variability of functional diversity, while decreasing environmental synchrony. This points to two complementary biological mechanisms in the control of temporal niche segregation. On the one hand, an increase in functional redundancy, as predicted by the insurance hypothesis (Naeem and Li, 1997; Yachi and Loreau, 1999); and on the other hand, a higher rate of phytoplankton immigration at high latitudes (Chust et al., 2013), as already mentioned. This last process may be especially relevant in polar biomes, where the existence of several months in the absence of solar radiation determines a cyclical restructuring of the communities of primary producers. This scenario contrasts with low latitude biomes. It has recently been shown that the location of the deep spring/summer chlorophyll maximum is strongly conditioned in large temperate and tropical regions by the location of the previous winter's mixed layer (Navarro and Ruiz, 2013). This hysteresis phenomenon reflects the high temporal autocorrelation in the environment at these latitudes, which also explains the increased multi-year fluctuations in community abundance at low latitudes. Indeed, in highly variable environments the impact of phytoplankton diversity on ecosystem functioning is specially important (Bestion et al., 2021). A particularly important result is the empirical confirmation of the ordering of the different stability metrics (Fig. 4.17). Given that world marine phytoplankton communities are already fluctuating with a reactive dynamics (a high initial resilience; see Fig. 4.12) this results suggests that the loss of initial resilience operates as an early-warning signal of the loss of asymptotic resilience (Tang and Allesina, 2014), and ultimately of structural stability (Arnoldi, Loreau, and Haegeman, 2016). This suggests that the future risk of extinction of some species/functional types can be predicted from their current transient dynamics (see Caswell and Neubert, 2005; Tang and Allesina, 2014; Arnoldi, Loreau, and Haegeman, 2016 for theoretical predictions).

Recently, the analysis of time series of phytoplankton abundance recorded over more than a decade in Scandinavian lakes revealed an increase in community stability, as measured by species replacement, with an increase in generic richness (Ptacnik et al., 2008). In the present study, the time series analysis of community abundance suggests that marine phytoplankton communities in the global pelagic region are dynamically stable, indicating high overall resilience despite increased inter-annual fluctuations at low latitudes. On the other hand, a clear latitudinal pattern was found in structural stability, which increases with latitude in both hemispheres along with the im-

pact of intra-specific competition. This suggests a decoupling of both stability measures, which are qualitatively different (Rohr, Saavedra, and Bascompte, 2014; Logofet, 2016), at the planetary level, and points to a greater resistance to demographic disturbances of high-latitude communities compared to those of low latitudes. As predicted by ecological theory (Barabás, J. Michalska-Smith, and Allesina, 2016; Logofet, 2016), the competitive ratio, governed in this case by an increase in the impact of intra-specific competition with latitude, has a positive effect on structural stability. Multi-annual studies carried out with freshwater phytoplankton communities also suggest a positive impact of intra-specific competition on community biomass stability (Jochimsen, Kümmerlin, and Straile, 2013). On the other hand, environmental synchrony has a multiple negative effect on structural stability, both directly and indirectly through the reduction of the competitive ratio. In summary, this points to functional diversity as a structural stabilization mechanism for marine phytoplankton communities on a global scale. The results further suggest that this mechanism is mediated by the temporal segregation of niches, independently of the direct impact of seasonality, temperature and productivity, as predicted by the insurance hypothesis.

Due to the impact of marine phytoplankton on global ecological processes and biogeochemical cycles (Falkowski, Barber, and Smetacek, 1998; Field, 1998; Feng et al., 2015; Casey et al., 2022), the results of this study may be especially relevant for predicting the dynamics of primary production and the carbon cycle at the planetary level in possible future scenarios of global change (Henson et al., 2021). Ensemble projections of future global change scenarios suggest that marine ecosystems are at a particular risk (Tittensor et al., 2021; Auber et al., 2022), and large and complex uncertainties remain to be solved (Flombaum et al., 2013; Henson et al., 2021; Anderson et al., 2021). A central result of this work resides in the discovery of the environmental control of the spatial variation in community stability properties through changes in functional diversity of marine phytoplankton on a global scale. Recent evidence suggests a planetary extension of oceanic oligotrophic zones (Irwin and Oliver, 2009; Irwin et al., 2015), and an increase in such areas is predicted in the future (Henson et al., 2021). This increase could be accompanied by a reduction in the functional diversity of primary producers (Acevedo-Trejos et al., 2014; Flombaum et al., 2013), as has been modeled in this study for the biogeochemical provinces located in the large oligotrophic zones of the planet. Furthermore, Earth System Models predict an increase in ocean surface temperature of up to 3°C in the coming decades (Bopp et al., 2013; Tittensor et al., 2021). The results obtained in this work suggest that the changes in the physical processes predicted as a consequence of ocean warming, such as an increase in vertical stratification and a decrease in the availability of nutrients at the surface (Steinacher et al., 2009), could have negative effects on the structural stability of global primary producer communities by reducing their functional diversity.

Potentially, these effects could spread throughout the food web, affecting not only to the efficiency of carbon transport to the deep ocean (Siegel et al., 2013), but also to the stability of energy supply at sea levels upper trophic levels of the global ocean (Chassot et al., 2010).

5 Mixotrophic interactions drive a complex marine food web to the edge of instability

Pablo Almaraz[1,2], Suzana G. Leles[3], Oscar Godoy[4]

1. Departamento de Ecuaciones Diferenciales y Análisis Numérico, Facultad de Matemáticas, Universidad de Sevilla, Sevilla, Spain.

2. Grupo de Oceanografía Operacional, Instituto de Ciencias Marinas de Andalucía, CSIC, Puerto Real, Spain.

3. Department of Biological Sciences, University of Southern California, Los Angeles, CA, USA

4. Instituto Universitario de Ciencias del Mar (INMAR), Departamento de Biología, Universidad de Cádiz, Puerto Real, Spain.

Abstract

Current ecological theory on the structure and dynamics of food webs focus exclusively on the role of species within horizontal compartments, such as competitors for resources, and vertical compartments, either as producers or consumers. However, in marine ecosystems a commonly neglected strategy is that of mixotrophy: planktonic species that act both as primary producers (autotrophs) and consumers (heterotrophs). Beyond classic interaction types, the role of mixotrophy on modulating long-term coexistence and stability of natural food webs remains unexplored. We analyze a long-term dataset of weekly biomass of a coastal marine plankton food web composed of 10 functional types of autotrophs, heterotrophs and mixotrophs. We fit a Bayesian non-linear Lotka-Volterra model with environmental effects to the community time-series, and implement an algorithm that performs a stochastic search through the model space to assign probabilities to the constellation of interaction networks compatible with observed data. The full constellation is made up by topologies with at least one interaction. While the aggregate probability of detecting inter-type interactions is low, a small-world module with diverse interactions is driving the dynamics: two mixotrophs exert a positive impact, and a large heterotroph a negative effect, on the growth rate of a small heterotroph. Both interaction network structure and dynamical complexity are nearly maximal and, while the global equilibrium is dynamically stable and feasible, the linearized system is found in the limit of structural instability. This render the system highly sensitive to internal and external perturbations. Our results provide empirical evidence of the major role that mixed trophic strategies may play in driving the long-term structure and dynamics of marine food webs,

with potentially far-reaching consequences for the control of primary production and biogeochemical cycles in variable environments.

KEYWORDS Bayesian state-space model, Coexistence, Entropy, Functional diversity, Mixotrophy, Network topology, Reactivity, SSVS, Structural stability, Plankton.

5.1 INTRODUCTION

Ecologists have long sought to understand the role of ecological interactions in modulating key features of ecological communities. Prior work has shown that the sign, strength and the architecture in which species interactions are embedded modulate the maintenance of biodiversity (e.g., species composition (Levine and HilleRisLambers, 2009), the stability and resilience of ecological communities to external perturbations (Mougi and Kondoh, 2012; Kondoh and Mougi, 2015; Adler et al., 2018) as well as their functioning (Miele et al., 2019; Cardinale, 2011; Godoy et al., 2020). Yet, the vast majority of studies in this subject does not validate whether the estimated structure of species interactions reproduces well the population dynamics of the interacting species that persist in the long-term. Therefore, it is poorly understood to what extent we are documenting transient (i.e. lasting only for a short period of time) or stable features of ecological systems.

The lack of connection between the structure of species interactions and long-term community and population dynamics is exemplified by the longstanding debate between complexity and stability. The seminal work by May, 1972 posits that the higher the number of interactions and species in a system, the more unstable a community is expected to be. However, if we focus on the number of viable communities in the long-term and not the overall number of starting communities, the pattern is reversed: and the more stable communities are the more complex ones (Roberts, 1974). This disconnection is also present in empirical works such as the qualitative characterizations commonly observed in bipartite mutualistic networks that describe whether a pair of species (e.g., plant and pollinator) are interacting or not (e.g., (Bascompte et al., 2003; Bartomeus, Vilà, and Santamaría, 2008; Chacoff et al., 2012) or quantitative estimations with neighborhood analyses of the sign and the strength of plant competition Godoy and Levine, 2014; Canham et al., 2006; Kunstler et al., 2016. For both examples, it is implicitly assumed that a thorough characterization of the structure of species interactions should reproduce well its population consequences. However, this assumption is not likely true for two main reasons. First, ecological communities are open systems subjected to continuous variation in environmental conditions in which population trajectories are highly influenced my dispersal processes and stochastic events Thompson et al., 2020; Shoemaker et al., 2019. Second, the same structure of species interactions can produce quite contrasted long-term dynamics due to historical and contingency factors such as

species abundances, legacy effects, or variation in intrinsic growth rates Song et al., 2020.

A first step towards building solid bridges connecting the structure of species interactions with the long-term dynamics of ecological communities requires solving two previous limitation. On the one hand, we need to be agnostic about which particular interactions are relevant for the dynamics of entire communities. For instance, multitrophic studies have place great in describing the interactions occurring among species belonging to different trophic levels but ignore self-limitation processes which are critical to regulate population dynamics Godoy et al., 2018. On the other hand, we also believe the sign of species interactions should not be predefined. This is a procedure that started with classic studies (e.g., Macarthur and Levins, 1967 but still is common in the literature in both mutualistic systems, in which pollinators are predifined to have a positive effect on plant fitness Bastolla et al., 2009; Rohr, Saavedra, and Bascompte, 2014, and in food webs, in which herbivores and pathogens are predefined to have a negative effect in plant fitness Maron, Agrawal, and Schemske, 2019. The change we advocate here in how we model ecological communities is justify by growing evidence showing that the sign of species interactions is labile Mougi and Kondoh, 2012; García-Callejas, Molowny-Horas, and Araújo, 2018. They can change from negative to positive and viceversa. Such is the case of changes from negative (competition) to positive (facilitation) interactions in many biological communities including terrestrial and marine communities along environmental stresses when environmental conditions change or resources become scarce Stoecker et al., 2016.

Here, we aim to overcome these two limitations to better understand the role of species interactions on their long-term persistence by focusing on the microscopic organisms that inhabit the sunlit ocean. Plankton communities are highly diverse in terms of species diversity, composition, function, and ecological interactions (Worden et al., 2015). Traditionally, plankton communities have been studied under the paradigm of a plant-animal dichotomy. However, these communities, and in particular protist plankton can act as both consumers and producers through mixotrophy (Stoecker et al., 2016; Selosse, Charpin, and Not, 2017), defined as a nutritional strategy in which organisms can perform photosynthesis as well as consume prey (Flynn et al., 2013). Mixotrophy is not a single strategy. Mixotrophs present a wide variety of sizes and strategies (Mitra et al., 2016; Stoecker et al., 2016), which reflect on different responses to environmental conditions and potential roles in carbon fluxes (Leles, 2019; Leles et al., 2021). A basic distinction can be made between those that possess (constitutive) or acquire (non-constitutive) the ability to photosynthesize (Mitra et al., 2016). Constitutive mixotrophs can choose to feed to meet their nutritional requirements (Caron et al., 1993; Adolf, Stoecker, and Harding, 2006) while non-constitutive forms must continuously replace the plastids acquired from phototrophic prey to survive (see Leles, 2019; Stoecker et al., 2016; McManus, Schoener, and Haberlandt, 2012). The latter can also be classified as generalists or specialists depending

on the type of prey that they must feed on to acquire their photosystems. Importantly, mixotrophy is ubiquitous among protist plankton in the global oceans (Leles, 2019), they play a critical role in food web dynamics and biogeochemical cycling in the oceans (Mitra et al., 2014; Mitra et al., 2016; Ward and Follows, 2016) as well as the size structure of plankton communities and the trophic transfer of carbon to upper trophic levels (Ward and Follows, 2016). Overall, this knowledge suggests that mixotrophy is a stable strategy along a wide range of environmental conditions and multitrophic interaction networks, yet how this stability is particularly influenced by environmental variation, self-limiting processes, and interspecific interactions remains unclear. Mixotrophy can enable the coexistence of species that compete for the same finite resource through intraguild predation (Jost et al., 2004; Wilken et al., 2013; Moeller et al., 2016). Yet to what extent this strategy is important to the stability and persistence of complex plankton communities across oceanographic gradients is not well understood (Cesar-Ribeiro et al., 2020). The lack of studies that incorporate multi-trophic interactions to investigate coexistence within and across trophic levels highlights this issue (Bartomeus et al., 2021).

Using an inverse modelling approach applied to a high-resolution time series of biomass fluctuations of 10 functional groups of autotrophs, mixotrophs, and heterotrophs spanning over five orders of magnitude of size, we ask three main questions: 1) What is the structure of interactions in terms of sign, strength, and network properties that reproduce with confidence the long-term dynamics of the plankton system? 2) What is the role of mixotrophy (and particular mixotrophy strategies) in the long-term persistence of the plankton system? 3) How the relative importance of species interactions versus environmental fluctuations vary for each of the functional groups considered?

5.2 Methods

5.2.1 *The L4 dataset*

We analysed a long-term time series dataset obtained at the L4 monitoring station, located about 7.25 nautical miles south southwest of Plymouth, in the Western English Channel, UK (50°15N, 4°13W). This time series is part of the Western Channel Observatory (`http://www.westernchannelobservatory.org.uk/`). The water at L4 is about 53 meters deep, and it has a complex temperature profile. During the winter, the water column is well mixed, but from April to September it becomes stratified, with a temperature difference of up to 2 degrees Celsius between the upper and lower layers. The site also experiences strong tidal currents, occasional riverine inputs and surface currents that can reach speeds of 0.5-0.6 meters per second. The surface temperature at L4 varies throughout the year, ranging from 8 ^{o}C in the middle of winter to between 17 and 18 ^{o}C in mid-August (Smyth et al., 2010; Tarran and Bruun, 2015). We used weekly data

obtained over a period of 9 years, from 2007 to 2015. We chose not to use data collected prior to 2006 due to a lack of taxonomic resolution that hampered the identification of mixotrophic taxa. Coupled to the taxonomic information, the L4 observational data used here includes temperature, salinity, mixed layer depth, inorganic nutrients, chlorophyll-a, and carbon biomass of all plankton functional types included in our analysis (Smyth et al., 2010; Widdicombe et al., 2010; Atkinson et al., 2015; Tarran and Bruun, 2015). The major nutrients, nitrate + nitrite, silicate and phosphate, follow a similar seasonal pattern as temperature. Chlorophyll-a levels are consistently low during late autumn and winter, and higher during spring and summer. There is a significant amount of month-to-month variability, and in some years a distinct bimodal distribution of peak chlorophyll-a concentration can be observed.

Roughly every week, the RV Plymouth Quest collected water samples from various depths (2, 10, 25, and 50 meters) using 10 L Niskin bottles and a rosette sampler with a Seabird 19+ CTD. The samples were transferred to clean containers and kept in a cool box until they were brought back to the laboratory. In some cases, the samples were treated with glutaraldehyde and stored at 4 ^{o}C for at least 30 minutes before being frozen in liquid nitrogen for analysis. The samples were either kept in liquid nitrogen or stored in a freezer at -80 ^{o}C until analysis. We analyzed Plankton data obtained at 10 m depth. For more details on sampling and data processing, we refer to previous studies (Smyth et al., 2010; Widdicombe et al., 2010; Atkinson et al., 2015; Tarran and Bruun, 2015).

5.2.2 *Functional grouping*

Our plankton community comprised populations with diverse trophic strategies and cell sizes. Following previous studies with this dataset (Leles et al., 2018; Leles, 2019), we first grouped taxa according to their trophic strategy among autotrophs (producers), heterotrophs (consumers), or mixotrophs (producers and consumers). We then assigned different functional groups based on size and mixotrophic functional diversity. Plankton taxa ranged over five orders of magnitude in size (pico- to meso- plankton, i.e., 0.2 μm – 2 cm). Our analysis included two autotrophs (picophytoplankton and diatoms), four heterotrophs (bacteria, nano-, micro- and meso- zooplankton), and four mixotrophs (including constitutive and non-constitutive forms). Mixotrophic taxa were assigned based on previous reviews as described by Leles, 2019. Specifically, all autotrophic flagellates that possess their own photosystems were assigned as constitutive mixotrophs (Table S1). These were then divided in two mixotrophic types according to cell size, i.e., nano- (2–20 μm) and micro- (20–200 μm) plankton. Dinoflagellate and ciliate taxa known to acquire photosynthetic capacity from their autotrophic prey were classified as non-constitutive mixotrophs. These were then divided between specialist and generalist forms according to

their ability to obtain plastids from specific or diverse prey types, respectively. All non-constitutive forms were in the microplankton size class. Figure 5.1 shows time-series plots of each of the ten functional types considered.

5.2.3 *Time series modelling of plankton community dynamics*

We adopt a Bayesian inverse modeling approach through state-space methods (e.g., Mutshinda, O'Hara, and Woiwod, 2011; Almaraz et al., 2012) to fit a Lotka-Volterra model with Ricker-type interactions and environmental abiotic effects to the L4 time-series of community plankton biomass. A state-space scheme is a fully stochastic model in which uncertainty is segregated into a state equation, modelling the system under study with an associated process variance; and an observation equation, liked to the state equation through a measurement process with observation error (Clark and Bjørnstad, 2004; Mutshinda, O'Hara, and Woiwod, 2011; Almaraz et al., 2012). In this approach, the 'true' state of the system is thus regarded as unobserved, or latent (Durbin and Koopman, 2001). Therefore, uncertainty is optimally handled and propagated across the model structure, therefore reducing the bias in the estimation of both the interaction network and environmental effects (see Almaraz and Amat, 2004; Mutshinda, O'Hara, and Woiwod, 2009; Mutshinda, O'Hara, and Woiwod, 2011; Almaraz et al., 2012).

Structure of the inverse state-space model The state (process) equation of the discrete-time version of the Lotka-Volterra model is written as:

$$n_{i,t+\delta_t} = n_{i,t} + \delta_t r_i \left(1 - \frac{\sum_{j=1}^{s} \alpha_{ij} N_{j,t}}{K_i}\right) + \delta_t \sum_{i=1}^{s} \sum_{m=1}^{p} \beta_{i,m} c_{m,t} + \delta_t \epsilon_{i,t} \quad \text{for} \quad i = 1, 2, ..., s \quad \text{and} \quad m = 1, 2, ..., p \tag{5.2.1}$$

where $n_{i,t}$ is the log_e of the latent (unobserved) biomass of the i functional type at time t, for a set of s functional types ($\forall i, j \in s$). Therefore, $N_{j,t}$ is the raw latent biomass at time t of the i functional type. The variable δ_t is the sampling interval among subsequent events in time. Although most of the time lapses among samplings were of 1 week, this figure varied across the full sampling scheme: for instance, there are no data available for some months. Rather than interpolating or imputing data, we treat this scheme as a case of uneven sampling interval (Clark and Bjørnstad, 2004; Clark, 2007), which affects the estimation of parameters and process error in Eqn. 5.2.1 (see below). The coefficients α_{ij} measure the *per*-capita direct effect of type j on population growth rate of type i, relative to the impact of type i on itself with all other species held constant (Levins, 1968; Novak et al., 2016). The α_{ii}'s are set to 1 to make the system dissipative (see Levins,

1968; Ranta, Lundberg, and Kaitala, 2006; Mutshinda, O'Hara, and Woiwod, 2011; Almaraz et al., 2012). The r_i are the intrinsic (instantaneous, *per*-capita) rates of increase for each functional type, and the K_i are their carrying capacities. The β's parameters, $\beta \in \mathbb{R}^{s \times m}$ stand for the impacts of m environmental variables c on the growth rate of each type i. Finally, $\epsilon_{i,t}$ represent for environmental stochasticity impacting on the population growth rate of each functional type i through a set of independent, identically distributed (white noise) random variables. The process variance of $\epsilon_{i,t}$ is denoted by σ^2.

The state equation in 5.2.1 is linked to the samples obtained by the RV Plymouth Quest (see above) through an observation model:

$$y_{i,t} = n_{i,t} + \rho_{i,t} \tag{5.2.2}$$

where $\rho_{i,t}$ is the measurement error, with an observation variance of τ_i^2. Finally, the initial state, $n_{i,0}$ for each functional type in the vector of latent states is specified as a normal distribution with mean $\mu_{i,0}$ and variance ϵ_0, $n_{i,0} \sim \mathcal{N}(\mu_{i,0}, \epsilon_0)$.

Written in Bayesian matrix (compact) form, the Lotka-Volterra-Ricker state-space model with environmental abiotic effects is:

$$\begin{aligned} \mathbf{n}_{t+\delta_t} &\sim \mathcal{MVN}\left(\mathbf{n}_t + \delta_t diag(\mathbf{r})\left(\mathbf{1}_S - \mathbf{A}\mathbf{N}_t\right) + \delta_t \mathbf{B}\mathbf{c}_t, \Sigma\right) \\ \mathbf{y}_t &\sim \mathcal{N}\left(\mathbf{n}_t, \mathbf{T}\right) \\ \mathbf{n}_0 &\sim \mathcal{N}\left(\mathbf{M}, \Sigma\right) \end{aligned} \tag{5.2.3}$$

where $\mathbf{n}_t = (n_{1,t}, \cdots, n_{s,t})^T$ and $\mathbf{N}_t = (N_{1,t}, \cdots, N_{s,t})^T$ are the vectors of log_e and raw population abundances of each functional type, respectively. $diag(\mathbf{r}) = (\mathbf{r}\mathbf{1}^T) \circ \mathbb{I}$ is the diagonal matrix formed with the *per*-capita (intrinsic) growth rates of each functional type, r_i; the symbol $\circ$ stand for the element-wise (Hadamard) product. The matrix $\mathbf{A}$ is formed by the coefficients of inter-type interactions scaled by the carrying capacities in the off-diagonal, α_{ij}/k_i. Matrix $\mathbf{A}$ is thus called the alpha matrix (Levins, 1968; Novak et al., 2016). The intra-type coefficients in the diagonal, α_{ii}, are k_i^{-1} (see Ranta, Lundberg, and Kaitala, 2006; Mutshinda, O'Hara, and Woiwod, 2009; Almaraz and Oro, 2011). $\mathbf{B}$ is the $s \times m$ matrix formed with the impacts of each of the m environmental covariates on the set of s functional types.

The matrix Σ in the state equation includes the variance of the unmodelled (stochastic) environmental factors impacting on single-type dynamics in the main diagonal, σ_i^2, and the (potentially) correlated joint responses to the common environment among all functional types, $cov(\sigma_i, \sigma_j)$, in the off-diagonal. Note that this matrix is implicitly impacted by the varying sampling intervals, δ_t in Eqn. 5.2.5. This matrix is, thus, positive semi-definite and symmetric (Almaraz et al., 2012): $\mathbf{E}_t \sim \mathcal{MVN}(0, \Sigma)$. Finally, the vector $\mathbf{T}$ includes the measurement errors for each functional type, and we consider that the cross-correlation

between these terms among functional types was negligible.

Evaluating the coexistence and stability of the mixotrophic community The Lotka-Volterra-Ricker state equation in 5.2.3 converges to the equilibrium, denoted by $\mathbf{N}^*$, when $\mathbf{N}_{t+1} = \mathbf{N}_t$. The system can be solved for this equilibrium,

$$\mathbf{N}^* = \mathbf{K}\mathbf{A}^{-1} \tag{5.2.4}$$

were $\mathbf{K}$ is the vector of carrying capacities of each functional type and $\mathbf{N}^*$ is the vector of functional-type abundances at the equilibrium (Levins, 1968; Ranta, Lundberg, and Kaitala, 2006). For generalized Lotka-Volterra systems, such as the state equation in 5.2.3, if an admissible equilibrium is found ($\mathbf{N}^* \geq 0$) this is also the global equilibrium of the system (Takeuchi, 1996). Besides, for an admissible equilibrium to be feasible, only positive components are allowed in vector $\mathbf{N}^*$, $\mathbf{N}^* > 0$ (Roberts, 1974). We define the probability of feasibility of the global equilibrium of Eqn. 5.2.3 as the frequency of non-null components in the posterior distribution of $\mathbf{N}^*$. Note that this is a measure of the probability of coexistence in a variable environment.

If and admissible equilibrium exist, it is possible to linearize 5.2.3 around this equilibrium $\mathbf{N}^*$, and evaluate the dynamical stability of the system to infinitesimal perturbations of initial conditions (Takeuchi, 1996; Elaydi, 2005). Upon linearization, and noting the varying sampling interval δ_t, the Jacobian matrix of the Lotka-Volterra-Ricker state-space model 5.2.3 is:

$$\mathbf{J}_t = \begin{pmatrix} 1 - \delta_t \frac{r_1}{K_1}\mathbf{N}_1^* & \cdots & -\delta_t \frac{\alpha_{1s} r_1}{K_1}\mathbf{N}_1^* \\ \vdots & \ddots & \vdots \\ -\delta_t \frac{\alpha_{s1} r_s}{K_s}\mathbf{N}_s^* & \cdots & 1 - \delta_t \frac{r_s}{K_s}\mathbf{N}_s^* \end{pmatrix} \tag{5.2.5}$$

The matrix 5.2.5 is also named the community matrix (Levins, 1968; Novak et al., 2016); note the differences with the alpha matrix $\mathbf{A}$ in 5.2.3 (see Novak et al., 2016). The Jacobian (community) matrix includes the direct *per*-capita effect of functional type j on the population growth rate of type j. In discrete-time models, the criteria for the dynamical stability of a system is that the spectral radius of the Jacobian should be strictly less than 1 (Elaydi, 2005). This means that the modulus of the dominant eigenvalue of matrix 5.2.5 should be contained within the unit circle in the complex plane. As with feasibility, we define the probability of dynamical stability of the system modeled with 5.2.3 as the frequency of spectral radii that were < 1 in the posterior distribution of the Jacobian. Note that the Jacobian is time-varying, given that the heterogeneous time step δ_t affects the linearized dynamics. However, this variability is due to a sampling artifact, and not to an unmodelled non-stationary process of the community. Therefore, for simplicity in the calculations, we considered the median value of δ_t which is, indeed, of 1 week. Hereafter, we denote

the Jacobian as **J**.

To characterize the posterior probabilities of coexistence and stability of the mixotrophic plankton community we derived the following metrics from the posterior distribution of the fitted Lotka-Volterra-Ricker model in 5.2.3:

1. **Departure from normality**: A first measure of the sensitivity of matrix **A** to perturbations is the scaled departure from normality, depn(**A**) (Barabás and Allesina, 2015). If depn(**A**) ≤ 1, the spectra of the matrix shows low sensitivity to perturbations; when depn(**A**) $= 1$, the the degree of nonnormality is that of a random matrix of the same dimension (Barabás and Allesina, 2015). In contrast, values of depn(**A**) > 1, are indicative of matrix spectra with a high sensitivity to perturbations.

2. **Robustness of coexistence**: The set of eigenvalues of the alpha matrix **A** describes the robustness of the dynamical system. In continuous time, the smaller the eigenvalue, the larger the sensitivity of the matrix to perturbations in that direction (Barabás et al., 2014; Pásztor et al., 2016): since the determinant of a matrix is the product of its eigenvalues, when its value approaches 0 the system becomes increasingly fragile to perturbations in specific directions. In particular, the geometric mean of the eigenvalues of **A** informs on the robustness of coexistence: in discrete time, values ≥ 1 are indicative of low robustness and high sensitive to perturbations.

3. **Dynamic dimensionality**: For any system with a matrix **A**, the perturbations to initial conditions will be dampened or propagated at different rates, according to the eigenvalue spectra of **A**, and directions, according to their associated eigenvectors (e.g., Trefethen and Embree, 2005). Therefore, a spectra with eigenvalues of similar magnitude will absorb perturbations at a similar rate irrespective of the direction, since no slow eigenvalue will dominate the dynamics. Such a system is said to have a high dynamic dimensionality (Gilljam, 2016). Dynamic dimensionality can be evaluated as the inverse of the Simpson index calculated for the modulus of the eigenvalues of the Jacobian matrix 5.2.5. If this index is low, this is indicative of a high probability of some eigenvalue dominating the response of perturbations in specific directions, therefore increasing the likelihood of species extinction (Gilljam, 2016).

4. **Entropy**: Measuring complexity in ecology, as in any physical system, is far from straightforward (e.g., Lloyd, 2001). For ecological networks, an internal measure of complexity related to the maximum physical information that can be compressed in a system (see Chaitin, 1994; Soler-Toscano et al., 2014) was recently introduced by Strydom, Dalla Riva, and Poisot, 2021, based on work by Gu and Shao, 2016. Applying Singular Value Decomposition (SVD) to the

alpha matrix $\mathbf{A}$, a measure of entropy is constructed by quantifying the scaled diversity of the spectra of the SVD:

$$\mathcal{E} = -\frac{1}{\ln(k)} \sum_{i=1}^{k} s_i \ln(s_i) \tag{5.2.6}$$

where k is the rank of the alpha matrix $\mathbf{A}$, and s_i is the singular value σ_i, scaled by the sum of the spectra of the SVD, $s_i = \sigma_i / sum(\sigma)$. The maximum complexity of an ecological network, as expressed in matrix $\mathbf{A}$, is achieved when the entropy is maximum, $\mathcal{E} = 1$.

5. **Resilience**: The asymptotic (long-term) response of the dynamical system in 5.2.3 linearized around the equilibrium $\mathbf{N}^*$ is driven by the dominant eigenvalue of the Jacobian 5.2.5 . Asymptotic resilience, R_∞, is the defined (Ives, 1995; Ives et al., 2003; Arnoldi, Loreau, and Haegeman, 2016) as the inverse of the absolute value of the real part of the dominant eigenvalue of $\mathbf{J}$, with units t^{-1}:

$$\mathrm{R}_\infty = \frac{1}{|\max[\mathrm{Re}(\lambda(\mathbf{J}))]|} \tag{5.2.7}$$

6. **Reactivity**: Besides asymptotic resilience, it is interesting to evaluate the initial response of the dynamical system in 5.2.3 to infinitesimal perturbations of the equilibrium $\mathbf{N}^*$. The initial resilience, R_0, measures the instantaneous (in contrast to asymptotic) response of the system to perturbations (Ives et al., 2003; Caswell and Neubert, 2005; Snyder, 2010). For discrete-time systems (Snyder, 2010),

$$\mathrm{R}_0 = \ln\left(\sqrt{\lambda_1(\mathbf{J}^T \times \mathbf{J})}\right) \tag{5.2.8}$$

where λ_1 is the dominant eigenvalue of the transpose of $\mathbf{J}$ times $\mathbf{J}$. It is the worst-case scenario (Ives et al., 2003).

7. **Stochastic structural stability**: Finally, Arnoldi and Haegeman, 2016 showed the fundamental relationships between measures of dynamical stability (i.e., resilience 5.2.7 and reactivity 5.2.8) and measures of structural stability of systems linearized around an equilibrium. This is an important result: it relates the response of dynamical systems to infinitesimal perturbations of initial conditions with their response to finite perturbations of the parameters of the system (Arnoldi, Loreau, and Haegeman, 2016; Arnoldi and Haegeman, 2016). Therefore, dynamical stability, quantified through the response to external perturbations, coincides with the minimal internal white-noise perturbation able to make the system unstable (Arnoldi and Haegeman, 2016). This unified measure is named stochastic invariability, or stochastic structural stability:

$$\mathcal{I}_s = -\frac{1}{\Delta t} \ln\left(1 - \frac{1}{\|(\mathbb{I} - \mathcal{J})^{-1}\|}\right) \tag{5.2.9}$$

where the lifted operator $\mathcal{J}$ is the tensor (Kronecker) product

of the community matrix over itself, $\mathbf{J} \otimes \mathbf{J}$. Large values of $\mathcal{I}_s$ are representative of systems robust to perturbations, both in a dynamical and structural sense.

Prior specification and parameter estimation We used Bayesian Markov Chain Monte Carlo integration (MCMC) through Gibbs sampling in the JAGS language (Just Another Gibbs Sampler, Plummer, 2003) to fit the Lotka-Volterra-Ricker state-space model to the community time series data. We used normal prior distributions for the parameters of the environmental effects, $\beta_{i,m} \sim \mathcal{N}(0, 1)$, and positively truncated normal distributions for the *per*-capita growth rates, $r_i \sim \mathcal{N}(0, 0.25)\mathrm{T}(0,)$ and the carrying capacities, $k_i \sim \mathcal{N}(\hat{k}_i, 0.25)\mathrm{T}(0,)$. Here, $\hat{k}_i$ is a prior estimate of the carrying capacity for each functional type obtained with preliminary runs of the model. This location parameters greatly improved the mixing and stabilization of MCMC chains. Unfortunately, no estimates for measurement error were available from the RV Plymouth Quest sampling scheme. Therefore, we use an estimate of sampling variance of 10% of the observed biomass for each functional type. Smaller or larger values did not significantly altered the results. We used a scaled inverse Wishart distribution (Huang and Wand, 2013) as a prior model to the covariance matrix for environmental noise, $\Sigma^{-1} \sim \mathrm{SWishart}(\zeta, S)$. The inverse Wishart distribution is the conjugate prior for the covariance matrix of a multivariate normal distribution (Gelman et al., 2020), but it is known to constrain the variance parameters. The scaled inverse Wishart (Huang-Wand distribution, Huang and Wand, 2013), allows for the estimation of a diagonal matrix of scale parameters (ζ) and an unscaled covariance matrix (S) that follow the Wishart distribution. With this distribution, the standard deviation and correlation parameters are marginally non-informative, in contrast to the inverse Wishart (see Huang and Wand, 2013), but still conditionally conjugate on the expanded space. We placed the same prior scale ($\boldsymbol{\zeta} = \mathbb{I}$) on all of the elements of the variance-covariance matrix. We set the number of degrees of freedom to the number of functional types, $s = 10$, which is the value placing marginal uniform distributions on the correlation parameters of the covariance matrix, $s \sim \mathcal{U}(0, 1)$.

With $s = 10$ functional types, and having induced dissipativity in the dynamics ($\alpha_{ii} =$ in Eqn. 5.2.3), there are $s(s$ - $1)$ inter-type interactions to estimate in matrix $\mathbf{A}$ of Eqn. 5.2.3; that is, 90 parameters in the off-diagonal, where $\alpha_{ij} \neq \alpha_{ji}$. It is known that serious practical parameter identifiability problems may arise with such high dimensional systems (Cole, 2020). Bayesian regularization techniques (e.g., Mutshinda, O'Hara, and Woiwod, 2011; Almaraz et al., 2012; Piironen and Vehtari, 2017) provide strategies to deal with the presence of sparse parameter compositions, namely a set of parameters of weak or effectively null value that may correlate during posterior simulation with other parameters and destroy identifiability (e.g, Machta et al., 2013; Chis et al., 2016; Cole, 2020). We took advantage of the abil-

ity of the Gibbs algorithm to sample from discrete distributions and use Stochastic Search Variable Selection (SSVS; George and McCulloch, 1993), also known as Spike-and-Slab priors (Piironen and Vehtari, 2017; Almaraz et al., 2022), to regularize the **A** matrix. Interestingly, while regularizing the inter-type alpha matrix, SSVS also allows the assignment of posterior probabilities to the constellation of interaction networks compatible with the observed data. See the next sections for further details.

Posterior probabilities of interaction. The prior distribution of the inter-type interaction coefficients were specified as:

$$\alpha_{ij} \sim \mathcal{N}(0, \nu_{ij}^2) \tag{5.2.10}$$

The hyperprior for the variance of the parameter, ν_{ij}^2, is further modeled as:

$$\nu_{ij}^2 = (1 - p_i) \times \gamma_0^2 + p_i \times \gamma_1^2 \tag{5.2.11}$$

were p_{ij} is the probability that a given inter-type interaction parameter is included in the model, while the auxiliary variables γ_0^2 and γ_1^2 are the variance when the parameter is either not-included or included in the model, respectively. We set these variances to $\gamma_0^2 = 10^{-3}$ and $\gamma_1^2 = 100$. The probability of inclusion of a given parameter, p_i, is given a Bernoulli distribution,

$$p_i \sim \text{Bern}(\rho) \tag{5.2.12}$$

where ρ is the prior probability of inclusion of the inter-type interaction parameters. The Bernoulli distribution is a discrete distribution, and can only take two values, either 0 or 1. In previous approaches a given constant was used as the prior ρ (see Almaraz and Oro, 2011; Mutshinda, O'Hara, and Woiwod, 2011; Almaraz et al., 2012). Here, we used a weakly informative beta distribution for ρ to let the model learn from sparsity during the posterior simulation, $\rho \sim \text{beta}(2, 2)$. The beta distribution is a family of distributions defined on the continuous interval $[0, 1]$. They are parameterized by two shape parameters, and it is the conjugate prior of the Bernoulli distribution (Gelman et al., 2020). In our case, we used a $\text{beta}(2, 2)$, which is a weakly informative prior centered on 0.5.

If the probability of inclusion p_i of a given inter-type interaction parameter α_{ij} is 1 during the simulation, according to ρ, this parameter is active and its variance (eqn. 5.2.11) becomes $\nu_{ij}^2 = p_i \times \gamma_1^2 = 100$. The prior is then automatically set to $\alpha_{ij} \sim \mathcal{N}(0, 100)$. This is the slab. On the other hand, if the probability of inclusion p_i of an inter-type interaction parameter is 0, this parameter is inactivated: $\nu_{ij}^2 = (1 - p_i) \times \gamma_0^2 = 10^{-3}$, and then the prior for the parameter is converted into $\alpha_{ij} \sim \mathcal{N}(0, 10^{-3})$. This is the spike. During the posterior simulation, those inter-type interaction parameters α_{ij} significantly affecting the posterior distribution will more often be in an activated

state. Therefore, the posterior probability of inclusion of a given parameter in the model is simply the proportion of times that the parameter was activated during the MCMC simulation (the number of times that $p_i = 1$). This posterior probability can be compared to the posterior probability of inclusion, ρ, which is common to all parameters. A Bayes factor, BF_i, (Kass and Raftery, 1995; Almaraz and Oro, 2011; Mutshinda, O'Hara, and Woiwod, 2011) can then be calculated for every inter-type interaction parameter in matrix **A**:

$$\mathrm{BF}_i = \frac{p_i}{1 - p_i} \times \frac{\rho}{1 - \rho} \tag{5.2.13}$$

According on the Kass-Raftery scale (Kass and Raftery, 1995), it is possible to evaluate the evidence in favor of the inclusion of a given inter-type interaction parameter in the Lotka-Volterra-Ricker state-space model (Egn. 5.2.3) based on its Bayes factor.

The architectures of interaction networks. The Spike-and-Slab prior, as implemented above in a SSVS scheme (George and McCulloch, 1993, 1997), performs a stochastic search through the model space during MCMC simulation (Fragoso, Bertoli, and Louzada, 2018). Due to the inclusion of the binary auxiliary variables γ in eqn. 5.2.11, during each iteration a matrix Γ will multiply the matrix **N** containing the variances (ν_{ij}^2) of the inter-type interaction parameters α_{ij}, $\Gamma \circ \mathbf{N}$. Note that, by model construction, $diag(\Gamma) = 1$. After a burn-in period, this means that during the MCMC simulation the Gibbs sampler will be selecting the set of indicator matrices Γ that tend to increase the joint posterior probability of the Lotka-Volterra-Ricker state-space model (Eqn. 5.2.3). In other words, of all the possible combinations of inter-type interaction parameters α_{ij}, the SSVS scheme will provide the suite of matrices Γ, representing the presence/absence of interactions, that most likely explain the observed pattern of temporal variation in community biomass.

Interestingly, rather than just providing a posterior estimate for the alpha matrix **A**, the SSVS scheme provides an estimate of **A** weighted by the individual probabilities of observing any inter-type interaction α_{ij}, as encoded in the posterior matrix Γ. This allows for the construction of two new objects. Firstly, a network of posterior probabilities of inter-type interactions. This is conceptually similar to a weighted connectivity matrix, where the weights are the probabilities of each inter-type interaction being active during the MCMC simulation. Secondly, it is straightforward to build the constellation of posterior interaction networks compatible with the observed pattern of community biomass fluctuations. In this constellation, the probability of a given architecture of interaction network is proportional to the frequency of this architecture in the posterior probability distribution, as encoded in its matrix Γ.

Model adequacy and parameter identifiability. To assess model adequacy we conducted posterior predictive checks with the fitted model (see Gelman et al., 2020). We generated predicted time series of community biomass from the posterior distribution during the MCMC iterations:

$$\hat{\mathbf{y}}_t \sim \mathcal{N}(\mathbf{n}_t, \mathbf{T}) \tag{5.2.14}$$

where $\hat{\mathbf{y}}_t = (\hat{y}_{1,t}, \cdots, \hat{y}_{s,t})^T$ is the vector of log_e posterior predicted population abundances of each functional type s (see Fig. 5.1).

While the Lotka-Volterra-Ricker state-space model (Eqn. 5.2.3) is structurally identifiable (Bellman and Åström, 1970; e.g., all parameters are conditioned on data), practical identifiability might become an issue in high-dimensional systems: in these scenarios, the ratio of estimable parameters to available data might be exceedingly large (Chis et al., 2016; Villaverde, 2019). To check for potential issues with practical parameter identifiability of the proposed modelling approach, we checked for parameter redundancy and sloppiness (Brown and Sethna, 2003; Gutenkunst et al., 2007; Chis et al., 2016; Villaverde, 2019; Cole, 2020; Monsalve-Bravo et al., 2022). If a model is weakly identifiable in practice, large posterior cross-correlations among parameters should become apparent during MCMC simulations. Since there are potentially $s(s\text{-}1)$ inter-type interactions (90 parameters), we produced heatmaps of cross-correlation among all the α_{ij}'s. Due to the sparsity-inducing SSVS scheme, it might be expected that these posterior cross-correlations should be weak. Additionally, sloppiness (Brown and Sethna, 2003) refers to the situation in which the posterior distribution is highly sensitive to perturbations of so-called stiff parameters, but otherwise insensitive to sloppy (practically unidentifiable) parameters. Sloppiness is then defined as a gap in the eigenvalue spectra of the Fisher's Information Matrix (FIM; Chis et al., 2016; Villaverde, 2019): stiff parameters are associated to large eigenvalues, while sloppy parameters are linked to small eigenvalues. The FIM is an approximation to the Hessian of the log-likelihood function, and it is also approximated (as a lower bound, Chis et al., 2016) by the inverse of the posterior parameters covariance matrix. In the extreme case of a structurally unidentifiable model, the FIM is theoretically singular, and no inverse is available. For a structurally identifiable model, sloppiness is regarded as significant when the ratio ($\mathcal{C}_{\mathcal{F}}$) of the smallest eigenvalue of the FIM to the largest eigenvalue is smaller than three orders of magnitude (Chis et al., 2016):

$$\mathcal{C}_{\mathcal{F}} = \frac{\lambda_{\min}}{\lambda_{\max}} \lesssim 10^{-3} \tag{5.2.15}$$

and in this case the model is regarded as weakly identifiable in practice (Chis et al., 2016).

The Lotka-Volterra-Ricker state-space model was written in the JAGS language (Plummer, 2003), compiled in `C++` languaje, version 4.3.0, and interfaced with the `R` environment (version 4.2.2,

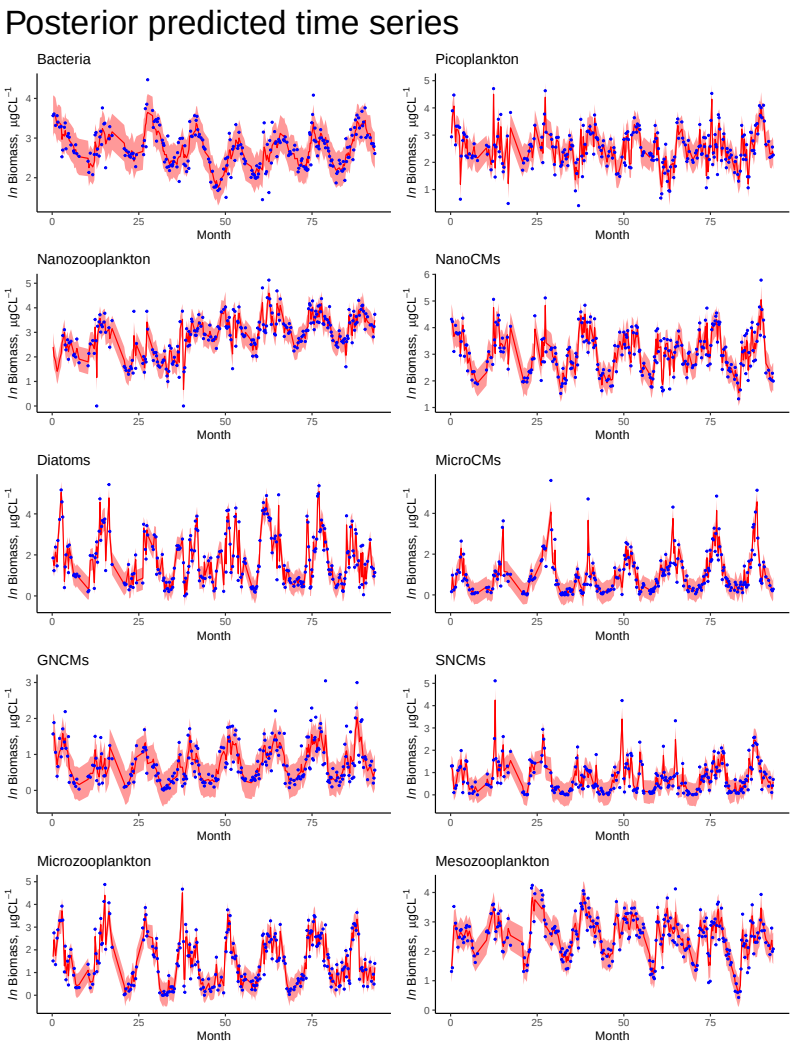

Figure 5.1: Posterior Predicted Checks performed with the stochastic formulation of the Lotka-Volterra-Ricker model shown in Eqn. 5.2.3 fitted to the community time series of the plankton community. Blue dots • denote the biweekly measured abundances for each functional type, and red lines ─ denote the posterior predicted average of 3000 synthetic biomass time series for each functional type. Red shaded regions contains the 90% HDI of the posterior predictions for each type.

RCoreTeam, 2021). The `runjags` package (Denwood, 2016) was used to parallelize the estimation. Posterior estimates for parameters, latent states, and missing data were obtained with three independent chains, after discarding the first 4×10^5 iterations as burn-in. Standard diagnostic tests (see Gelman et al., 2020) were conducted to assess the convergence of the chains to a stationary distribution, using the package `ggmcmc` (Fernández-Marín, 2016). When summarizing the posterior distribution, we will give the Maximum A Posteriori probability estimates (MAP) and the 90 % Highest Density Intervals (HDI), (MAP [HDI]), using the `bayestesR` package (Makowski, Ben-Shachar, and Lüdecke, 2019).

5.3 Results

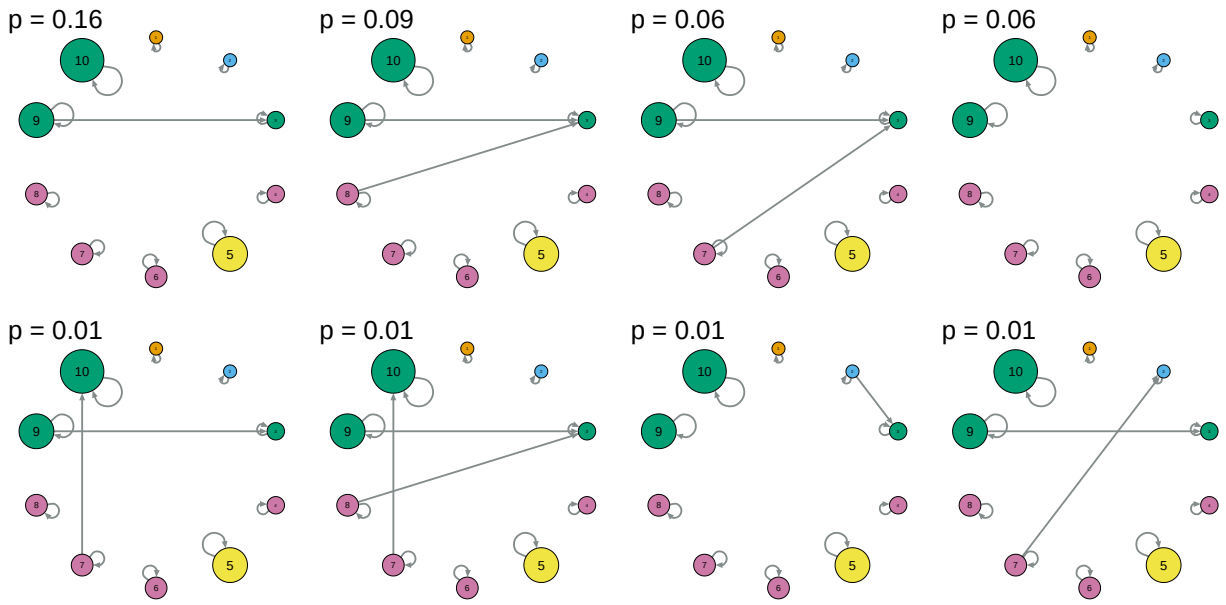

Figure 5.2: Most probable network architectures, with individual probabilities of observing a particular topology denoted with p above each graph. Nodes are functional types, with size proportional to plankton size class, and edges stand for the directed interactions between pairs of nodes (see legend in Fig. 5.3 for the color and numeric identification of nodes). Self-loops stand for intra-specific (intra-type) interactions. By model construction, their probability is 1.

5.3.1 *Model adequacy and calibration*

The posterior predicted time-series of community biomass simulated from the fitted bayesian Lotka-Volterra-Ricker state-space model (Eqn. 5.2.3) agree very well with the observations derived from the RV Plymouth Quest (Figure 5.1). Except for the most extreme observations, that in some cases fall beyond the credible intervals, the average posterior simulated values are strongly correlated with the true observations. This indicates that the fitted model does not display a pathological behavior.

The heatmap for the posterior cross-correlation in the estimation of the inter-type interaction coefficients, α_{ij}, is shown in Fig. S5.8 in the Supplementary Material). The cross-correlation among parameters was negligible in all cases. However, the degree of sloppiness of the matrix $\mathbf{A}$ is of 6.7% (Fig. S5.9 in the Supplementary Material); this suggests that the posterior estimation of matrix $\mathbf{A}$ is likely insensitive to variation in some interaction coefficients, that may be only weakly identifiable.

5.3.2 *Characterizing the emerging network architecture*

The constellation of posterior network architectures compatible with the observed community dynamics, as selected by the SSVS algorithm, is composed of 1047 networks of differing topologies. Of these, 16 % of the networks selected during the MCMC simulation conform to a topology with only inter-type interactions (Fig. 5.2): Microzooplankton on Nanozooplankton. Interestingly, a completely sparse topology (only intra-type interactions) or a completely saturated one (all inter-type interactions present) were virtually unrepresented (only 1 out of 1047 topologies for each one). The remaining topologies always included at

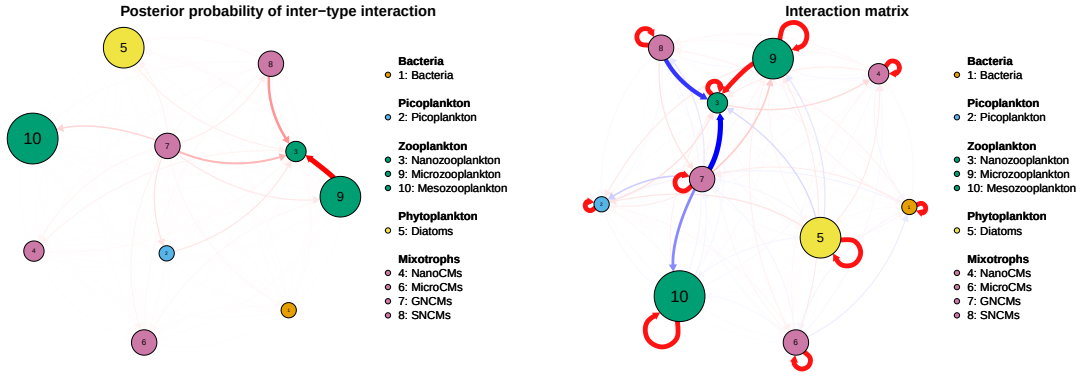

(a) Posterior probability of inter-type interaction

(b) Interaction matrix.

Figure 5.3: In (**a**), Network of posterior probability of interactions, constructed with the marginal probabilities of interactions across the 1047 posterior networks explored by the SSVS algorithm. Arrows (edges) indicate the direction of the effect and its magnitude (thickness), from 0 to 1. For clarity, self-loops are omitted (their probability is 1 by model construction). In (**b**), network of interactions as expressed in the interaction (alpha) matrix. Interactions are depicted as directed arrows. In this figure, blue arrows denote a positive effect (negative α_{ij}), while red arrows denote a negative impact (positive α_{ij}); arrow thickens depicts the relative magnitude of the effect. Size of nodes is proportional to size of the plankton class, and colors identify different trophic classes.

least one inter-type interaction. The most abundant topology is one including 4 inter-type interactions (31.33 % of the explored networks; see Fig. 5.10 in the Supplementary Material). Overall, the emerging probability of observing at least one interaction across the posterior constellation of network topologies, conditioned on the observed data, is of 99.99 %.

5.3.3 *Estimation of inter-type interactions and environmental effects*

In spite of a relatively informative prior distribution for the probability of inclusion of interactions, the posterior matrix $\mathbf{A}$ was very sparse (see Fig. S5.11 in the Supplementary Material): the posterior distribution of the probability of inclusion of inter-type interactions (p_i in Eqn. 5.2.12) in the community dynamics model had a maximum posterior mode of (0.035 [0.008, 0.087]). Indeed, out of a potential number of 90 inter-type interactions, only 8 yielded a Bayes Factor worth mentioning (Fig. S5.12 in the Supplementary Material). Of these, only the interactions among Nanozooplankton, GNCMs, SNCMs, Microzooplankton, Mesozooplankton had a decisive support conditioned on the observed data.

These interactions can be explored in the network of posterior probability of interactions (Fig. 5.3a). A small-world of a strongly interactive sub-module is evident for these species, with Nanozooplankton as the keystone species: according to the interaction matrix (Fig. 5.3b), there is a strong positive impact of both GNCMs and SNCMs on the growth rate of Nanozooplankton, while the impact of Microzooplankton on Nanozooplankton is negative. The positive impact of SNCMs on Mesozooplankton is weaker, but non-negligible according to the Bayes Factor (Fig. S5.11 in the Supplementary Material). Interestingly, no impact of Nanozooplankton on other functional types emerge from the community matrix: no outgoing arrow was detected from this functional type.

Figure 5.4 shows the impact of measured environmental variability on growth rate of each functional type. In general, the effects of nutrients and temperature were strong and negative for all functional types, with all other variables having a mixed, generally weak, effect.

Interestingly, only the dynamics of heterotrophic bacteria and generalist non-constitutive mixotrophs (GNCMs) were largely independent of nutrients and temperature. Temperature, indeed, had a negative impact on the biomass and availability of all nutrients, which were strongly correlated among them. This is expected from oceanographic conditions (see Discussion).

The cross-covariation of the biomasses of functional types in the fluctuations of the common environment, as measured through the environmental stochastic effects (the matrix Σ in 5.2.3) is positive in nearly all cases (See Fig. S5.14 in the Supplementary Material).

5.3.4 *Stability, feasibility and coexistence of the community*

The equilibrium of the linearized Lotka-Volterra-Ricker state-space model was dynamically stable with a very large probability (effectively 99.85 %, Fig. 5.5a): nearly all of the posterior estimated dominant eigenvalues of the Jacobian 5.2.5 fall within the unit circle. However, it is interesting that the posterior distribution of dominant eigenvalues is nevertheless close to the nonhyperbolic case, where the eigenvalue is 1. This drives the system close to instability, and induces a relatively slow resilience (1.036 [1, 1.065] t^{-1}, see Fig. 5.5). This also determines a reactivity with a strongly positively skewed distribution (Fig. 5.6): although the maximum posterior mode was negative, the posterior distribution included a large mass of positive values (-0.045 [-0.126, 1.064]; the 66 % of the distribution included positive values). This indicates that the system is largely reactive: perturbations of the initial conditions are initially propagated, although asymptotically absorbed. This is also in agreement with the relatively low stochastic invariability, or structural stability, of the system (0.003 [0.0002, 0.090]). Both the dynamical and structural stabilities of the systems are thus sensitive to perturbations of either the initial conditions or system parameters.

The relatively large sensitivity of the system to perturbations is also expressed in the bimodal distribution of the departure from normality of the alpha matrix $\mathbf{A}$ (Fig. 5.6). The posterior dominant mode is above 1, (1.223 [0.283, 1.303]), but there is a second mode at 0.496. Therefore, while this provides evidence that the matrix $\mathbf{A}$ is highly sensitive to perturbations, the second mode indicates that the SSVS explored with a large probability model spaces with large robustness to perturbations. Indeed, the posterior entropy of $\mathbf{A}$ is nearly maximal (0.982 [0.791, 0.995]), which suggests that the complexity of the interaction pattern is also maximal. This is in accordance with the large dynamic dimensionality (9.940 [9.878, 9.975]) of the linearized system, which suggest that there are no specific sensitive perturbation directions in which the system is particularly fragile. The posterior correlations among the metrics of stability suggest an interesting pattern (Fig. S5.13 in the Supplementary Material): increases in entropy are strongly and negatively correlated with reactivity, and strongly and positively (although nonlinearly) correlated with structural stability. The pattern of posterior cross-correlation with departure from nor-

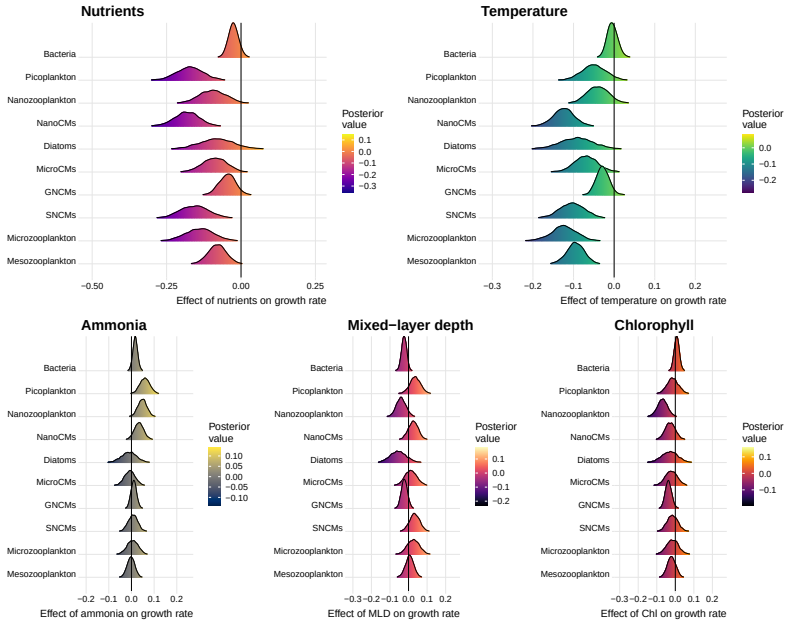

Figure 5.4: Posterior distribution of the environmental effects on the growth rate of each plankton functional type. All values correspond to the measured environment at a depth of 10 m. The variable nutrient includes nitrates, silicate and phosphate. These three variables were strongly positively correlated (Fig. S5.7) Units: Nutrients, Ammonia, μM: Chlorophyll: μC L^{-1}; Temperature, ^{o}C; Mixed-layer depth: m.

mality is the opposite. Note that these are cross-correlations among posterior generated quantities.

With respect to the metrics of coexistence, the probability of feasibility is also close to 1 (Fig. 5.5b). This means that, at equilibrium, the linearized system is saturated with all functional types, even though the posterior estimated abundances and carrying capacities vary largely. However, the posterior estimated robustness of coexistence of the community is centered around 1 (1.001 [0.963, 1.042], 5.6). This suggests that coexistence is indeed relatively sensitive to perturbations. In particular, the posterior vector of equilibrium abundances included some negative values for MicroCMs, GNCMs and SNCMs, compatible with extinction (Fig. 5.5b).

5.4 Discussion

Our findings revealed that a small-world mixotrophic interaction ensemble in a temperate coastal ecosystem drove a plankton food web to the edge of instability in an otherwise feasible community (Figs. 5.5 and 5.3). This is of particular importance considering the effect of trophic position and diversity on fluctuations and extinctions in natural communities (Segura et al., 2017; Gerhard, Mori, and Striebel, 2021; Selaković, Säterberg, and Heesterbeek, 2022). Thus, our analysis on diverse trophic modes contributes to the broad literature that seeks to understand how competition drives species coexistence (Tilman, 1987; McCann, 2010; Levine and HilleRisLambers, 2009; Segura et al., 2013). An interesting finding suggests that an increase in the complexity of the pattern of mixotrophic interactions reduces the reactivity and increases the structural stability of the system (Fig. S5.13 in the Supplementary Material).

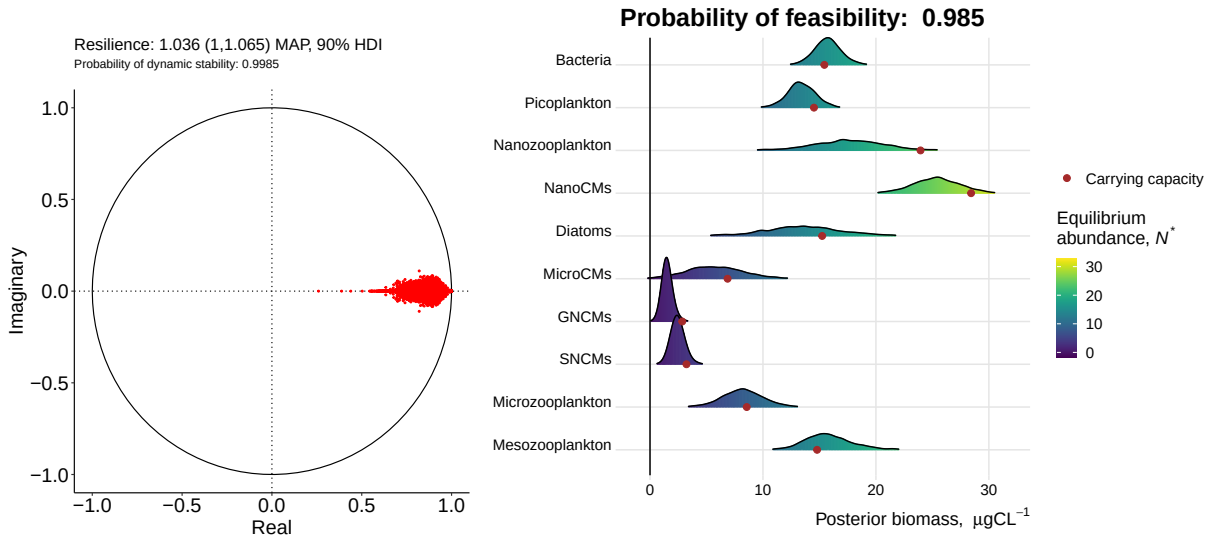

(a) Eigenvalues in the complex plane

(b) Probability of feasibility

Figure 5.5: In (**a**), the posterior eigenvalues of the Jacobian 5.2.5 matrix are shown in the unit circle of the complex plane. The probability of stability is the fraction of eigenvalues strictly smaller than 1 in the posterior distribution. In (**b**), the posterior distribution of each component of the equilibrium vector $\mathbf{N}^*$ is shown for each functional group; for comparison, the MAP estimate for the carrying capacities are shown as red circles. The probability of feasibility is the fraction of posterior estimates of the equilibrium vector that are strictly positive.

Mixotrophy was the core of the interaction set of the analyzed plankton food web. Plastic responses promoted by mixotrophy can lead to asynchrony which tends to stabilize biological systems. Overall, we found that intraspecific interactions were stronger than interspecific interactions at the equilibrium (Figs, 5.3. This result was expected according to theory that predicts intraspecific interactions to be more important in highly connected and diverse communities (Barabás, J. Michalska-Smith, and Allesina, 2016). It is well recognized that species (or functional groups) can evolve to use different resources to decrease interspecific competition (e.g., Moosmann et al., 2021). This is clearly shown in our plankton food web, in which diverse trophic strategies and cell sizes result in weak interspecific interactions in the long-term. However, competition can also drive diversification within functional groups (Svanbäck and Bolnick, 2007). In fact, one can expect high trait diversity within a single plankton functional type (Kruk et al., 2010; Kruk et al., 2011; Irwin et al., 2015). This can in part explain why mixotrophic species fall within a continuum of nutritional modes from mainly autotrophy to heterotrophy (Stoecker et al., 2016; Leles, 2019).

Our analysis also revealed a "small world" interaction between a mixotroph and two heterotrophs that drives the system towards instability (Figs. 5.5 and 5.3). Interestingly, this seems to agree to our second prediction which is based on mixotrophy promoting stronger interactions between functional groups which, in turn, likely act decreasing the stability of the system. Small world patterns are characterized by most functional groups being weakly connected except for a few that are highly linked (Dunne, Williams, and Martinez, 2002; Sinha, 2005). These can be widespread in diverse and complex food webs in nature and they have been suggested to promote fast responses to perturba-

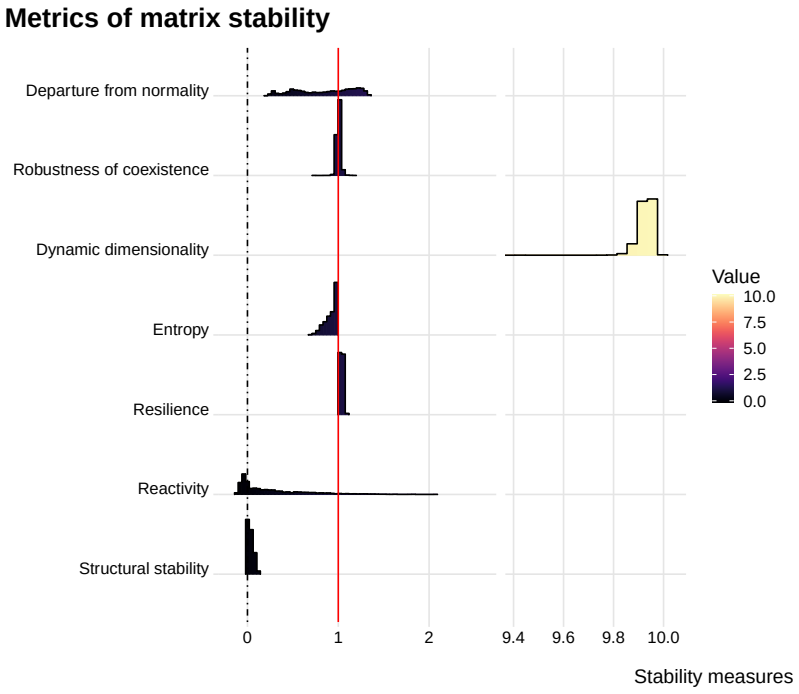

Figure 5.6: Posterior distribution of the different metrics of matrix stability and community coexistence.

tions (Montoya, Rodríguez, and Hawkins, 2003). The "small world" observed on this study involved heterotrophs and a non-constitutive mixotroph within the nano- and microplankton size classes. These groups correspond to the main consumers of primary production in the oceans (Schmoker, Hernández-León, and Calbet, 2013). By being smaller and having growth rates similar to their prey, nano- and micro- grazers can take advantage of an often-limited environment and respond quickly to increases in primary production (Schmoker, Hernández-León, and Calbet, 2013).

The interactions among the functional groups within the "small world" can be interpreted looking at size differences and trophic strategy. The small world comprised the nano- and micro- zooplankton and the generalist non-constitutive (GNCMs) and specialists (SNCMs) mixotrophs. While all four of them compete for the smallest prey in the food web (picoplankton), nanozooplankton are also an accessible prey to the micro grazers, i.e., microzooplankton, GNCMs and SNCMs. This explains the observed negative impact of microzooplankton on nanozooplankton. The positive impact of GNCMs and SNCMs on nanozooplankton can be related to mixotrophy. The predation impact of GNCMs on nanozooplankton can be expected to be smaller than that of microzooplankton for two reasons. First, GNCMs engage on phototrophy to support part of their respiratory demands (Stoecker et al., 2016 and references therein), which can alleviate the need to consume prey. Second, they are obligate mixotrophs and need to constantly acquire new chloroplasts from their autotrophic prey to photosynthesize since they are not able to keep acquired chloroplasts for

more than a few weeks (McManus, Schoener, and Haberlandt, 2012). This suggests that they might preferentially consume autotrophic prey vs heterotrophic prey (Dolan and PÉrez, 2000). However, our results represent the long-term response of the food-web at equilibrium, and it is known that ecological interactions can fluctuate over time (Deyle et al., 2016; Cenci and Saavedra, 2019).

Functional differences among mixotrophs were found to be important to understand the impact of mixotrophy in the stability of the system, particularly to identify the small world pattern. In addition, constitutive forms seem to be under stronger self-regulation and environmental control compared to generalist non-constitutive forms and their heterotrophic competitors. Specifically, mixotrophic and heterotrophic nanoplankton seem to be playing slightly different ecological roles, which could help to explain their persistence across the global oceans (Edwards, 2019; Leles, 2019). Among non-constitutive mixotrophs, we found that specialist forms are under strong self-regulation, particularly when compared to generalist mixotrophs. Generalist forms rely on diverse types of prey to acquire chloroplasts and, contrary to specialists, tend to be mainly heterotrophic (Mitra et al., 2016). This agrees with theory which predicts that diversifying resources can decrease intra-specific interactions (e.g., Svanbäck et al., 2008; Svanbäck and Bolnick, 2007).

Regarding other functional groups, heterotrophic bacteria and diatoms were found to be under strong self-regulation and/or highly influenced by stochasticity. For instance, bacteria are quite insensitive to what is happening to the rest of the food web. This is expected due to their metabolism, which is driven mainly by organic material dynamics, depending on the quality, size and how labile the organic matter is, as well as bacterial community diversity (Enke et al., 2018). Diatoms were the type most affected by stochasticity, which can be explained by their strategy of achieving the highest growth rates, their dependence on silicate to growth, and their investment on defense traits which can alleviate predation (Litchman et al., 2007; Grønning and Kiørboe, 2020).

The stability of our food web system did not seem highly influenced by measured abiotic factors. On the other hand, environmental stochasticity accounted for nearly half of biomass variability across functional types. This is a common result when analyzing plankton food webs through inverse methods (Griffiths et al., 2016; Barraquand et al., 2018). Additionally, environmental synchrony in the response to the common environment was strongly and significantly positive for nearly all functional types (Fig. S5.14 in the Supplementary Material), and this suggests that shared unmeasured niche dimensions are inducing a significant covariation in the temporal fluctuations of plankton biomass. The patchy nature of plankton assemblages in the oceans, the role of advection transporting cells horizontally, sinking rates, and

plankton vertical migration in the water column are all sources that enter inverse model in the form of stochastic fluctuations. Still, one could expect a bigger role of abiotic factors considering how plankton communities are tightly linked to their physico-chemical environment (Reynolds, 2006; Sommer and Lewandowska, 2011). As mentioned previously, our results are the long-term response of the food web at equilibrium. However, ecological interactions are known to vary in time and space due to environmental fluctuations (Deyle et al., 2016; Cenci and Saavedra, 2019; Kortsch et al., 2019). Considering how mixotrophy is modulated by environmental conditions, future studies focusing on fluctuating interactions could ultimately define the direction of its impact on the stability of food webs. This is particularly relevant considering their different seasonal patterns and functional roles across gradients of oceanographic conditions (Leles et al., 2021). As the open oceans get warmer and more stratified and coastal seas continue to be heavily impacted by eutrophication, mixotrophy is expected to be even more dominant across microbial communities (Burkholder, Glibert, and Skelton, 2008; Stoecker et al., 2016). Ultimately, assigning multi-trophic interactions and diverse trophic modes will be critical to understand how communities will respond to climate change and affect ecosystem functioning.

Overall, our analysis showed the importance of analyzing biological communities beyond the lens of producers or consumers, acknowledging how diverse trophic modes modulate the persistence of communities. Mixotrophy was found to be key to promote the long-term stability of a plankton food web, but it was also part of a "small world" pattern that could drive the system towards instability. Acknowledging multi-trophic interactions and the functional differences among mixotrophs was key to interpret how mixotrophy affected the stability of our system.

5.5 Supplementary Material

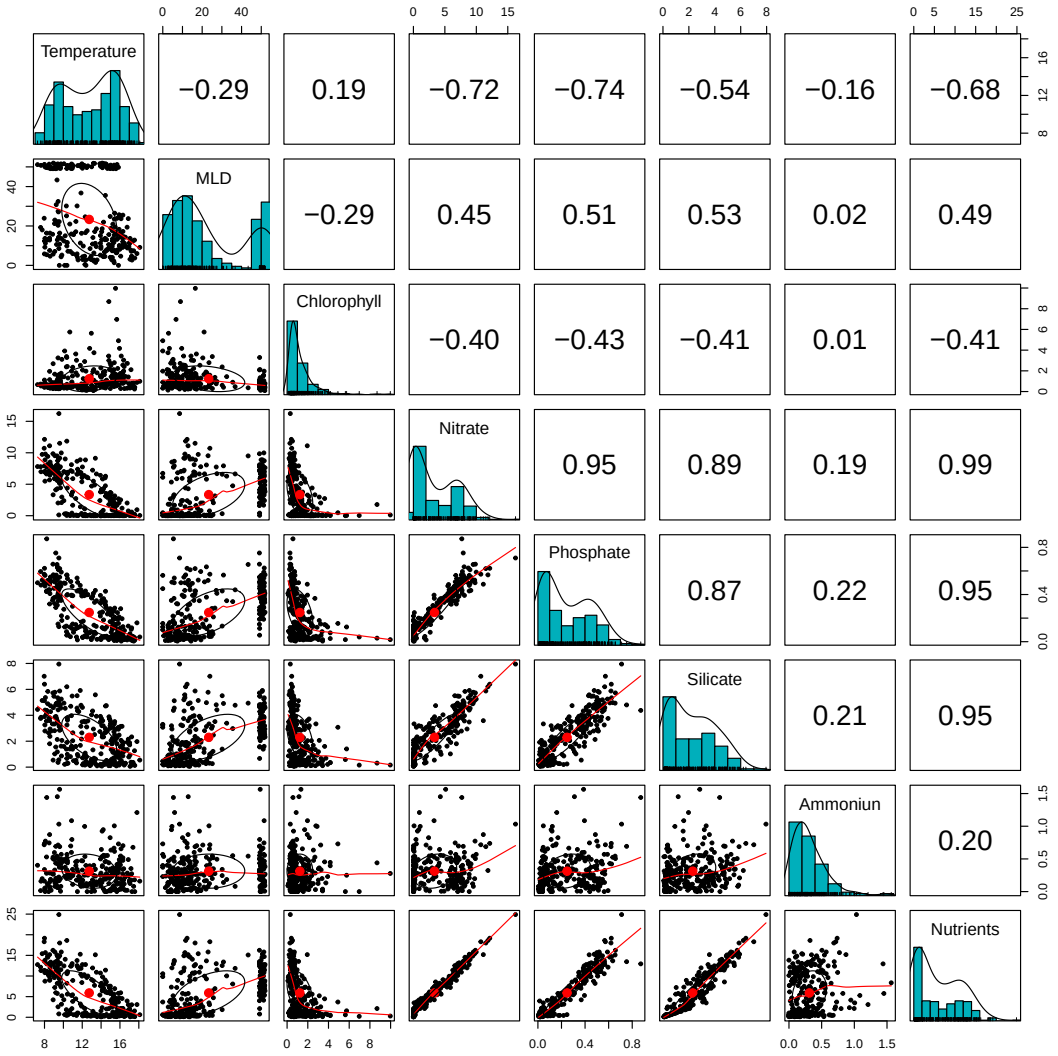

Figure 5.7: Matrix of posterior cross-correlations among the environmental variables measured in the study area at a depth of 10 m. Bivariate scatter plots are shown below the diagonal, histograms on the diagonal, and the Pearson correlation above the diagonal. The robust regression fittings through LOESS smoothed regressions are shown in red, while the correlation ellipses are shown in black with the centroid in red.

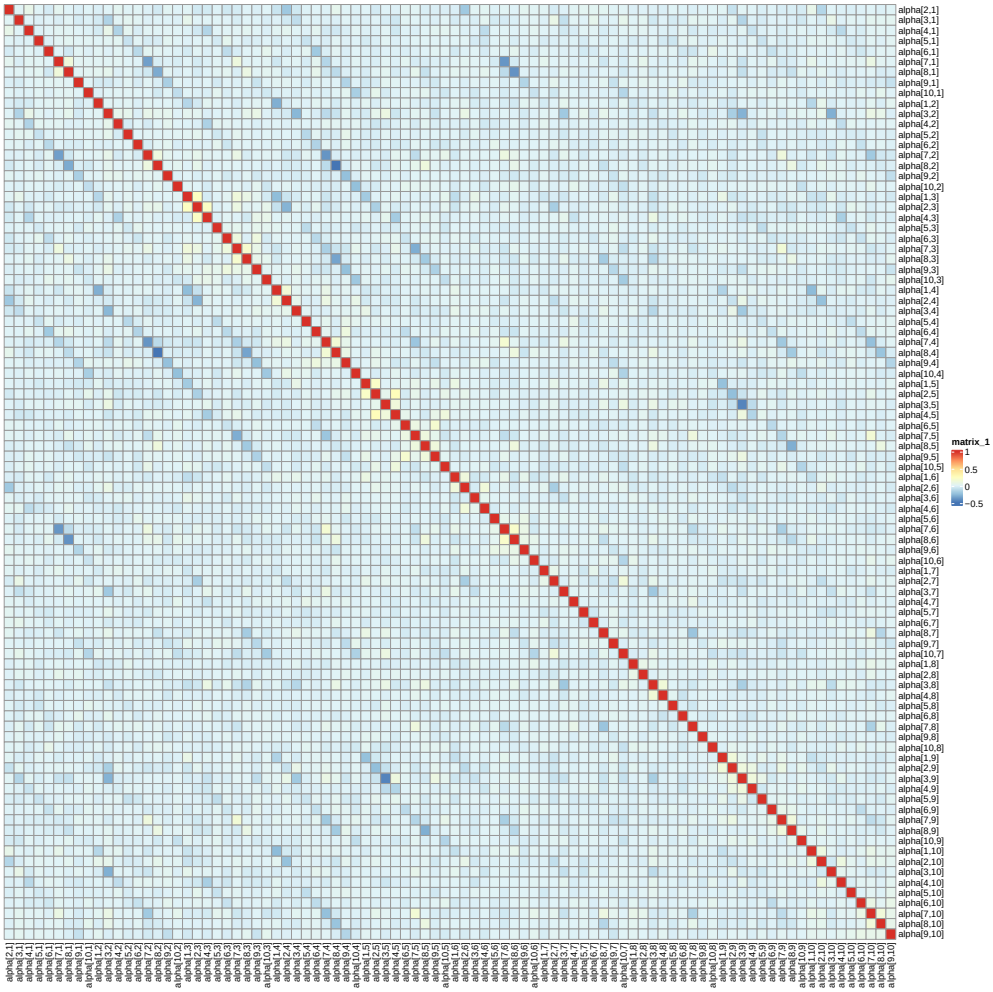

Figure 5.8: Heatmap of the posterior cross-correlation among the inter-type interaction coefficients, α_{ij}. The value of the main diagonal is 1, since it is the value for the correlation of a parameter with itself.

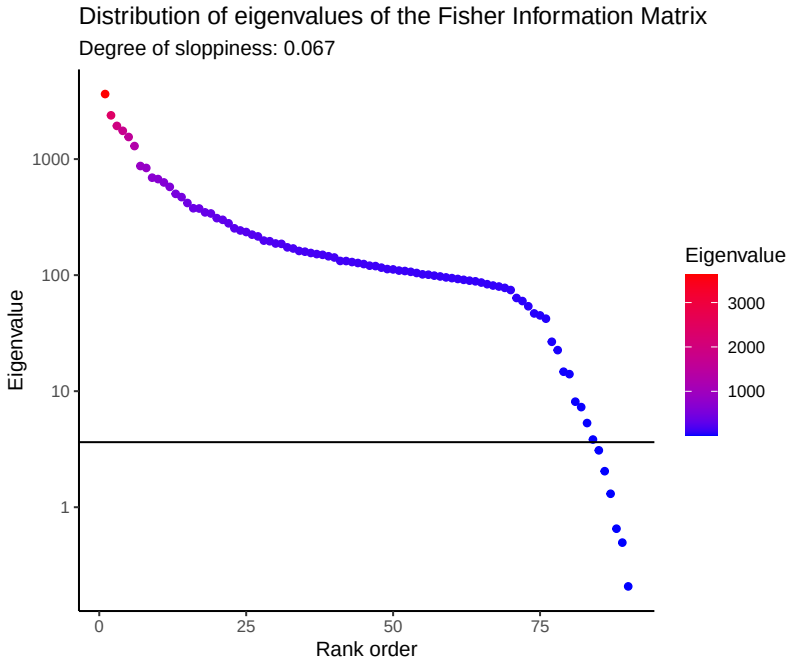

Figure 5.9: Rank distribution of the eigenvalues of the Fisher Information Matrix, estimated as the inverse of the covariance matrix of the inter-type interaction posterior matrix $\mathbf{A}$. The degree of sloppiness is calculated as the proportion of eigenvalues with a value at least three orders of magnitude smaller that the largest eigenvalue. This can be interpreted as the proportion of inter-type interaction coefficients, α_{ij}, with a negligible effects on the posterior estimation.

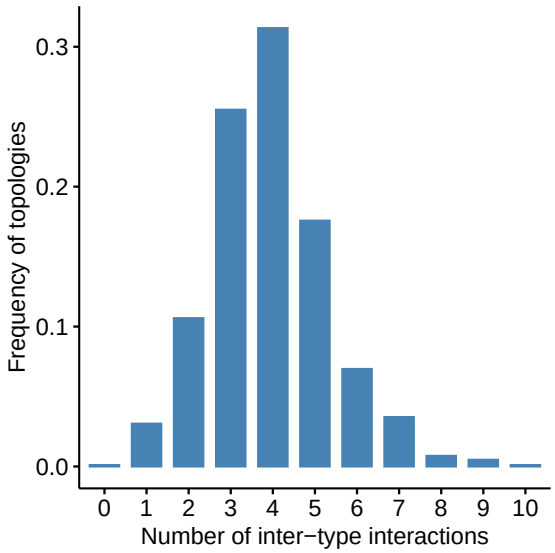

Figure 5.10: Frequency in the posterior distribution of the network topologies with different numbers of inter-type interactions, selected by the SSVS in the search through the model space.

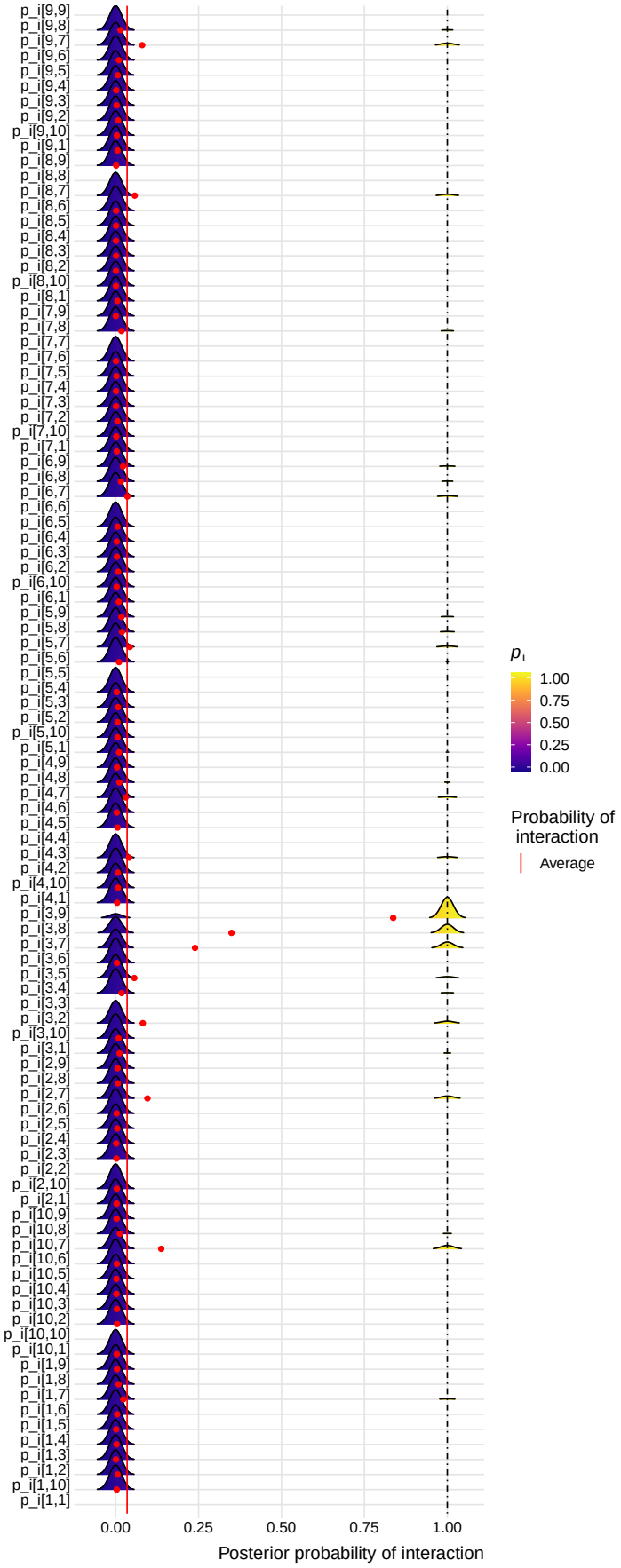

Figure 5.11: Posterior distributions of the probabilities of inclusion of every coefficient of inter-type interaction, p_i (Eqn. 5.2.12). Since p_i follows a Bernoulli distribution, during the MCMC simulations this parameter takes only values of 0 or 1. Therefore, the posterior distributions of those inter-type interactions, α_{ij} with a large probability, will be shifted to 1. Conversely, those parameters with a negligible effect will be shifted to 0. Red dots indicate the posterior average of the Bernoulli process, and the vertical red line is the posterior value of ρ, the probability of inclusion of the inter-type interaction parameters (see Eqn. 5.2.12).

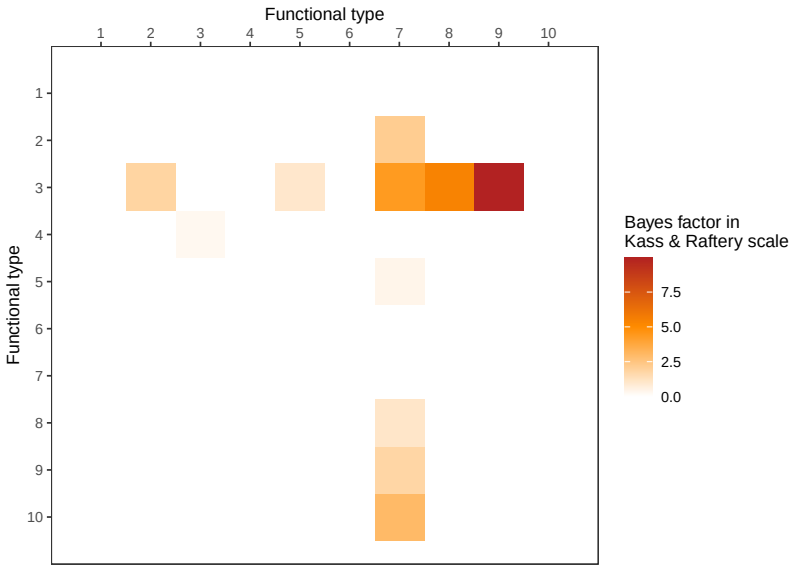

Figure 5.12: Matrix of Bayes Factors of inter-type interactions in matrix **A**, colored according to the Kass and Raftery, 1995 scale. Colored positions in the matrix refer to the degree of support in the posterior distribution. Only 8 out of 90 interactions yielded a factor worth mentioning. In particular, interactions among Nanozooplankton (3), GNCMs (7), SNCMs (8), and Microzooplankton (9) had a decisive support conditioned on the observed data.

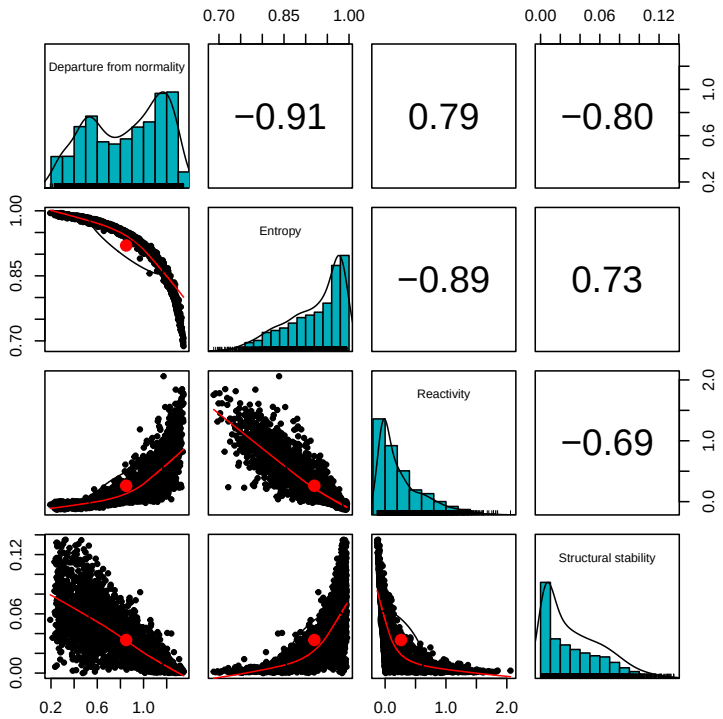

Figure 5.13: Matrix of posterior cross-correlations among departure from normality, entropy, reactivity and structural stability. Bivariate scatter plots are shown below the diagonal, histograms on the diagonal, and the Pearson correlation above the diagonal. The robust regression fittings through LOESS smoothed regressions are shown in red, while the correlation ellipses are shown in black with the centroid in red.

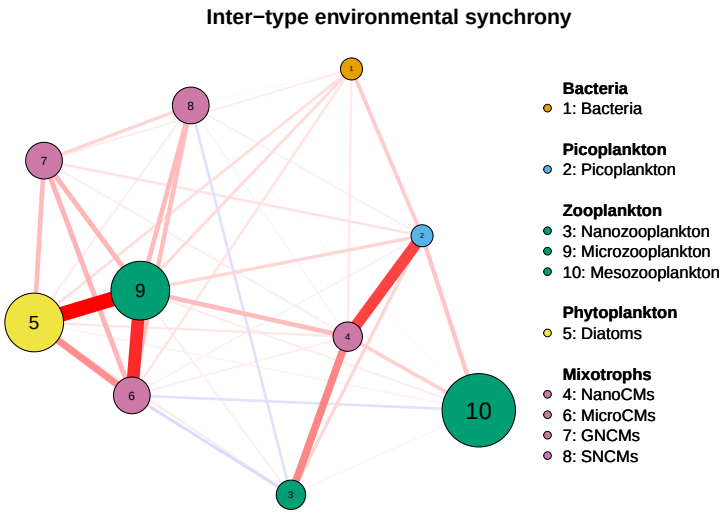

Figure 5.14: Inter-type environmental synchrony. Shown are the covariances between every pair of functional types in the response to the common environment, as measure by the off-diagonal terms of the matrix Σ in Eqn. 5.2.3. Red links denote positive correlation, blue stand for negative ones. Link thickness is proportional to the magnitude of covariation.

6 Alternative Stable States in the Dynamics of a Bird Community Triggered by a Planetary-Scale Environmental Catastrophe

Pablo Almaraz[1,2], Javier Bustamante[2], Miguel A. Rendón[2], Eduardo Aguilera[2], Andy J. Green[2]

1. Departamento de Ecuaciones Diferenciales y Análisis Numérico, Facultad de Matemáticas, Universidad de Sevilla, Sevilla, Spain.

2. Departamento de Ecología de Humedales, Estación Biológica de Doñana, CSIC, Sevilla, Spain.

6.1 Abstract

Until recently, standard environmental research was dominated by a focus on the asymptotic behaviour of ecological systems, but transient features, regime shifts and alternative stable states can have a profound effect on dynamics and persistence of natural ecosystems. Here, we show a strong non-stationary coupling of structural shifts in the environmental, anthropogenic and ecological subcomponents of one the world's major Mediterranean wetland ecosystems. Recurrent changes in the seasonal structure of rainfall prompted sudden reorganizations in community size, diversity and trends of a guild of 10 wintering waterfowl species during a 36-year period. A major ecological shift in 1992, correlated with a severe dry and cold period in the Northern Hemisphere induced by the catastrophic volcanic eruption of Mt. Pinatubo, prompted an abrupt shift to an alternative state that still persist today. Indeed, community size, and population size of most species, has not recovered since even though the external triggering variables did change, and the dynamical and structural stability properties of the wintering community are similar in both fluctuating states. A stochastic catastrophe model suggest that the spatiotemporal persistence of cold and dry conditions in the wintering areas, coupled with warm and wet conditions in the breeding grounds, is modulating local wintering conditions and subsequently inducing a shift in the global pattern of wintering philopatry. Our study provides evidence linking abrupt planetary-scale climatic changes to rapid reorganizations in the multi-decadal population and community dynamics of terrestrial vertebrates.

KEYWORDS alternative stable states, catastrophe theory, climate, community ecology, ecological disturbance, Mediterranean basin, regime shifts, volcanism.

6.2 INTRODUCTION

The stability of populations and communities in response to environmental perturbations is currently one of the most relevant research topics in the field of global change ecology (Bjornstad, 2001; Post, 2013; Vellend, 2016; Yang et al., 2019). In spite of early appreciation that ecosystems might operate under more than one stable state (e.g., Holling, 1973; May, 1977), the major focus of theoretical ecology is still dominated by the asymptotic stability of time-independent ecological models. However, a growing body of evidence suggests that many ecological systems might operate under nonlinear dynamics characterized by abrupt, transient shifts from one stable state to another usually preceded by tipping points (Fukami and Nakajima, 2011; Petraitis, 2013; Yletyinen et al., 2016; Rocha et al., 2018; Clements and Ozgul, 2018; Dakos et al., 2019; Chen et al., 2020). This behaviour, usually referred to as alternative stable states, is common in marine, freshwater and terrestrial ecosystems (Steele, 1996; Knowlton, 2004; Capon et al., 2015; Gsell et al., 2016; review in Rocha, Peterson, and Biggs, 2015).

In global change scenarios, understanding this non-linear behaviour is regarded as a major research goal (Rockström et al., 2009; Barnosky et al., 2012; Steffen et al., 2015; Nash et al., 2017). Progress in this field has to some extent been limited by semantic and statistical confusions on the specific mechanisms, processes and patterns involved in the characterization of alternative stable states (Suding, Gross, and Houseman, 2004; Capon et al., 2015; Kuiper et al., 2015). A regime shift denotes a statistical change in the parameters forcing a system, while a phase transition alludes to a change in the state of some attribute of the system (Scheffer, 2009). From this it follows that regime shifts should most of the times translate to phase transitions, but the detection of the latter does not necessarily demonstrate the existence of the former (e.g., Rudnick and Davis, 2003). Indeed, evaluating weather alternative states are stable is far from trivial (Scheffer, 2009; Stelzer et al., 2021). Alternative stable states give rise to hysteresis: under the same concurrent environmental conditions there may exist several stable states and, not only the present, but also the historical conditions explain the location of the system in that particular state (Scheffer, 2009; Clements and Ozgul, 2018).

The overall consequence of this is that the abrupt phase transitions detected within ecological time-series are not always explicitly linked to the regime shifts potentially triggering them, thus yielding a rather phenomenological understanding of alternative stable states and regime shifts (Hastings, 2004; Montoya, Donohue, and Pimm, 2018;

Hastings et al., 2018; Hillebrand et al., 2020). Thus, to date it is unclear how abrupt regime shifts at different levels of ecological organization are intertwined, and to what extent this non-linear behaviour stem from external disturbances or internal dynamics (Scheffer, 2009). For example, abrupt ecological disturbances have only recently been linked mechanistically to extreme climatic events, such as large volcanic eruptions and heavy hurricanes (e.g., Kuhnt et al., 2005; Schoener and Spiller, 2006; Vázquez-Loureiro et al., 2019; Osland et al., 2020). In particular, volcanism is regarded as one of the major perturbations not only to planetary climate (Osipov et al., 2021; Millán et al., 2022), but also to ecological systems at all organizational, temporal and spatial scales (Sadler and Grattan, 1999; Oppenheimer, 2003; Crisafulli et al., 2015; Jiang et al., 2022; Green, Renne, and Keller, 2022; Chen et al., 2022; Cabon and Anderegg, 2022). One of the most recent catastrophic volcanic eruptions was that of the Mount Pinatubo on Luzon Island, Philippines, on 1991 (e.g., Labitzke and McCormick, 1992). After producing the largest stratospheric volcanic aerosol cloud of the 20th century, the climatic impacts of Mt. Pinatubo eruption were of planetary-scale and lasted for several years (McCormick, Thomason, and Trepte, 1995; Robock, 2002; Douglass and Knox, 2005). The Mt. Pinatubo eruption provided a natural experiment testing the response of the global atmosphere and biosphere to catastrophic geological phenomena (Soden et al., 2002; Church, White, and Arblaster, 2005; Khodri et al., 2017; Booth et al., 2012). Consequently, a suite of ecological effects of this transient major perturbation were detected in several world ecosystems (Genin, Lazar, and Brenner, 1995; Lucht et al., 2002; Gu et al., 2003; Kuhnt et al., 2005; Trenberth and Dai, 2007). Nevertheless, by definition, the frequency of such events is rare, so there are few opportunities to study the effects of single catastrophic perturbations on ecological dynamics on the long-term, specifically accounting for system dynamics before and after the perturbation.

Using a 36-year dataset of abundance fluctuations of a wintering waterfowl community, we provide evidence on the coupling of abrupt shifts in the environmental, anthropogenic and biological subcomponents in one of the largest and best preserved Mediterranean wetland ecosystems in the world (Doñana Marshes, SW Spain; Rendón et al., 2008; Almaraz et al., 2012). This major ecosystem, historically hoarding more than 1 million wintering birds from breeding grounds across the Palearctic, is a Biosphere Reserve and a UNESCO World Heritage site. In spite of this, it is currently considered under severe threat due to several human pressures (Scheffer et al., 2015; Green et al., 2017; Camacho et al., 2022). Using a Bayesian Dynamic Factor Analysis (Almaraz and Oro, 2011; Ward et al., 2022) we indeed detect an abrupt shift in 1992 towards a significantly lower local wintering population, when a sudden drop of more than 60 % of the population still persists today. However, a multivariate state-space model (Almaraz et al., 2012) suggests that the stability and feasibility of the wintering community is similar before and after the regime shift. Finally, we apply

a stochastic cusp catastrophe model (Poston and Stewart, 1979; Cobb and Watson, 1980; Grasman, Maas, and Wagenmakers, 2009) to show that this regime shift among two alternative stable states was likely triggered by a transient perturbation of planetary climate induced by the explosion of the Mt. Pinatubo. Based on evidence from around the breeding and wintering grounds of waterfowl in the Palearctic, we suggest that the cold and dry conditions for wintering in our study area during the transient perturbation translated to persistent behavioral shifts in the philopatry and the migratory behaviour of waterfowl. Our study provides an example linking abrupt climatic changes to regime shifts and alternative stable states in both the population and community dynamics of vertebrates.

6.3 Material and methods

6.3.1 *Study area, environmental data and bird community time series*

The Doñana Marshes are located in South-western Spain, and are composed of a complex mosaic of natural wetland ecosystems and artificial salt pans, ricefields, and fish farms within the large (>150.000 Ha) inner delta of the Guadalquivir river (Rendón et al., 2008; Almaraz et al., 2012). This area is one of the best preserved Mediterranean wetland ecosystems in the world, and is one of the major wintering and stopover sites for waterbirds breeding throughout the Western Palearctic (Marín and García, 2006; Scheffer et al., 2015; Green et al., 2017; Camacho et al., 2022). A total of 100.000 ha have been surveyed from the air on a monthly basis by the same two expert observers since 1973, providing absolute numbers for the 10 most abundant wintering waterfowl (Anatidae) species: the Pintail (*Anas acuta*), Shoveler (*Spatula clypeata*), Common Teal (*Anas crecca*), Eurasian Wigeon (*Mareca penelope*), Mallard (*Anas platyrynchos*), Gadwall (*Mareca strepera*), Greylag goose (*Anser anser*), Common Pochard (*Aythya ferina*), Red-crested pochard (*Netta rufina*), and Shelduck (*Tadorna tadorna*). Complete data exist for every species from 1978 until nowadays. We used two wintering counts every year (December and January). The wintering population size ranged from maximum of 534.460 birds to a minimum of 61282.

The population abundance of waterfowl depends strongly on the amount of flooded surface, which itself determines the extent of ricefields in Mediterranean ecosystems (Marín and García, 2006). To assess the potential coupling between phase transitions in waterfowl populations and environmental dynamics, we used annual figures for the extent of winter flooding in the surveyed area, obtained from satellite imagery and averaged from November to February, for the surface covered with cultivated ricefields each year (see Almaraz et al., 2012 for details). Finally, we used monthly rainfall and temperature time-series gathered within Doñana National Park area from 1978 onwards; to extend the time-series further back in the past, we collected rainfall data from two nearby stations from which

data is available since 1951, using the World Monthly Surface Station Climatology of the National Center for Atmospheric Research (http://dss.ucar.edu/datasets/ds570.0/). Both time series correlate strongly ($r > 0.95$). To explore the fine-scale structure of non-stationarity in the weather time series we applied Scale Dependent Correlations plot (SDC, Rodríguez-Arias and Rodó, 2004; Rodó and Rodríguez-Arias, 2006) to monthly rainfall in the study area. We complemented the SDC plot of rainfall time-series by extending the temporal analysis to the frequency domain through wavelet analysis (Torrence and Compo, 1998; Cazelles et al., 2008).

6.3.2 *Climatic and volcanic database*

We constructed a synoptic climatology of the western Palearctic, including both the breeding and wintering grounds of the ten waterfowl species considered, for the studied time period and during all seasons except summer. This included the region from 30N to 80N, and from 20W to 45E (Fig. 6.3). We extracted time-series data from the Version 3 (V3) of The Twentieth Century Reanalysis Project (https://psl.noaa.gov/data/20thC_Rean/), developed by the Physical Sciences Laboratory of the National Oceanographic and Atmospheric Administration. We reconstructed the fields for air temperature and precipitation rate, and produced plots of composite anomalies for both variables: as suggested by the SDC and wavelet analyses, a transient dry and cold period was detected from 1992 to 1995. We thus compared the composite anomalies for air temperature and precipitation rate from 1978 to 2013 (excluding the transient period 1992-1995), with the composite anomalies of the transient period (1992-1995).

Several indices are available for characterizing the magnitude of volcanic eruptions (e.g., Crosweller et al., 2012; Constantinescu et al., 2021). The multi-decadal variability in the North Atlantic climate is under strong forcing by stratospheric aerosols (Otterå et al., 2010; Booth et al., 2012; Knudsen et al., 2014). Volcanic activity is one of the main natural sources of aerosols to the stratosphere (Otterå et al., 2010; Constantinescu et al., 2021), so an index of Volcanic aerosol optical depth of the stratosphere (SAOD, Booth et al., 2012) has been suggested as a surrogate for evaluating the impacts of Volcanic activity on global climate through the forcing of the upper atmosphere. We used the monthly AOD index for the Northern Hemisphere (35.2 ^{o}N and 58.7 ^{o}N) from Booth et al., 2012 as a surrogate for climatic forcing of volcanic activity in the breeding and wintering areas of Palearctic waterfowl (See Fig. 6.2).

6.3.3 *Detecting community trends and regime shifts*

We used bayesian state-space Dynamic Factor Analysis (Almaraz and Oro, 2011; Ward et al., 2022) to detect and characterize major trends, and potentially regime shifts, in the long-term wintering community

time-series of the waterfowl community. A state-space DFA model has two equations: a (latent) process, or state equation; and an observation or measurement model linking the state process to the observations. The DFA can be written as:

$$\begin{aligned} \mathbf{x}_{t+1} &= \mathbf{S}(\mathbf{x}_t) + \mathbf{w}_t \\ \mathbf{y}_t &= \mathbf{Z}\mathbf{x}_t + \mathbf{e}_t \end{aligned} \tag{6.3.1}$$

were $\mathbf{x}$ is an $T \times K$ matrix of K latent trends and T years. The process error, $\mathbf{w}_t$, follows a multivariate normal distribution, $\mathbf{w}_t \sim \mathcal{MVN}(0, \mathbf{Q})$ where Q is generally assumed to be a $T \times K$ identity matrix. The trends x_t are linked to the observations y_t (the wintering waterfowl counts each year) through the observation or measurement model. In this case, $\mathbf{Z}$ is a matrix of estimated factor loadings, dimensioned as $P \times K$, were P is the number of time series. Again, the residual errors are assumed to be multivariate normally distributed, $\mathbf{e}_t \sim \mathcal{MVN}(0, \mathbf{R})$.

The term $\mathbf{S}$ represent flexible P-Spline functions (Eilers and Marx, 1996; Ward et al., 2022) implemented for the temporal variation of each common trend modeled. We fit a DFA with two common trends ($K = 2$), and each P-Spline was fitted with 16 knots; this is the value minimizing the leave-on-out cross validation score (see Ward et al., 2022). We implemented the DFA to two wintering counts each year: December and January, to account for variable observation errors among years in a long-format scheme (see Ward et al., 2022) After estimating the common trends, we used a Hidden Markov Model (HMM, Fraser, 2008) with two regimes to detect and localize potential regime shifts in the common trends. We used the `bayesdfa` `R` package (Ward et al., 2022), which implements the Hamiltonian Monte Carlo NUTS algorithm of the `Stan` language (Carpenter et al., 2017), to fit the DFA in Eqn. 6.3.1.

6.3.4 *Modeling community dynamics and stability*

After characterizing the existence and location of the regime shift (see Fig. 6.4), we fitted a state-space Lotka-Volterra-Ricker (LVR) model to each of the regimes to evaluate their relative stability properties. We denote the first regime identified by the DFA (Fig. 6.4) with the subscript 1 for each of the parameters, and the second regime with the subscript 2. The LVR regime-dependent state-space model can be written as:

$$n_{i,t+1} = \begin{cases} n_{i,t} + r_{1,i}\left(1 - \frac{\sum_{j=1}^{s} \alpha_{1,ij} N_{j,t}}{K_{1,i}}\right) + \epsilon_{1,i,t} & \text{for } 1978 < t < 1992 \\ n_{i,t} + r_{2,i}\left(1 - \frac{\sum_{j=1}^{s} \alpha_{2,ij} N_{j,t}}{K_{2,i}}\right) + \epsilon_{2,i,t} & \text{for } 1995 < t < 2013 \end{cases} \tag{6.3.2}$$

$$y_{i,t} = \begin{cases} n_{i,t} + b_{1,i,k} + \tau_{1,t,i} & \text{for } 1978 < t < 1992 \\ n_{i,t} + b_{2,i,k} + \tau_{2,t,i} & \text{for } 1995 < t < 2013 \end{cases} \tag{6.3.3}$$

$$n_{i,0} = \begin{cases} \mu_{1,i,0} + \epsilon_{1,i,0} & \text{for } 1978 < t < 1992 \\ \mu_{2,i,0} + \epsilon_{2,i,0} & \text{for } 1995 < t < 2013 \end{cases} \tag{6.3.4}$$

where $n_{i,t}$ is the log_e population abundance of each waterfowl species i during each winter, and $N_{i,t}$ is the raw population abundance. The *per*-capita (intrinsic) growth rates of each waterfowl species is denoted by r_i; the symbol $\circ$ stand for the element-wise product. The interaction matrix $\mathbf{A}$ is formed by the coefficients of inter-specific interactions scaled by the carrying capacities of each waterfowl species in the study area in the off-diagonal, α_{ij}/k_i. The intra-specific coefficients in the diagonal, α_{ii}, are k_i^{-1} (see Ranta, Lundberg, and Kaitala, 2006; Mutshinda, O'Hara, and Woiwod, 2009; Almaraz and Oro, 2011). We used Stochastic Search Variable Selection (SSVS) to regularize the interaction matrix (see Almaraz et al., 2012). The initial state, $n_{i,0}$ for each waterfowl species in the vector of latent states is specified as a normal distribution with mean $\mu_{i,0}$ and variance ϵ_0, $n_{i,0} \sim \mathcal{N}(\mu_{i,0}, \epsilon_0)$.

The matrix Σ in the state equation includes the variance of the unmodelled (stochastic) environmental factors impacting on single-species dynamics in the main diagonal, σ_i^2, and the (potentially) correlated joint responses to the common environment among all species, $cov(\sigma_i, \sigma_j)$, in the off-diagonal. This matrix is, thus, positive semi-definite and symmetric (Almaraz and Oro, 2011; Almaraz et al., 2012): $\mathbf{E}_t \sim \mathcal{MVN}(0, \Sigma)$. The matrix Ω includes the measurement errors for each functional type in the main diagonal, and we also modeled the covariance between these terms in the off-diagonal. Finally, the coulmn vectors $\mathbf{b}_k$ include the correction factors for the average fluctuation level of each wintering census (December and January) and for each waterfowl species. The correction factors for the December replicate were set to 0, while the other parameters were estimated freely. This allowed for identifiability (Mutshinda, O'Hara, and Woiwod, 2011; Almaraz et al., 2012).

Finally, to evaluate the stability of the equilibrium for each regime detected by the DFA, we constructed the Jacobian matrix of the LVR model; for simplicity, we omit the subscript for each regime, but we recall that there are two Jacobians:

$$\mathbf{J} = \begin{pmatrix} 1 - \frac{r_1}{k_1}\mathbf{n}_1^* & \cdots & -\frac{\alpha_{1s} r_1}{k_1}\mathbf{n}_1^* \\ \vdots & \ddots & \vdots \\ -\frac{\alpha_{s1} r_s}{k_s}\mathbf{n}_s^* & \cdots & 1 - \frac{r_s}{k_s}\mathbf{n}_s^* \end{pmatrix} \tag{6.3.5}$$

The criteria for the dynamical stability of a in discrete-time system is that the spectral radius of the Jacobian should be strictly less than 1 (Elaydi, 2005). We tested if the modulus of the dominant eigenvalue of matrix 6.3.5 is contained within the unit circle in the complex plane during the different regime shifts detected (see Results). We define

the probability of dynamical stability of the LVR state-space model 6.3.2 as the frequency of spectral radii that were < 1 in the posterior distribution of the Jacobian. If these conditions are fulfilled during the distinct regimes detected, this provides evidence of the existence of alternative stable states.

6.3.5 *Stochastic cusp catastrophe modeling*

Finally, we applied stochastic catastrophe theory (Cobb and Watson, 1980; Cobb and Zacks, 1985; Grasman, Maas, and Wagenmakers, 2009) to model the possible links between the global climatic transient forcing induced by the Mt. Pinatubo eruption on the regime shifts in the wintering waterfowl community. We hypothesize that this link operates through the transient perturbation of the large-scale weather conditions in the full distribution area of the studied waterfowl species, namely the weather Palearctic. This transient perturbation reorganized the wintering populations at a continental scale, with potentially long-lasting shifts in the migratory behaviour (see Discussion).

As a branch of nonlinear dynamical systems and bifurcation theory, catastrophe theory, originally developed by René Thom (Thom, 1975, 1977; Zeeman, 1988), has seen some applications in marine sciences over the last decades. For example, catastrophic dynamics has been recently suggested as an explanation for the collapse of Atlantic Cod (*Gadus morhua*) fisheries during the last decades (Sguotti et al., 2019; Sguotti et al., 2020). The perspective provided by catastrophe theory is particularly relevant for systems characterized by sudden shifts between alternative stable states induced by smooth changes in control parameters (Casti, 1979, 1982; Loehle, 1989).

As a theorem for the classification of dynamical systems, catastrophe theory identifies seven canonical, so-called elementary catastrophes (see Thom, 1975; Arnold, 1994). Currently, the majority of applications of catastrophe theory in ecology are based on the fold model: a single control parameter induces sudden changes in systems between alternative stable states, separated by unstable parameter regions that induce hysteresis (Dakos et al., 2019; Scheffer, 2009). Here, we used the second canonical catastrophe, the cusp, to test the hypothesis linking planetary-scale perturbations to alternative stable states in the wintering waterfowl community. With an additional control parameter, the cusp catastrophe model considers that some external variables may modulate the behaviour of the bifurcation parameter, inducing a discontinuous, nonlinear behavior in a previously smooth, continuous dynamics. Here, we briefly introduce the cusp catastrophe model. Consider a deterministic dynamical system with a state variable $y(t)$, a control parameter c, and a potential function of the system, $V(y; c)$:

$$\frac{\partial y}{\partial t} = \frac{\partial V(y;c)}{\partial y}, \quad y \in R^k, c \in R^p \tag{6.3.6}$$

The minimum of the potential $V(y;c)$, is achieved at equilibrium, $\frac{\partial y}{\partial t}$. Interestingly, catastrophe theory classifies the behaviour of dynamical systems such as Eqn. 6.3.6 in the vicinity of degenerate critical points of the potential $V(y;c)$. This set of points can be classified in only seven canonical forms, or universal unfoldings. The simplest of these canonical forms is the cusp:

$$-V(y;\alpha,\beta) = -\frac{1}{4}y^4 + \frac{1}{2}\beta y^2 + \alpha y \tag{6.3.7}$$

The equilibrium points of the cusp unfolding, as a function of α and β, is

$$\alpha + \beta y - y^3 = 0 \tag{6.3.8}$$

There is a range of solutions that the cusp can take, depending on the Cardan's discriminant: $\delta = 27\alpha - 4\beta^3$. If $\delta > 0$, the system has only one solution. But if $\delta < 0$, there are three solutions of the system defined by 6.3.7. The set of values of α and β for which $\delta = 0$ is, indeed, the bifurcation set. It is in this region were the system exhibits alternative stable states (see Thom, 1975; Casti, 1979; Casti, 1997; Grasman, Maas, and Wagenmakers, 2009 for further details). Cobb (Cobb and Watson, 1980) provided a stochastic approach to the cusp catastrophe. Adding to Eqn. 6.3.6 a Wiener process $dW(t)$ with variance σ^2, we get:

$$dY = \frac{\partial V(Y;\alpha,\beta)}{\partial Y}dt + dW(t) \tag{6.3.9}$$

which, for the case of the cusp, can be rewrtitten as

$$dZ_t = (-Z(t)^3 + \beta Z(t) + \alpha)dt + \sigma_z dW(t) \tag{6.3.10}$$

were the term within brackets is the drift term and σ_z is the diffusion parameter. Thus, the model in 6.3.10 reduces to a maximum-likelihood problem if data for fitting α, β and Z is available (see Cobb and Zacks, 1985; Grasman, Maas, and Wagenmakers, 2009 for details). In our case, we tested the hypothesis that the major community trend detected by the DFA (x_1, see section 6.3.3) is represented by the canonical variable, Z. The canonical (control) asymmetry variable, α will be modeled by the interactive changes in the spatial flooding extension (F) and the wintering waterfowl community size (N_s). Finally, the canonical bifurcation variate is represented in our model by the temporal changes in the Volcanic aerosol optical depth of the stratosphere (SAOD). The final model is, thus:

$$\begin{aligned} \alpha &= \alpha_0 + \alpha_1 F + \alpha_2 N_s + \alpha_3 F N_s \\ \beta &= \beta_0 + \beta_1 SAOD \\ Z &= \omega_0 + \omega_1 x_1 \end{aligned} \tag{6.3.11}$$

Therefore, our phenomenological hypothesis is that the smooth temporal changes in the impact of the spatial flooding extension and the density-dependent effects, as represented by the community size,

on community trends can become nonlinear and discontinuous, and exhibit regime shifts to alternative stable states, under the forcing of Volcanic-induced shifts in planetary climate fluctuations.

We used the `R` package `cusp` to fit the cusp catastrophe model through maximum-likelihood methods (Grasman, Maas, and Wagenmakers, 2009). The fitting of a linear and a non-linear (logistic) model was compared with the cusp catastrophe using information criteria and $pseudo - R^2$.

Model	$pseudo - n_p$	R^2	***log*Lik**	**AICc**	**BIC**
Linear	6	0.447	-36.914	94.724	101.328
Logistic	7	0.743	-26.101	70.201	77.286
Cusp	8	0.956	1.648	18.038	25.373

Table 6.1: Comparison of model fits between a linear model, a logistic model and the cusp catastrophe model. n_p is the number of parameters; pseudo $- n_p$ specifies the proportion of variance explained by each model; *log*Lik is the minimized log-likelihood function; AIC is the small-sample corrected Akaike Information Criterion, and BIC the Bayesian Information Criterion.

6.4 Results

6.4.1 *Weather and climate fluctuations*

The long-term variability in the local precipitation of the study area is shown in Figure 6.1. Both the scale-dependent correlation plot and the wavelet analysis suggests significant signals of seasonality (a periodicity of 12 months) throughout the time series. However, this signal was sometime disrupted: in particular, during the period 1991-1995, no significant cyclic signal is detected. Additionally, a nearly significant period of eight years is evident from 1951 to 1980. This long wave was never recovered.

Figure 6.2 shows the fluctuations in the stratospheric optical depth in the northern hemisphere, temperature, rainfall and spatial flooding extension of the study area from 1978 to 2013. While seasonality in the signal for temperature is strong and was never lost, rainfall did exhibit a more irregular pattern (see also Fig. 6.1). The wavelet power spectrum is shown again for rainfall: the 1991-1995 period stand out as a particularly irregular period. Finally, the volcanic aerosol optical depth shows two salient peaks coinciding with the two largest volcanic eruptions of the study period. The inset figure shows the standardized values for rainfall, temperature and flooding for volcanic vs. non-volcanic years. During volcanic years, the local weather was significantly cooler, drier and the extension of flooded are was smaller.

The synoptic fields of composite anomalies for 1978 to 2013 obtained from the Twentieth Century Reanalysis Project (Fig. 6.3) reveal a clearly temporal and spatial divergent pattern at a continental scale: the reconstructed anomalies for temperature and precipitation rate for the period of transient climatic perturbation of Mt. Pinatubo eruption (1991-1995) shows a particularly dry and cold period for southern Europe and northern Africa, and a relatively warm and wet period

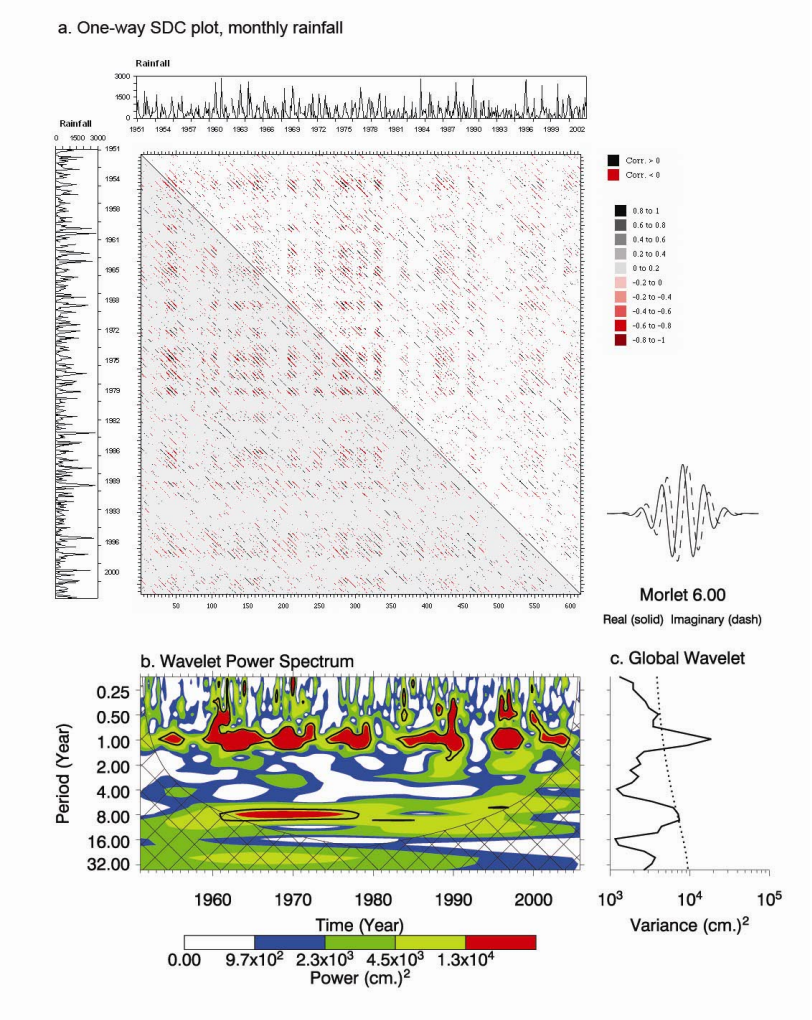

Figure 6.1: In **a**) the scale dependent correlation is shown for the monthly precipitation time series from 1951 to 2006 (Rodríguez-Arias and Rodó, 2004; Rodó and Rodríguez-Arias, 2006). The size of the sliding correlation fragment is 6 months, and only the significant local correlations are colored (significance was calculated through 1000 Monte Carlo randomizations at each point). In **b**) the wavelet power spectrum, using the Morlet transform (Torrence and Compo, 1998; Cazelles et al., 2008), aplied to the precipitation time series. The power regions surround by a solid line are significant at the 5% level. In the global wavelet, the significant period of the signal are those to the right of the doted significance line.

for the northern Palearctic. When excluding these years, this pattern is reversed: relatively warm and wet period characterized winters in the southern Palearctic.

6.4.2 *Major trends in the community*

The major waterfowl community trends modeled by the state-space Dynamic Factor Analysis (DFA) are shown in Figure 6.4). A first trend display a downward peak around 1992, and a further increase through time. In contrast, the second trend display a clear abrupt shift in 1991 towards significantly lower levels, a shift that was sustained through time. A DFA with only on trend select this second trend as the dominant, but is a worst model according to the leave-one-out cross-validation information criterion, LOOIC: 1961.8 vs. 1906.4, respectively. Indeed, the Hidden Markov Model (HMM) of regime shifts, when applied to this second trend (Fig. 6.5), suggest a highly significant shift in 1992. A HMM with no regime shift is a much worst predictor than a HMM with at least one regime shift (LOOIC, 317.652 vs. 1.451, respectively). The fitting of species-specific trends is

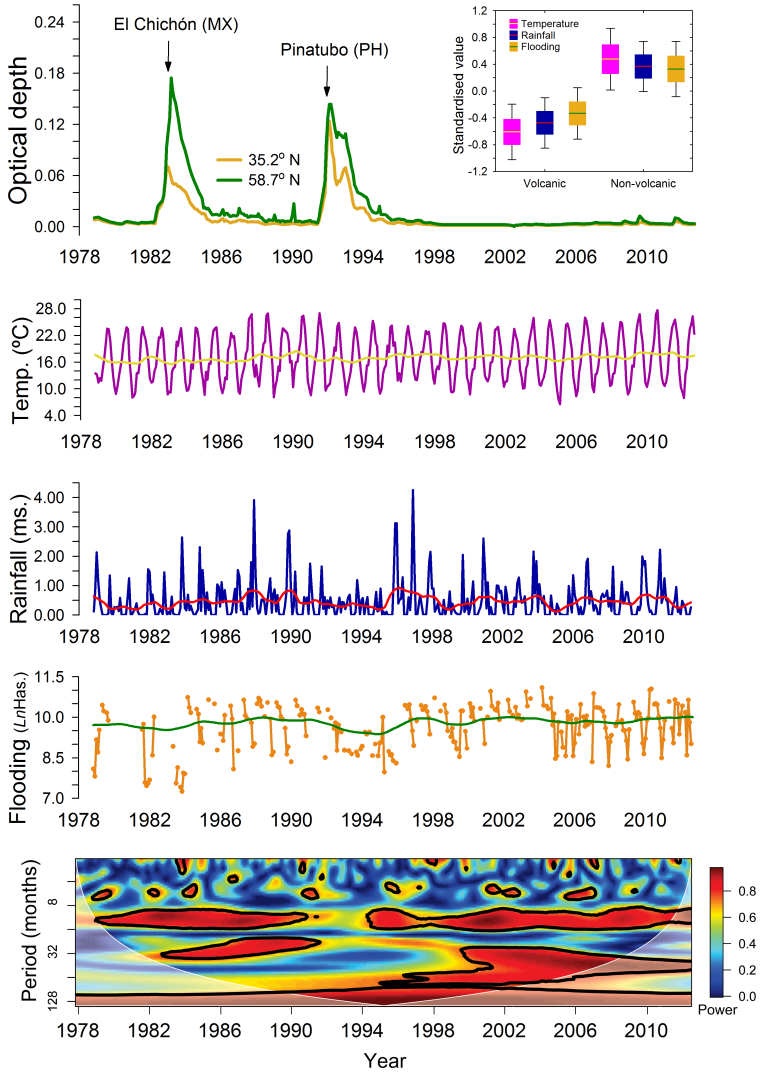

Figure 6.2: Time series (1978-2013) for the stratospheric aerosol optical depth in the Northern hemisphere, temperature, rainfall and spatial flooding extension in the study area. The wavelet spectrum is shown for the rainfall time series. The inset figure shows the average standardized values for temperature, rainfall and spatial flooding extension, during volcanic and non-volcanic years. For the local weather variables, the smoothed trends are shown as loess fittings.

shown in Figure 6.6, with associated loading factors in Figure 6.7. All species, except for the Common Pochard and the Pintail have positive factor loadings for the second trend. The depth of the abrupt shift in 1992 differed somewhat among species, and is particularly strong for some, such as the Common Teal, the Eurasian Wigeon and the Greylag Goose. Overall, the DFA analysis suggest that the abrupt shift in 1992 is a generalized dynamic shift across the community, with weak, subsequent recoveries only for some species.

6.4.3 *Characterizing alternative stable states*

According to the community regime shift detected by the DFA in 1992, and the transient period towards the second fluctuation level, that started in 1995 (Fig. 6.5), the state-space LVR model was fitted to two separate periods: from 1978 to 1992; and from 1995 to 2013.

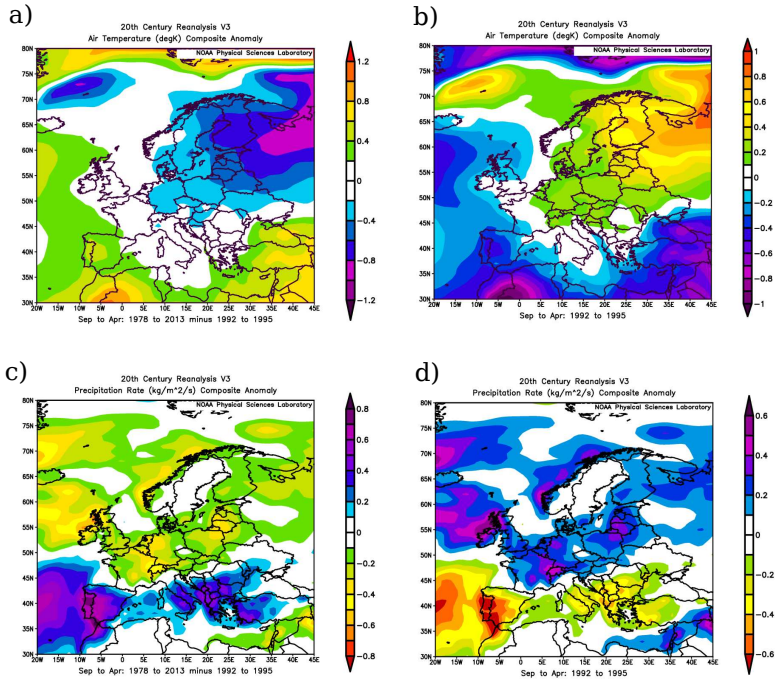

Figure 6.3: Synoptic fields of composite anomalies obtained from the V3 of the Twentieth Century Reanalysis Project (https://psl.noaa.gov/data/20thC_Rean/). The composite anomaly from 1978 to 2013, excluding the transient period 1992-1995, are shown for air temperature (**a**) and precipitation rate (**c**). The composite anomaly for the transient period, 1992-1995, is shown for air temperature (**c**) and precipitation rate (**d**). The seasonal period considered exclude the summer months.

The posterior quality checking of model fitting suggests that MCMC chains mixed well and showed evidence of convergence in both periods. The probability of inter-specific interaction, as selected by SSVS, was low in both periods (less than 0.03). Interestingly, both the posterior probability of dynamic stability and resilience are the same for both periods (Figure 6.8). While the posterior distribution of the dominant eigenvalues of the Jacobian are close to 1 in both periods, the linearized dynamics around the equilibrium is stable. This is strong evidence of alternative stable states.

6.4.4 *Cusp catastrophe modeling*

The results of the fitting of the cusp catastrophe modeling to the major community trend is shown in Table 6.1. The cusp model (Eqn. 6.3.11) is clearly the best one for explaining the observed pattern of covariation of the major community trend, the volcanic aerosol stratospheric optical depth (SAOD) and spatial flooding extension. This model accounts for the 95.6% of variance of the major DFA trend displaying a regime shift (Fig. 6.5). Table 6.2 shows the maximum-likelihood estimates, and their associated uncertainty, of the parameter of the cusp catastrophe model (Eqn. 6.3.11). The effect of spatial flooding extension, in particular the interaction between flooding and community size, and the SAOD are very strong.

The diagnostic plot for the fitted cusp catastrophe model (Fig. 6.9) suggest that nearly all values are located in the region of the bifurcation set, providing strong evidence for alternative stable states and hysteresis. A 3D plot of the cusp catastrophe model (Fig. 6.10)

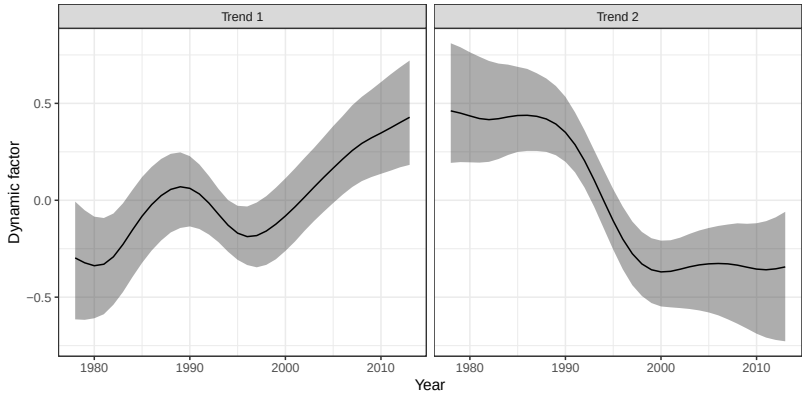

Figure 6.4: Posterior estimated community common trends of the state-space Dynamic Factor Analysis (Ward et al., 2022) applied to the wintering waterfowl community, and 95 % credible intervals.

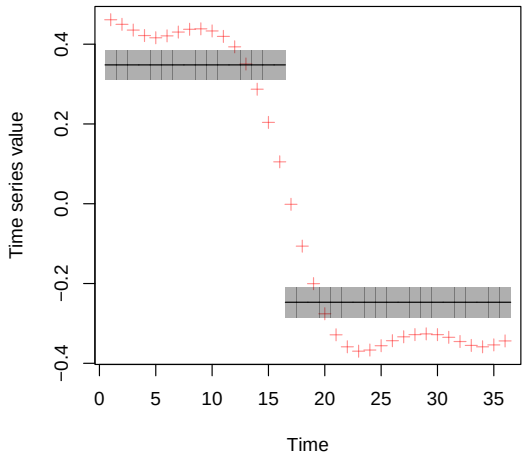

Figure 6.5: Posterior regime shift identified by a Hidden Markov Model applied to the second common trend of the state-space DFA (Fig. 6.4). The values of the common trend are depicted as red axes, and the average (and 95% Credible Intervals) of each regime is denote in grey.

verifies that the waterfowl community fluctuated during the full 36 year period in the region of multi-stability. This more clearly assessed in the transition plot of the major community trend (Fig. 6.11): two fluctuating regimes, clearly separated by an abrupt transition, indicate a fundamental regime shift between alternative stable states after a tipping point in 1992.

6.5 Discussion

We have found a persistent regime shift between two alternative stable states in the environmental and biological components of one of the major Mediterranean wetland ecosystem in the world. As examples of abrupt shifts in birds, Durant et al., 2004 recently showed the existence of regime shifts in breeding parameters of a seabird linked to oceanographic changes in the Norwegian Sea, and Jenouvrier, Weimerskirch, et al., 2005 found discrete shifts in the cycling dynamics of three seabirds breeding in the Antarctic correlated to changes in the climatic conditions of the Southern Ocean. In the present paper, a detailed pattern of covariation between external forcing variables and

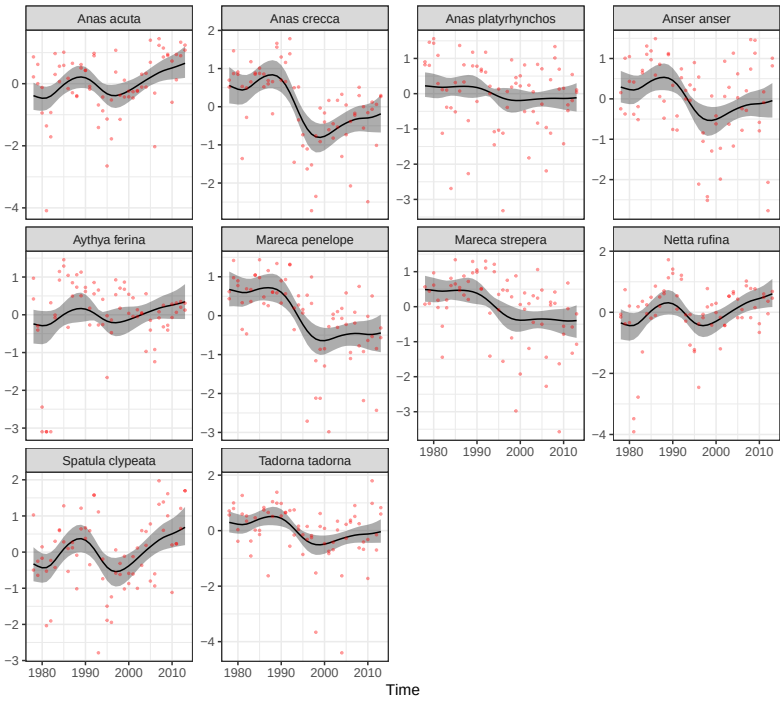

Figure 6.6: Posterior estimated common trends of the state-space Dynamic Factor Analysis for each wintering waterfowl species in Doñana marshes, 1978-2013. The red dots denote the aerial count estimate for December and January of each wintering season. The solid line is the average posterior value, and the shaded region is 95 % credible intervals.

Parameter	**Average**	**95 CI**
α_0	-0.231	(-0.500, 0.037)
$\alpha_1 F$	-0.181	(-0.421, 0.058)
$\alpha_2 N_s$	0.602	(0.189, 1.015)
$\alpha_3 F \cdot N_s$	0.308	(0.021, 0.594)
β_0	4.821	(3.657, 5.986)
$\beta_1 SAOD$	-1.103	(-1.707, -0.499)
ω_0	-0.326	(-0.446, -0.205)
$\omega_1 x_1$	2.194	(1.949, 2.439)

Table 6.2: Average parameter values, along with the 95 % confidence interval for the cusp catastrophe model (Eqn, 6.3.11) fitted to the wintering waterfowl community of Doñana marshes.

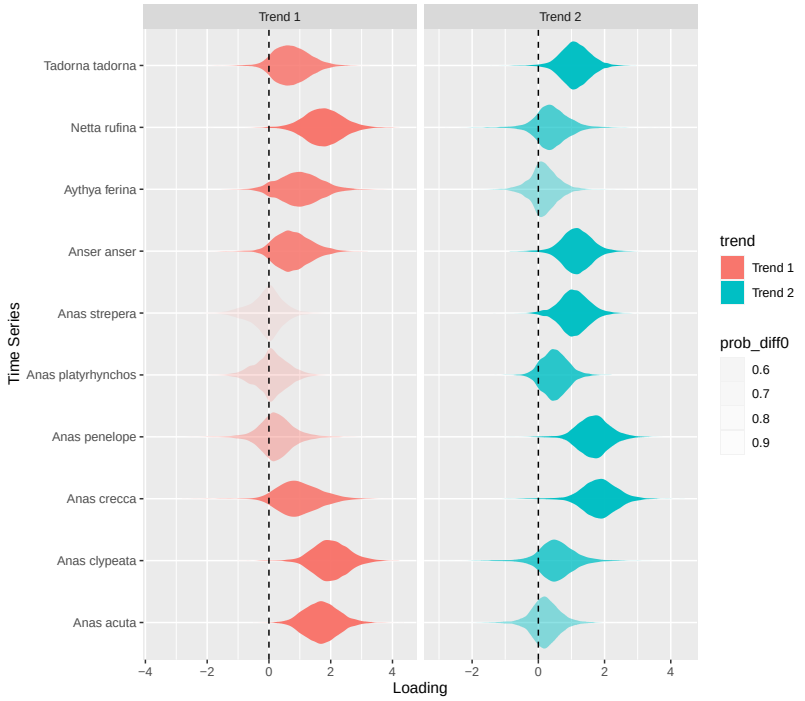

Figure 6.7: Factors loadings of the state-space Dynamic Factor Analysis for each wintering waterfowl species and dynamic common trend (shown in Figs. 6.4 and 6.6). Violin plots included the posterior density for each loading and species, and the sharing is proportional to the probability that the loading is different from 0.

the biological trend of a wintering waterfowl community conform very well to a cusp catastrophe, where the ecological dynamics depend not only on the local environmental conditions, but also on the external, large-scale forcing climatic conditions modulating the transition from linear to nonlinear behaviour of the biological variable. Indeed, the modeled shift has been statistically linked to an abrupt transient perturbation of planetary climate for which a detailed forcing mechanism has been elucidated, namely the eruption of Mt. Pinatubo, Philippines, in June 1991 (Hansen et al., 1992; Labitzke and McCormick, 1992; Robock, 2000, 2002; Douglass and Knox, 2005). A general, transient (2-3 years) worldwide cooling of the troposphere, inducing cold summers and warm winters in the Northern Hemisphere and even a transient reversal of the global warming trend (Robock, 2000, 2002; Lucht et al., 2002; Church, White, and Arblaster, 2005; Smith et al., 2016), points to the Mt. Pinatubo eruption, with more that 20 megatons of SO_2 injected into the stratosphere (Hansen et al., 1992), as the single most important catastrophic geological event of the 20th century. The transient pattern of cooling in southern Europe and Warming of Northern Europe immediately after the eruption (e.g., Robock, 2002; Lucht et al., 2002) was reproduced in this study, and suggest long-lasting shifts in the behaviour of migrating birds. Several biological signals have already been linked to Mt. Pinatubo eruption, such as the remote control of net primary production (Lucht et al., 2002; Krakauer and Randerson, 2003) shifts in deep-sea communities and oceanographic conditions (Hess et al., 2001; Kuhnt et al., 2005; Yao and Hoteit, 2018), fish biology (Gaston, Woo, and Hipfner, 2003), changes in coral survival (Genin, Lazar, and Brenner, 1995), global

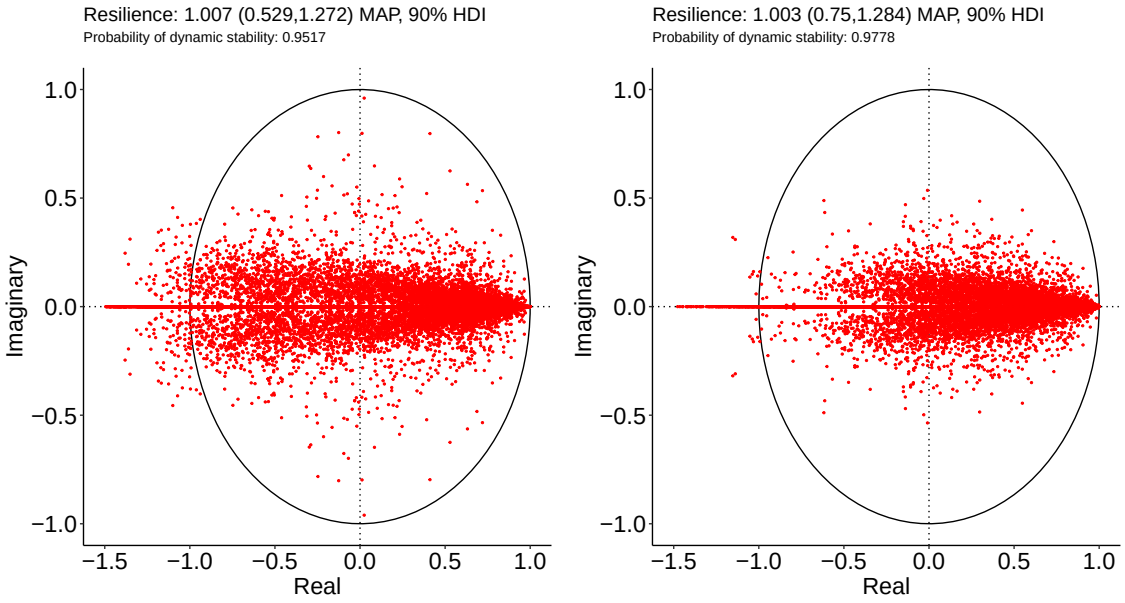

(a) Probability of stability pre-Pinatubo

(b) Probability of stability post-Pinatubo

Figure 6.8: Figure **a**) shows the distribution in the unit circle of the complex plane of the posterior eigenvalues of the Jacobian 6.3.5 matrix of the LVR state-space model fitted to the pre-Pinatubo community time series (1978-1992), as suggested by the regime shift modeled in the dominant common trend of the DFA (Fig 6.5). The probability of stability is the fraction of eigenvalues strictly smaller than 1 in the posterior distribution. In figure **b**) the posterior distribution is shown for the Jacobian 6.3.5 matrix of the LVR state-space model fitted to the post-Pinatubo community time series (1995-2013). MAP is the maximum a posteriori density, and 90% HDI the highest density interval (Makowski, Ben-Shachar, and Lüdecke, 2019).

hydrological cycles (Trenberth and Dai, 2007), etc.

With more than one million birds wintering in some years, our study area, Doñana marshes, are the key wintering and stopover wetlands for all migrating waterbirds of the Western Palearctic (Marín and García, 2006; Rendón et al., 2008; Green et al., 2017; Camacho et al., 2022). The wintering conditions in this region are linked to the survival and breeding output in the breeding headquarters of many waterfowl species in the Western Palearctic (Rendón et al., 2008; Almaraz et al., 2012; Green et al., 2017). Interestingly, Ganter and Boyd, 2000 presented qualitative evidence of an arctic-wide decline in breeding performance of waterbirds in the summer following the Mt. Pinatubo eruption, with potentially negative effects on wintering waterfowl populations in Southern Europe. This large-scale breeding failure in 1992 was confirmed by local studies with Eurasian Wigeons in Denmark and the UK (Mitchell et al., 2008), and by a reduced hunting bag of several waterfowl species in Denmark from 1982 to 2010 (Christensen and Fox, 2014). Given the global relevance of Doñana marshes, it is very likely that the abrupt regime shift detected in 1992 was due to a combination of two factors: 1) a generalized failure of breeding success in the breeding grounds (Ganter and Boyd, 2000; Mitchell et al., 2008; Christensen and Fox, 2014); and 2) a particularly harsh (cold and dry) condition in the study area during the 1992 winter, compared to other continental wintering grounds (Fig. 6.3). As shown by the wavelet and SDC analyses of the long-term, high resolution weather variables in the study area (Fig. 6.2 and 6.1), these conditions persisted until 1995. While the evidence suggest that most European waterfowl populations recovered rapidly from the 1992 breeding failure (Ganter and Boyd, 2000; Mitchell et al., 2008; Christensen and Fox, 2014), it is in-

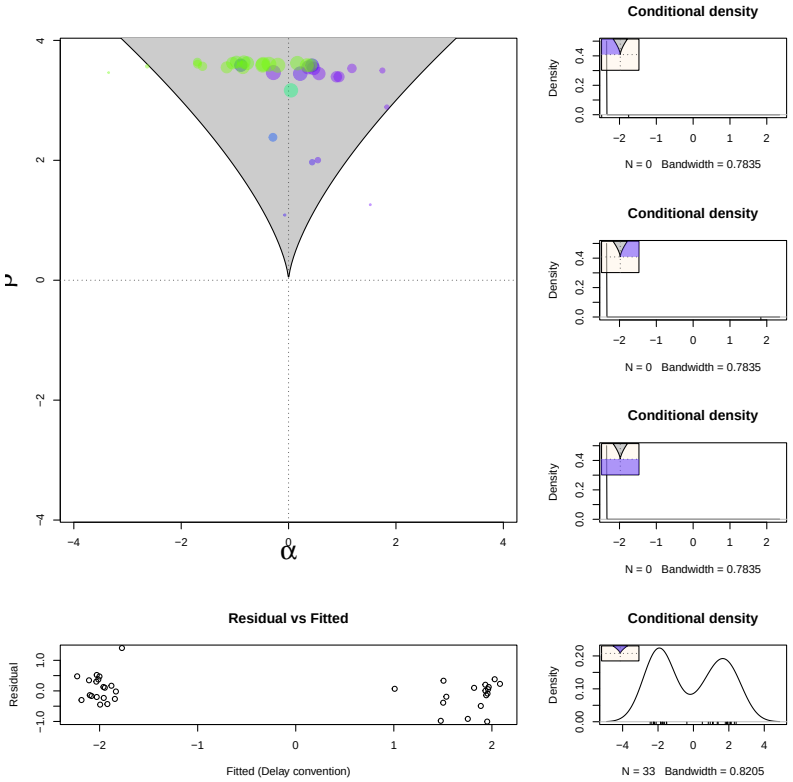

Figure 6.9: Diagnostic plot for the fitted stochastic cusp catastrophe model (Eqn. 6.3.11). The shaded region in the $\alpha - \beta$ plane is the bifurcation set of the cusp catastrophe: the set of points for which the Cardan's discriminant is 0. The crossing of the dotted lines, were $\alpha = \beta = 0$, is the cusp (tipping) point. The conditional density plots show the relative distribution of observed values that are located in each region of the plane. Green dots are above the folded region of the 3D cusp, purple dots are below the folded region.

triguing that the wintering population of Doñana marshes entered an alternative stable state of significantly lower community abundance, even though local conditions returned to the normal statistical behavior. Although the stochastic cusp catastrophe model we use is a phenomenological approach (Casti, 1979; Casti, 1997), we suggest a biological mechanism explaining the regime shift to an alternative stable state induced by behavioural plasticity.

Studies on waterfowl migration point to a stronger breeding philopatry compared to site fidelity to wintering grounds in this taxa (e.g., Guillemain, Sadoul, and Simon, 2005; Davis et al., 2014; Clausen and Madsen, 2016; Clausen et al., 2018). While geese and swans have been traditionally regarded as bearing stronger fidelity to wintering grounds relative to dabbling ducks and pochards (Robertson and Cooke, 1999; Coulson, 2016), most recent data suggest that geese are indeed very plastic and can shift flyways with a large probability (Clausen and Madsen, 2016; Clausen et al., 2018). At a continental scale, changes in migration propensity and shifts in flyways and wintering sites are common responses of European ducks to cold or warm spells (Ridgill and Fox, 1990). Abmigration, the ability to shift flyways depending on environmental conditions, is indeed a common strategy in waterfowl: during the last decades, ringing data support the hypothesis that breeding populations Palearctic Common Teal easily shift North-Western European and Mediterranean flyway routes with a large prob-

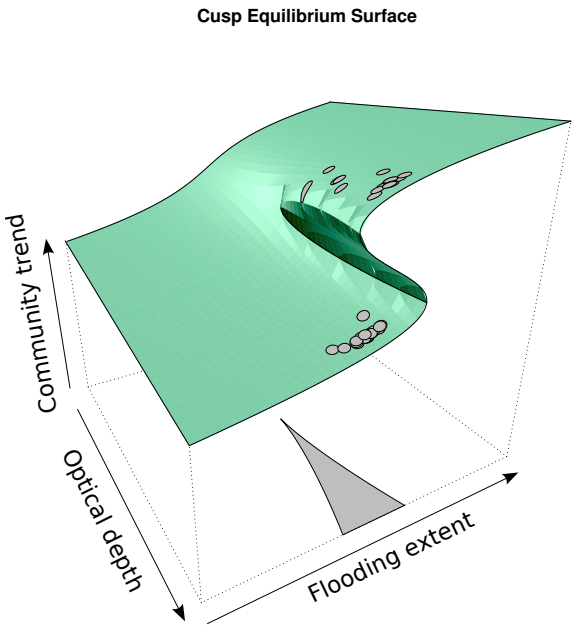

Figure 6.10: Three-dimensional representation of the fitted stochastic cusp catastrophe model (Eqn. 6.3.11), with the fitted values plotted in the maximum-likelihood cusp equilibrium surface (Grasman, Maas, and Wagenmakers, 2009). The volcanic aerosol stratospheric optical depth is the bifurcation parameter, and spatial flooding extension is the asymmetry parameter.

ability (Guillemain, Sadoul, and Simon, 2005; Parejo et al., 2015). Pink-footed geese wintering in Denmark, the Netherlands and Belgium, show an average 54% probability of changing migrating strategy during a 25 year period (Clausen et al., 2018). Importantly, site fidelity is usually female-biased in waterfowl and, contrary to other taxa, pair formation occurs in wintering grounds (Robertson and Cooke, 1999). As a behavioral strategy under such a strong selective pressure, plasticity in flyways shifting behavior in response to rapidly changing environments is thus regarded as adaptive in waterfowl (Clausen and Madsen, 2016; Clausen et al., 2018). We suggest the possibility that the abrupt regime shift detected in Doñana marshes, followed by an alternative stable state, might be a consequence of a permanent shift to alternative wintering grounds prompted by a perturbation-induced-behavioral shift in philopatry: the reversed synoptic climatic conditions uncovered here during the Mt. Pinatubo transient perturbation (6.3) point to an increase in quality for wintering conditions of alternative wintering grounds. Once waterfowl populations undergo a shift in site use in response to local changes in environmental conditions, they may become faithful to the new sites, even if the conditions in the original site improve (Clausen and Madsen, 2016; Clausen et al., 2018). Indeed, even though Doñana Marshes are considered the main wintering site for Greylag goose in the Western Palearctic, the negative shift detected in 1995 has not yet reversed, and remarkable population increases have been observed in northern Spain and several European wintering sites from the mid nineties onwards (Madsen, Cracknell, and Fox, 1999).

Recently, theoretical and empirical approaches are addressing the study of nonlinear population dynamics in social species driven by behavioral rapid shifts in response to perturbations, social feedbacks and

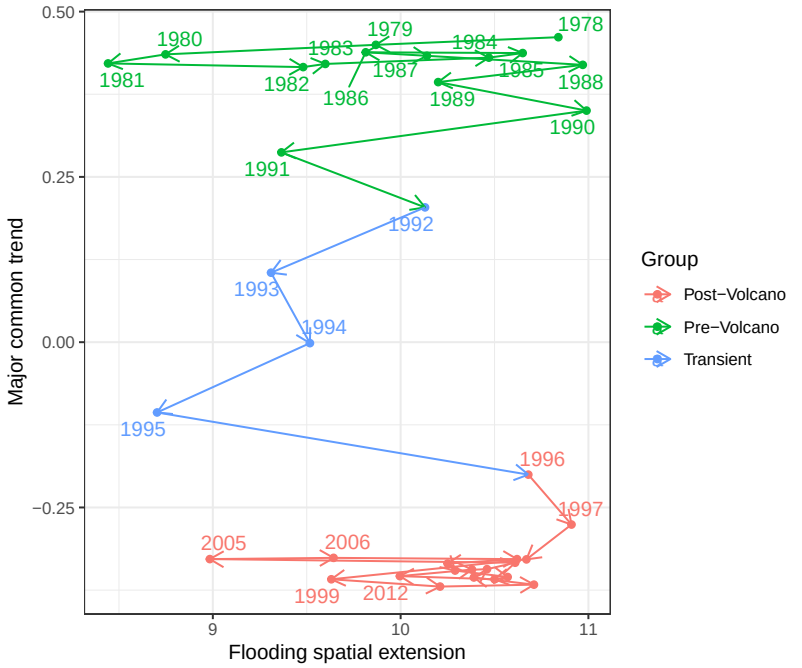

Figure 6.11: Transition of the values of the dominant common trend of the DFA (Fig 6.5) from 1978 to 2013, depicted as a function of the flooding spatial extension of Doñana marshes derived from satellite imaging (see Almaraz et al., 2012). The values for the pre-Pinatubo period (in green) drop abruptly to the post-Pinatubo period (in red) through a transient period (in blue).

tipping points (Oro, 2020; Oro and Freixas, 2021). According to this perspective, changes in social behaviour induced by disturbances in breeding or wintering grounds may feedback at the population level to induce a highly non-linear dynamics, i.e., a population crash triggered by breeding site abandonment in response to predation (Almaraz and Oro, 2011). In the case of Doñana marshes, we hypothesize that the regime shift to an alternative stable state induced by the transient, large scale climatic perturbation of the Mt. Pinatubo eruption, might be a remarkable an example of non-linear feedbacks between behaviour and population dynamics (See Figure 6.12): under this scenario, a persistent reversal of the synoptic climatic fields, with cold and dry conditions in the wintering area, might trigger a trans-generational plastic behavioral shift in migrating birds that persist even under the reversal of the normal synoptic conditions. In this conditions, wintering birds might remain in alternative wintering grounds even if the local conditions return to normal. This might be the mechanism giving rise to hysteresis, as evidenced here in the cusp catastrophe model (Figs. 6.9 and 6.10).

Overall, in a rapidly changing world ecological dynamics over short time-scales, at which transient (non-asymptotic) dynamics may govern persistence, arise as a research area of paramount importance (Hastings et al., 2021). Processes operating with diverging spatial and temporal rates of change, may yield surprises if time lags and alternative stable states are not correctly identified (Watts et al., 2020; Williams, Ordonez, and Svenning, 2021; Scheffer, 2009) This is the fundamental scale of most ecological processes, and may have an overriding effect on ecosystem supplies and resilience (Folke et al., 2004). Predicting

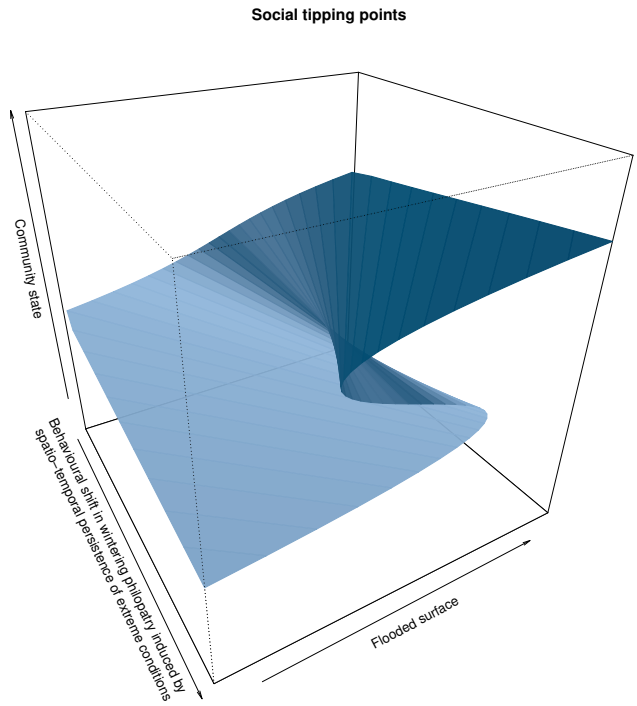

Figure 6.12: Hypothesized impact of the spatio-temporal persistence of continental-scale climatic anomalies on regime shifts in the wintering waterfowl community size, operating through behavioral shifts in wintering philopatry of migrating birds.

the consequences of transient environmental dynamics on biological systems is thus essential in global change ecology, with benefits ranging from improved knowledge on ecosystem functioning to informed management of harvested populations (Suding, Gross, and Houseman, 2004; Scheffer, 2009; He and Biswas, 2019). Our results provide an empirical example of a potentially catastrophic dynamics in a major hotspot induced by an abrupt geological disruptions with global impacts on the atosphere, the bisophere and the ocean.

7 Long-term demographic dynamics of a keystone scavenger disrupted by human-induced shifts in food availability

Published paper: Almaraz et al., 2022 *Ecological Applications* (2022), 32 (6), e2579. https://esajournals.onlinelibrary.wiley.com/doi/10.1002/eap.2579. Includes Supplementary Material.

Open Research statement: Data, code, and scripts are available in Zenodo at https://doi.org/10.5281/zenodo.5718953.

Pablo Almaraz[1], Félix Martínez[2], Zebensui Morales-Reyes[3], José A. Sánchez-Zapata[3], Guillermo Blanco[4]

1. Department of Ecology and Coastal Management, Instituto de Ciencias Marinas de Andalucía, ICMAN-CSIC, Campus Río San Pedro, 11510, Puerto Real, Spain.
2. Escuela Internacional de Doctorado, Universidad Rey Juan Carlos (URJC), C/ Tulipán s/n, E-28933 Móstoles, Madrid, Spain.
3. Department of Applied Biology, Centro de Investigación e Innovación Agroalimentaria y Agroambiental (CIAGRO-UMH), Miguel Hernández University of Elche, Avda. de la Universidad, s/n, 03202 Elche, Spain.
4. Department of Evolutionary Ecology, Museo Nacional de Ciencias Naturales (MNCN-CSIC), José Gutiérrez Abascal 2, 28006 Madrid, Spain.

Abstract

Scavenging is a key ecological process controlling energy flow in ecosystems and providing valuable ecosystem services worldwide. As long-lived species, the demographic dynamics of vultures can be disrupted by spatio-temporal fluctuations in food availability, with dramatic impacts on their population viability and the ecosystem services provided. In Europe, the outbreak of Bovine Spongiform Encephalopathy (BSE) in 2001 prompted a restrictive sanitary legislation banning the presence of livestock carcasses in the wild at a continental scale. In long-lived vertebrate species the buffering hypothesis predicts that the demographic traits with the largest contribution to population growth rate should be less temporally variable. The BSE outbreak provides a unique opportunity to test for the impact of demographic buffering in a keystone scavenger suffering abrupt but transient food shortages. We study the 42-year dynamics (1979-2020) of one of the world's largest breeding colonies of Eurasian griffon vultures (*Gyps fulvus*). We fit-

ted an inverse Bayesian state-space model with density-dependent demographic rates to the time-series of stage-structured abundances to investigate shifts in vital rates and population dynamics before, during and after the implementation of a restrictive sanitary regulation. Prior to the BSE outbreak the dynamics was mainly driven by adult survival: 83% of temporal variance in abundance was explained by variability in this rate. Moreover, during this period the regulation of population size operated through density-dependent fecundity and sub-adult survival. However, after the onset of the European ban, a one-month delay in average laying date, a drop in fecundity and a reduction in the number of fledglings induced a transient increase in the impact of fledgling and sub-adult recruitment on dynamics. Although adult survival rate remained constantly high, as predicted by the buffering hypothesis, its relative impact on the temporal variance in abundance dropped to 71% during the sanitary legislation and to 54% after the ban was lifted. A significant increase in the relative impact of environmental stochasticity on dynamics was modeled after the BSE outbreak. These results provide empirical evidence on how abrupt environmental deterioration may induce dramatic demographic and dynamic changes in the populations of keystone scavengers, with far-reaching impacts on ecosystem functioning worldwide.

KEYWORDS carrion, inverse demographic modelling, mad cow disease, matrix modelling, state-space modelling, scavenging, vultures.

7.1 INTRODUCTION

Predictable food subsidies from humans are increasingly altering ecosystem structure and functioning in multiple ways, with far-reaching consequences for environmental conservation worldwide (Oro et al., 2013). Such food subsidies are known to influence the population size and trends of different generalist vertebrate species. For example, seabirds usually benefit from fisheries discards (e.g., Bicknell et al., 2013), garden birds from supplementary feeding in urban areas (e.g. Fuller et al., 2008) or game species including mammals and birds from diversionary and management feeding (e.g. Putman and Staines, 2004). Scavengers are among these vertebrates that are tightly linked to food subsidies derived from human activities including shepherding, hunting and supplementary feeding (Donazar, 1993; Mateo-Tomás and Olea, 2010; Blanco, 2014; Cortés-Avizanda et al., 2016). Interactions between humans and scavengers have been closely connected since the Late Pliocene when early hominids probably competed for food with other scavengers (Moleón, Sánchez-Zapata, Margalida, et al., 2014). Nowadays, even if wild ungulate carcasses from hunting are an important source of food for scavengers, these species mostly rely on livestock for food worldwide (Donazar, 1993; Mateo-Tomás et al., 2015; Lambertucci et al., 2009; Lambertucci et al., 2018). Indeed, beyond the ecological function of eliminating wild ungulate carcasses, vertebrate scavengers provide an important ecosystem service by elim-

inating both domestic ungulate carcasses from agricultural waste, and carcasses derived from hunting (Moleón, Sánchez-Zapata, Selva, et al., 2014; Morales-Reyes et al., 2015; DeVault et al., 2016)

Among vertebrates, vultures are one of the most threatened scavengers worldwide (Buechley and Şekercioğlu, 2016). The main extrinsic threats for vultures include dietary pollutants (i.e. poisoning and veterinary drugs such as diclofenac and antibiotics), collision and electrocution with electric infrastructures, direct persecution and reduction in food availability (Ogada, Keesing, and Virani, 2012; Blanco et al., 2016; Buechley and Şekercioğlu, 2016). Carcass availability might be subject to changes related to socioeconomic shifts in livestock production and management (e.g. the abandonment of traditional farming practices; Olea and Mateo-Tomás, 2009), rewilding processes (e.g. increase of wild ungulate populations; Cortés-Avizanda, Donázar, and Pereira, 2015) or sanitary regulations (Margalida et al., 2010; Blanco, 2014). Thus, these changes might affect not only resource availability but also their predictability and quality (Donázar, Margalida, and Campión, 2009; Cortés-Avizanda et al., 2012; Blanco, 2014; Blanco, Junza, and Barrón, 2017; Blanco et al., 2019). These factors can have a profound influence on population dynamics by driving key demographic parameters ultimately determining population dynamics, age structure and reproductive performance. The life-history strategies of long-lived species in fluctuating environments are predicted to evolve to reduce the temporal variability of population growth rate (Roff, 2002; Doak et al., 2005). In particular, the demographic buffering hypothesis (Pfister, 1998) predicts that those demographic rates with a larger contribution to growth rate, and hence with a larger impact on extinction probability, should be less variable across time. Since population growth rate is particularly sensitive to adult survival in long-lived species (Saether and Bakke, 2000; Gaillard and Yoccoz, 2003), canalized adult survival is predicted to stabilize long term dynamics (e.g., Rotella et al., 2012). In unpredictable environments, in particular in the presence of abrupt perturbations on demographic rates induced by human activities, the ability of populations of long-lived species to buffer those rates more strongly affecting population growth will determine their extinction probability. Nevertheless, there is little evidence on the magnitude of the effects of changes in food availability on the long-term demography and population dynamics of long-lived scavenger species (Margalida, Colomer, and Oro, 2014).

In Europe, the outbreak of Bovine Spongiform Encephalopathy (BSE) led to the subsequent application of a restrictive sanitary legislation that critically limited the use of animal by-products not intended for human consumption (Regulation EC 1774/2002). This legislation banned the disposal of livestock carcasses in the field, which originated a major conservation problem, namely a new source of greenhouse gases emissions associated with the destruction of carcasses in authorized plants (Morales-Reyes et al., 2015), and further

affected the ecosystem services provided by scavengers (Margalida and Colomer, 2012; Blanco, 2014; Moleón, Sánchez-Zapata, Selva, et al., 2014; Morales-Reyes et al., 2015). This conflict between sanitary and environmental policies led to an intense debate about the European dispositions that regulated the use of animal by-products and their implications for conservation of necrophagous birds (Tella, 2001; Donázar, Margalida, and Campión, 2009; Margalida et al., 2010). In particular, virtual population modelling predicts that food shortage derived from sanitary regulations may induce rapid population declines in the Eurasian griffon vulture (*Gyps fulvus*) (Margalida and Colomer, 2012). This colonial species is by far the most abundant and widespread obligate scavenger in Europe, and is also considered the dominant species in scavenger guilds (Cortés-Avizanda et al., 2012). Roughly, 30000-37000 pairs currently breed in Spain ($>$ 95% of the EU population (Del Moral and Molina, 2018). However, there is a lack of knowledge on the long-term breeding biology and on the demographic consequences of sanitary regulation on vultures' population dynamics and conservation.

Here, we take advantage of the long-term monitoring of one of the largest colonies of Eurasian griffon vultures in Europe to analyse multidecadal changes in the demographic dynamics of this species. The different trophic scenarios that arose after the dramatic change in food availability derived from the European sanitary regulations provides an excellent opportunity to conduct a natural experiment to study aspects of demography and population dynamics directly dependent on food availability that can be hardly reproduced experimentally. The main goal of this analysis will be to model the long-term dynamics of vital rates before, during and after the implementation of the European sanitary regulation EC 1774/2002, in order to explore potential temporal shifts in the demographic structure induced by abrupt environmental deterioration. According to the buffering hypothesis (Pfister, 1998) we predict that adult survival of vultures remained constant in spite of the abrupt food shortage. In particular, within this scenario we evaluated how a large shift in food availability derived from the application of sanitary regulations affected, i) the population size, ii) stage structure, iii) laying dates and iv) breeding success of Eurasian griffon vultures, and how these traits impacted upon long-term population dynamics.

7.2 Materials and methods

7.2.1 *Study area and fieldwork*

We collected demographic data in the gorges of the Riaza River (41º31'N, 3º36'W), north of Segovia Province, Central Spain. The area includes a complex of cliffs and canyons where a large population of about 716 pairs of Eurasian griffon vulture were breeding in 2020. We censused the colony every two or three years from 1984 to 1994 and then annually until 2020; further information was obtained

from the national census of 1979 and other sources (http://www.naturalicante.com/mochila/Montejo/Hojas-e-Informes-censo.htm; Fernández y Fernández-Arroyo, 1996). We conducted five complete surveys each breeding season in order to detect all pairs (Martinez, Rodriguez, and Blanco, 1997). We examined both partners of each breeding pair to assess whether they were morphologically adults or sub-adults; individuals were categorized as sub-adults when they had not acquired full adult appearance (at 5-6 years old) on the basis of their general body colour, bill colour and, especially the colour, length and shape of the ruff feathers (Elosegui, 1989; Blanco and Martinez, 1996; Duriez, Eliotout, and Sarrazin, 2011). The age structure of pairs was recorded in three possible combinations: adult-adult, adult-sub-adult and sub-adult-sub-adult (Blanco and Martinez, 1996; Blanco, Martinez, and Traverso, 1997). To control for errors in the stage-classification of the monitored individuals due to uncertain ageing, we specified a state-space approach (King et al., 2010) linking the demographic process to the data through an observation model (see subsection Observation model).

Breeding Eurasian griffon vultures are year-round residents in the study area. Egg laying began in late December and the last clutches were laid by mid-March (Martínez, Blanco, and Rodríguez-Martínez, 1998). We conducted regular and intensive monitoring throughout the breeding season to determine whether the pairs laid (breeding pairs) or do not laid (non-breeding pairs) despite they showed typical pair-bonding behavior, including close contact, nest building and defense, and copulation. We observed at a distance the presence of eggs in the nests, recorded the start of incubation and calculated the date of hatching based on nestling age (Elosegui, 1989). Taking into account all these criteria and an incubation period of 55 days we determined laying dates within 10-day periods from 10 December onward (Martínez, Blanco, and Rodríguez-Martínez, 1998). Nests were regularly checked to verify breeding failure or the success of each pair in fledgling young; young fledged from June-August (Fargallo et al., 2018). All observations were made by telescope at distances that avoided disturbing the birds in the colony. Besides the long-term monitoring of breeding pairs in the colony, we focused on the behavior of 456 individuals ringed as nestlings since 1990. Of these individuals, only 9 bred outside the focal colony and most in colonies ¡50 Kms. away from there. In contrast, 136 birds bred or attempted to bred in the focal colony, some for more than 20 years. These data point to the strong philopatry of the Eurasian griffon vulture to the study area (F. Martínez and G. Blanco in prep.). These results agree with the dispersal behavior of the studied species in other colonies (Zuberogoitia et al., 2013). Overall, we considered breeders in this population as highly philopatric to their natal colony

7.2.2 *Stage-structured density-dependent population dynamics model*

Demographic population modelling is usually conducted through the use of population projection matrices (Caswell, 2001). This direct approach uses empirical estimates of vital rates, such as age-dependent fecundity and survival, to project the rate of increase of a population. In the presence of age- or stage-structured population time series, an alternative approach is to use inverse demographic modelling (Wood, 1997; Caswell, 2001). In this approach, vital rates are estimated through the fitting of a set of difference equations describing the life-history of a species to age- or stage-structured time series data (Wood, 1994; Caswell, 2001; Gross, Craig, and Hutchinson, 2002; Wielgus et al., 2008). In this study, we fit an inverse Bayesian stage-structured stochastic density-dependent demographic model to data assembled from distance observations of multiple cohorts of individuals during a 42-year period. As a non-invasive demographic approach (Wielgus et al., 2008), this method allows for the estimation of demographic vital rates from population-abundance data, with no need of capturing-recapturing individuals across time. Although this approach has been used previously (Gross, Craig, and Hutchinson, 2002; Wielgus et al., 2008), these implementations were deterministic. In contrast, here we propose a fully stochastic strategy taking into account demographic and environmental stochasticity, as well as sampling error and missing data. Our Bayesian approach thus allows for the efficient propagation and classification of uncertainty from the data to vital rates and population growth rates.

The demographic model for the Eurasian griffon vulture is based on the standard avian life cycle (Bennett and Owens, 2002). This model considers three separate demographic stages: fledglings, sub-adults and adults (Supplementary Material, Appendix S1: Fig. S1). Three transitions among life stages and two survival probabilities define the time-relationships between stages, so a set of three difference equations, including environmental and demographic stochasticity, can be derived to model the life cycle. A nonlinear density-dependent function of the Beverton-Holt type was included for each vital rate. This specification is suitable because it is a discrete-time analogous of the continuous-time logistic equation (Bohner and Warth, 2007), and considers an asymmetric resource partitioning among individuals in a scenario of contest competition typical of colonial species (the results, however, are insensitive to alternative functional specifications of density-dependence).

7.2.3 *Model construction*

Process model We let $n_{f,t}, n_{s,t}$ and $n_{a,t}$ represent the number of fledglings, sub-adults and adults in the breeding population at time t, respectively. We stress here that the adult stage also includes a variable proportion of sub-adults individuals that eventually paired

with an adult or another sub-adult; the breeding success of these mixed-aged and sub-adult pairs is invariably lower that adult breeding pairs. Some adult pairs may not breed in a given year, but they are regarded as adults. We let F represent the average fecundity (mean number of fledglings produced per adult per time step); be G_f (fledgling recruitment) and G_s (sub-adult recruitment) the average probabilities that a fledgling and a sub-adult recruits to the next stage, respectively (recruitment probabilities); and we let S_s (sub-adult survival) and S_a (adult survival) represent the average probabilities that a sub-adult and an adult survives (remains in the same stage) to the next time step, respectively. We let β_i represent the parameters encapsulating the strength of density-dependence modulating each vital rate i, and N_{t-1} the population size at time t-1 summed across stages ($N_{t-1} = n_{f,t-1} + n_{s,t-1} + n_{a,t-1}$). Note that, if the parameter β_i of a given vital rate is estimated to be 0, that vital rate becomes density-independent. The density-dependent demographic model can then be written as:

$$\begin{aligned} n_{f,t} &= \tfrac{F}{1+\beta_1 N_{t-1}} n_{a,t-1} + \varepsilon_{f,t} \\ n_{s,t} &= \tfrac{G_f}{1+\beta_2 N_{t-1}} n_{f,t-1} + \tfrac{S_s}{1+\beta_3 N_{t-1}} n_{s,t-1} + \varepsilon_{s,t} \\ n_{a,t} &= \tfrac{G_s}{1+\beta_4 N_{t-1}} n_{s,t-1} + \tfrac{S_a}{1+\beta_5 N_{t-1}} n_{a,t-1} + \varepsilon_{a,t} \end{aligned} \tag{7.2.1}$$

where $\varepsilon_{.,t}$ denotes environmental and demographic stochasticity impacting on each life stage (see below). The set of density-dependent difference equations in Eqn. 7.2.1 can be written in compact form as:

$$\mathbf{N}_t = \mathbf{L}\mathbf{N}_{t-1} + \boldsymbol{\varepsilon_t} \tag{7.2.2}$$

where $\mathbf{N_t} = (n_{f,t}, n_{s,t}, n_{a,t})^T$ is the vector of stage-structured population sizes and $\mathbf{L}$ is the Lefkovitch matrix (Lefkovitch, 1965) including the density-dependent vital rates for each stage:

$$\mathbf{L} = \begin{pmatrix} 0 & 0 & \frac{F}{1+\beta_1 N_{t-1}} \\ \frac{G_f}{1+\beta_2 N_{t-1}} & \frac{S_s}{1+\beta_3 N_{t-1}} & 0 \\ 0 & \frac{G_s}{1+\beta_4 N_{t-1}} & \frac{S_a}{1+\beta_5 N_{t-1}} \end{pmatrix} \tag{7.2.3}$$

Finally, in Eqn. 7.2.2, $\boldsymbol{\varepsilon}_t$ is a vector of sequentially independent random shocks distributed according to a multivariate normal distribution of mean 0, $\varepsilon_t \sim MVN(0, \Sigma_t)$. The variance-covariance matrix Σ_t is decomposed into an environmental (C) and demographic component (D_t), $\Sigma_t = C + D_t$ (see, Mutshinda, O'Hara, and Woiwod, 2011; Almaraz and Oro, 2011). The environmental matrix includes the variance of the stochastic environmental factors impacting on the dynamics of each life-stage in the main diagonal (σ^2), as well as the covariance terms for the pairwise (stage-by-stage) joint responses to these factors, $\zeta_{i,j}$ (for $i \neq j$), in the off-diagonal. The diagonal matrix $D_t = [\delta_f^2/n_f, \ldots, \delta_a^2/n_a]^T$ reflects the demographic variance affecting the transition of each demographic stage from time t-1 to t, which scales inversely with population size. See Supplementary Material, Appendix S1: Section S1 for details.

Given the density-dependent Lefkovitch matrix in eqn. 7.2.3 it is possible to estimate both the density-independent and density-dependent components of each vital rate. For example, in eqn. 7.2.3 the parameter F is the maximum attainable fecundity at very low population sizes (that is, when N_{t-1} is close to 0). Hence, it is a density-independent quantity. In contrast, the density-dependent component of fecundity is $\frac{F}{1+\beta_1 N^*}$, where N^* is the total population size at equilibrium. This is the size at which the population growth rate is 0. Indeed, it is straightforward to estimate a transient rate of increase, encapsulating the realized rate at which the stage-structured population grows, and an asymptotic rate of increase. This rate is, for a density-dependent model, the real part of the dominant eigenvalue of the Lefkovitch matrix evaluated at the equilibrium N^*, and should be 1 for a population to be stabilized through density-dependent mechanisms. See Supplementary Material, Appendix S1: S3.

Observation model The reliability of vital rates estimates depends on the correct classification of individuals according to a given demographic stage, either fledgling, sub-adult or adult. Individual variations in phenotypic characteristics might introduce some error in the assignment of a stage to an individual (see subsection Study area and fieldwork). To control for this we introduced three observation equations, linking the real (latent, or unobserved) abundance of fledglings, sub-adults and adults, $n_{f,t}, n_{s,t}$ and $n_{a,t}$ in Eqn. 7.2.1, to the demographic stage assignments made to every individual during the long-term monitoring of the colony. We let $y_{f,t}$, $y_{s,t}$ and $y_{a,t}$ be the number of pairs assigned to the fledgling, sub-adult and adult stage at time t, respectively, Then, we specified the real abundance for each stage as following a Poisson distribution across time with the mean as the observed (field-assigned) abundance:

$$\begin{aligned} y_{f,t} &\sim \mathcal{P}(n_{f,t}) \\ y_{s,t} &\sim \mathcal{P}(n_{s,t}) \\ y_{a,t} &\sim \mathcal{P}(n_{a,t}) \end{aligned} \tag{7.2.4}$$

A Poisson distribution is suitable in this case given the discrete nature of abundance, and due to the linear scaling of the observation variance with the mean abundance. The set of equations in 7.2.4 are called observation equations, while the set of equations in 7.2.1 are called process equations. The linking of the observation and process equations is called a state-space model (King et al., 2010). This strategy efficiently separates the uncertainty arising from the observation process, in our case the uncertain assignment of a demographic stage to an individual, from the variability due to the ecological process under study. Thus, this approach is fully stochastic.

7.2.4 *Parameter specification, posterior estimation and model validation*

The inverse state-space stage-structured model was fitted to the stage-structured time series of the Eurasian griffon vulture using Bayesian

Markov Chain Monte Carlo (MCMC) integration through Gibbs sampling (Gelman et al., 2014). We performed a review of the available literature searching for empirical natural history data on the vital rates of the Eurasian griffon vulture (Supplementary Material, Appendix S1: Table S1). This data was used to construct weakly informative priors for all the vital rates in our model (eqn. 7.2.1), which greatly improved posterior convergence of parameters and latent states. A Stochastic Search Variable Selection scheme (SSVS; George and McCulloch, 1993) was implemented to automatically set to 0 the density-dependent parameters with a negligible effect on demography during the MCMC simulation (see Mutshinda, O'Hara, and Woiwod, 2011; Almaraz and Oro, 2011 for further details). As a sparsity-inducing method (see Gelman et al., 2014.) with SSVS it is possible to estimate the posterior probability of inclusion of a density-dependent vital rate, and therefore evaluate the Bayes factor associated to each one. This allows evaluating the evidence in favor of including a given density-dependent vital rate. Finally, given the use of time-series abundance data it is also possible to estimate the relative contribution of each vital rate and stochastic component in the stage-structured model to the observed temporal variance in population dynamics (see Almaraz and Oro, 2011; Mutshinda, O'Hara, and Woiwod, 2011). This is analogous to Life Table Response Experiments (Caswell, 2010) applied to inverse, time series models. The construction of the model for the priors, the specification of SSVS and the description of variance component estimation are described in detail in Supplementary Material, Appendix S1: Sections S1-S3.

The Bayesian model was written in the JAGS language (Plummer, 2003), version 4.3.0, using the `R` environment (version 4.1.2, RCoreTeam, 2021) through the `runjags` package (Denwood, 2016). The JAGS code is available in DataS1. Three models were fitted to separate datasets: the first one models the demographic dynamics of the Eurasian griffon vulture prior to the BSE outbreak (from 1978 to 2001), the second one models the dynamics during the term of the Regulation EC 1774/2002 (2002-2011), and the third one models the dynamics after the ban was lifted (2012-2020). Three MCMC chains with diffuse random priors were run for 10^6 iterations for each model. Posterior estimates for parameters, latent states, missing data and variance components were obtained after discarding the first 5×10^5 iterations as burn-in. Standard diagnostic tests (see Gelman et al., 2014) were conducted to assess the convergence of the chains to a stationary distribution, using the package `ggmcmc` (Fernández-Marín, 2016).

Posterior predicted checks To check for potential issues with parameter identifiability of the proposed modelling approach, we generated synthetic time series from scenarios with known demographic rates and stochastic effects. The state-space density-dependent demographic

model (Eqns. 7.2.1 and 7.2.4) was then fitted to each of these time-series, and the resulting distribution of posterior parameter values were compared with the ground-truth estimates. The results of this exercise suggest that the model is highly successful in recovering the original demographic rates (See Supplementary Material, Appendix S1: Section S5). We also conducted posterior predictive checks on the fitted model (see Gelman et al., 2014) to assess model adequacy. We simulated 50 synthetic stage-structured time series from the fitted models and fit the model to each one. If the posterior estimates of vital rates are identifiable, we expect that the vital rates recovered by the model with the synthetic time series will approach the values of the model fitted to the observed data (Gelman et al., 2014). That is, a clustering of the posterior fits to simulated data around the Y=X line is indicative of parameter identifiability.

7.3 Results

7.3.1 *Temporal trends and shifts in breeding parameters*

From 1978 to the BSE outbreak in 2001, population numbers expanded from 128 to 334 breeding pairs in the focal colony (Fig. 7.1A). The proportion of breeding pairs made up by either an adult plus a sub-adult (mixed-age pairs) or two sub-adults also increased consistently from 1985 to 2001, but these positive trends ended abruptly in 2001, indicating that most sub-adults withdrew from the reproducing population (Fig. 7.1B). These shifts are concurrent with the onset of the BSE outbreak, with a peak in 2003 (Fig. 7.1A). Moreover, a phenological advancement in mean laying date of roughly two weeks from 1985 ended with an abrupt shift in 2001-2003, amounting to an average delay in one month up to 2011 (Fig. 7.1C). Another clear abrupt shift to very low breeding success took place in 2004 for both (Fig. 7.1D). These shifts in breeding structure and phenology were accompanied by similar trends in the stage-structured time series (Fig. 7.1A). From the BSE outbreak in 2001 to the end of the restrictive regulation (2011), the breeding population dropped with a time lag similar to the age of first breeding in the Eurasian griffon vulture (4-5 years), while the non-breeding population stabilized. However, a particularly dramatic crash was observed in the number of fledglings throughout this period (Fig. 7.1A). After the ban was lifted (2011-2020), mean-laying date abruptly dropped to pre-outbreak levels and breeding success increased for both the adults only and adults plus sub-adults pairs.

7.3.2 *Inverse stage-structured demographic modelling*

Model-based estimates of vital rates obtained with the state-space inverse demographic model suggest a severe drop in fecundity after the BSE outbreak, from 0.629 ± 0.027 (1SD) chicks per breeding adult prior to the outbreak, to 0.465 ± 0.047 during the BSE epidemic (Fig. 7.2A). After the BSE outbreak (when the food-shortage period ended)

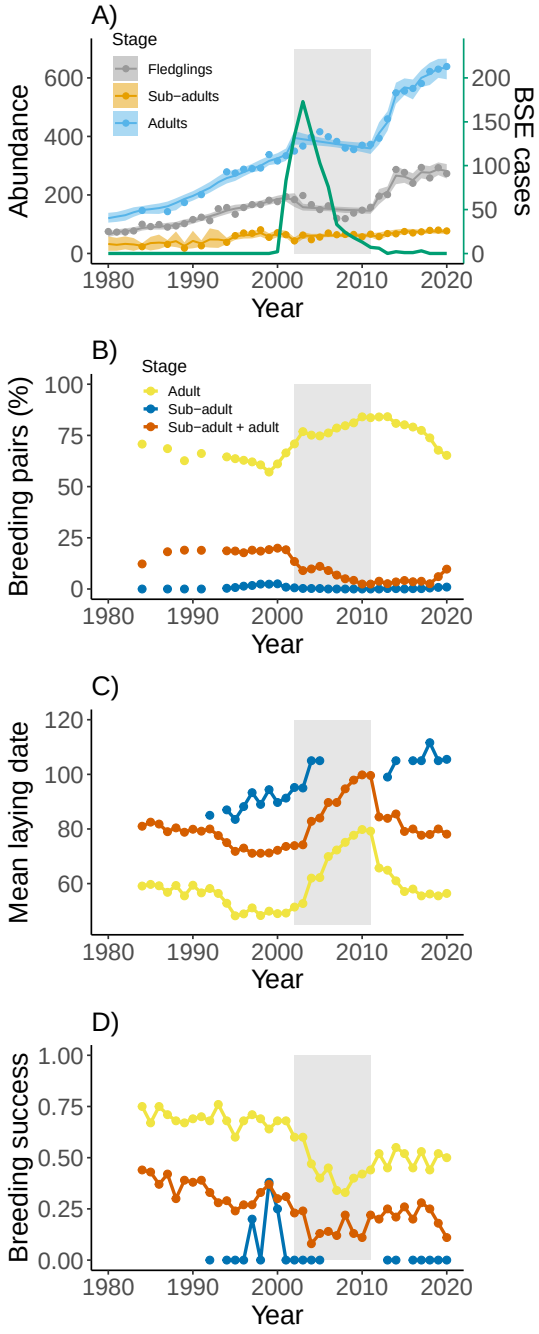

Figure 7.1: Long-term dynamics of the abundance, breeding parameters and phenology of the Eurasian griffon vulture in Central Spain from 1984 to 2020. **A**. Time series of adult breeding pairs (red dots), non-breeding pairs made up by sub-adults (blue dots), and fledglings (green dots). The impact of observation uncertainty arising from the stage classification errors is shown as shaded bands. These areas encompass the 90% credible intervals of the posterior estimates for the latent abundances of adults (red shade), fledglings (green shade) and sub-adults (blue shades). The orange time-series stand for the yearly reported cases of Bovine Spongiform Encephalopathy in Spain provided by the Spanish Ministry of Agriculture (MAPAMA, 2018). **B**. Proportion of breeding pairs (%) formed by adults only (red dots), by an adult plus a sub-adult (green dots) and pairs formed by sub-adults only (blue dots). **C**. Mean laying date in Julian days for the three types of breeding pairs. **D**. Breeding success, estimated as the number of fledglings per breeding pair are shown structured by stages. In all figures, the gray shaded rectangle covers the time window during which the European legislation banned carrion disposal in the wild.

fecundity increased again (0.487 ± 0.034). These figures agree very well with the data on breeding success obtained through the individual-based long-term monitoring of the colony (Fig. 7.1D). Sub-adult recruitment to the breeding adult population dropped during the epidemic, with a correlated rise in sub-adult survival (a larger fraction of sub-adults remained as such during the epidemic; Fig. 7.2A). Adult survival, in contrast, remained constantly high during the 42-year period (0.992 ± 0.008 during the pre-BSE period, 0.991 ± 0.007 during the food-shortage, and 0.985 ± 0.017 after the food-shortage; Fig. 7.2A).

The relative impact of vital rates on the temporal variance of the stage-structured population suffered a significant shift after the BSE outbreak: prior to 2001 adult survival explained a large proportion of the variance observed at the population level (83.1%), followed by fecundity (10.6%, Fig. 7.2B). During the BSE outbreak the impact of adult survival decreased to 71.3%, and a further decrease to a 53.8% was modeled but after this event (Fig. 7.2B). Moreover, after the BSE outbreak the variance component of environmental stochasticity increased to 42.5%, while it was negligible during the previous periods (Fig. 7.2B). Overall, the shifts in demographic rates translated to shifts in the transient rate of increase, which was larger before (1.036 ± 0.004) and after (1.059 ± 0.010) than during the BSE outbreak (0.990 ± 0.006, Fig. 7.3A). Note that the transient rate of increase of the stage-structured population overlapped 1 during the BSE outbreak (95% Credible Interval, CI: 0.971-1.002), but neither before (95% CI: 1.028-1.044) nor after this period (95% CI: 1.040-1.079).

7.3.3 *Impact of density-dependent vital rates on population stabilization*

The density at equilibrium predicted by the stage-structured density-dependent model differed significantly among the three time periods (Supplementary Material, Appendix S1: Section S4): 793.397 ± 59.925 (1SD) individuals before the BSE outbreak, 153.854 ± 30.887 individuals during the BSE outbreak and 398.113 ± 185.558 individuals after the BSE outbreak. Compared to the observed number of individuals across time (Fig. 7.1A), this suggests that prior to the BSE outbreak the Eurasian griffon vulture population was approaching the equilibrium density, while both during the BSE outbreak and after this period it was fluctuating above its carrying capacity. The posterior asymptotic rates of increase of the density-dependent model evaluated at the population size at equilibrium were centered around 1 in all three periods, consistent with a long-term stabilized population (Fig. 7.1B; See Supplementary Material, Appendix S1: Section S4).

The probability of detecting density-dependence across the life cycle was relatively low for all time periods (Supplementary Material, Appendix S1: Table S2), ranging from 0.280 before the BSE outbreak to 0.264 during the BSE outbreak and 0.255 after the BSE outbreak. The posterior probability of density dependence was indeed very low for most vital rates during all time periods, which overall suggest weak density-dependent regulation across the life cycle. However, the posterior probability of density-dependence in sub-adult survival before the BSE outbreak was of 0.466, with an associated Bayes factor of 2.248. This is regarded as barely worth mentioning evidence according to the Kass-Raftery scale (Supplementary Material, Appendix S1: Table S2). Both during and after the BSE outbreak, very weak evidence for density-dependence was found for sub-adult recruitment, but not survival. Due to the low sample sizes of these latter periods,

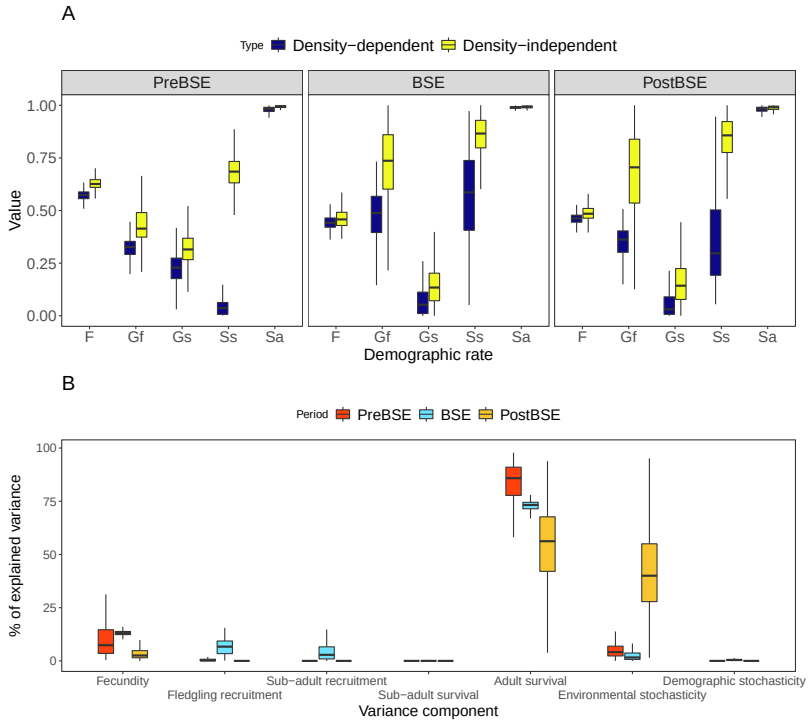

Figure 7.2: Demographic modelling of the Eurasian griffon vulture in Central Spain. An inverse stage-structured model was fitted to the population dynamics prior to the BSE outbreak (PreBSE, 1978-2000), for the dynamics during the term of the sanitary regulation EC 1774/2002 (BSE, 2001-2011) and after the sanitary regulation was lifted (PostBSE, 2012-2020). **A**. The posterior distribution of the vital rates estimates considered in the life cycle during the three time periods, shown for both the density-independent (yellow) and density-dependent rates (blue, see main text); F = Fecundity; Gf = Fledgling recruitment; Gs = Sub-adult recruitment; Ss = Sub-adult survival; and Sa = Adult survival. **B**. The relative impact of the set of vital rates, and environmental and demographic stochasticity, on the temporal variance of the stage-structured population (measured as the % of explained variance in abundance). In the box-plot, horizontal black line stand for the posterior median of each rate and stochastic component; the box represents the inter-quantile range and whiskers show the 95% percentiles.

Type II error in the detection of density dependence cannot be ruled out. Finally, breeding success of adult and mixed-aged pairs showed a slight decrease from 1985 as a likely consequence of density-dependent processes, only significant for the time series of mixed-aged pairs (r = 0.66, p-value = 0.003; see Fig. 7.1D).

The impact of density-dependence on the different vital rates can be assessed in Figure 7.2A. While most vital rates are only weakly depressed at equilibrium in all time periods, sub-adult survival is severely reduced when the population approaches the equilibrium population size. As expected, this is particularly the case before the BSE outbreak, when the evidence for density-dependence is significant.

7.3.4 *Posterior predictive checks and model validation*

With only 50 synthetic time series, the inverse demographic model was able to successfully recover the original vital rates estimates with simulated stage-structured data (Fig. 7.4A-C): most of the posterior predicted vital rates cluster around the Y=X regression line. Importantly, fecundity and adult survival, which are the vital rates most strongly impacting on temporal dynamics (Fig. 7.2B) are also the vital rates more accurately recovered by the posterior predictive checking (Fig. 7.4). The posterior predicted abundance time-series agree very well with the true abundance for all demographic stages and temporal periods (Fig. 7.4D-F).

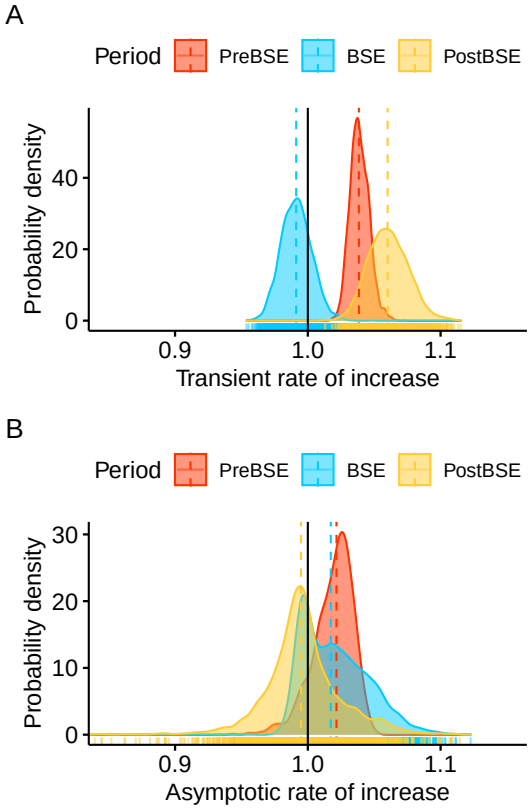

Figure 7.3: Rates of increase of the stage-structured Eurasian griffon vulture population during a 42-year period. **A**. Posterior distributions of the transient rates of increase before the BSE outbreak (PreBSE, 1978-2001), during the BSE outbreak (BSE: 2002-2011), and after the BSE outbreak (PostBSE: 2012-2020). **B**. Posterior distributions of the asymptotic rates of increase, λ_s, predicted from the model evaluated at the equilibrium population size N^* for the three time periods (Supplementary Material, Appendix S1: Section S4). In all figures, vertical dotted lines indicate the mean of each posterior distribution, and the solid black line denotes the rate of increase 1, at which the population achieves long-term stability.

7.4 Discussion

Based on 42 years of monitoring of one of the largest colonies of Eurasian griffon vultures in Europe, we found that temporal, abrupt variability in food availability derived from human activities and induced by an epidemic outbreak had profound effects on the population dynamics of this long-lived species. The influence of food availability on the dynamics of wildlife populations has been widely discussed (see review in Ostfeld and Keesing, 2000). Human activities have played an important role in ecosystem functioning by generating anthropogenic food subsidies (Oro et al., 2013). Vertebrate scavengers are one of the most susceptible group to changes in the availability of these subsidies (Cortés-Avizanda et al., 2016). Several studies suggest a negative impact of food scarcity arising from the application of the European sanitary policy on the populations of some scavengers of conservation concern. For example, dietary changes in vultures (Donázar, Cortés-Avizanda, and Carrete, 2010) and other avian scavengers (Blanco, 2014), as well as large carnivores (Lagos and Bárcena, 2015; Llaneza and López-Bao, 2015; Northrup and Boyce, 2012), impacts on the movement patterns (Arrondo et al., 2018) or changes in demographic parameters of vultures (e.g. decrease in survival and breeding success or delay in egg-laying dates; Donázar, Margalida, and Campión, 2009; Martínez-Abraín et al., 2012; Margalida et al., 2014; Donázar et al., 2020). However, while some studies have suggested that food shortage

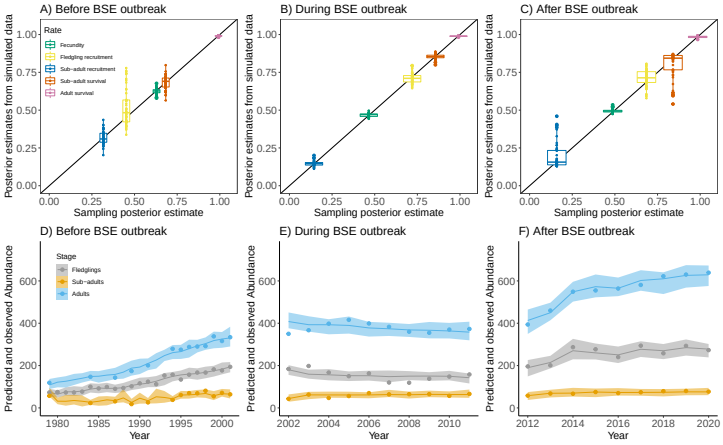

Figure 7.4: Results of the numerical experiment testing the ability of the inverse demographic model to recover the demographic dynamics of the Eurasian griffon vulture before, during and after the BSE outbreak. **A**-**C**. The posterior estimates for the vital rates of the inverse state-space demographic model fitted to each of the 50 posterior predicted time series are plotted against the sampling posterior estimate of the real dataset used to generate them during the three temporal periods. The box-plots show the median (horizontal line), inter-quantile range (box) and 95% percentiles (whiskers). The thickness of the box is proportional to the posterior density of the estimates within the inter-quantile range. The Y=X regression line (in black) is plotted as a reference. **D**-**F**. Time series of the observed abundance for the three demographic stages (adults: blue dots; sub-adults: green dots; fledglings: red dots) during the three demographic periods (Before, during and after de BSE outbreak). The time series of the abundance predicted by the 50 posterior simulated models are shown for each stage as lines (average of predicted abundance) and shaded regions (95% credible interval).

derived from sanitary regulations may affect the Eurasian griffon vulture (Margalida and Colomer, 2012), few studies have attempted to study the effects of food shortages on the basic demographic parameters of this species on the long-term.

Our inverse Bayesian demographic modelling approach uses long time-series of stage-structured abundance data (Wood, 1994; Gross, Craig, and Hutchinson, 2002) to decompose the temporal variability of population abundance into the relative impact of the constituent vital rates. Our method thus allows for the estimation of the effects of transient perturbations on the long term demographic variability and population dynamics by using only stage-structured abundance data. The results suggests that some vital rates of this keystone avian scavenger, in particular fecundity, might be very sensitive to severe food shortages derived from the shifts in sanitary regulations (i.e., reduction of carcasses availability in the field). In the Iberian Peninsula, the Eurasian griffon vulture primarily depended on free-ranging livestock in the past, especially sheep in lowland areas and cattle in mountain ranges (Donazar, 1993). The declining trend in the abundance of extensive herds over the last decades, especially of sheep and goats, along with the sanitary regulations forbidding the abandonment of cattle carcasses in the countryside, were concurrent with an increase in the number of factory farms of fattening pigs and poultry and with increasing stabled conditions of ungulate livestock (Blanco, 2014). As a consequence, the populations of this and other vultures now largely depend on livestock carcasses from intensive exploitations in the study area and other regions across its distribution range in Spain (Camiña and Montelío, 2006; Donázar, Cortés-Avizanda, and Carrete, 2010; Blanco et al., 2019). It should be noted, though, that the application of the policy that banned the abandonment of carcasses in the countryside due to the BSE crisis was not applied homogeneously across time and space, but it supposed a general crash in the availability of carrion in most of the range of distribution of vultures in Spain (Donázar, Margalida, and Campión, 2009; Margalida et al., 2010). In general, the application of the restrictive policy was not conducted immediately af-

ter the new regulation, but it delayed a variable time period depending on regions with different government administrations. In addition, the discard of carcasses in the countryside continued occurring illegally in some regions in the first years after the implementation of the sanitary policy, and still occurs, but this practice was increasingly persecuted later. Overall, these factors led to a time lag between the new regulation and its effective application, which was reflected in the lowest carcass availability around 1-2 years after the emergence of the BSE crisis (Donázar, Margalida, and Campión, 2009; Blanco, 2014).

Prior to the BSE outbreak, an advancement in the mean laying date, along with an increase in the proportion of mixed-aged and subadults pairs suggest that food availability was relatively high in the study colony and other areas (Blanco, Martinez, and Traverso, 1997; Blanco, 2014; Parra and Tellería, 2004). During the implementation of the European sanitary regulation a dramatic reduction of available livestock carcasses induced a severe environmental deterioration that triggered the modeled structural change in stage structure, productivity and phenology. Among these effects the delay in laying date and the dramatic drop in fecundity were particularly large. This is likely due to the high cost of reproduction and other life-history traits of vultures, evolved as a result of unpredictable food conditions (see Donazar, 1993; Bennett and Owens, 2002; Carrete, Donázar, and Margalida, 2006). In contrast, as a long-lived species, adult survival is expected to be very high and its temporal variability relatively low, owing to the canalization of this vital rate (Stearns and Kawecki, 1994; Saether and Bakke, 2000; Pfister, 1998; Sæther et al., 2013). Eurasian griffon vultures would exhibit relatively constant adult survival but large plasticity in other traits like reproduction (Fargallo et al., 2018), as has been described for different organisms with a slow pace of life (e.g. Bennett and Owens, 2002; Benton, Plaistow, and Coulson, 2006; Sæther et al., 2013). Thus, the combination of fixed and variable traits might have dampened the effects of sanitary policies and allow for a quick recovery of population structure and dynamics once the EU sanitary policies allowed for the disposal of carcasses (Margalida et al., 2010; Blanco, 2014). Interestingly however, while most of the observed and modeled demographic parameters promptly reversed to pre-outbreak values after the ban was lifted, their relative impact on population dynamics shifted across the 42-year period: the variance component associated to adult survival consistently decreased across time even though this rate remained constantly high, while the environmental stochastic component of the dynamics increased dramatically. This suggest that the relative dynamical impacts of constant and variable vital rates across time can vary in rather non-intuitive ways in stochastic environments.

Several studies have shown the importance of food competition driven by density-dependent processes on population dynamics of long-lived birds such as gulls (see e.g. Payo-Payo et al., 2016). Likewise,

breeding productivity of the semi-colonial cinereous vulture (*Aegypius monachus*) and the territorial bearded vulture (*Gypaetus barbatus*) was affected by density-dependent mechanisms (Carrete, Donázar, and Margalida, 2006; Fernández-Bellon et al., 2016). For the Eurasian griffon vulture in our study area, observed breeding success consistently declined across time, particularly for the mixed-aged pairs formed by an adult and a sub-adult. Moreover, our modeling results indicated that before the BSE outbreak, density-dependent sub-adult survival likely played a role on population regulation: at the onset of the sanitary regulation the population was fluctuating close to the equilibrium population size, the size at which the population growth rate is 0. From this moment to the end of the time-series, the fluctuations were above the estimated equilibrium population size, particularly during the BSE outbreak. In other raptor species, density-dependence also operates through sub-adult demographic stages (e.g., Carrete et al., 2006), since juveniles disperse to other areas or may skip breeding at high population densities. In our case, the reduced sub-adult survival suggests that a fraction of sub-adult individuals abandoned the population when the colony approached the transient carrying capacity. This is reflected in the abrupt drop in the proportion of sub-adult and mixed-aged pairs during the BSE outbreak. Finally, a consistent delay in laying date for adults, sub-adults and mixed-aged pairs during the term of the sanitary regulation point to a severe environmental deterioration. Life history theory indeed predicts that pulse perturbations, such as severe food shortages, may induce long-lived species to reduce breeding effort and hence maintain large survival rates across time (e.g. Saether and Bakke, 2000). While age and sex might influence differential patterns of survival in some vulture species (Sanz-Aguilar et al., 2017), data from 66 GPS-tagged adult Eurasian griffon vultures throughout Spain suggest that mortality was mainly related to landscape anthropization and only secondarily to sex and sub-population (Arrondo et al., 2020), but no information is available for fledglings and sub-adults.

Overall, our findings suggest that the changes in food availability related to shifts in European sanitary regulations have had negative consequences on key demographic parameters of the colonial Eurasian griffon vultures with significant detrimental effects on the population dynamics of this species. Vultures have coevolved with a rich but ephemeral food resource (DeVault, Rhodes, and Shivik, 2003). Carcass availability and predictability can be largely variable depending among others on the source of food (i.e. wild vs. domestic ungulates) and the processes involved (Moleón, Sánchez-Zapata, Selva, et al., 2014). Vultures have been able to cope with this variability for eons (Moleón, Sánchez-Zapata, Margalida, et al., 2014). In contrast, other environmental changes increasing mortality such as illegal poisoning, the use of veterinary drugs like diclofenac, or even collision with wind turbines (Martínez-Abraín et al., 2012; Margalida et al., 2021) are known to negatively impact on vultures' populations (Green et

al., 2006; Serrano et al., 2020). Our results confirm the impact of domestic ungulate carcasses availability as the major source of food resources for Eurasian griffon vultures in Spain, in spite of the importance of wild ungulate populations (Mateo-Tomás et al., 2015; Blanco et al., 2019). Nearly twenty years after the BSE outbreak, the consensus among scientists, conservationists and managers led to the implementation of a new European regulation (EC 142/2011), which allows farmers to leave the carcasses of livestock in the field. Our results show that, although most of the changes in demographic parameters of Eurasian griffon vultures promptly reversed to pre-BSE outbreak scenario after the ban was lifted and the new legislation EC 142/2011 was implemented, the dynamical impacts of the abrupt demographic changes can still be seen in the population more than a decade after the BSE outbreak. Nevertheless, although the new and encouraging legislation represents an important improvement in the conservation of European scavengers and the environment, some aspects should still be improved to ensure the long-term conservation of vultures (Mateo-Tomás et al., 2019; Morales-Reyes et al., 2017; Blanco et al., 2016; Blanco et al., 2019). Given the tight intertwining of sanitary and conservation policies, further research is needed to evaluate the demographic changes derived from the application of new sanitary regulations that may impact vulture conservation and the ecosystem services they provide.

Acknowledgements

The authors thank Fidel José Fernáandez y Fernáandez- Arroyo and those who have worked over the years to protect the Riaza Gorges as a Fauna Refuge and Natural Park (WWF Spain and Junta de Castilla y León). The constructive comments made by the editor and two anonymous reviewers greatly improved the quality of a previous version of the manuscript. Pablo Almaraz was supported by a pre- doctoral fellowship through the program Formacion del Profesorado Universitario FPU of the Spanish Ministry of Education (FPU16/00626). ZMR was supported by two post- doctoral contracts cofunded by the Generalitat Valenciana and the European Social Fund (APOSTD/2019/016) and funded by the Junta de Andalucía (POSTDOC-21-00353). Funds were provided by the projects CGL2009-12753-C02- 01/BOS, CGL2010-15726, and PID2019-109685GB-I00 of the Spanish Ministry of Science and Innovation.

Conflict of interest

The authors have no conflicts of interest to declare for the manuscript.

Authors contributions

Guillermo Blanco, José A. Sánchez-Zapata, and Pablo Almaraz conceived the study; Guillermo Blanco and Félix Martínez undertook the

surveys; Pablo Almaraz designed and conducted the analyses; Pablo Almaraz led manuscript writing with inputs from all authors.

8 Covariation among life history traits, demographic rates, and population dynamics in a globally threatened taxa

Pablo Almaraz[1,2]

1. Departamento de Ecuaciones Diferenciales y Análisis Numérico, Facultad de Matemáticas, Universidad de Sevilla, Sevilla, Spain.

2. Departamento de Ecología de Humedales, Estación Biológica de Doñana, CSIC, Sevilla, Spain.

Abstract

The theory of evolutionary strategies predicts a "slow-fast" continuum in the covariation between demographic rates, life history characteristics and population dynamic patterns. Fast species, for example, are those that have high fecundity and low survival rates. Outside this continuum, however, there are some species with high survival rates and high fertility rates. This strategy has been called "risk dispersal," and it has evolved in species that live in highly unpredictable environments. Among birds, waders (Order Charadriiformes) have been suggested as an example of a "risk disperser" species. Surprisingly, more than 40% of the world's wader bird populations have been categorized as in decline, despite the fact that less than 14% of the species are classified as Endangered by the IUCN. Here, the method of comparative population dynamics, combining time series analysis of counts and demographic matrix modeling, is used to define a potential ecological and evolutionary basis that explains the unusual decline observed in this bird taxon. Through the analysis of 15 time series and demographic data belonging to 13 migratory species, this study shows that the analyzed species show an internal tendency to exhibit fluctuations over a very long period (years or decades). The variation in these stability properties is related to central features of the vital strategy, such as body size or the existence of sexual selection. Although adult survival rate is the demographic parameter that has the greatest impact on the population growth rate, particularly in declining populations, this parameter is positively correlated with the magnitude of environmental stochasticity that impacts on temporal dynamics. This suggests a close environmental control of the demo-

graphic parameter with the greatest impact on population growth rate. Taking into account the dynamic population consequences of the "risk dispersal" strategy, these results may provide an evolutionary basis for the large proportion of global wader bird populations in decline under a scenario of planetary reduction in habitat quantity and quality.

KEYWORDS demography, Lyapunov exponent, matrix models, stochasticity, theta-logistic model, time-series.

8.1 INTRODUCTION

Stochastic and deterministic factors have been shown to jointly influence population dynamics of vertebrates (Turchin, 2003; Lande, Engen, and Saether, 2003; Sæther et al., 2013). Inter-specific variation in the relative effects of these factors has been recently related to variation in demographic characteristics and life-history strategies of ungulates (Gaillard and Yoccoz, 2003) and birds (Saether and Bakke, 2000; Sæther et al., 2013; Sæther et al., 1996). This attempt to characterize the relative effects of stochasticity and determinism in the pattern of population regulation and life-history variation has been termed the comparative population dynamics approach (Sæther et al., 1996; Coulson, Lindström, and Cotgreave, 2002). The fundamental assumption of this approach is that the dynamical characteristics of a time-series of population counts, such as the cycle period and the signal-to-noise ratio (Turchin, 2003), will somehow reflect the particular life-history and demographic characteristic of the species. Indeed, the most recent modelling schemes build on this assumption to predict the structure of covariation in serial population data from the knowledge of life-histories strategies (see Lande, Engen, and Saether, 2003).

Within this field, birds stand out as a particularly valuable ecological model because a great deal of data currently exists on every feature of their biology and ecology (Bennett and Owens, 2002). Based on adult survival rates and clutch sizes from 104 bird species, Sæther et al., 1996 hypothesize that a 'slow-fast' continuum of life-history variation can be defined as a gradient in which a group of highly fecund species with low life expectancy is located in the "fast" extreme, and a cluster of survivorship species, with smaller clutches (usually only 1 egg) and high survival rates is found at the "slow" end. Outside this continuum, a bet-hedging category denotes species with large clutch sizes and still large survival rates (Saether and Bakke, 2000). Shorebirds, gulls and terns (Order Charadriiformes) are such an example among birds (Sæther et al., 1996).

Risk-spreading, or bet-hedging (Slatkin, 1974; Seger and Brockmann, 1987) is a life history strategy evolved in organisms living in highly unpredictable environments in which fitness is maximized at the cost of an increased variance of some vital rates, such as fecundity (Gillespie, 1977). When the stochastic component of fitness is mostly environmental rather than developmental, the geometric mean fitness is consistently smaller than the arithmetic mean fitness (see Gillespie,

1977; Charlesworth, 1994), so Bulmer, 1985 suggested an adaptive decrease in arithmetic fitness through a compensatory reduction in the temporal variance of some of its components, such as adult survival rate. Such an effect, named environmental canalization, was recently reported in ungulate populations (Gaillard and Yoccoz, 2003; Pfister, 1998). Indeed, Gaillard and Yoccoz, 2003 suggest that the apparent canalization of adult survival rate in ungulates is the ecological consequence of the evolution of bet-hedging strategies in this group.

However, some recent theoretical analyses have shown that the annual reproductive cost in iteroparous species should be variable if the environment fluctuates largely among breeding episodes (Orzack and Tuljapurkar, 2001). The biological consequence of this external variability, and hence the cause for the variable cost of reproduction, is the existence of multiple adaptive optima for reproductive effort. Thus, this should limit the ability of life-history strategies to filter environmental stochasticity into a realized reduction of the temporal variance in vital rates (the so-called environmental canalization). In this scenario, the optimal individual strategy would be to produce a large progeny with differing phenotypes in order to compensate for bad years on the long-term; in other words, large environmental stochasticity necessarily translates to a reduced arithmetic fitness at the individual level (Grafen, 1999) and to an increased temporal variability of demographic rates at the population level, which in practice should appear to be under environmental control. This might pave the way for the evolution of extreme bet-hedging strategies (see Jenouvrier, Barbraud, et al., 2005 for a recent example). Overall, as a general ecological hypothesis we can predict for extreme bet-hedgers an internally generated population destabilization coupled with large external stochastic effects on life-history and dynamics; a specific demographic hypothesis is that adult survival would still have a large relative impact on growth rate despite a high fecundity (Saether and Bakke, 2000). These predicted population dynamical consequences of bet-hedging remain largely unexplored so far in a single order of organism.

The present work proposes a framework integrating different modelling strategies within the comparative population dynamics approach. Available studies either provide unstructured analyses of time-series of population counts (Turchin, 2003) or age-/stage-structured modelling of demographic data (Caswell, 2001). The present study aims at merging both approaches in a single analysis of population time-series, demographic rates and life-history traits of a set of species, which in practice might provide the link between largely ecological processes (environmental stochasticity and quantitative dynamic probes measured through time-series analysis) and largely evolutionary patterns (extant inter-specific variation in demographic rates and life-history traits measured through structured population modelling). As a model ecological system this work will focus on 13 migratory wader species wintering in Great Britain. This choice is suitable for two main reasons. Firstly, shorebirds are an ideal focus among birds due to their unusually high diversity in life-strategies (Bennett and Owens, 2002;

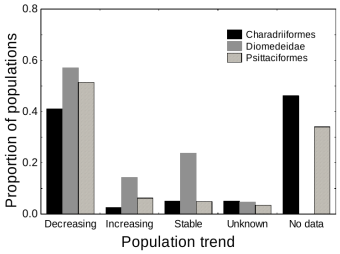

Figure 8.1: Proportion of populations from the Charadriiformes, Psittaciformes, and Diomedeidae belonging to any of the IUCN categories for which data for the temporal trend could be obtained (`http://www.iucnredlist.org`; see Appendix A for further details).

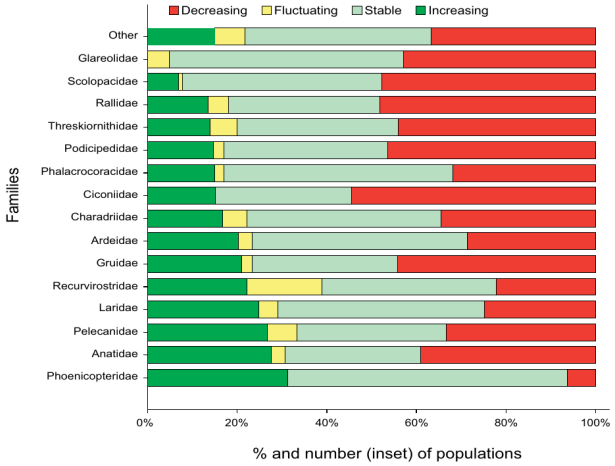

Figure 8.2: Population trends by selected waterbird families, from WetlandsInternational, 2012.

Baker et al., 2004). Indeed, the early suggestion by Sæther et al., 1996 that shorebirds are bet-hedgers provides one of the first opportunities to test the population dynamical consequences of this strategy. Secondly, an intriguing worldwide decline affecting more than 40% of the known shorebird populations (Figures 8.1 and 8.2) has been recently observed (International Wader Study Group, 2003; Paleczny et al., 2015; Roomen et al., 2012; Kenyon Ross et al., 2012; WetlandsInternational, 2012). Although many anthropogenic causal factors have been proposed (see Rehfisch et al., 2003; Norris, Atkinson, and Gill, 2004; Wilson and Lundberg, 2004; WetlandsInternational, 2012; Lindström et al., 2015), the global character of this decline might point to ecological and evolutionary causal factors behind it (e.g., Peach, Thompson, and Coulson, 1994; Baker et al., 2004; Dougall et al., 2005). Hence, this study explores whether world shorebirds are prone to decline as a result of their unusual bet-hedging life history strategy. Hence, due to the close connection between bet-hedging and population vulnerability (Boyce, Kirsch, and Servheen, 2002) this research might help to shed light on the possible biological causes behind this global decline.

8.2 Material and methods

8.2.1 *The dataset*

A search for time-series of population counts of shorebirds (excluding Gulls and Terns) spanning at least 15 years with no missing counts was conducted using the Global Population Dynamics Database `https://knb.ecoinformatics.org/view/doi:10.5063/F1BZ63Z8` (e.g., Inchausti and Halley, 2001) and standard literature search. Although some datasets with less than 15 years were found in the literature, only figures equal or bigger than this were selected to provide a reasonable statistical power. In order to avoid the effect of factors other than biological characteristics, I excluded three datasets and included only datasets from a single spatial location (Great Britain). Overall, 15 time-series from 13 migratory shorebirds species belonging to three re-

lated families were located (see Table 8.3 in Appendix B). Both population dynamic properties and life-history characteristics has been shown to be correlated with latitude in some groups (Bjornstad, Falck, and Stenseth Chr., 1995; Turchin, 2003). A key approach of this study is the analysis of multi-species data from a single spatial unit, thus ruling out the possible confounding effect of latitude on population dynamics. In any case, little geographic variability in life-history traits and demographic rates has been revealed in shorebirds (e.g., Wennerberg, Klaassen, and Lindström, 2002; Summers and Nicoll, 2004; Dougall et al., 2005).

Several life-history traits and demographic rates which are supposed to affect population dynamic properties were quantified in all the species studied (e.g., Charlesworth, 1994; Bennett and Owens, 2002; Sæther, Engen, and Matthysen, 2002): 1) Predictions from a model II regression between body weight and wing length were used as an index of body size (Peig and Green, 2009); 2) Plumage dichromatism between sexes was used as a surrogate for the operation of sexual selection (Doherty et al., 2003). Since body size was a good predictor of quantitative dynamic probes (see Results), a general linear model (GLM) with identity link function and normal error structure (Dobson and Barnett, 2018) was constructed to test for the effect of sexual dimorphism on population dynamics characteristics while controlling for body size; 3) Number of broods per breeding season; 4) Nest size and hatching success, from which an estimate of brood size was obtained; 5) fledgling success; 6) α, or age at first breeding (Charlesworth, 1994); and 7) Annual juvenile and adult mortality and age of the oldest bird ringed. Most of these figures are available in the literature (see Table 8.4 in Appendix C).

8.2.2 *Population time-series modelling: the unstructured scheme*

In order to assess their dynamical characteristics, four quantitative probes (sensu Turchin, 2003) were calculated for each time series, namely: 1) the coefficient of variation, as a measure of relative variability (Pimm and Redfearn, 1988; Inchausti and Halley, 2003); 2) The global Lyapunov exponent (GLE, Λ_∞), which measures the long-term exponential rate of system trajectory divergence and provides a probe of deterministic dynamic instability (Hilborn, 2000). Λ_∞ was estimated through generalised cross-validation using a response surface model (Hilborn, 2000; Turchin, 2003):

$$r_t = P_q\left(N_{t-1}^{\phi_1}, N_{t-2}^{\phi_2}, \cdots, N_{t-P}^{\phi_P}\right) + \epsilon_t \tag{8.2.1}$$

where r_t is the population growth rate (N_t/N_{t-1}, where N_t is population size at time t), P_q is a polynomial of degree q, p is the time lag (or process order), ϕ are transformation parameters, and ϵ_t is the residual variance (Box and R., 1987). Once the generalised cross-validation method selects the optimal model for each time-series, the matrix including the partial derivatives of the optimal function in eqn. 8.2.1 (called the Jacobian matrix, J_t; Hilborn, 2000) was evaluated both at

the initial time (J_0) and at successive points of the time-evolved system ($J_t, J_{t+1}, \ldots, J_{t+K}$). The global Lyapunov exponent is then defined as the mean product of the Jacobians, using some matrix norm, such as the dominant eigenvalue of J, for matrix multiplication (Hilborn, 2000; Turchin, 2003):

$$\Lambda_\infty = \frac{1}{t} \parallel J_{t-1} \cdot J_{t-2} \cdots J_0 \parallel \tag{8.2.2}$$

Therefore, Λ_∞ measures the average exponential rate of divergence of the time-evolved system from the initial trajectory. A useful analogy is to consider two trajectories beginning at very close initial conditions: positive values of Λ_∞ imply trajectory divergence and chaos (bounded fluctuations with sensitive dependence on initial conditions), while negative values indicates trajectory convergence and stability, whether stable points or stable limit cycles. When $\Lambda_\infty = 0$, quasiperiodic cycles arise Hilborn, 2000. Although the GLE estimates in stochastic systems have been severely criticised Dennis et al., 2003, it should be emphasized that this paper is concerned with the pattern of covariation between life-history traits and quantitative dynamic probes measured in a standardised way, not with point GLE values. 3) The characteristic period of fluctuation and 4) the value of the autocorrelation function at this point. This will check for the existence of cycles and their period (Turchin, 2003). Altogether, these probes will check for the variability and cyclicity of each time-series and its relationship to the deterministic component of the system (Hilborn, 2000).

The particular pattern of density-dependence in a population would translate to a characteristic autocovariance structure in its temporal evolution (Royama, 1992; Bjornstad, Falck, and Stenseth Chr., 1995). An intuitive model capturing this structure can be written as an autoregressive process of second order (an AR(2) model, sensu Royama, 1992; Bjornstad, Falck, and Stenseth Chr., 1995):

$$X_t = \beta_0 + (1 + \beta_1)X_{t-1} + \beta_2 X_{t-2} + \epsilon_t \tag{8.2.3}$$

where X_t is $\ln N_t$, β_0 is a constant, $(1 + \beta_1)$ denotes direct statistical density-dependence, β_2 lagged density-dependence, and ϵ_t stands for Gaussian (independent and identically distributed, IID) noise. The statistical properties of the AR(2) model are very well studied (e.g., Royama, 1992). Indeed, in the presence of moderate stochasticity this model can produce a wide range of dynamical behaviours (from dampened stability to long-term cycles to extinction). The AR(2) model was fitted to the time-series through Maximum-Likelihood techniques, after testing for the additivity and linearity assumptions inherent to the statistical theory of AR models (see the Appendix D). Note that the reason for fitting a second-order autoregressive process is to provide a comparison of the asymptotic dynamic properties of the time-series, and not finding the appropriate process order of the dynamics.

To test for the shape of density-dependence and the form of population regulation in each population, the theta-logistic model of population growth (Gilpin, 1973; Sæther, Engen, and Matthysen, 2002)

was fitted to each stationary time-series:

$$\frac{N_{t+1}}{N_t} = e^{\beta\left[1-\left(\frac{N_t}{K}\right)^{\theta}\right]} \tag{8.2.4}$$

where K stands for the carrying capacity, β for the intrinsic specific growth rate, and θ for the shape of density-dependence (Sæther, Engen, and Matthysen, 2002); ϵ_t is a set of IID random variables following a normal distribution with variance σ^2. The variance of this distribution will give a standardised estimate of the environmental stochasticity impacting on the deterministic dynamics if we consider demographic stochasticity to be negligible; the amount of first-order autocorrelation in σ^2, (ρ) was estimated for each time series. Although demographic stochasticity is an important source of life-history variation in many bird populations (Sæther et al., 2004), no detailed data on individual-based demographic rates is currently available in the wader literature. The theta-logistic model was chosen due to their well known statistical properties (Sæther, Engen, and Matthysen, 2002); for values of $\theta < 1$, the population is regulated below the carrying capacity, suggestive of highly variable populations for a constant value of ϵ_t. In contrast, when $\theta > 1$, the population is regulated in the vicinity of the carrying capacity, which stabilises the population. If $\theta = 1$, eqn. 8.2.4 reduces to the standard logistic or Ricker equation (Hilborn, 2000; Turchin, 2003), while a value of $\theta = 0$ correspond to the Gompertz (density-independent) model. Therefore, both the Ricker and Gompertz types of population growth were considered as null hypotheses. When evidence for non-stationarity was found in a time-series, the stochastic diffusion model (Dennis, Munholland, and Scott, 1991) was used to derive statistical estimates of σ^2 in this case (see also Sæther et al., 2004).

8.2.3 *Demographic analysis: the structured scheme*

In contrast to time-series analysis, structured modelling regards population dynamics as a process in which the variation of population size through time is age-or stage-dependent. A stage-structured population model derived from the standard bird life cycle was constructed using matrix population modelling (Caswell, 2001; Bennett and Owens, 2002; see Appendix E). Three stages (fledgings, juveniles and adults) were considered. The asymptotic growth rate of the structured population (λ) can be calculated as the largest real root of the demographic transition matrix. Numerical simulation was implemented to calculate λ using Tuljapurkar, 1982; Tuljapurkar, 1990 approximation for small-noise, Markovian (IID) environments; with this method it is possible to infer if positive covariances among the vital rates in a given life history are increasing the variance of matrix entries and hence reducing the stochastic growth rate (see Appendix E). Besides, I calculated the proportional contribution of each demographic rate to the asymptotic growth rate, which is called the elasticity (proportional sensitivity) of λ to each rate. Additionally, a set of stochastic simulations were

Species	Trend	P_{boot}	μ	$\theta \pm SE$	$\sigma^2 \pm SE$	$\rho \pm SE$	**Type**
Dunlin	-0.417	0.030	–	0.736 ± 1.846	0.015 ± 0.017	0.128 ± 0.241	Ricker
Ringed plover	0.322	0.086	–	0.615 ± 2.640	0.012 ± 0.018	0.010 ± 0.243	Ricker
Sanderling	-0.210	0.170	–	1.074 ± 0.866	0.031 ± 0.034	-0.196 ± 0.238	Ricker
Ruddy turnstone	0.706	0.000	1.025	–	0.026 ± 0.025	-0.375 ± 0.224	Gompertz
Redshank	0.094	0.309	–	1.490 ± 0.450	0.020 ± 0.037	0.260 ± 0.234	K
Redknot	-0.116	0.318	–	1.511 ± 0.438	0.022 ± 0.024	-0.310 ± 0.231	K
Grey plover	0.971	0.000	1.094	–	0.040 ± 0.042	-0.174 ± 0.239	Gompertz
Greenshank	0.558	0.005	1.000	–	0.074 ± 0.073	-0.292 ± 0.247	Gompertz
Bar-tailed godwit	0.387	0.050	–	1.762 ± 0.322	0.024 ± 0.023	-0.476 ± 0.213	K
Black-tailed godwit	0.779	0.000	1.054	–	0.047 ± 0.048	-0.356 ± 0.227	Gompertz
Eurasian oystercatcher	0.099	0.179	–	1.228 ± 0.664	0.007 ± 0.016	-0.103 ± 0.210	K
Eurasian curlew	0.418	0.027	–	0.765 ± 1.709	0.011 ± 0.014	-0.044 ± 0.242	Ricker

Table 8.1: Results of the fitting of the theta-logistic and stochastic diffusion models to time series of population counts of shorebirds. Species are sorted according to increasing body size. The trend of population size through time was calculated for each time-series with the non-parametric ρ correlation; 1000 bootstrapped samples were used to construct unbiased point estimates and P-values (P_{boot}). For the time-series with significant drift through time ($P_{boot} < 0.01$), the stochastic diffusion model Dennis, Munholland, and Scott, 1991 was fitted to find parameter values for the diffusion rate (μ), the environmental variance (σ^2), and residual autocorrelation (ρ). For stationary series the theta-logistic model was fitted to find values for the theta-parameter (θ) and environmental variance. The type of population growth of each stationary population was defined according to two density-dependent, null hypotheses: Ricker ($\theta = 1$) and Gompertz ($\theta = 0$). Only populations of K type seem regulated above the carrying capacity.

conducted with the matrix model derived for each species, in order to calculate the population trends and quasi-extinction probability (the probability that simulated populations drop below the 10% of initial population size) of density-dependent and density-independent models under both demographic and environmental stochasticity.

The value of λ in structured populations can be interpreted as the Maximum-Likelihood estimate of an 'invasion' exponent, yielding information on the expected temporal fate of a population or phenotype (McGraw and Caswell, 1996; Ferriere and Gatto, 1995; Caswell, 2001). In principle, it says nothing regarding the propensity of the modelled system to move away from this central exponent. However, a measure of the relative variability of density-dependent vs. density-independent simulated population trajectories would help in comparing the long-term effect of both forms of population growth on the variance, and not only the mean, of population size. When dealing with the population dynamical consequences of bet-hedging strategies, the measures of population variance are critical. Based on the statistical theory of the variance ratio, I develop a measure of the long-term average rate of growth in the variance of local growth rates. For reasons of space, this measure is developed in detalil in Appendix E).

8.3 Results

8.3.1 *Correlates of unstructured dynamics and life-history characteristics*

Eleven out of the fifteen time-series were constructed through an abundance index, so estimates of the coefficient of variation are not standardized within the database; however, using only those 11 datasets, and excluding the series with a significant trend through time, there appears to be a marginal negative relationship between the body size index and the relative population variability (r = -0.75, n = 8, signification obtained through Monte Carlo simulation with 1000 randomizations, $p_{MC} = 0.056$). Moreover, using the whole database, a strong negative relationship between body size and the GLE was found (r = -0.71, n = 13, $p_{MC} = 0.006$; Fig. 8.3a). Albeit values for the GLEs

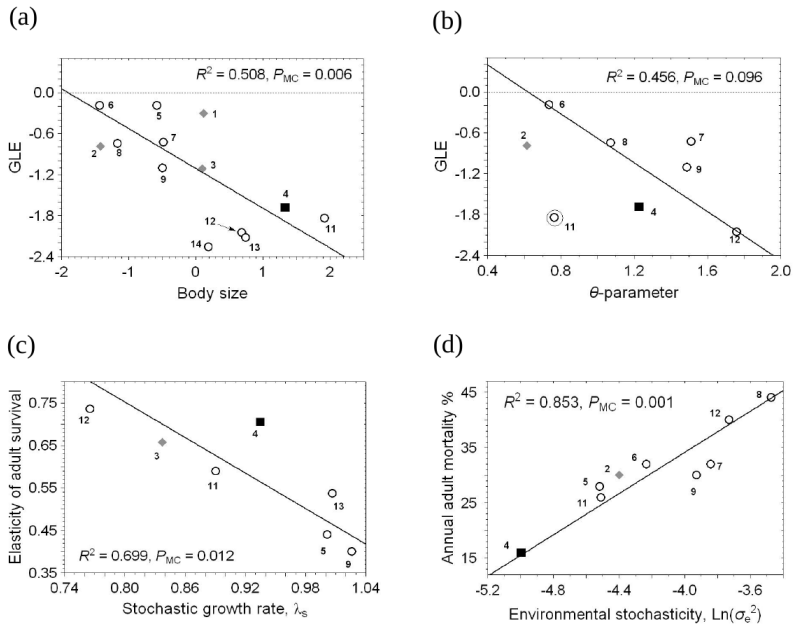

Figure 8.3: Relationship between quantitative dynamic probes, life-history traits and demographic rates of shorebirds; a) regression of the general Lyapunov exponent (Λ_∞, GLE) of each time-series on the specific body size index; b) regression of the GLE on the value of the theta-parameter of the stationary time-series. The circle denotes an outlier; c) regression of the elasticity of adult survival on the Tuljapurkar, 1982; Tuljapurkar, 1990 approximation of λ, λ_S; d) regression of annual adult mortality of each species on the loge-residual variance $ln(\sigma^2)$ of the population dynamics models fitted to each time-series. The regression line within each graph was fitted using a model II regression (major axis regression), and P-values (p_{MC}) were obtained from 1000 random samples using Monte Carlo simulation. Numbers within the panels stand for: 1) Grey plover; 2) Ringed plover; 3) Lapwing; 4) Eurasian Oystercatcher; 5) Ruddy turnstone; 6) Dunlin; 7) Red knot; 8) Sanderling; 9) Redshank; 11) Eurasian curlew; 12) Bar-tailed godwit; 13) Black-tailed godwit; and 14) Greenshank. In panels a), c), and d), open circles belong to species from the Scolopacidae family, grey diamonds to the Charadriidae, and the black box to the Haematopodiidae.

were always negative, suggestive of asymptotically stable dynamics in all cases, this result identifies a gradient in which smaller species are relatively more affected by stochasticity than bigger ones.

Sexually monomorphic species exhibited less autocorrelation than did dimorphic species (rACF = 0.22 ± 0.14 vs. 0.65 ± SE 0.05; GLM, Wald test = 4.48, d.f. = 1, p = 0.034); additionally, the impact of environmental stochasticity was lower in the dynamics of monomorphic species compared to dimorphic species ($ln(\sigma^2)$ = -3.95 ± 0.15 vs. -4.63 ± 0.18; GLM, Wald test = 6.35, d.f. = 1, p = 0.011). Both relative population variability and the Lyapunov exponent were mainly affected by body size (GLM, $p < 0.05$) relative to sexual dimorphism (GLM, $p > 0.08$), while sexual dimorphic species seemed to have less cyclic and more stochastically fluctuating time-series relative to non-dimorphic species, with no effect of body size in this case (p ¿ 0.85). Therefore, since no relationship was found between sexual dimorphism and body size in the analysed subset of species (t-test, t = -1.30, d.f. = 11, p = 0.21), it is the joint effect of sexual selection and body size what seems to affect population dynamic probes in shorebirds. Due to unbalanced sample sizes, the GLM yielded unreliable estimates for the other quantitative probes. Fig. 8.4 shows the location of the wader time-series in the parameter space of the AR(2) model. The stochastic asymptotic dynamics range clearly between dampened stability and multi-annual cycles (greater than 4 years), and are achieved mainly through variation in the strength of statistical direct density-dependence. Stochastic calculations of cycle period suggest, indeed, that long-term (multi-annual to multi-decadal) fluctuations are expected in most shorebird populations. Furthermore, nearly all the time-series analysed here can be successfully described using linear statistical theory (see Table A3 in the Appendix D in the

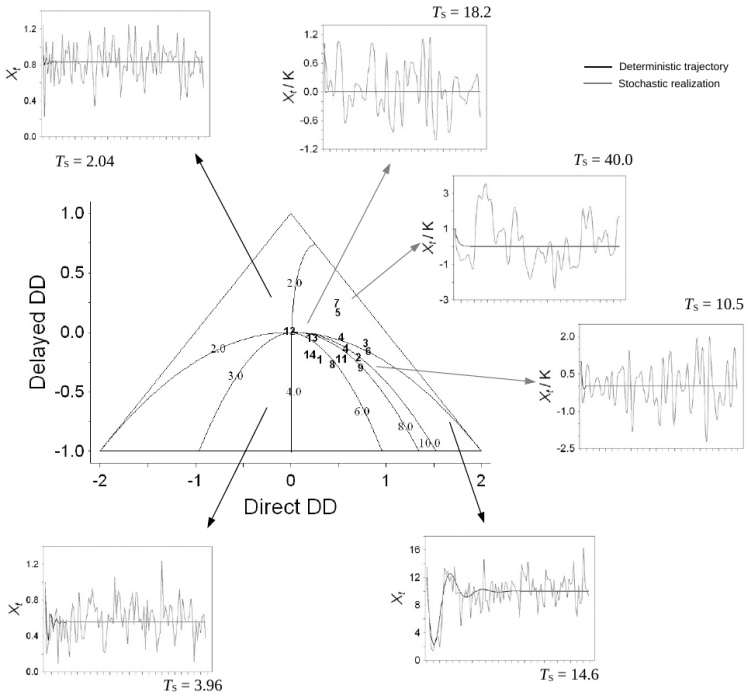

Figure 8.4: Location of time-series of shorebirds in the parameter space of a deterministic AR(2) process (Royama, 1992). Outside the triangle, populations tend to extinction, and below the parabola multi-annual cycles arise; within the area between the triangle and the parabola the populations exhibit dampened stability (on the right) or two-year cycles (on the left). The lines within the parabola give the contours of cycle period (T), from 2.0 years on the left to an infinite period on the right; these changes can be achieved either through a reduction of lagged DD (β_2) or through an increase in the strength of direct DD ($1 + \beta_1$). Since the AR(2) is a linear model, sustained fluctuations can only persist in the presence of moderate stochasticity; three sets of simulated trajectories were constructed and plotted in the region of cycle periods 2.0, 3.5 and 15.0 years by implementing Gaussian noise, $N \sim (0, 1)$ on the deterministic skeleton. Numbers within the triangle denote the position of each shorebirds time series (see Fig. 8.3). Deterministic and stochastic trajectories (the later derived from the probability distribution of fitted parameter values; see Appendix) are plotted for Red knot, Redshank and Bar-tailed godwit. The stochastic asymptotic fluctuation period (TS) is calculated in each case from a series of 1000 years, using spectral analysis; only the first 300 years are plotted. The simulated stochastic time-series were smoothed with a high-pass filter, which removed cycles of less than 3 years.

online edition of American Naturalist), so these long-term fluctuations can only be sustained in nature under small to moderate levels of stochasticity.

The fitting of the theta-logistic model to the stationary time series was very good for all of them, with weakly correlated or uncorrelated residuals in all cases (Durbin-Watson test with lags up to three years, P > 0.05; see Table 8.1). However, the time-series for the Lapwing did not converge correctly, so it was dropped from subsequent analysis. 5 out of 8 analysed time-series had a value of θ greater than 1 (Table 8.1), suggesting either Ricker (logistic) or K-type of density-dependent population growth. A strong negative relationship was found between the θ-value and the mean growth rate (r = -0.81, n = 9, p_{MC} = 0.009), suggesting across-species population regulation irrespective of the type of population growth. Additionally, a decrease in the GLE with increasing magnitude of the θ-parameter was apparent (r = -0.67, n = 7, p_{MC} = 0.092) only after deleting the Eurasian Curlew from the analysis (Fig. 8.3b). Interestingly, this correspondence would suggest that the response surface constructed to estimate the GLE correctly reflects the density-dependent properties of the bounded theta-logistic model. Therefore, the closer the onset of regulation is to carrying capacity, the greater the ability of the population to filter environmental stochasticity.

8.3.2 *Correlates of stage-structured dynamics and life-history characteristics*

Irrespective of the estimation method, the density-independent asymptotic growth rate estimated through the structured approach (either

Species	λ	λ_{DD}	λ_S	QEP_{DI}	QEP_{DD}	$e_{ij}F_1$	$e_{ij}G_1$	$e_{ij}G_2$	$e_{ij}P_1$
Ruddy turnstone	1.008 (1.005, 1.012)	1.001 (0.956, 1.045)	1.001	0.355	0.557	0.178	0.185	0.183	0.454
Redshank	1.030 1.026, 1.034)	1.010 (0.868, 1.151)	1.026	0.076	0.409	0.192	0.199	0.197	0.412
Lapwing	0.843 (0.840, 0.846)	1.004 (0.961, 1.047)	0.838	1.000	0.416	0.107	0.116	0.113	0.664
Bar-tailed godwit	0.770 (0.767, 0.772)	0.991 (0.848, 1.134)	0.765	1.000	0.390	0.093	0.099	0.092	0.717
Black-tailed godwit	1.014 (1.011, 1.018)	1.002 (0.964, 1.040)	1.007	0.276	0.485	0.148	0.157	0.153	0.542
Eurasian oystercatcher	0.943 (0.940, 0.947)	1.002 (0.945, 1.058)	0.935	0.774	0.398	0.098	0.108	0.099	0.694
Eurasian curlew	0.897 (0.894, 0.900)	1.002 (0.965, 1.039)	0.891	0.986	0.377	0.134	0.142	0.136	0.588

Table 8.2: Stage-structured population modelling and stochastic simulations with available demographic data for shorebirds. Shown are the stochastic growth rate (λ) along with the 95% confidence interval. λ_{DD} denotes the stochastic estimate of the density-dependent growth rate and associated confidence intervals. λ_S is the Tuljapurkar, 1982 approximation of λ for Markovian, small-noise environments. Also shown is the quasi-extinction probability (QEP) in both density-dependent and density-independent stochastic simulations (subscripts DD and DI, respectively). The last four columns give the stochastic elasticities (e_{ij}) of λ to annual fecundity (F_1), and fledgling (G_1), juvenile (G_2), and adult (P_1) survival rates. 10000 random matrices were used for the stochastic calculations. See the Appendix D

the standard or Tuljapurkar's approximation) was smaller than 1.0 in 4 out of 7 species, suggesting a declining trend for such species; additionally, the quasi-extinction probability was > 0.77 in these cases (8.2). The rest of species displayed increasing trends, with no cases in which the long-term average of λ approached 1, even in the presence of environmental and demographic stochasticity (see Fig. Figure in Appendix E). However, the inclusion of stochastic density-dependence in the simulations, in the form of scramble competition (see Appendix E), stabilized all populations around a value of λ_{DD} close to 1 (Table 2; note, that although some point values did not approach 1 all the confidence intervals overlap 1).

On the other hand, note that the long-term average rate of growth in the variance of local growth rates, which stand for a probe of the variability of population size at the equilibrium was positive in all density-dependent simulations and similar to density-independent values (see Table in Appendix E); in the Bar-tailed godwit the density-dependent rate was even negative. Thus, simulation results suggest that wader populations stabilized in density-dependent environments relative to density-independent environments (8.2), but that the long-term variability of population size increased accordingly. Interestingly, the elasticity of λ to adult survival was nearly four times greater than to any other trait in all species (adjusted $R^2 = 0.55$, $F_{3,24} = 11.82$, $P_{MC} < 0.0001$; GLM-ANOVA; see 8.2). This suggests that a change in adult survival has, on average, a fourfold effect on the population trajectory relative to changes in any other rate. Even more interestingly, the elasticity of λ to adult survival correlates negatively with population growth rate (r = -0.84, n= 7, $P_{MC} = 0.016$; Fig. 8.3c), which suggests that adult survival is relatively more important than any other demographic rate in decreasing relative to increasing populations.

8.3.3 *Merging unstructured and structured approaches*

The amount of environmental stochasticity impacting on each population measured through time series analysis ($ln(\sigma^2)$), correlates closely and positively with the annual adult mortality obtained from the liter-

ature ($r = 0.92$, n = 9, $P_{MC} = 0.001$; Fig. 8.3d). The small sample size (n=4) precluded a direct comparison between the long-term average rate of growth in the variance of local growth rates in stage-structured density-dependent simulations and the theta-parameter. Interestingly however, this variance ratio correlates negatively but weakly with the GLE estimated through time-series analysis (r = -0.69, n = 7, P_{MC} = 0.108). Notably, in spite of the negative relationship found between the theta-parameter and the GLE, the parameters θ and $ln(\sigma^2)$ were not correlated ($r = 0.51$, n = 9, $P_{MC} = 0.160$) in the subset of analyzed species, even though a negative relationship was expectable from previous studies. Overall, although sample size is too small this strongly suggests that the joint effect of the deterministic component and the stochastic component on the variance increase in density-dependent simulations is mainly additive, non interactive.

8.4 Discussion

The main patterns arising from this study are: 1) A larger body size, the absence of sexual selection and an increase in the convexity of the theta-logistic model were all related to population stabilization through the buffering of environmental impacts in shorebirds; 2) Structured population modelling suggest that shorebirds have an inherently unstable dynamics, whether through increasing or decreasing trends in density-independent stochastic environments, or through an amplification of fluctuations under density-dependent stochastic environments in otherwise long-term stable populations; 3) time-series analyses suggest that this amplification might be the consequence of a population dynamics regulated below the carrying capacity but not of an increased role of environmental stochasticity; and 4) Adult mortality in shorebirds might be under strong inter-specific environmental control, implying a main role for extrinsic sources on the variability of this demographic rate. Surprisingly however, adult survival was the demographic rate with the largest impact on growth rate, especially for declining populations.

An increase in relative population variability with decreasing body size is a general pattern in nature Pimm, 1984; Fagan et al., 2001; Inchausti and Halley, 2003, and also holds for the subset of wader species analysed here. However, the role of sexual selection on population dynamic characteristics has seldom been explored. After controlling for body size, the present study supports the theoretical prediction that increased stochasticity may have a larger impact on sexually selected species Tanaka, 1996, since dichromatic shorebirds had less cyclic populations (as shown by the low value of the rACF) with an increased role for environmental variation. Previous empirical work (e.g., Promislow, Montgomerie, and Martin, 1992; Sorci, Møller, and Clobert, 1998) also suggest a larger extinction probability for dichromatic species. However, Doherty et al., 2003 found evidence of an increased rate of not only local extinction but also population turnover in sexually selected species of North America, which might provide an explanation to the

apparently counterintuitive observation of increased species richness in sexual selected clades Bennett and Owens, 2002 (Bennett and Owens 2002). Moreover, Prinzing et al., 2002 found no evidence for an effect of sexual selection on population trends in a subset of Central European non-Passerines species. Therefore, the commonly supported relationship between sexual selection and population dynamics seems more complex than previously acknowledged.

The set of shorebirds time-series compiled here could be fairly described using linear statistical theory. Autoregressive modelling located shorebird populations in the dynamic region between dampened stability and multi-annual cycles. Due to the phase-forgetting nature of linear dynamic models Hilborn, 2000, the long average fluctuation period of the time-series (12.7 $\pm$ 7 years, ranging from 2.7 to 25.5; see Table A3 in the Appendix D) can only be maintained in nature under small to moderate levels of stochasticity, whether demographic or environmental. Indeed, although according to the age of first reproduction (1 year in nearly all cases) it would be expectable to find 2-year cycles only evidence for cycles greater than 3 years, including multi-decadal cycles, was found (Fig. 8.4). Additionally, 7 out 12 time series were classified as non-stationary. Available studies (e.g., Dougall et al., 2005) suggest indeed a long fluctuation period for single shorebirds populations, and, interestingly, some time series classified here as non-stationary displayed opposite trends during recent years (Rehfisch et al., 2003). Additionally, Peach, Thompson, and Coulson, 1994 found a major role for climatic fluctuations on inter-annual variability in some demographic rates of Lapwings in Britain. Since most climatic variables display reddened and even black spectra (Pimm and Redfearn, 1988; Cuddington and Yodzis, 1999), the multi-decadal cycles and long-term trends of shorebirds could be a consequence of the climatic control on the variability of some of its vital rates.

On the other hand, irrespective of the particular life-history or form of population regulation, the available data on demographic rates suggest that shorebirds have an inherently unstable dynamics, since no evidence for long-term population stabilization was found. Recent empirical and theoretical explorations (BJØRNSTAD, NISBET, and FROMENTIN, 2004) suggest that in species with age-structured life-histories inter-cohort interactions might prompt long-term trends superimposed on short-term fluctuations due to the amplification of environmental noise among cohorts (the so-called "cohort resonance effect", BJØRNSTAD, NISBET, and FROMENTIN, 2004). This means that an intrinsic dynamics alone, when interacting with environmental noise, can produce long-term trends. Although no empirical evidence is available to date to support this notion in shorebirds, recent results with the Black-tailed godwit (Gill et al., 2001) might suggest a role for intrinsic dynamics in the generation of long-term trends and variance, as suggested by the present study. Gill et al., 2001 results shows that the fourfold increase of Black-tailed godwits observed throughout the United Kingdom during the last 30 years (see Table 8.1) was the consequence of local populations increasing in individual estuaries of poor

quality. Given that the environment remained constant through time and that prey intake and survival rates were lower in such estuaries, the long-term trend was the consequence of intrinsic dynamics through behavioural mechanisms (the buffer effect; see Gill et al., 2001; Norris, Atkinson, and Gill, 2004). It is likely that the buffer effect operates in many other shorebirds species, and it might provide an explanation to the peculiar population dynamics identified here. Overall, the finding of negative GLEs in all cases (which appeared indeed determined by body size), the statistical evidence for strong population regulation in more than half of the species, and the significant impact of stochasticity on shorebirds life-history traits and population processes point to an additive interaction between stochasticity and determinism as the candidate for long-term trends generation. However, the extent to which the long-term fluctuation period of single shorebirds populations is a consequence of internal dynamics or external forcing requires future research.

In accordance to recent analyses (e.g., Pfister, 1998; Crone, 2001; Gaillard and Yoccoz, 2003), the present study confirms the finding that adult survival is usually the demographic rate yielding the largest elasticity in iteroparous species (Caswell, 2001). Given that fecundity is relatively high in shorebirds and their age of maturation is relatively short, the finding of a larger elasticity in adult survival than in fecundity provides strong evidence for the evolution of a bet-hedging strategy in this group of birds (see Saether and Bakke, 2000). Strikingly, this rate is the likely demographic driver of the population trajectory in declining shorebirds (Fig. 8.3c; see Baker et al., 2004). Owing to adult survival yielding the largest elasticity in all species, it would be expectable a species-wide reduction in the variance of this demographic rate due to the canalizing effect of natural selection (Stearns and Kawecki, 1994; Crone, 2001; Pfister, 1998; Gaillard and Yoccoz, 2003). Although information on the temporal variability of vital rates in shorebird populations is lacking, the large inter-specific variation in adult survival (0.49-0.84) might suggest that shorebirds may fail to canalize this rate in nature; some particular examples on the potential of adult survival rates to display large temporal variability in single populations are Peach, Thompson, and Coulson, 1994; Baker et al., 2004; Dougall et al., 2005.

Two explanations might account for this lack of canalization. First, it might be possible that the positive covariance between juvenile and adult survival found here ($r = 0.85$, n = 9, $P_{MC} = 0.016$) precludes this variance reduction (Stearns and Kawecki, 1994; Caswell, 2001). Indeed, Peach, Thompson, and Coulson, 1994 show a positive temporal covariance between juvenile and adult survival for the Lapwing *Vanellus vanellus* in Great Britain. Additionally, Tuljapurkar, 1982 approximation of λ, although highly correlated to the other measures, was slightly but consistently smaller across species, which might indicate that the correlated vital rates could further decrease the long-term stochastic growth rate. Secondly, the finding of a strong inter-specific environmental control of adult survival (Fig. 8.3d) provides the novel

example of an external control of the demographic rate yielding the largest elasticity. This provides the striking inter-specific connection between environmental stochasticity and population dynamics through the control of demographic rates with a large impact on growth rate. Since Peach, Thompson, and Coulson, 1994 demonstrates a close climatic control of the temporal covariation between adult and juvenile survival in a shorebird, note that these explanations are not mutually exclusive.

Altogether, these results point to the evolution of extreme bet-hedging strategies in shorebirds, and suggest further that this life-history strategy might have a visible impact on their population dynamical characteristics through the generation of internal long-term variability. This opens the exciting possibility for an intrinsic cause behind the observed world-wide "decline", namely that the long-term trends displayed by some populations might be the consequence of a reddened dynamics, in which the medium-term trends ($\approx$ 15 years) form part of a larger cycle (see Dougall et al., 2005 for a potential example). Indeed, although nearly the half of the known shorebirds populations is declining, probably by a global reduction in habitat quantity and quality (WetlandsInternational, 2012), a non-negligible 16% of populations are increasing (International Wader Study Group, 2003); overall, the fact that nearly the 70% of the world shorebird populations display temporal non-stationarity can be regarded as a fingerprint of the population dynamical consequences of bet-hedging strategies. Individual-based data on demographic rates of shorebirds and its temporal variation should be obtained in different species and population in order to test the general validity of this conclusion.

Family	Taxon name	Common name	Location	Years	Source
Haematopodidae	*Haematopus ostralegus*	Eurasian oystercatcher	British coastline	1971-1991	[1]
Haematopodidae	*Haematopus ostralegus*	Eurasian oystercatcher	Skokholm Island	1946-1979	[2]
Haematopodidae	*Haematopus ostralegus*	Eurasian oystercatcher	Skokholm Island	1953-1967	[3]
Haematopodidae	*Haematopus ostralegus*	Eurasian oystercatcher	Skokholm Island	1963-1977	[4]
Charadriidae	*Vanellus vanellus*	Lapwing	Skokholm Island	1946-1979	[2]
Charadriidae	*Pluvialis squatarola*	Grey plover	British coastline	1971-1991	[1]
Charadriidae	*Charadrius hiaticula*	Ringed plover	British coastline	1971-1991	[1]
Scolopacidae	*Limosa limosa*	Black–tailed godwit	British coastline	1971-1991	[1]
Scolopacidae	*Limosa lapponica*	Bar–tailed godwit	British coastline	1971-1991	[1]
Scolopacidae	*Arenaria interpres*	Ruddy turnstone	British coastline	1971-1991	[1]
Scolopacidae	*Calidris alpina*	Dunlin	British coastline	1971-1991	[1]
Scolopacidae	*Calidris canutus*	Red knot	British coastline	1971-1991	[1]
Scolopacidae	*Calidris alba*	Sanderling	British coastline	1971-1991	[1]
Scolopacidae	*Tringa totanus*	Redshank	British coastline	1971-1991	[1]
Scolopacidae	*Numenius arquata*	Eurasian curlew	British coastline	1971-1991	[1]
Scolopacidae	*Tringa nebularia*	Greenshank	Kyle of Tongue	1964-1982	[5]

Table 8.3: Phylogeny, geographic location, temporal location and bibliographic source of the time-series of population counts from migratory waders used in the comparative population dynamics analysis. Sources: [1] Prys-Jones, Underhill, and Waters, 1994; [2] Williamson, 1983; [3] Lack, 1969; [4] Safriel et al., 1984; [5] Thompson, Thompson, and Nethersole-Thompson, 1986.

8.5 Appendix

8.5.1 *Appendix A: Data on the extinction risk of shorebirds relative to other highly threatened bird taxa*

As a comparison with Charadriiformes, both Psittaciformes and *Diomedeidae* were selected for having a large number of species categorized by the IUCN (n = 144 and 21, respectively) and also a large proportion of species threatened (> 65% and > 90%). In contrast, Charadriiformes (Fam. *Scolopacidae*, *Charadriidae* and *Haematopodidae*) has a large number of classified species (n = 39) but a low proportion of them are classified as threatened (<14%). Nevertheless, a Tukey-type test for multiple comparisons of proportions suggests that the proportion of populations with declining trend is similar across taxa (p-value > 0.10 in all cases). Moreover, the proportion of stable and/or increasing populations is larger in Diomedeidae, one of the most threatened avian families (IUCN, 2020), relative to Charadriiformes (p-value < 0.05). Indeed, a large proportion (¿ 56%) of populations from Caradriiformes has an unknown/no data trend status, in contrast to Diomedeidae. Therefore, it can be concluded that the risk of population decline in Charadriiformes might be similar to other well known, highly threatened taxa. Raw data to conduct the analysis were obtained from `http://www.iucnredlist.org`.

8.5.2 *Appendix B: Description of the species, locations and time-series, and bibliographic sources*

Besides the dataset contained in the Global Population Dynamics Database, some references including time-series of wader counts of ¿ 15 years were located. These included a time series of the number of waders ringed in Eliat, Israel from 1984 to 2000 (Yosef, 2001), data from a long-term (1946-1995) monitoring program in Ottenby, Sweden, including counts from the Red Knot (*Calidris canutus*) and the Curlew sandpiper (*C. ferruginea*) (Blomqvist et al., 2002), and fur returns from hunted woodcocks (*Scolopax rusticola*) in Sussex, UK (Middleton,

Species	Length (mm.)	Weight (grs.)	Broods	Nest size	Hatching success	Brood size	Fledging success	α	Juvenile mortality	Adult mortality	Oldest bird
Haematopus ostralegus	43.75	622.5	1	3.5	48	1.68	20	3	36	16	35
Vanellus vanellus	29.5	229	1	3	65	1.95	16	1	40	27	18
Pluvialis squatarola*	29	247	1	4	67	2.68	–	3	–	–	20
Charadrius hiaticula	19	60	2	3.5	36	1.26	20	1	–	30	10
Limosa limosa*	40	300	1	4	49	1.96	40	1	37.6	20	15
Limosa lapponica*	39	295	1	3.5	–	1.22	–	2	79	40	32
Arenaria interpres*	23.5	137	1	3	57	1.71	62	2	39.5	28	20
Calidris alpina*	19	59	1	3.5	60	2.1	–	1	68.5	32	24
Calidris canutus*	24	152.5	1	3.5	54	1.89	27	2	–	32	16
Calidris alba*	20.5	74.5	1	3.5	33	1.16	–	2	62	44	11
Tringa totanus*	28	100	1	4	86	3.44	50	1	55	30	17
Tringa nebularia	32.5	207.5	1	4	74	2.96	32	1	–	–	12
Numenius arquata	55	885	1	3.5	47	1.64	37	2	53	26	31

Table 8.4: Values of the life history traits and demographic rates for the 14 waders species considered in the comparative population dynamics analysis (Tobias et al., 2022). Species with an asterisk display sexual plumage dichromatism, according to the detection of any colour difference between males and females (Doherty et al., 2003). Since data for brood size was lacking for most species, this figure was calculated as the product of nest size and (hatching success/100). α stands for age at first breeding (in years). Age of the oldest bird ringed, in years.

1934). However, these time-series were not included in the analysis due to the uneven sampling effort (Yosef, 2001), high local predation pressure from Arctic foxes (Blomqvist et al., 2002), and potentially non-natural fluctuations in population size (Middleton, 1934).

Additionally, four references were located that included long time-series (>21 years) of counts from the Oystercatcher (*Haematopus ostralegus*). However, three of them (Lack, 1969; Williamson, 1983; Safriel et al., 1984) referred to the same location (Skokholm, Wales, UK), so the longest complete time-series (34 years, Williamson, 1983) was used. In order to obtain single quantitative dynamic probes for the Oystercatcher and hence avoid pseudoreplication (Purvis et al., 2000), unified estimates for each statistic were achieved by weighting each estimate by the length of each time series. For instance, be θ_1 and θ_2 a statistic (the density-dependent exponent of the theta-logistic equation in the accompanying paper) for two time series X and Y, respectively, and be n1 and n2 the length of time-series X and Y. A unified estimate of θ, θ_U would be:

$$\theta_U = \theta_1 \left(\frac{n1}{n1+n2} \right) + \theta_2 \left(\frac{n2}{n1+n2} \right) \tag{8.5.1}$$

8.5.3 *Appendix C: Table including demographic information and life-history data for shorebirds*

8.5.4 *Appendix D: Detailed description of the autoregressive modelling, including a Table with parameter values and statistical tests for non-linearity and additivity, and other quantitative probes*

Autoregressive modelling is usually advocated for studying the asymptotic properties of time-series (Royama, 1992). Framed within the standard scheme of stochastic difference equations, an autoregressive model of k orders (an AR(k)) can be written as:

$$R_t = X_{t+1} - X_t = g(X_t, X_{t+1}, \cdots, X_{t-k(k-1)}, \epsilon_t) \tag{8.5.2}$$

where R_t is the population growth rate, X_t the ln-population density, and ϵ_t a set of independent and identically distributed random variables, following a Gaussian distribution. The function g($\cdot$) usually takes a linear and negative form in both X_t and ϵ_t (Bjornstad, Falck,

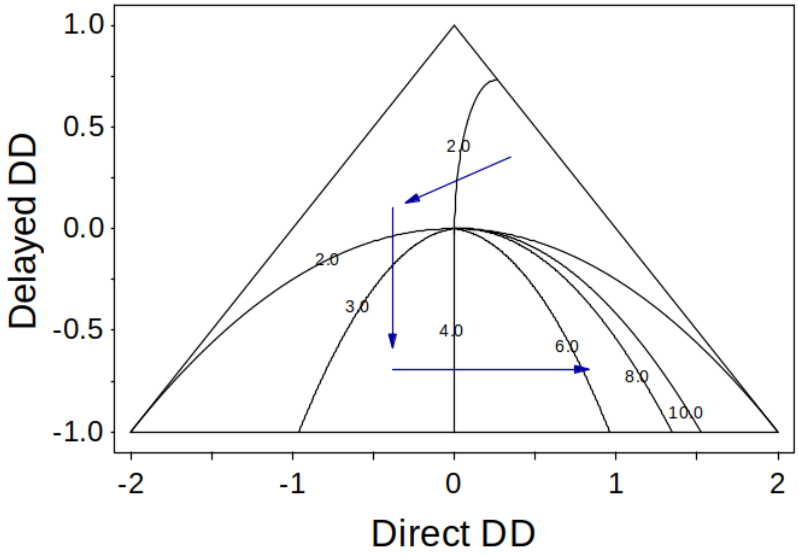

Figure 8.5: Cycle period as a function of direct $(1 + \beta_1)$ and delayed density-dependence (β_2) in the AR(2) model (Royama, 1977). Parameters outside the triangle lead to long-term extinction, while populations within it persist under moderate levels of stochasticity, either through dampened stability to 2-years cycles to multiannual fluctuations. These main gradients from short to long-period fluctuations are indicated by the arrows. The figures inside the triangle (2.0, 3.0, ... , 10.0) denote the cycle length in years.

and Stenseth Chr., 1995). After some algebra, the AR(k) model simplifies to (Royama, 1992; I follow Bjornstad, Falck, and Stenseth Chr., 1995 in the notation):

$$X_t = \beta_0 + (1 + \beta_1)X_{t-1} + \beta_2 X_{t-2} + \cdots + \beta_k X_{t-k} + \epsilon_t \qquad (8.5.3)$$

The ecological interpretation of the AR(k) is that the parameter β_0 denotes the average diffusion of the population through time, β_1 indicates the strength of direct density-dependence, and parameters β_2 to β_k stand for the lagged effects of past densities on current density. The dynamical behaviour of the AR(k) model varies greatly with the values of the β_i parameters. For instance, assuming an AR(2) model the effect of the second order parameter on fluctuation period length can be depicted in the parameter space of the Royama's diagram, shown in Figure 8.5.

Given that the model is linear, the long-term dynamics of the system will be phase-forgetting, which means that any sustained fluctuation would persist only in the presence of external perturbations (Hilborn, 2000). Additionally, the AR(2) model assumes that the time-series can be described reasonably well with an additive rather than multiplicative model. To test these assumptions, the Lagrange multiplier test for additivity (CHEN, LIU, and TSAY, 1995) and the Tukey one-degree-of-freedom test for linearity (TSAY, 1986) were applied to each time-series studied (see Bjornstad, 2001 for further descriptions and an ecological example).

The results of the tests are shown in Table 8.5. As can be seen, the null hypotheses of additivity and linearity could not be rejected in nearly any case. Therefore, the AR(2) model was fitted to each time series (detrended when necessary) through Maximum-Likelihood techniques (see Table A2). Since the goal of the analysis with the AR(2)

Species	Order (CVd)	Additivity (p-value)	Linearity (p-value)	Period	$(1+\beta_1) \pm SE$	$\beta_1 \pm SE$	R^2
Haematopus ostralegus (1)	3 (1.035)	0.1686	0.0023	12.5	0.5595 ± 0.1602	-0.1452 ± 0.1912	0.19
Haematopus ostralegus (2)	1 (0.930)	0.3265	0.7945	25.5	0.5233 ± 0.1303	-0.0470 ± 0.1527	0.21
Vanellus vanellus	1 (0509)	0.2727	0.7977	25.5	0.7879 ± 0.0678	-0.0921 ± 0.1097	0.55
Pluvialis squatarola*	1 (0.201)	0.7064	0.6013	5.8	0.3121 ± 0.2069	-0.2332 ± 0.2117	0.01
Charadrius hiaticula	1 (0.547)	0.2419	0.8943	15	0.7103 ± 0.1142	-0.2106 ± 0.1586	0.36
Limosa limosa*	1 (0.491)	0.0201	0.3828	12.5	0.2243 ± 0.2236	-0.0476 ± 0.2292	0
Limosa lapponica	1 (1.011)	0.9882	0.7127	2.7	-0.0099 ± 0.2357	0.0098 ± 0.2357	0
Arenaria interpres*	4 (0.282)	0.7634	0.1117	15	0.4879 ± 0.1770	0.1693 ± 0.1998	0.23
Calidris alpina	1 (0.676)	0.3567	0.6644	15	0.8081 ± 0.0808	-0.1503 ± 0.1357	0.55
Calidris canutus	1 (0.716)	0.7442	0.9755	15	0.4833 ± 0.1751	0.2467 ± 0.1938	0.31
Calidris alba	1 (0.960)	0.3631	0.4013	5.8	0.4339 ± 0.1840	-0.2739 ± 0.1964	0.11
Tringa totanus	1 (0.686)	0.2751	0.811	15	0.7315 ± 0.1048	-0.2914 ± 0.1471	0.43
Numenius arquata*	1 (0.706)	0.0558	0.4845	8.3	0.5370 ± 0.1632	-0.2297 ± 0.1883	0.17
Tringa nebularia*	2 (0.746)	0.1978	0.1288	4.5	0.2062 ± 0.2349	-0.1921 ± 0.2356	0

Table 8.5: Quantitative dynamic probes and results of the fitting of the AR(2) model to the time-series of migratory waders analyzed in the present study. The order of each time series selected by cross-validation (Order(CVd)) of the linear autoregressive model, using conditional least-squares; p-values are shown for the Lagrange multiplier test for additivity (Additivity test) and the Tukey one-degree-of-freedom test for linearity in time series. The dominant period of fluctuation of each time series was assessed through spectral analysis. Due to the shortness of most time series the median of the first and second periods with the greatest periodogram values is shown; the first and second Maximum-likelihood parameters with associated standard errors, and the proportion of explained variance (R^2) of the AR(2) model are also shown. R^2 values were adjusted for time series length. The sources for *Haematopus ostralegus* are: Prys-Jones, Underhill, and Waters, 1994 (1) and Williamson, 1983 (2). Time series with the symbol '*' were detrended prior to the analyses.

model is to compare the asymptotic properties between time series (see accompanying paper), no model selection procedures were applied to select for the optimal order of each time series (see, however, the second column in Table 8.5). Since the assumption of linearity works very well with slightly non-linear time-series (Royama, 1992), the violation of the linearity assumption in one of the Eurasian oystercatcher time-series (Table A2) would not overestimate the number of lags, and an AR(2) model will capture the essential dynamical properties of the time series examined here.

The additivity and linearity tests, and the order selection for each time series were performed with the `nlts` 1.0-2 `R` package, developed by Ottar N. Bjørnstad (`http://ento.psu.edu/directory/onb1`), using `R` version 4.2.1 (RCoreTeam, 2021). The AR(2) models were fitted using the package `tseries` 0.10-51.

8.5.5 *Appendix E: Detailed description of the stage-structured modelling, including extended results and a full description of the calculation of the variance-ratio*

Structured population modelling: construction A tacit assumption of unstructured population modelling, such as the theta-logistic model of the accompanying paper, is that the demography of individuals does not differ with respect to age, size or stage (Caswell, 2001). However, this assumption seldom holds within any natural population, hence the exploration of the population dynamical consequences of age-, stage-, or size-dependent life histories should be performed with structured population modelling.

Therefore, I considered a bird life cycle composed of three stages, common to all birds (Saether and Bakke, 2000; Bennett and Owens, 2002): fledglings, including individuals not completely emancipated from their parents; juveniles, including individuals from the fledging period to the moment previous to their first breeding attempt; and adults, including birds from the first breeding attempt to death. A set of demographic transitions can be defined among these stages, namely: survival from fledglings to juveniles (G1), from juveniles to

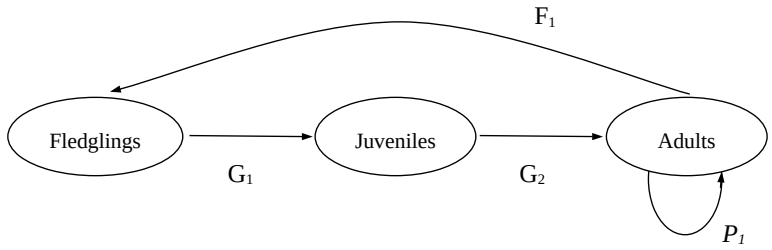

Figure 8.6: Bird life cycle graph used in the present analysis.

adults (G2) and adult survival (P1). Additionally, a fecundity function (F1) connecting adults with fledglings may stand for brood size. The bird life cycle graph is shown in Figure 8.6.

Assuming that a population of total size N, summed up by subpopulations of fledglings (n1), juveniles (n2), and adults (n3), evolve from time t to time t + 1 according to the set of demographic rates defined above, the bird life cycle can be translated into the following matrix difference equations (Lefkovitch, 1965):

$$\begin{pmatrix} n_1 \\ n_2 \\ n_3 \end{pmatrix}_{t+1} = \begin{pmatrix} 0 & 0 & F \\ G_1 & 0 & 0 \\ 0 & G_2 & P_1 \end{pmatrix} \times \begin{pmatrix} n_1 \\ n_2 \\ n_3 \end{pmatrix}_t \tag{8.5.4}$$

with right and left population vectors at time t and $t + 1$, and a Lefkovitch transition matrix ($\mathbf{L}$) connecting both of them through time. The Lefkovitch matrix is the stage-structured version of the Usher-Leslie model, commonly used in species with age-dependent demographic rates (see Caswell, 2001). Therefore, using the data from Table A3, a matrix was constructed for each of the species from which complete information on the demographic transitions defined above was available (7 out of 13).

Parameter estimation The largest real root of the Lefkovitch matrix (denoted by λ), which can be found by solving its characteristic equation, is the asymptotic growth rate of the population structured by stages (Caswell, 2001). I estimated λ through three different methods:

1. Point estimate of the mean matrix.

2. Stochastic estimate and confidence intervals using the mean, maximum (1.25*mean matrix entry, corresponding to a coefficient of variation of 0.25, see below) and minimum (0.75*mean matrix entry) matrix.

3. Tuljapurkar, 1982; Tuljapurkar, 1990's approximation of λ for Markovian (IID) small-noise environments, using the matrices derived from the joint probability distribution of the set of vital rates, as method 2). After some analytical derivations, and assuming that environments are independent, Tuljapurkar's approximation

($ln\lambda_S$) to the dominant ln-eigenvalue of the average projection matrix ($ln\lambda_1$) reduces to:

$$ln\lambda_S \approx ln\lambda_1 - \frac{V(ln\lambda_1)}{2ln\lambda_1^2} \tag{8.5.5}$$

where $V(ln\lambda_1)$ is the long-term variance of the dominant eigenvalue of the mean matrix. If we assume that the temporal variation around the mean matrix is small, $ln\lambda_S$ is a small-IID noise approximation to structured growth rate. Overall, Tuljapurkar's approximation suggests that an increase in the variance of matrix entries, for instance, a positive covariance among vital rates, reduces the stochastic growth rate $ln\lambda_S$.

Although Tuljapurkar's approximation is analytical, numerical simulations where implemented to provide a stochastic estimate of λ_1 assuming relatively small IID temporal noise, which seems a rather realistic assumption given the small to moderate temporal environmental autocorrelation of most wader time-series (see Table 1 of the accompanying paper). Therefore, for the methods 2) and 3) above, the simulation scheme uses asymmetrical probabilities (Morris and Doak, 2002) to draw a matrix from the mean (probability of resample = 0.5), minimum and maximum (probability of resample = 0.25 each) matrix at each time step, and calculates λ during each transition for 10000 runs (1 run = 1 time step). With Tuljapurkar's method, λ_S is calculated from the normalized difference between consecutively simulated matrices, so that a final approximation to $ln\lambda_S$ is reached (see Morris and Doak, 2002 for a similar procedure).

An interesting parameter from an ecological, evolutionary, and conservation standpoint, is the elasticity or proportional sensitivity (e_{ij}), which measures the relative response of λ to changes in any of the demographic rates (Caswell, 2007). The elasticity of λ to changes in the ij_{th} element of the matrix can be calculated as the ratio of the partial derivative of the ln of λ and the partial derivative of the log of the a_{ij} element:

$$e_{ij} = \frac{a_{ij}}{\lambda}\frac{\partial\lambda}{\partial a_{ij}} = \frac{\partial ln\lambda}{\partial lna_{ij}} \tag{8.5.6}$$

That is, the elasticity e_{ij} is the slope of the asymptotic growth rate plotted against lna_{ij}. Since the elasticity of λ to all of the transitions in a matrix sum up to 1 (Mesterton-Gibbons, 1993; Caswell, 2007), a direct comparison between rates in their impact on λ can be obtained. Stochastic point estimates of elasticities were constructed with 10000 random matrices for each species, using the probability distribution of methods 2) and 3) above. Specifically, the following distributions were specified:

$$\begin{aligned} G_{1-2} &\sim \text{beta}(\mu, \sigma^2) \\ P_1 &\sim \text{beta}(\mu, \sigma^2) \\ F_1 &\sim \text{gaussian}(\mu, \sigma^2) \end{aligned} \tag{8.5.7}$$

where μ is the mean and σ^2 the variance of the given distribution (Kendall & Stuart 1958).

An implicit assumption of the model outlined above is that demographic rates are density-independent, which might not hold for waders (see the accompanying paper). Therefore, an alternative density-dependent model was constructed considering that the structured population might be regulated through scramble, or interference competition. In this model, the amount of resources per individual decreases as the population size increases, which might be representative of wader ecology since a density-dependent decrease in foraging intake and prey density has been suggested (Szekely and Bamberger, 1992; Goss-Custard et al., 2002). Indeed, the scramble type competition model is similar to the Ricker or Logistic equation ($\theta = 1$ in the theta-logistic model), lying somewhere in between the pattern detected for waders (see Table 8.1). However, using the contest (Beverton-Holt) type of model yielded similar results (not shown).

The `popbio` 2.7 `R` package was used for the stochastic estimation of elasticities, and for the matrix parameter estimation for each species and subsequent stochastic calculations.

Population dynamics simulation scheme Up to here, one key assumption of the above model is that the demographic rates are temporally invariant. However, this is a largely unrealistic assumption of matrix population models, and waders might be a group with particularly variable demographic rates (Bennett and Owens, 2002). Therefore, since information on the temporal variability of wader demography is overall lacking, I decided to implement a 25% of variability (that is, a coefficient of variation of 0.25) for each mean rate within each species. This range is very similar to other species in nature (see review in Caswell, 2001). Since here the variability is inherent to the vital rate and not to the population size, this source of variance will account for environmental variability (stochasticity) in the simulations (Lande, Engen, and Saether, 2003; Lande, Engen, and Sæther, 2017). In particular, the demographic rates are specified as random variables following beta distributions for survival rates and a normal distribution for the fecundity function, both with mean μ and variance σ^2 (see Eqns.8.5.7).

Additionally, demographic stochasticity, which accounts for the impact of stochastic deaths and birth discrete processes on the population growth rate (Lande, Engen, and Saether, 2003), was implemented in the simulation as a probability function depending on population size. In particular, survival rates are specified as a binomial process and fecundity rates as a Poisson process (see Morris and Doak, 2002). Overall, at each time step the model draw at random a value from the probability distribution of the demographic rates (G1-3, F1) and evaluates the current population size, adjusting the birth and death schedule accordingly. This means that the simulation accounts simultaneously for environmental and demographic stochasticity. Additionally, in density-dependent simulations the model assumes that the total

Species	$\Delta \mathrm{Var} R_t$DI	$\Delta \mathrm{Var} R_t$DD
Ruddy turnstone	0.054 (0.031,0.077)	0.055 (0.033,0.078)
Redshank	0.054 (0.029,0.079)	0.037 (-0.003,0.077)
Lapwing	0.051 (0.031,0.071)	0.029 (0.010,0.049)
Bar-tailed godwit	-0.001 (-0.007,0.005)	0.019* (0.016,0.023)
Black-tailed godwit	0.037 (0.021,0.052)	0.044 (0.028,0.059)
Eurasian oystercatcher	0.029 (0.017,0.0245)	0.027 (0.018,0.037)
Eurasian curlew	0.043 (0.022,0.064)	0.031 (0.020,0.042)

Table 8.6: Estimates (95% confidence limits) of the long-term average rate of growth in the variance of local growth rates ($\Delta \mathrm{Var} R_t$) for wader populations, simulated in DD and DI environments. The confidence limits were calculated upon the 50 years of simulated data. The symbol '*' denotes statistically significant differences at $p < 0.05$, using the variance ratio test (Lewontin, 1966a; Markowski and Markowski, 1990).

abundances of all stages affect the demographic rates proportionally, therefore simplifying the simulation scheme and its interpretation. A summary of the stage-structured population dynamics simulation for each species can be found in Figure 8.7.

Long-term trend of variability vs. long-term trend of density at equilibrium Based on the statistical theory of the variance ratio (Markowski and Markowski, 1990), I develop below a measure of the long-term average rate of growth in the variance of local growth rates. Population modelling efforts based on the statistical theory of stochastic diffusion processes (Dennis, Munholland, and Scott, 1991) provide Maximum-Likelihood measures of the diffusion rate of a population and the dispersion of this process through time. However, this measure of dispersion relates to the amount of variance around the diffusion rate within a given time scale or sampling interval, and says nothing on the mean rate of variation of the process among consecutive time steps. Since the choice of the time scale and/or sampling interval is not trivial (Heino, Ripa, and Kaitala, 2000), we can construct a measure of the long-term average growth rate in the variance of local growth rates, in contrast to the measures of the variance in local growth rates. First, keep in mind that Lewontin, 1966a demonstrated that the ratio of the variances of two log-variables asymptotically follows an F-distribution. Based on this assumption, and denoting population size as Nt, we can write the long-term average rate of growth in the variance of local growth rates ($\Delta \mathrm{Var} R_t$) as:

$$\Delta \mathrm{Var} R_t = \sum_{i=n_1}^{k} \left[\frac{\sigma^2 \ln N_t}{\sigma^2 \ln N_{t-i}} \right] \left[\frac{1}{n} \right] \tag{8.5.8}$$

where n is the length of the period over which $\Delta \mathrm{Var} R_t$ is measured. Given that the Central Limit Theorem states that the average of a large group of sampling averages is similar to the population average, the quantity $\Delta \mathrm{Var} R_t$ converges to an F-distribution asymptotically (a mathematical proof would be rather cumbersome here). This property is desirable since a straightforward comparison between DD and DI estimates of the quantity $\Delta \mathrm{Var} R_t$ is possible using the variance ratio test (Lewontin, 1966a; Markowski and Markowski, 1990).

For heuristic purposes, the biological interpretation of $\Delta \mathrm{Var} R_t$ is rather similar to the interpretation of the Global Lyapunov Exponent

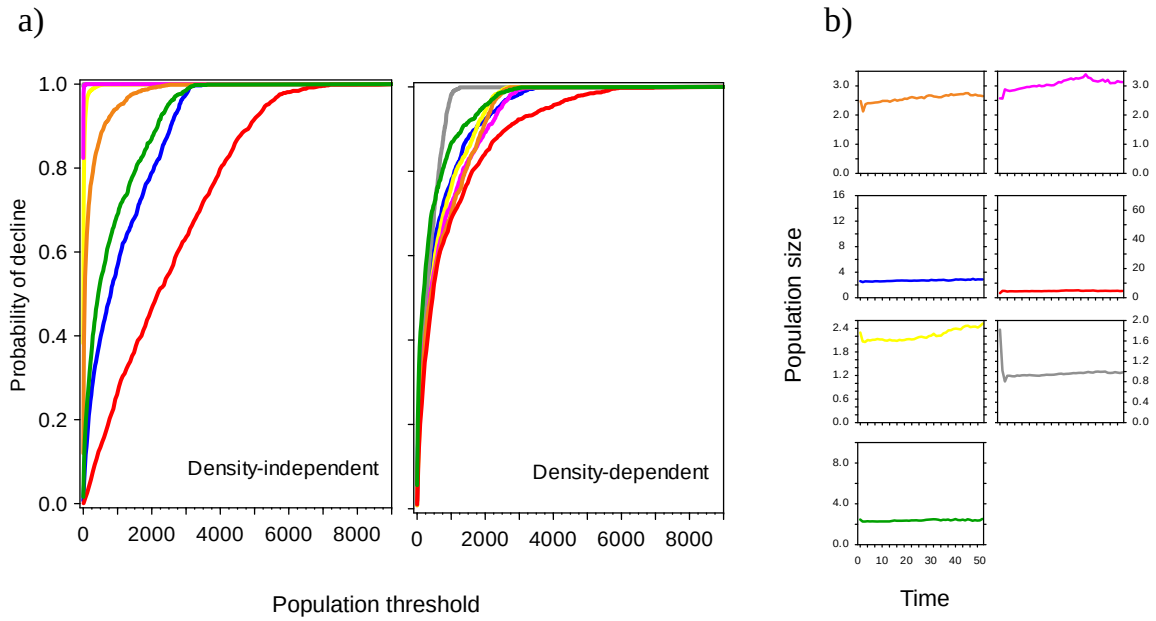

Figure 8.7: Results of the stochastic simulations performed with the standard stage-structured model constructed for waders. In a), the cumulative distribution of the proportion of simulated populations dropping below the threshold shown in the x-axis is represented as the probability of decline of the mean population with increasing population size. Both density-independent and density-dependent results are shown. In b), the mean trajectory during 50 years of the stochastic realizations is shown for each species, in both density-independent (dotted lines) and density-dependent (solid lines) versions of the simulation. 1,000 stochastic matrices were used in the analysis. Species shown are: Eurasian Oystercatcher (orange), Lapwing (pink), Black-tailed godwit (blue), Redshank (red), Eurasian curlew (yellow), Bar-tailed godwit (grey), and Ruddy turnstone (green).

in time series analysis. For instance, a positive value in the average ratio would indicate a steady increase in the inter-annual variance of population size, irrespective of its long-term mean. Values distinct to 0 are thus expected in density-independent populations, since they describe an unbounded process. On the other hand, density-dependent populations should yield a value close to 0 due to the bounded process they describe. Although it may seem counterintuitive, chaotic dynamics should indeed produce long-term stochastic values close to 0, since they also describe a bounded process (see Dennis et al., 2003 for a discussion of boundedness in ecology). The finding of a variance ratio distinct to 0 in a DD population would point to a particular life-history (internal) structure that is not able to filter environmental perturbations into long-term variance stability, thus producing a steady increase in population variance. An example of this would be a life-history with positive covariances between one ore several vital rates (e.g., Caswell, 2001).

In any case, it is stressed here that the calculation of $\Delta \mathrm{Var} R_t$ in single populations explicitly simulated with estimation error on vital rates would be inaccurate, since the inter-annual variance in Nt would be obviously inflated by the estimation error variance. Thus, accurate measures of $\Delta \mathrm{Var} R_t$ can only be achieved through numerical simulation, assuming that the point estimate of Nt is accurate enough.

Table A4 shows the value of the quantity $\Delta \mathrm{Var} R_t$ for wader species in DD and DI simulation environments. As can be shown, the quantities are virtually the same between DD and DI simulations, and even greater in DD vs. DI environments in the Bar-tailed godwit; additionally, except for the Redshank the confidence limits of the DD versions of $\Delta \mathrm{Var} R_t$ do not overlap 0, which suggest a stochastic increase in

the variance of local growth rates through time. This might stand as evidence for an internally generated increase in population variance, irrespective of long-term equilibrium density stabilization in stochastic DD simulations.

Overall, results tentatively suggest that the internal structure of a standard wader life cycle might be able to increase the long-term variability of population size irrespective of the amount of environmental variability. However, the small subset of species analyzed here renders this conclusion as rather speculative, so more stage- or age-structured models for waders should be analyzed.

Discussion 9

9.1 General patterns emerging from the case studies analyzed

In the present dissertation I have analyzed five case studies from different marine and terrestrial natural ecosystems, with the major goal of providing insights into several major questions on the **diversity, variability and persistence of ecosystems in variable environments**. These case studies span a wide range of spatial scales, from the global ocean to a single breeding population; organizational levels, from single species to diverse communities of functional types; different habitats, from the pelagic zone, to coastal areas, marshes and mountain regions; and temporal dimensions and resolutions, from weekly biomass data to multi-decadal data on population size. In spite of (or, more precisely, because of) this huge diversity, several major patterns can be outlined:

1. The strategy of **mathematical modelling as a strategy of abstraction** has been very useful as a first-order approximation to natural dynamical systems (Pimm, 1991; Kingsland, 1995; Abrams, 2022). This dissertation has used a wide range of dynamical system approaches (Chapters 2 and 3), and provided a deep exploration of different stability notions and their interconnections (for example, Figs. 4.16, 4.17, 5.6, 5.13). Going from linear and equilibrium based approaches (Chapter 4) to nonlinear (Chapter 5) and highly nonlinear and far-from-equilibrium (Chapter 6) approaches, the lesson learned is that an abstraction is useful if it illuminates those aspects of a problem believed to be instrumental in nature according to the structural realistic approach. If an abstraction obscures the process, or if the only insight provided by the model is about itself, the strategy of abstraction is a failure (Levins, 2007). Overall, the family of models used in this dissertation: MARSS models, (Chapter 4), Lotka-Volterra state-space models (Chapters 5 and 6), state-space stage-structured inverse models (Chapter 7), and AR models (Chapter 8), were shown to be very well calibrated to the problems studied (for example, Figs. 4.8, 5.1 and 7.4). They are **useful abstractions**. In the sense used by Levins, 1966 and Wimsatt, 2007, they conform to a family of **robust models**: in spite of the diverse landscape of problems explored in this dissertation, the mathematical tools used in each case were successful, and conform to **structurally stable family of models** in the sense of Casti, 1997 (Figure 9.1). Smooth transformations allow moving from the simple, linear and univariate models used in

"In theories as in faces, beauty can be an artifact" (Pitelka, 1974)

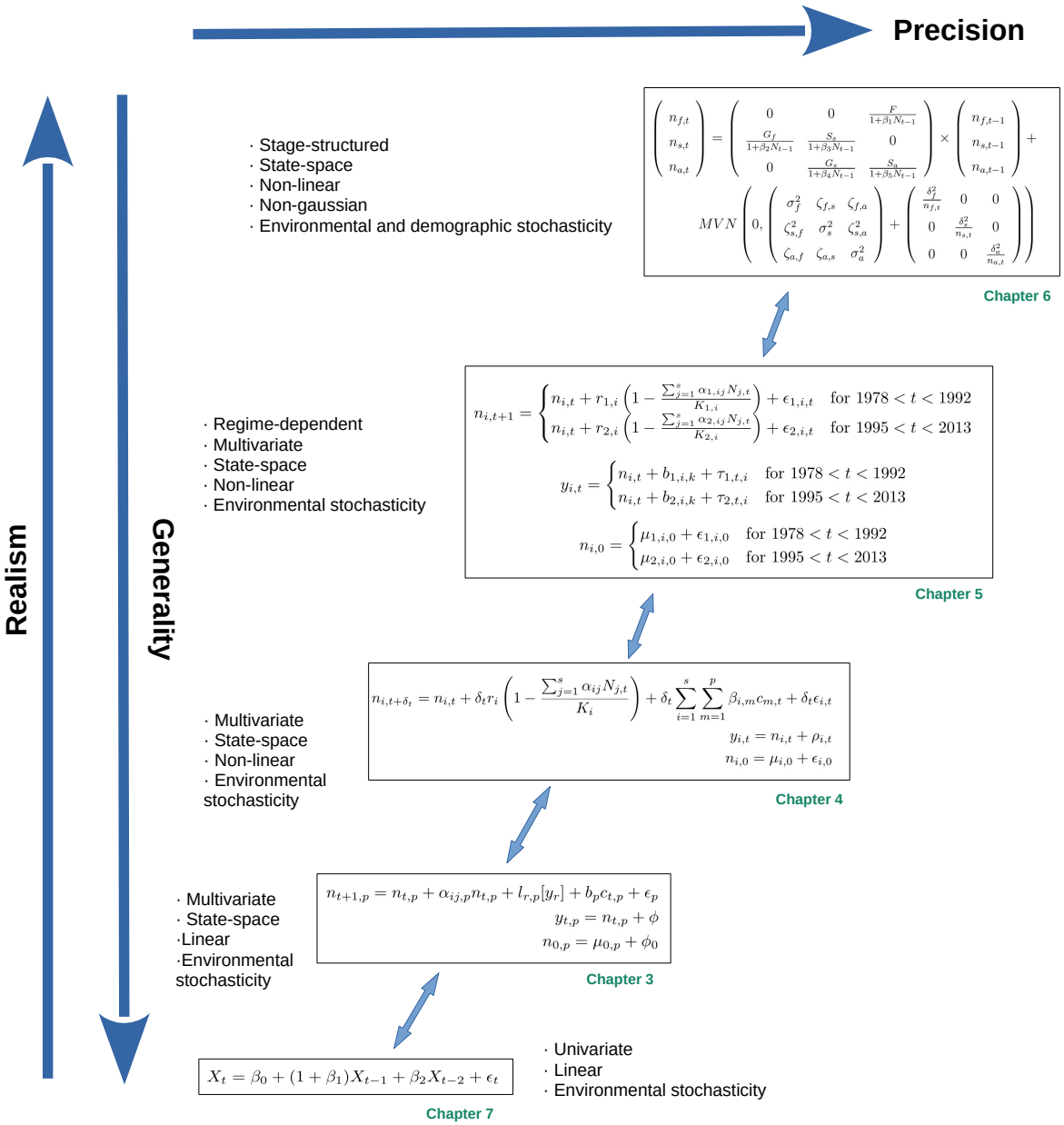

Flow among modeling strategies in each chapter of the dissertation, according to the three axes of variation of the strategy of **robust model building** (Levins, 1966; Orzack and Sober, 1993; Levins, 1993; Wimsatt, 2007; Levins, 2007). From top to bottom, smooth transformations allow shifting from models with little realism, high generalism and low precision in the bottom left (Chapter 8) to models with high realism, low generalism and high precision in the upper right (Chapter 7). In this route, at least one degree-of-freedom is gained during the transformation; the *local* characteristics of each model are placed besides each one. Since transformations are smooth, under the structural realistic framework (Casti, 1997) this is a family of globally **robust models**, or **structurally stable models**.

Figure 9.1: Smooth mapping among models

Chapter 8, to the stage-structured, non-linear, non-gaussian state-space model used in Chapter 7.

2. A second, major theme emerging from the set of examples presented in this dissertation is the following: irrespective of the level of ecological or taxonomic organization, of the type of ecosystem considered and of the spatial or temporal resolution explored, **natural systems seem to track their common environment very closely**. For the case of plankton food webs, it is very well known that the coupling between oceanographic conditions and biomass production in the ocean is very strong (Longhurst, 2007), and this what we found in this dissertation (Chapters 4 and 5). In the case of the wintering bird community (Chapter 6) and the breeding colony of scavenger bird (Chapter 7), a salient result was the highly non-linear dynamics induced at the population and community levels by abrupt, non-stationary shifts in the environment, both from geological catastrophes (Chapter 6) or human perturbations (Chapter 7). Moreover, there is a clear evolutionary, deep-time signal in how different species respond to the current environment (Chapter 8): the impact of environmental stochasticity on the population stability and demography of shorebirds is closely modulated by life-history traits under strong selection, such as body size or sexual dimorphism. Overall, in this dissertation I show that **current environmental conditions and evolutionary legacies should be jointly taken into account for explaining and predicting the dynamics of population and communities**.

9.2 Do the systems studied conform to the complexity criteria?

As laid out in the introduction, ecological systems are currently conceptualized by ecologist as *complex systems*. While this term is usually given a very loose meaning, several criteria were discussed (Rzevski and Skobelev, 2014) to assess whether ecological systems are really complex systems. In the light of the case studies explored in this dissertation, is this the case?

9.2.1 *Connectivity*

In three of the case studies explored, a network approach to the dynamical connectivity among species in communities, expressed in ecological interaction networks, suggest a rich pattern: the interaction networks were relatively sparse for the case of global phytoplankton communities (Chapter 4) and for the wintering waterfowl community (Chapter 6). In contrast, for the mixotrophic plankton food web (Chapter 5) a *small-world* pattern emerged from the interaction network, with a few functional types strongly interacting among them, but very weakly with others. Diverse *connectivity* patterns is the rule.

9.2.2 *Autonomy*

A general pattern in all the case studies is the finding that the probability of interaction between species or functional types in a network is much lower that the probability of *self-loops*: the strength with which the average individual of a species interact with conspecifics is larger than the strength with which it interacts with heterospecifics (Chapters 4, 5 and 6). In other words: interactions are **localized**, and modify the global stability properties (see below).

9.2.3 *Emergence*

A direct consequence of the diverse connectivity pattern, from sparse (Chapter 4) to small-world (Chapter 5), and of the fundamental dominance across networks of intra-specific interactions over inter-specific interactions, is that the global properties of the communities are such that **stability is maximized**. In particular, the entropy of the modeled mixotrophic plankton food web (Chapter 5) is maximal, even though this system is located at the limit of instability. Thus, stability in the systems studied is an *emergent* property. This is in accordance with recent views of stability as an emergent property of ecological systems selected at higher levels (Borrelli et al., 2015).

9.2.4 *Non-equilibrium*

The small-world pattern detected in mixotrophic plankton food web (Chapter 5), with a few functional types involved in relatively strong interactions, is driving this community to the edge of instability (Fig. 5.5), a non-equilibrium condition. The case of the wintering waterfowl community (Chapter 6) is particularly prominent: a stochastic cusp catastrophe model points to an abrupt regime shift among two alternative stable states. This is an extreme example of non-equilibrium dynamics (Scheffer, 2009; Petraitis, 2013).

9.2.5 *Non-linearity*

In the present dissertation, an example of a highly nonlinear behaviour is provided by the catastrophic dynamics of the wintering waterfowl community in Doñana marshes (Chapter 6): the presence of a regime shift among two alternative stable states after the crossing of a tipping point induced by an external, planetary geological event. This tipping point is a degenerate equilibrium, in which the dynamics abruptly shifts from smooth and linear to discontinuous and nonlinear. The dynamics of the mixotrophic plankton food web (Chapter 5) is another example of a non-linear behaviour in the frontier of instability, and in this case the mechanism is internal: a strongly interacting small-world.

9.2.6 *Self-organization*

The evidence of self-organization in the case studies presented in this dissertation are diverse: in the case of phytoplankton communicates of the world ocean (Chapter 4), a latitudinal increase in structural and dynamical stability in response to a larger functional diversity points to a community self-organization induced by an increase in environmental variability (Fig. 4.19). This is an example of the phenomena of *order through fluctuations* (Prigogine, 1978, 1980), characteristic of complex systems evolving in non-equilibrium conditions. Additionally, the remaining case studies show some degree of self-organization. For example, the wintering waterfowl community, in spite of an abrupt regime shift, reorganize in an alternative stable state (Fig. 6.8). The strong covariation between evolutionary traits and population dynamics properties in shorebirds (Chapter 8) provides evidence of self-organization at a larger evolutionary scale.

9.2.7 *Coevolution*

Finally, the coevolution between the ecological systems studied in this dissertation and their common environment is a direct consequence of their *persistence*: as shown above, self-organization requires some degree of interaction with the environment, both the biotic and abiotic (Prigogine, 1980; Borrelli et al., 2015). For example, in the case of phytoplankton communities in the global ocean (Chapter 4) one of the most abundant species of bacterioplaknton is *Prochlorococcus* (Fig. 4.7), the major niche constructor in the oceans of the planet (Flombaum et al., 2013). Additionally, the mixotrophic plankton food web (Chapter 5), is composed of species that can act as phototrophs and heterotrophs, and these strategies by definition shits the environmental conditions. Also, the microbial loops present in these two systems (Chapters 4 and 5) is one of the main mechanisms for the remineralization of organic matter and, as such, operates as a niche construction strategy.

9.3 Ecology in changing times: towards a non-stationary, non-autonomous perspective?

The discussion above firmly suggest that the case studies analyzed in the present dissertation are **complex** in a rigorous sense. What does this means for the general interpretation and implications of the results (Fig. 9.3)? Two lines of further research are identified in this final section, related with the **diversity**, **variability** and **persistence** of fluctuating ecological systems:

1. **Time**. As shown in this dissertation, time is of essence for ecological systems. Inverse modeling has stand out as the fundamental tool for understanding the fluctuations of ecological systems in variable environments. Whether this variability is predictable, such as the strong seasonal signal in plankton systems (Chapters 4 and 5),

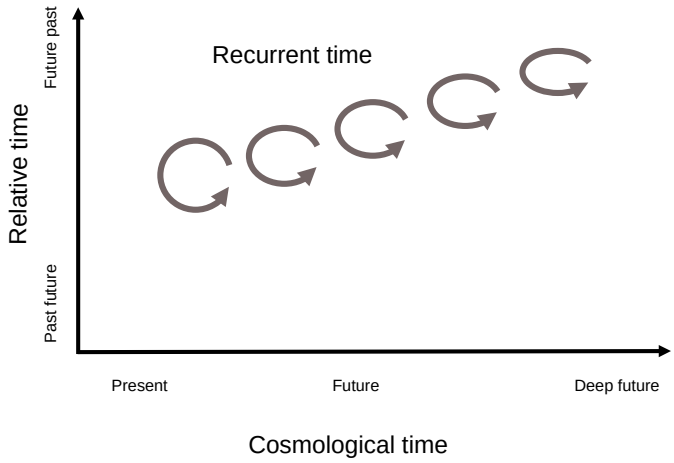

Figure 9.2: The tree types of time in ecology are bound to change in the future: a general warming trend will be followed by a compressions of seasons in the Northern Hemisphere.

or unpredictable, as in the geological catastrophe triggering regime shifts in bird communities (Chapter 6), quantitative ecology must expand its toolbox. In climate change scenarios, for example, seasons are predicted to become shorter (compressed in time, e.g,, Gallinat, Primack, and Wagner, 2015), in a generally warming trend (Fig. 9.2). Climate change, as a non-stationary, non-autonomous process (Drótos, Bódai, and Tél, 2016) provides an avenue of research: the application of **non-autonomous dynamical systems theory** (Langa, Robinson, and Suárez, 2003; Carvalho, Langa, and Robinson, 2013; Chesson, 2019). Although beyond the scope of this dissertation, a non-autonomous perspective could be instrumental to harness the problem of understanding systems in which parameters themselves are a function of time. Indeed, in both micro- and macroevolutionary models, parameters are both the subject and object of selection (Morris and Lundberg, 2011), so an extension of the non-autonomous perspective to eco-evolutionary models is a promising way. This is a way forward in ecology suggested by the complexity of the diverse case studies analyzed here.

2. **Dimensionality**. The examples presented in this work span from the demography of single-species (Chapters 7 and 8) to the ecosystem characteristic of a diverse community of functional types (Chapter 5). In spite of this, the species diversity of natural systems is typically much larger than the diversity that standard mathematical models can handle. This is an open problem. But there is yet another dimension that stand out as completely neglected by ecologists: the existence of a large **stability landscape** even for simple, generalized Lotka-Volterra models, beyond the global stable equi-

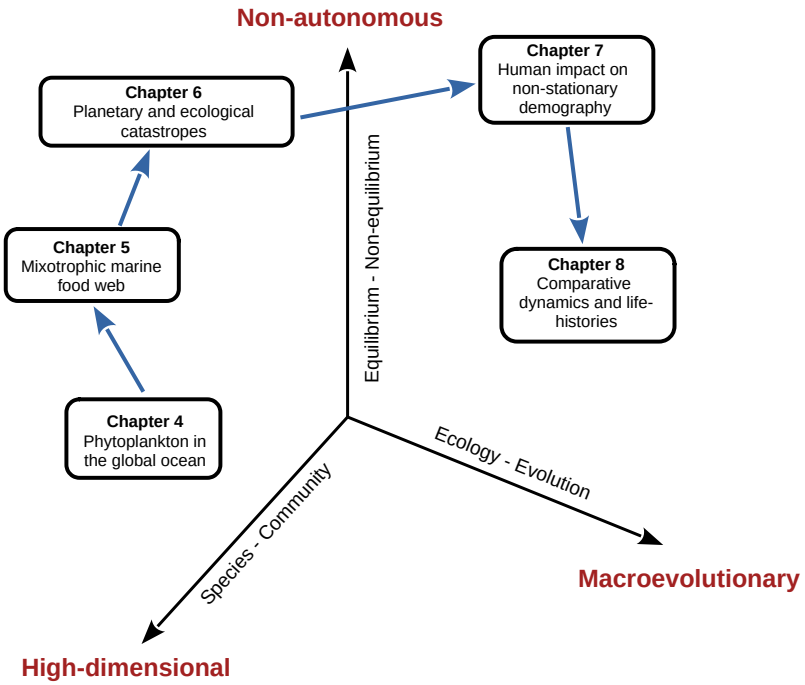

Figure 9.3: Three axes for an extended quantitative ecology suggested by the results of the present dissertation.

librium (e.g., Esteban et al., 2018; Bortolan, Carvalho, and Langa, 2020; Soler-Toscano et al., 2022). To introduce an extension of the models used in this dissertation to the field of stability landscapes, or **informational structures** (Kalita, Langa, and Soler-Toscano, 2019; Portillo, Soler-Toscano, and Langa, 2022), in Figure 9.4 I show the informational structure of the small-world network of five plankton functional types identified in Figure 5.3. This structure is the **global attractor** of the system: it is composed by all the equilibria, whether stable (asymptotic) or unstable (transient), and their connections in the state space (Conley, 1978; Norton, 1995; Hurley, 1995; Kalita, Langa, and Soler-Toscano, 2019). The globally stable equilibrium (the node in the cusp in Fig. 9.4) is feasible: all species are present. Interestingly however, there is a *deep state space* below this global equilibrium composed of **unstable equilibria**, connected to the global equilibrium by invasion events. Due to the very stochastic nature of fluctuations in ecological systems (both demographic and environmental), these equilibria are exerting a mechanical impact on the system: ignoring them hides away a largely unexplored explanation for the prevalence of transients in ecology (Hastings et al., 2018). As an illustration, Figure 9.5 shows a new measure of *non-equilibriumness* of dynamical systems suggested by the results of this dissertation. In this figure, the distance to the global attractor (the informational structure in Fig. 9.4) measures how close the system is, at any time, to the globally stable equilibrium (the cusp in Fig. 9.4), and to the closest *transient* (unstable) equilibrium in the attractor. For this system,

"Maybe ecological complexity persists by virtue of the transience of any ecological system" (Taylor, 1988)

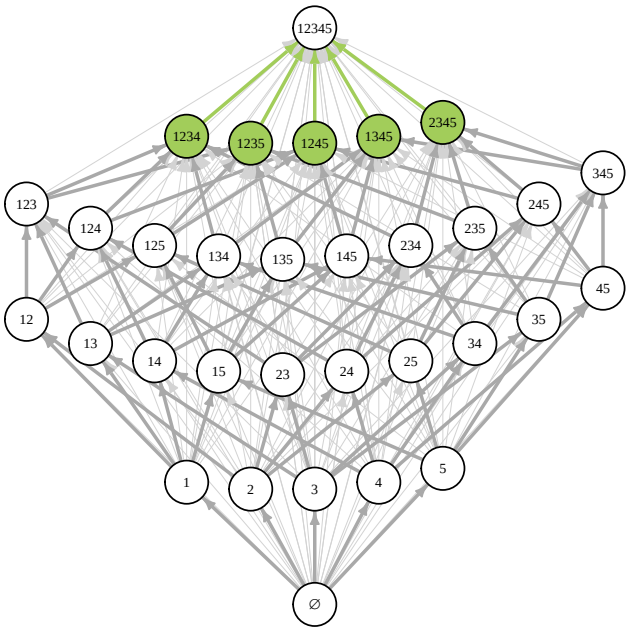

Figure 9.4: The **informational structure**, or **global attractor**, for the mixotrophic plankton food web (Chapter 5). The fitting of the Lotka-Volterra model to the small-world network of interactions identified in Figure 5.5, yields a total of 2^n equilibria, were n is the number of functional types ($n = 5$). These equilibria are represented in the nodes as subcommunities, composed by up to 5 species labeled with numbers, and invasions (arrows) are possible among these communities from a bare environment at the bottom, ∅, to the globally stable community (Takeuchi, 1996), in the cusp of the graph. This community is stable and feasible, but the rest of transient equilibria are unstable. Green nodes and edges denote positive invasion growth rates for those species. For Volterra-Lyapunov stable systems (Almaraz, Langa, and Kalita, 2022), this informational structure is identical to the invasion graph (Hofbauer and Schreiber, 2022)

even in this autonomous case, as the euclidean distance to the transient points is systematically smaller, most of the time the biomass of the small-world planktonic food web is fluctuating in regions of the state space densely populated by transient, unstable manifolds. This results is, indeed, what is expected in thermodynamical systems fluctuating away from the stable equilibrium (Prigogine, 1980): they self-organize through fluctuations.

What is the importance, then, of the globally stable equilibrium?

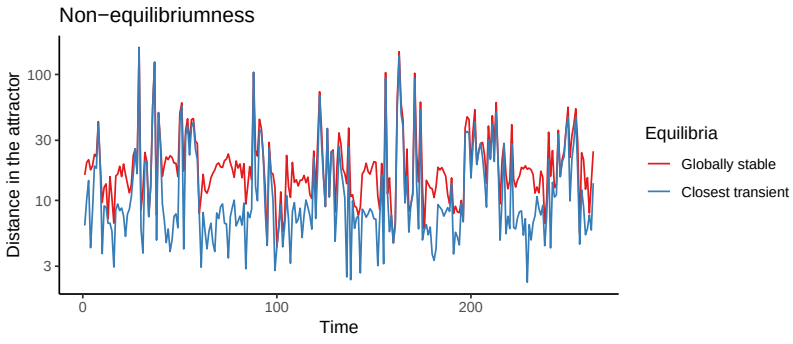

Figure 9.5: Closeness of the observed vector of biomass of the small-world network of mixotrophic plankton (Figure 5.3) to the globally stable equilibrium of the global attractor shown in Figure 9.4 (in red), compared to the distance to the closest transient (unstable) equilibrium (in a kind of blue). This euclidean distance measures the *non-equilibriumness* of a dynamical system.

Conclusions 10

1. Under the philosophical framework of structural realism, the strategy of inverse mathematical modeling as a strategy of abstraction has proven very useful for understanding the complex mechanics of fluctuations in five natural ecosystems used as case studies. These systems span a range of spatial scales, from the global ocean to a single population; organizational levels, from single species to diverse communities of functional types; different habitats, from the pelagic zone, to coastal areas, marshes and mountain regions; and temporal dimensions and resolutions, from weekly biomass data to multi-decadal data on population size.

2. An increase in functional diversity with latitude stabilizes phytoplankton communities at a planetary scale, in spite of an increase in environmental harness with latitude. At a local scale, a small-world interactive network of mixotrophic interactions in a temperate, coastal plankton food web drives the system to the edge of instability in a scenario of maximum interaction entropy. These case studies provide evidence of self-organization through fluctuations, both internal and external.

3. The dynamics of the major wintering waterfowl community in Doñana mashes displayed an abrupt regime-shift to alternative stable states during a 36-year period. This extreme non-equilibrium dynamics conforms to a cusp catastrophe likely operating through behavioral shifts in response to a volcanic eruption inducing a transient reversal of climatic conditions. The demographic dynamics of one of the world's largest breeding population of a keystone scavenging bird was severely disrupted by human-induced environmental perturbations during a 42-year period. The population dynamics displayed a highly plastic demography, with very fast recoveries. Again, these case studies provide evidence of self-organization through both internal and external fluctuations.

4. A comparative population dynamics analysis suggest that the current demography and stability of the wintering shorebird community in coastal UK is under strong control of life-history traits with a large selection pressure, such as body size and sexual dimorphism. This indeed suggest that this community is also self-organized through internal and external fluctuations, this time operating at deeper evolutionary time scales.

5. From this quantitative and theoretical exploration of a diversity of case studies, a major pattern emerging is that natural systems are able to closely track their local and global environments. These environments, and the heterogeneous dynamical patterns they in-

duce, are coped thanks to the complex nature of the studied ecosystems. The evidence presented supports that these systems indeed posses the features of complex systems: connectivity, autonomy, emergence, non-equilibrium, non-linearity, self-organization and co-evolution. Whether these ecosystems will be able to robustly respond to future changing conditions in a global change scenario, is an open question.

6. The results of this dissertation point to non-autonomous dynamical system approaches, where model parameters are a function of time, as a fundamental approach to foster the merging of complex systems dynamics and non-stationary environments. As a first step, the global attractor of the small-word mixotrophic food web is studied in detail, and a measure of non-equilibriumness is introduced for dynamical systems. This novel perspective points to the relevance of considering the transient dynamics as an integral, mechanical part of natural ecosystems in rapidly changing environments.

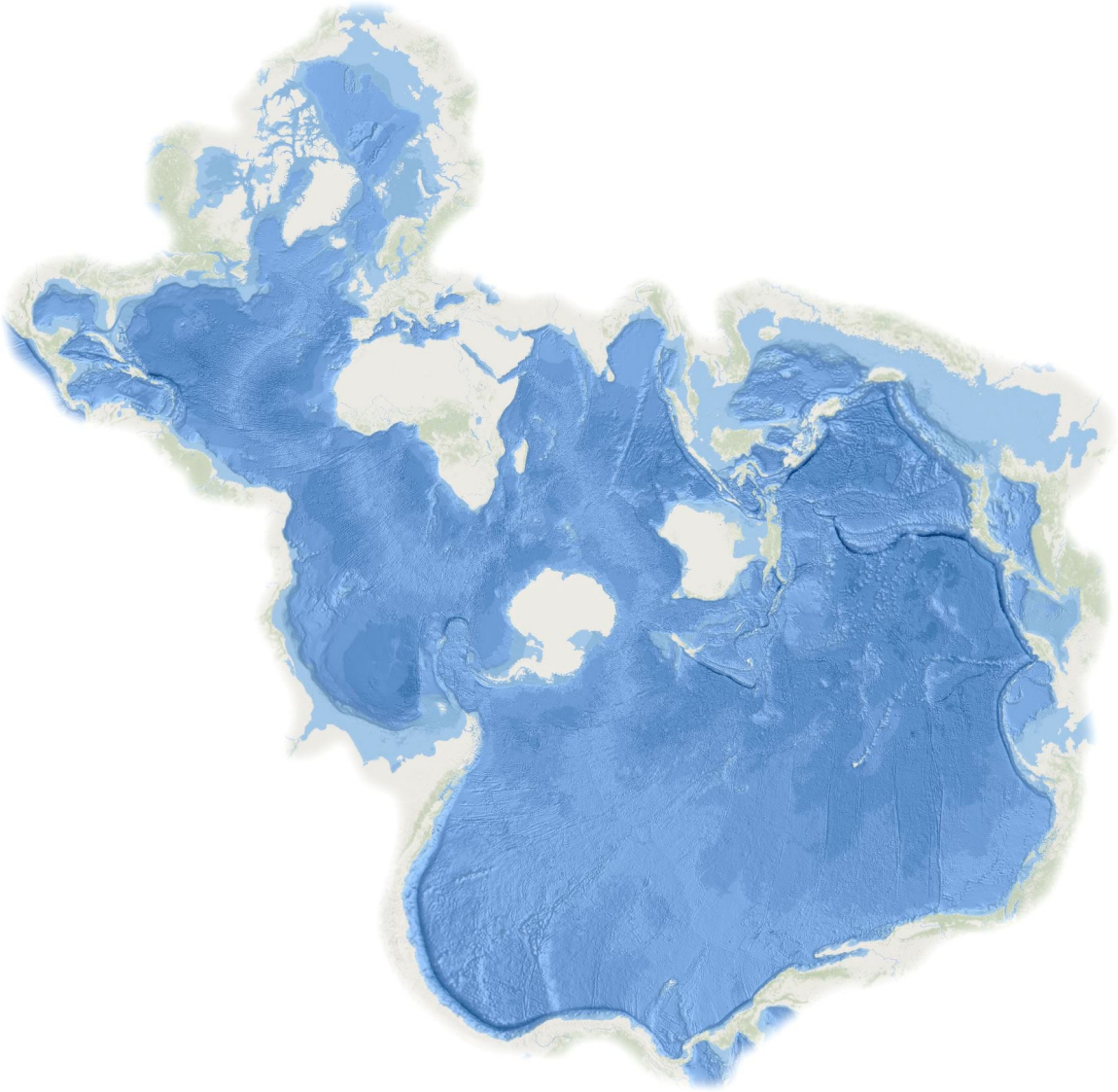

"Mystics and ecologists say that the world is one"
Leigh Van Valen, 1976

Bibliography

Abrams, P. A. 2022. *Competition Theory in Ecology*. Oxford, UK: Oxford University Press. doi:10.1093/oso/9780192895523.001. (see p. 187).

Acevedo-Trejos, E., G. Brandt, J. Bruggeman, and A. Merico. 2015. *Mechanisms shaping size structure and functional diversity of phytoplankton communities in the ocean.* Scientific reports 5:8918. doi:10.1038/srep08918. (see pp. 67, 84).

Acevedo-Trejos, E., G. Brandt, M. Steinacher, and A. Merico. 2014. *A glimpse into the future composition of marine phytoplankton communities*. Frontiers in Marine Science 1 (July): 1–12. doi:10.3389/fmars.2014.00015. (see pp. 64, 84, 86).

Adler, P. B., D. Smull, K. H. Beard, R. T. Choi, T. Furniss, A. Kulmatiski, J. M. Meiners, A. T. Tredennick, and K. E. Veblen. 2018. *Competition and coexistence in plant communities: intraspecific competition is stronger than interspecific competition*. Edited by L. Comita. Ecology Letters 21 (9): 1319–1329. doi:10.1111/ele.13098. (see p. 90).

Adolf, J. E., D. K. Stoecker, and L. W. Harding. 2006. *The balance of autotrophy and heterotrophy during mixotrophic growth of Karlodinium micrum (Dinophyceae)*. Journal of Plankton Research 28 (8): 737–751. doi:10.1093/plankt/fbl007. (see p. 91).

Allen, T. F. H., and T. B. Starr. 2017. *Hierarchy*. University of Chicago Press. doi:10.7208/chicago/9780226489711.001.0001. (see pp. 23, 24).

Almaraz, P. 2014. *Simple models, complex models, useful models: can we tell them from the flap of a butterfly's wings?* Frontiers in Ecology and Evolution 2:54. doi:10.3389/fevo.2014.00054. (see p. 28).

Almaraz, P., and J. A. Amat. 2004. *Complex structural effects of two hemispheric climatic oscillators on the regional spatio-temporal expansion of a threatened bird*. Ecology Letters 7 (7): 547–556. doi:10.1111/j.1461-0248.2004.00612.x. (see p. 94).

Almaraz, P., A. J. Green, E. Aguilera, M. A. Rendón, and J. Bustamante. 2012. *Estimating partial observability and nonlinear climate effects on stochastic community dynamics of migratory waterfowl*. Journal of Animal Ecology 81 (5): 1113–1125. doi:10.1111/j.1365-2656.2012.01972.x. (see pp. 69, 94, 95, 99, 100, 121, 122, 125, 135, 138).

Almaraz, P., J. A. Langa, and P. Kalita. 2022. *Structural stability of invasion graphs for generalized Lotka–Volterra systems*. arXiv 2209.09802:1–28. (see p. 194).

Almaraz, P., F. Martínez, Z. Morales-Reyes, J. A. Sánchez-Zapata, and G. Blanco. 2022. *Long-term demographic dynamics of a keystone scavenger disrupted by human-induced shifts in food availability*. Ecological Applications 32 (6). doi:10.1002/eap.2579. (see pp. 30, 73, 100, 141).

Almaraz, P., and D. Oro. 2011. *Size-mediated non-trophic interactions and stochastic predation drive assembly and dynamics in a seabird community*. Ecology 92 (10): 1948–1958. doi:10.1890/11-0181.1. (see pp. 95, 100, 101, 121, 123, 125, 138, 147, 149).

Alvain, S., H. Loisel, and D. Dessailly. 2012. *Theoretical analysis of ocean color radiances anomalies and implications for phytoplankton groups detection in case 1 waters*. Optics Express 20 (2): 1070. doi:10.1364/OE.20.001070. (see pp. 68, 69, 70).

Alvain, S., C. Moulin, Y. Dandonneau, and F. M. Bréon. 2005. *Remote sensing of phytoplankton groups in case 1 waters from global SeaWiFS imagery*. Deep-Sea Research Part I: Oceanographic Research Papers 52 (11): 1989–2004. doi:10.1016/j.dsr.2005.06.015. (see p. 68).

Alvain, S., C. Moulin, Y. Dandonneau, and H. Loisel. 2008. *Seasonal distribution and succession of dominant phytoplankton groups in the global ocean: A satellite view*. Global Biogeochemical Cycles 22 (3): 1–15. doi:10.1029/2007GB003154. (see pp. 68, 75).

Anderson, P. W. 1997. *Is measurement itself an emergent property?* Complexity 3 (1): 14–16. doi:10.1002/(SICI)1099-0526(199709/10)3:1<14::AID-CPLX5>3.0.CO;2-E. (see p. 23).

Anderson, S. I., A. D. Barton, S. Clayton, S. Dutkiewicz, and T. A. Rynearson. 2021. *Marine phytoplankton functional types exhibit diverse responses to thermal change*. Nature Communications 12 (1): 6413. doi:10.1038/s41467-021-26651-8. (see p. 86).

Andronov, A., and C. E. Chaikin. 1949. *Theory of Oscillations.* Princeton, NJ.: Princeton University Press. (see p. 45).

Andronov, A., and L. Pontryagin. 1937. *Systèmes grossiers*. Dokl. Akad. Nauk SSSR 14 (5): 247–250. (see pp. 43, 45).

Arnold, L. 1974. *Stochastic Differential Equations : Theory and Applications*. New York: John Wiley & Sons. (see p. 41).

Arnold, V. I. 1988. *Geometrical methods in the Theory of Ordinary Differential Equations.* 2nd ed. New York: Springer-Verlag. (see pp. 43, 44, 45, 46).

———. 1994. *Dynamical Systems V. Bifurcation Theory and Catastrophe Theory.* Berlin: Springer-Verlag. (see p. 126).

Arnoldi, J.-F., and B. Haegeman. 2016. *Unifying dynamical and structural stability of equilibria*. Proceedings of the Royal Society A: Mathematical, Physical and Engineering Sciences 472 (2193): 20150874. doi:10.1098/rspa.2015.0874. (see pp. 41, 43, 47, 48, 59, 64, 72, 98).

Arnoldi, J.-F., M. Loreau, and B. Haegeman. 2016. *Resilience, reactivity and variability: A mathematical comparison of ecological stability measures*. Journal of Theoretical Biology 389:47–59. doi:10.1016/j.jtbi.2015.10.012. (see pp. 35, 41, 42, 43, 44, 59, 64, 72, 82, 85, 98).

Arrondo, E., M. Moleón, A. Cortés-Avizanda, J. Jiménez, P. Beja, J. A. Sánchez-Zapata, and J. A. Donázar. 2018. *Invisible barriers: Differential sanitary regulations constrain vulture movements across country borders*. Biological Conservation 219:46–52. doi:10.1016/j.biocon.2017.12.039. (see p. 154).

Arrondo, E., A. Sanz-Aguilar, J. M. Pérez-García, A. Cortés-Avizanda, J. A. Sánchez-Zapata, and J. A. Donázar. 2020. *Landscape anthropization shapes the survival of a top avian scavenger*. Biodiversity and Conservation 29 (4): 1411–1425. doi:10.1007/s10531-020-01942-6. (see p. 157).

Atkinson, A., R. A. Harmer, C. E. Widdicombe, A. J. McEvoy, T. J. Smyth, D. G. Cummings, P. J. Somerfield, J. L. Maud, and K. McConville. 2015. *Questioning the role of phenology shifts and trophic mismatching in a planktonic food web*. Progress in Oceanography 137:498–512. doi:10.1016/j.pocean.2015.04.023. (see p. 93).

Auber, A., C. Waldock, A. Maire, E. Goberville, C. Albouy, A. C. Algar, M. McLean, et al. 2022. *A functional vulnerability framework for biodiversity conservation*. Nature Communications 13 (1): 4774. doi:10.1038/s41467-022-32331-y. (see p. 86).

Bacciotti, A., and L. Rosier. 2005. *Liapunov Functions and Stability in Control Theory*. 2nd. Berlin: Springer-Verlag. (see p. 40).

Baker, A. J., P. M. González, T. Piersma, L. J. Niles, I. de Lima Serrano do Nascimento, P. W. Atkinson, N. A. Clark, C. D. T. Minton, M. K. Peck, and G. Aarts. 2004. *Rapid population decline in red knots: fitness consequences of decreased refuelling rates and late arrival in Delaware Bay*. Proceedings of the Royal Society of London. Series B: Biological Sciences 271 (1541): 875–882. doi:10.1098/rspb.2003.2663. (see pp. 163, 164, 174).

Barabás, G., and S. Allesina. 2015. *Predicting global community properties from uncertain estimates of interaction strengths*. Journal of The Royal Society Interface 12 (109): 20150218. doi:10.1098/rsif.2015.0218. (see p. 97).

Barabás, G., M. J. Michalska-Smith, and S. Allesina. 2016. *The Effect of Intra- and Interspecific Competition on Coexistence in Multispecies Communities*. The American Naturalist 188 (1): E1–E12. doi:10.1086/686901. (see pp. 62, 86, 108).

Barabás, G., L. Pásztor, G. Meszéna, and A. Ostling. 2014. *Sensitivity analysis of coexistence in ecological communities: theory and application*. Edited by F. Adler. Ecology Letters 17 (12): 1479–1494. doi:10.1111/ele.12350. (see p. 97).

Barnosky, A. D., E. A. Hadly, J. Bascompte, E. L. Berlow, J. H. Brown, M. Fortelius, W. M. Getz, J. Harte, A. Hastings, P. A. Marquet, et al. 2012. *Approaching a state shift in Earth's biosphere*. Nature 486 (7401): 52–58. doi:10.1038/nature11018. (see p. 120).

Barnosky, A. D., N. Matzke, S. Tomiya, G. O. U. Wogan, B. Swartz, T. B. Quental, C. Marshall, et al. 2011. *Has the Earth's sixth mass extinction already arrived?* Nature 471 (7336): 51–57. doi:10.1038/nature09678. (see p. 62).

Barraquand, F., C. Picoche, D. Maurer, L. Carassou, and I. Auby. 2018. *Coastal phytoplankton community dynamics and coexistence driven by intragroup density-dependence, light and hydrodynamics*. Oikos 127 (12): 1834–1852. doi:10.1111/oik.05361. (see p. 110).

Bartomeus, I., S. Saavedra, R. P. Rohr, and O. Godoy. 2021. *Experimental evidence of the importance of multitrophic structure for species persistence*. Proceedings of the National Academy of Sciences 118 (12): e2023872118. doi:10.1073/pnas.2023872118. (see p. 92).

Bartomeus, I., M. Vilà, and L. Santamaría. 2008. *Contrasting effects of invasive plants in plant–pollinator networks*. Oecologia 155 (4): 761–770. doi:10.1007/s00442-007-0946-1. (see p. 90).

Barton, A. D., A. J. Pershing, E. Litchman, N. R. Record, K. F. Edwards, Z. V. Finkel, T. Kiørboe, and B. A. Ward. 2013. *The biogeography of marine plankton traits*. Edited by J. Elser. Ecology Letters 16 (4): 522–534. doi:10.1111/ele.12063. (see pp. 67, 84).

Bascompte, J., P. Jordano, C. J. Melian, and J. M. Olesen. 2003. *The nested assembly of plant-animal mutualistic networks*. Proceedings of the National Academy of Sciences 100 (16): 9383–9387. doi:10.1073/pnas.1633576100. (see p. 90).

Bascompte, J., and A. Ferrera. 2020. *A structural theory of mutualistic networks*. In Theoretical Ecology, edited by M. K. G. and Gellner, 93–115. Oxford University Press. doi:10.1093/oso/9780198824282.003.0007. (see p. 25).

Bascompte, J., P. Jordano, and J. M. Olesen. 2006. *Asymmetric Coevolutionary Networks Facilitate Biodiversity Maintenance*. Science 312 (5772): 431–433. doi:10.1126/science.1123412. (see p. 25).

Bastolla, U., M. a. Fortuna, A. Pascual-García, A. Ferrera, B. Luque, and J. Bascompte. 2009. *The architecture of mutualistic networks minimizes competition and increases biodiversity.* Nature 458 (7241): 1018–1020. doi:10.1038/nature07950. (see p. 91).

Behrenfeld, M. J., and P. G. Falkowski. 1997. *Photosynthetic rates derived from satellite-based chlorophyll concentration*. Limnology and Oceanography 42 (1): 1–20. doi:10.4319/lo.1997.42.1.0001. (see p. 65).

Behrenfeld, M. J., R. T. O'Malley, E. S. Boss, T. K. Westberry, J. R. Graff, K. H. Halsey, A. J. Milligan, D. a. Siegel, and M. B. Brown. 2016. *Revaluating ocean warming impacts on global phytoplankton*. Nature Climate Change 5:323–330. doi:10.1038/nclimate2838. (see p. 64).

Bellman, R., and K. Åström. 1970. *On structural identifiability*. Mathematical Biosciences 7 (3-4): 329–339. doi:10.1016/0025-5564(70)90132-X. (see p. 102).

Benincà, E., J. Huisman, R. Heerkloss, K. D. Jöhnk, P. Branco, E. H. Van Nes, M. Scheffer, and S. P. Ellner. 2008. *Chaos in a long-term experiment with a plankton community*. Nature 451 (7180): 822–825. doi:10.1038/nature06512. (see p. 25).

Bennett, P. M., and I. P. Owens. 2002. *Evolutionary ecology of birds: life histories, mating systems, and extinction.* Oxford, UK: Oxford University Press. (see pp. 146, 156, 162, 163, 165, 167, 173, 179, 182).

Benton, T. G., S. J. Plaistow, and T. N. Coulson. 2006. *Complex population dynamics and complex causation: devils, details and demography*. Proceedings of the Royal Society B: Biological Sciences 273 (1591): 1173–1181. doi:10.1098/rspb.2006.3495. (see p. 156).

Bernhardt, J. R., M. I. O'Connor, J. M. Sunday, and A. Gonzalez. 2020. *Life in fluctuating environments*. Philosophical Transactions of the Royal Society B: Biological Sciences 375 (1814): 20190454. doi:10.1098/rstb.2019.0454. (see p. 27).

Bestion, E., B. Haegeman, S. Alvarez Codesal, A. Garreau, M. Huet, S. Barton, and J. M. Montoya. 2021. *Phytoplankton biodiversity is more important for ecosystem functioning in highly variable thermal environments*. Proceedings of the National Academy of Sciences 118 (35): e2019591118. doi:10.1073/pnas.2019591118. (see p. 85).

Bicknell, A. W. J., D. Oro, K. C. Camphuysen, and S. C. Votier. 2013. *Potential consequences of discard reform for seabird communities*. Edited by J. Blanchard. Journal of Applied Ecology 50 (3): 649–658. doi:10.1111/1365-2664.12072. (see p. 142).

Bjornstad, O. N., W. Falck, and N. Stenseth Chr. 1995. *A geographic gradient in small rodent density fluctuations: a statistical modelling approach*. Proceedings of the Royal Society of London. Series B: Biological Sciences 262 (1364): 127–133. doi:10.1098/rspb.1995.0186. (see pp. 165, 166, 177, 178).

Bjornstad, O. N. 2001. *Noisy Clockwork: Time Series Analysis of Population Fluctuations in Animals*. Science 293 (5530): 638–643. doi:10.1126/science.1062226. (see pp. 120, 178).

BJØRNSTAD, O. N., R. M. NISBET, and J.-M. FROMENTIN. 2004. *Trends and cohort resonant effects in age-structured populations*. Journal of Animal Ecology 73 (6): 1157–1167. doi:10.1111/j.0021-8790.2004.00888.x. (see p. 173).

Bjørnstad, O. N., M. Peltonen, A. M. Liebhold, and W. Baltensweiler. 2002. *Waves of Larch Budmoth Outbreaks in the European Alps*. Science 298 (5595): 1020–1023. doi:10.1126/science.1075182. (see p. 25).

Blanco, G. 2014. *Can livestock carrion availability influence diet of wintering red kites? Implications of sanitary policies in ecosystem services and conservation*. Population Ecology 56 (4): 593–604. doi:10.1007/s10144-014-0445-2. (see pp. 142, 143, 144, 154, 155, 156).

Blanco, G., A. Cortés-Avizanda, Ó. Frías, E. Arrondo, and J. A. Donázar. 2019. *Livestock farming practices modulate vulture diet-disease interactions*. Global Ecology and Conservation 17:e00518. doi:10.1016/j.gecco.2018.e00518. (see pp. 143, 155, 158).

Blanco, G., A. Junza, and D. Barrón. 2017. *Food safety in scavenger conservation: Diet-associated exposure to livestock pharmaceuticals and opportunist mycoses in threatened Cinereous and Egyptian vultures*. Ecotoxicology and Environmental Safety 135 (July 2016): 292–301. doi:10.1016/j.ecoenv.2016.10.009. (see p. 143).

Blanco, G., A. Junza, D. Segarra, J. Barbosa, and D. Barrón. 2016. *Wildlife contamination with fluoroquinolones from livestock: Widespread occurrence of enrofloxacin and marbofloxacin in vultures*. Chemosphere 144:1536–1543. doi:10.1016/j.chemosphere.2015.10.045. (see pp. 143, 158).

Blanco, G., and F. Martinez. 1996. *Sex Difference in Breeding Age of Griffon Vultures (Gyps fulvus)*. The Auk 113 (1): 247–248. doi:10.2307/4088957. (see p. 145).

Blanco, G., F. Martinez, and J. M. Traverso. 1997. *Pair bond and age distribution of breeding Griffon Vultures Gyps fulvus in relation to reproductive status and geographic area in Spain*. Ibis 139 (1): 180–183. doi:10.1111/j.1474-919X.1997.tb04522.x. (see pp. 145, 156).

Blomqvist, S., N. Holmgren, S. Åkesson, A. Hedenström, and J. Pettersson. 2002. *Indirect effects of lemming cycles on sandpiper dynamics: 50 years of counts from southern Sweden*. Oecologia 133 (2): 146–158. doi:10.1007/s00442-002-1017-2. (see pp. 176, 177).

Blum, H. F. 1968. *Time's arrow and evolution*. Princeton, NJ.: Princeton University Press. (see p. 26).

Bohner, M., and H. Warth. 2007. *The Beverton–Holt dynamic equation*. Applicable Analysis 86 (8): 1007–1015. doi:10.1080/00036810701474140. (see p. 146).

Booth, B. B. B., N. J. Dunstone, P. R. Halloran, T. Andrews, and N. Bellouin. 2012. *Aerosols implicated as a prime driver of twentieth-century North Atlantic climate variability*. Nature 484 (7393): 228–232. doi:10.1038/nature10946. (see pp. 121, 123).

Bopp, L., L. Resplandy, J. C. Orr, S. C. Doney, J. P. Dunne, M. Gehlen, P. Halloran, et al. 2013. *Multiple stressors of ocean ecosystems in the 21st century: Projections with CMIP5 models*. Biogeosciences 10 (10): 6225–6245. doi:10.5194/bg-10-6225-2013. (see p. 86).

Borrelli, J. J., S. Allesina, P. Amarasekare, R. Arditi, I. Chase, J. Damuth, R. D. Holt, et al. 2015. *Selection on stability across ecological scales*. Trends in Ecology and Evolution 30 (7): 417–425. doi:10.1016/j.tree.2015.05.001. (see pp. 190, 191).

Bortolan, M. C., A. N. Carvalho, and J. A. Langa. 2020. *Attractors Under Autonomous and Non-autonomous Perturbations*. Providence, RI: American Mathematical Society. (see p. 193).

Box, G. E. P., and D. N. R. 1987. *Wiley Series in Probability and Mathematical Statistics Empirical model-building and response surfaces.* John Wiley & Sons, Ltd. (see p. 165).

Boyce, M. S., E. M. Kirsch, and C. Servheen. 2002. *Bet-hedging applications for conservation*. Journal of Biosciences 27 (4): 385–392. doi:10.1007/BF02704967. (see p. 164).

Brown, K. S., and J. P. Sethna. 2003. *Statistical mechanical approaches to models with many poorly known parameters*. Physical Review E 68 (2): 021904. doi:10.1103/PhysRevE.68.021904. (see p. 102).

Buechley, E. R., and Ç. H. Şekercioğlu. 2016. *The avian scavenger crisis: Looming extinctions, trophic cascades, and loss of critical ecosystem functions*. Biological Conservation 198:220–228. doi:10.1016/j.biocon.2016.04.001. (see p. 143).

Buitenhuis, E. T., M. Vogt, R. Moriarty, N. Bednar??ek, S. C. Doney, K. Leblanc, C. Le Qu??r??, et al. 2013. *MAREDAT: Towards a world atlas of MARine Ecosystem DATa*. Earth System Science Data 5 (2): 227–239. doi:10.5194/essd-5-227-2013. (see pp. 76, 77).

Buitenhuis, E., W. Li, D. Vaulot, M. Lomas, M. Landry, F. Partensky, D. M. Karl, et al. 2012. *Picophytoplankton biomass distribution in the global ocean*. Earth System Science Data Discussions 5 (1): 221–242. doi:10.5194/essdd-5-221-2012. (see pp. 66, 67).

Bulmer, M. G. 1985. *Selection for Iteroparity in a Variable Environment*. The American Naturalist 126 (1): 63–71. doi:10.1086/284396. (see p. 163).

Burkholder, J. M., P. M. Glibert, and H. M. Skelton. 2008. *Mixotrophy, a major mode of nutrition for harmful algal species in eutrophic waters*. Harmful Algae 8 (1): 77–93. doi:10.1016/j.hal.2008.08.010. (see p. 111).

Cabon, A., and W. R. L. Anderegg. 2022. *Large volcanic eruptions elucidate physiological controls of tree growth and photosynthesis*. Ecology Letters, no. June: 1–11. doi:10.1111/ele.14149. (see p. 121).

Camacho, C., J. J. Negro, J. Elmberg, A. D. Fox, S. Nagy, D. J. Pain, and A. J. Green. 2022. *Groundwater extraction poses extreme threat to Doñana World Heritage Site*. Nature Ecology & Evolution: 2–3. doi:10.1038/s41559-022-01763-6. (see pp. 121, 122, 135).

Camiña, A., and E. Montelío. 2006. *Griffon Vulture Gyps fulvus Food Shortages in the Ebro Valley (Ne Spain) Caused by Regulations Against Bovine Spongiform Encephalopathy (BSE)*. Acta Ornithologica 41 (1): 7–13. doi:10.3161/068.041.0106. (see p. 155).

Canham, C. D., M. J. Papaik, M. Uriarte, W. H. McWilliams, J. C. Jenkins, and M. J. Twery. 2006. *Neighborhood analyses of canopy tree competition along environmental gradients in New England forests*. Ecological Applications 16 (2): 540–554. doi:10.1890/1051-0761(2006)016[0540:NAOCTC]2.0.CO;2. (see p. 90).

Capon, S. J., A. J. J. Lynch, N. Bond, B. C. Chessman, J. Davis, N. Davidson, M. Finlayson, et al. 2015. *Regime shifts, thresholds and multiple stable states in freshwater ecosystems; a critical appraisal of the evidence*. Science of the Total Environment 534:122–130. doi:10.1016/j.scitotenv.2015.02.045. (see p. 120).

Capone, F., R. De Luca, and S. Rionero. 2013. *On the stability of non-autonomous perturbed Lotka-Volterra models*. Applied Mathematics and Computation 219 (12): 6868–6881. doi:10.1016/j.amc.2013.01.003. (see p. 51).

Cardinale, B. J. 2011. *Biodiversity improves water quality through niche partitioning.* Nature 472 (7341): 86–89. doi:10.1038/nature09904. (see p. 90).

Caron, D., R. Sanders, E. Lim, C. Marrase, L. Amaral, S. Whitney, R. Aoki, and K. Porters. 1993. *Light-dependent phagotrophy in the freshwater mixotrophic chrysophyte Dinobryon cylindricum*. Microbial Ecology 25 (1): 93–111. doi:10.1007/BF00182132. (see p. 91).

Carpenter, B., A. Gelman, M. D. Hoffman, D. Lee, B. Goodrich, M. Betancourt, M. Brubaker, J. Guo, P. Li, and A. Riddell. 2017. *Stan : A Probabilistic Programming Language*. Journal of Statistical Software 76 (1). doi:10.18637/jss.v076.i01. (see p. 124).

Carrete, M., J. A. Donázar, and A. Margalida. 2006. *Density-dependent productivity depression in Pyrenean Bearded Vultures: Implications for conservation*. Ecological Applications 16 (5): 1674–1682. doi:10.1890/1051-0761(2006)016[1674:DPDIPB]2.0.CO;2. (see pp. 156, 157).

Carrete, M., J. A. Sánchez-Zapata, J. L. Tella, J. M. Gil-Sánchez, and M. Moleón. 2006. *Components of breeding performance in two competing species: Habitat heterogeneity, individual quality and density-dependence*. Oikos 112 (3): 680–690. doi:10.1111/j.0030-1299.2006.14528.x. (see p. 157).

Cartwright, N. 1983. *How the Laws of Physics Lie*. Oxford, UK: Oxford University Press. doi:10.1093/0198247044.001.0001. (see pp. 28, 29).

Carvalho, A. N., J. A. Langa, and J. C. Robinson. 2013. *Attractors for infinite-dimensional non-autonomous dynamical systems*. Vol. 182. Applied Mathematical Sciences. New York, NY: Springer New York. doi:10.1007/978-1-4614-4581-4. (see p. 192).

Casey, J. R., R. M. Boiteau, M. K. M. Engqvist, Z. V. Finkel, G. Li, J. Liefer, C. L. Müller, N. Muñoz, and M. J. Follows. 2022. *Basin-scale biogeography of marine phytoplankton reflects cellular-scale optimization of metabolism and physiology*. Science Advances 8 (3). doi:10.1126/sciadv.abl4930. (see pp. 84, 86).

Casti, J. 1979. *Connectivity, Complexity, and Catastrophe in Large-Scale Systems*. New York, NY: John Wiley & Sons, Inc. (see pp. 25, 126, 127, 136).

———. 1982. *Catastrophes, control and the inevitability of spruce budworm outbreaks*. Ecological Modelling 14 (3-4): 293–300. doi:10.1016/0304-3800(82)90024-2. (see p. 126).

Casti, J. L. 1997. *Reality Rules*. New York, NY. (see pp. 127, 136, 187, 188).

Caswell, H. 2001. *Matrix population models: construction, analysis, and interpretation.* Sunderland, MA: Sinauer Associates. (see pp. 146, 163, 167, 168, 174, 179, 180, 182, 184).

———. 2007. *Sensitivity analysis of transient population dynamics*. Ecology Letters 10 (1): 1–15. doi:10.1111/j.1461-0248.2006.01001.x. (see pp. 37, 181).

———. 2010. *Life table response experiment analysis of the stochastic growth rate*. Journal of Ecology 98 (2): 324–333. doi:10.1111/j.1365-2745.2009.01627.x. (see p. 149).

Caswell, H., and M. G. Neubert. 2005. *Reactivity and transient dynamics of discrete-time ecological systems*. Journal of Difference Equations and Applications 11 (4-5): 295–310. doi:10.1080/10236190412331335382. (see pp. 37, 85, 98).

Cazelles, B., M. Chavez, D. Berteaux, F. Ménard, J. O. Vik, S. Jenouvrier, and N. C. Stenseth. 2008. *Wavelet analysis of ecological time series*. Oecologia 156 (2): 287–304. doi:10.1007/s00442-008-0993-2. (see pp. 123, 129).

Cenci, S., and S. Saavedra. 2019. *Non-parametric estimation of the structural stability of non-equilibrium community dynamics*. Nature Ecology & Evolution 3 (6): 912–918. doi:10.1038/s41559-019-0879-1. (see pp. 25, 110, 111).

Cermeño, P., E. Marañón, D. Harbour, F. G. Figueiras, B. G. Crespo, M. Huete-Ortega, M. Varela, and R. P. Harris. 2008. *Resource levels, allometric scaling of population abundance, and marine phytoplankton diversity*. Limnology and Oceanography 53 (1): 312–318. doi:10.4319/lo.2008.53.1.0312. (see p. 83).

Cermeño, P., T. Rodríguez-Ramos, M. Dornelas, F. G. Figueiras, E. Marañón, I. G. Teixeira, and S. M. Vallina. 2013. *Species richness in marine phytoplankton communities is not correlated to ecosystem productivity*. Marine Ecology Progress Series 488:1–9. doi:10.3354/meps10443. (see p. 83).

Cesar-Ribeiro, C., F. R. Piedras, L. C. da Cunha, D. T. de Lima, L. Q. Pinho, and G. A. O. Moser. 2020. *Is Oligotrophy an Equalizing Factor Driving Microplankton Species Functional Diversity Within Agulhas Rings?* Frontiers in Marine Science 7 (December): 1–16. doi:10.3389/fmars.2020.599185. (see p. 92).

Chacoff, N. P., D. P. Vázquez, S. B. Lomáscolo, E. L. Stevani, J. Dorado, and B. Padrón. 2012. *Evaluating sampling completeness in a desert plant-pollinator network*. Journal of Animal Ecology 81 (1): 190–200. doi:10.1111/j.1365-2656.2011.01883.x. (see p. 90).

Chaitin, G. 1994. *Randomness and complexity in pure mathematics*. International Journal of Bifurcation and Chaos 04 (01): 3–15. doi:10.1142/S0218127494000022. (see p. 97).

Charlesworth, B. 1994. *Evolution in age-structured populations*. Cambridge, UK: Cambridge University Press. (see pp. 163, 165).

Chassot, E., S. Bonhommeau, N. K. Dulvy, F. Mélin, R. Watson, D. Gascuel, and O. Le Pape. 2010. *Global marine primary production constrains fisheries catches*. Ecology Letters 13 (4): 495–505. doi:10.1111/j.1461-0248.2010.01443.x. (see pp. 64, 87).

Chen, N., K. Yu, R. Jia, J. Teng, and C. Zhao. 2020. *Biocrust as one of multiple stable states in global drylands*. Science Advances 6 (39): eaay3763. doi:10.1126/sciadv.aay3763. (see p. 120).

CHEN, R., J. S. LIU, and R. S. TSAY. 1995. *Additivity tests for nonlinear autoregression*. Biometrika 82 (2): 369–383. doi:10.1093/biomet/82.2.369. (see p. 178).

Chen, Z.-Q., D. A. Harper, S. Grasby, and L. Zhang. 2022. *Catastrophic event sequences across the Permian-Triassic boundary in the ocean and on land*. Global and Planetary Change 215:103890. doi:10.1016/j.gloplacha.2022.103890. (see p. 121).

Chesson, P. 2000. *Mechanisms of Maintenance of Species Diversity*. Annual Review of Ecology and Systematics 31:343–66. doi:10.1146/annurev.ecolsys.31.1.343. (see p. 84).

———. 2017. *AEDT: A new concept for ecological dynamics in the ever-changing world*. Edited by M. Loreau. PLOS Biology 15 (5): e2002634. doi:10.1371/journal.pbio.2002634. (see p. 37).

———. 2019. *Contributions to nonstationary community theory*. Journal of Biological Dynamics 13 (sup1): 123–150. doi:10.1080/17513758.2018.1526977. (see p. 192).

Chesson, P., S. Pacala, and C. Neuhauser. 2001. *Environmental niches and ecosystem functioning*. In The Functional Consequences of Biodiversity, edited by A. Kinzig, S. Pacala, and D. Tilman, 2:213–245. 4. Princeton, NJ.: Princeton University Press. (see pp. 76, 84, 85).

Chis, O. T., A. F. Villaverde, J. R. Banga, and E. Balsa-Canto. 2016. *On the relationship between sloppiness and identifiability*. Mathematical Biosciences 282:147–161. doi:10.1016/j.mbs.2016.10.009. (see pp. 99, 102).

Christensen, T. K., and A. D. Fox. 2014. *Changes in age and sex ratios amongst samples of hunter-shot wings from common duck species in Denmark 1982–2010*. European Journal of Wildlife Research 60 (2): 303–312. doi:10.1007/s10344-013-0787-7. (see p. 135).

Church, J. A., N. J. White, and J. M. Arblaster. 2005. *Significant decadal-scale impact of volcanic eruptions on sea level and ocean heat content*. Nature 438 (7064): 74–77. doi:10.1038/nature04237. (see pp. 121, 134).

Chust, G., X. Irigoien, J. Chave, and R. P. Harris. 2013. *Latitudinal phytoplankton distribution and the neutral theory of biodiversity*. Global Ecology and Biogeography 22 (5): 531–543. doi:10.1111/geb.12016. (see pp. 66, 83, 84, 85).

Clark, J. S. 2007. *Models for Ecological Data.* Princeton, NJ.: Princeton University Press. (see pp. 58, 72, 74, 94).

Clark, J. S., and O. N. Bjørnstad. 2004. *Population time series: Process variability, observation errors, missing values, lags, and hidden states*. Ecology 85 (11): 3140–3150. doi:10.1890/03-0520. (see pp. 70, 71, 94).

Clark, J. S., M. Dietze, S. Chakraborty, P. K. Agarwal, I. Ibanez, S. LaDeau, and M. Wolosin. 2007. *Resolving the biodiversity paradox*. Ecology Letters 10 (8): 647–662. doi:10.1111/j.1461-0248.2007.01041.x. (see p. 57).

Clark, T. J., and A. D. Luis. 2020. *Nonlinear population dynamics are ubiquitous in animals*. Nature Ecology & Evolution 4 (1): 75–81. doi:10.1038/s41559-019-1052-6. (see p. 25).

Clausen, K. K., J. Madsen, F. Cottaar, E. Kuijken, and C. Verscheure. 2018. *Highly dynamic wintering strategies in migratory geese: Coping with environmental change*. Global Change Biology 24 (7): 3214–3225. doi:10.1111/gcb.14061. (see pp. 136, 137).

Clausen, K. K., and J. Madsen. 2016. *Philopatry in a changing world: response of pink-footed geese Anser brachyrhynchus to the loss of a key autumn staging area due to restoration of Filsø Lake, Denmark*. Journal of Ornithology 157 (1): 229–237. doi:10.1007/s10336-015-1271-9. (see pp. 136, 137).

Clayton, S., S. Dutkiewicz, O. Jahn, and M. J. Follows. 2013. *Dispersal, eddies, and the diversity of marine phytoplankton*. Limnology & Oceanography: Fluids & Environments 3:182–197. doi:10.1215/21573689-2373515. (see p. 83).

Clements, C. F., and A. Ozgul. 2018. *Indicators of transitions in biological systems*. Edited by J. Metcalf. Ecology Letters 21 (6): 905–919. doi:10.1111/ele.12948. (see p. 120).

Cobb, L., and B. Watson. 1980. *Statistical catastrophe theory: An overview*. Mathematical Modelling 1 (4): 311–317. doi:10.1016/0270-0255(80)90041-X. (see pp. 122, 126, 127).

Cobb, L., and S. Zacks. 1985. *Applications of Catastrophe Theory for Statistical Modeling in the Biosciences*. Journal of the American Statistical Association 80 (392): 793–802. doi:10.1080/01621459.1985.10478184. (see pp. 126, 127).

Cole, D. J. 2020. *Parameter Redundancy and Identifiability*. Boca Raton : CRC Press, [2020]: Chapman / Hall/CRC. doi:10.1201/9781315120003. (see pp. 99, 102).

Conley, C. 1978. *Isolated Invariant Sets and the Morse Index*. Conference Board of the Mathematical Sciences Series No. 38. (see p. 193).

Constantinescu, R., A. Hopulele-Gligor, C. B. Connor, C. Bonadonna, L. J. Connor, J. M. Lindsay, S. Charbonnier, and A. C. M. Volentik. 2021. *The radius of the umbrella cloud helps characterize large explosive volcanic eruptions*. Communications Earth & Environment 2 (1): 3. doi:10.1038/s43247-020-00078-3. (see p. 123).

Cortés-Avizanda, A., R. Jovani, M. Carrete, and J. A. Donázar. 2012. *Resource unpredictability promotes species diversity and coexistence in an avian scavenger guild: a field experiment*. Ecology 93 (12): 2570–2579. doi:10.1890/12-0221.1. (see pp. 143, 144).

Cortés-Avizanda, A., G. Blanco, T. L. DeVault, A. Markandya, M. Z. Virani, J. Brandt, and J. A. Donázar. 2016. *Supplementary feeding and endangered avian scavengers: benefits, caveats, and controversies*. Frontiers in Ecology and the Environment 14 (4): 191–199. doi:10.1002/fee.1257. (see pp. 142, 154).

Cortés-Avizanda, A., J. A. Donázar, and H. M. Pereira. 2015. *Top Scavengers in a Wilder Europe*. In Rewilding European Landscapes, 85–106. Cham: Springer International Publishing. doi:10.1007/978-3-319-12039-3{_}5. (see p. 143).

Coulson, J. C. 2016. *A Review of Philopatry in Seabirds and Comparisons with Other Waterbird Species*. Waterbirds 39 (3): 229–240. doi:10.1675/063.039.0302. (see p. 136).

Coulson, T., J. Lindström, and P. Cotgreave. 2002. *Seeking New Recruits*. Science 295 (5562): 2023–2024. doi:10.1126/science.1070514. (see p. 162).

Cowie, R. H., P. Bouchet, and B. Fontaine. 2022. *The Sixth Mass Extinction: fact, fiction or speculation?* Biological Reviews 97 (2): 640–663. doi:10.1111/brv.12816. (see p. 62).

Crisafulli, C. M., F. J. Swanson, J. J. Halvorson, and B. D. Clarkson. 2015. *Volcano Ecology*. In The Encyclopedia of Volcanoes, Second Edi, 1265–1284. Elsevier. doi:10.1016/B978-0-12-385938-9.00073-0. (see p. 121).

Crone, E. E. 2001. *IS SURVIVORSHIP A BETTER FITNESS SURROGATE THAN FECUNDITY?* Evolution 55 (12): 2611–2614. doi:10.1111/j.0014-3820.2001.tb00773.x. (see p. 174).

Crosweller, H. S., B. Arora, S. K. Brown, E. Cottrell, N. I. Deligne, N. O. Guerrero, L. Hobbs, et al. 2012. *Global database on large magnitude explosive volcanic eruptions (LaMEVE)*. Journal of Applied Volcanology 1 (1): 4. doi:10.1186/2191-5040-1-4. (see p. 123).

Cuddington, K. M., and P. Yodzis. 1999. *Black noise and population persistence*. Proceedings of the Royal Society B: Biological Sciences 266 (1422): 969. doi:10.1098/rspb.1999.0731. (see p. 173).

Cushing, J. M., R. F. Costantino, B. Dennis, R. A. Desharnais, and S. M. Henson. 2003. *Chaos in Ecology. Experimental Nonlinear Dynamics*. San Diego, CA: Academic Press. (see p. 28).

Dai, L., D. Vorselen, K. S. Korolev, and J. Gore. 2012. *Generic Indicators for Loss of Resilience Before a Tipping Point Leading to Population Collapse*. Science 336 (6085): 1175–1177. doi:10.1126/science.1219805. (see p. 25).

Dakos, V., B. Matthews, A. P. Hendry, J. Levine, N. Loeuille, J. Norberg, P. Nosil, M. Scheffer, and L. De Meester. 2019. *Ecosystem tipping points in an evolving world*. Nature Ecology & Evolution 3 (3): 355–362. doi:10.1038/s41559-019-0797-2. (see pp. 120, 126).

Danovaro, R., C. Gambi, A. Dell'Anno, C. Corinaldesi, S. Fraschetti, A. Vanreusel, M. Vincx, and A. J. Gooday. 2008. *Exponential Decline of Deep-Sea Ecosystem Functioning Linked to Benthic Biodiversity Loss*. Current Biology 18 (1): 1–8. doi:10.1016/j.cub.2007.11.056. (see p. 64).

Davis, J. B., M. Guillemain, R. M. Kaminski, C. Arzel, J. M. Eadie, and E. C. Rees. 2014. *Habitat and resource use by waterfowl in the northern hemisphere in autumn and winter*. Wildfowl, no. 4: 17–69. (see p. 136).

DeBaggis, H. F. 1953. *III. Dynamical Systems with Stable Structures*. In Contributions to the Theory of Nonlinear Oscillations (AM-29), Volume II, 37–60. Princeton University Press. doi:10.1515/9781400882700-004. (see pp. 29, 45).

Del Moral, J. C., and B. Molina. 2018. *El buitre leonado en España, población reproductora en 2018 y método de censo*. Madrid: SEO/BirdLife. doi:10.31170/0066. (see p. 144).

DeLong, J. P., V. E. Forbes, N. Galic, J. P. Gibert, R. G. Laport, J. S. Phillips, and J. M. Vavra. 2016. *How fast is fast? Eco-evolutionary dynamics and rates of change in populations and phenotypes*. Ecology and Evolution 6 (2): 573–581. doi:10.1002/ece3.1899. (see p. 37).

Demarcq, H., G. Reygondeau, S. Alvain, and V. Vantrepotte. 2012. *Monitoring marine phytoplankton seasonality from space*. Remote Sensing of Environment 117:211–222. doi:10.1016/j.rse.2011.09.019. (see p. 75).

Dennis, B., R. A. Desharnais, J. M. Cushing, S. M. Henson, and R. F. Costantino. 2003. *Can noise induce chaos?* Oikos 102 (2): 329–339. doi:10.1034/j.1600-0706.2003.12387.x. (see pp. 166, 184).

Dennis, B., P. L. Munholland, and J. M. Scott. 1991. *Estimation of Growth and Extinction Parameters for Endangered Species*. Ecological Monographs 61 (2): 115–143. doi:10.2307/1943004. (see pp. 167, 168, 183).

Denwood, M. J. 2016. *runjags : An R Package Providing Interface Utilities, Model Templates, Parallel Computing Methods and Additional Distributions for MCMC Models in JAGS*. Journal of Statistical Software 71 (9). doi:10.18637/jss.v071.i09. (see pp. 103, 149).

DeVault, T. L., J. C. Beasley, Z. H. Olson, M. Moleón, M. Carrete, A. Margalida, and J. A. Sánchez-Zapata. 2016. *Ecosystem Services Provided by Avian Scavengers*. Chap. 8 in Why Birds Matter, edited by C. H. Sekercioglu, D. G. Wenny, and C. J. Whelan, 235–270. Chicago, ILL.: University of Chicago Press. doi:10.7208/chicago/9780226382777.003.0008. (see p. 143).

DeVault, T. L., O. E. Rhodes Jr., and J. A. Shivik. 2003. *Scavenging by vertebrates: behavioral, ecological, and evolutionary perspectives on an important energy transfer pathway in terrestrial ecosystems*. Oikos 102 (2): 225–234. doi:10.1034/j.1600-0706.2003.12378.x. (see p. 157).

Deyle, E. R., R. M. May, S. B. Munch, and G. Sugihara. 2016. *Tracking and forecasting ecosystem interactions in real time*. Proceedings of the Royal Society B: Biological Sciences 283 (1822): 20152258. doi:10.1098/rspb.2015.2258. (see pp. 110, 111).

Dirzo, R., and P. H. Raven. 2003. *Global state of biodiversity and loss*. Annual Review of Environment and Resources 28 (1): 137–167. doi:10.1146/annurev.energy.28.050302.105532. (see p. 62).

Doak, D. F., W. F. Morris, C. Pfister, B. E. Kendall, and E. M. Bruna. 2005. *Correctly Estimating How Environmental Stochasticity Influences Fitness and Population Growth*. The American Naturalist 166 (1): E14–E21. doi:10.1086/430642. (see p. 143).

Dobson, A. J., and A. G. Barnett. 2018. *Generalized Linear Models*. Boca Raton, FL: CRC Press. (see p. 165).

Doherty, P. F., G. Sorci, J. A. Royle, J. E. Hines, J. D. Nichols, and T. Boulinier. 2003. *Sexual selection affects local extinction and turnover in bird communities*. Proceedings of the National Academy of Sciences 100 (10): 5858–5862. doi:10.1073/pnas.0836953100. (see pp. 165, 172, 177).

Dolan, J. R., and M. T. PÉrez. 2000. *Costs, benefits and characteristics of mixotrophy in marine oligotrichs*. Freshwater Biology 45 (2): 227–238. doi:10.1046/j.1365-2427.2000.00659.x. (see p. 110).

Donazar, J. A. 1993. *Los buitres ibéricos. Biología y conservación.* Madrid: J.M. Reyero. (see pp. 142, 155, 156).

Donázar, J. A., A. Cortés-Avizanda, O. Ceballos, E. Arrondo, J. M. Grande, and D. Serrano. 2020. *Epizootics and sanitary regulations drive long-term changes in fledgling body condition of a threatened vulture*. Ecological Indicators 113 (February): 106188. doi:10.1016/j.ecolind.2020.106188. (see p. 154).

Donázar, J. A., A. Margalida, and D. Campión. 2009. *Vultures, feeding stations and sanitary legislation: a conflict and its consequences from the perspective of conservation biology.* San Sebastián: Society of Sciences Aranzadi. (see pp. 143, 144, 154, 155, 156).

Donázar, J. A., A. Cortés-Avizanda, and M. Carrete. 2010. *Dietary shifts in two vultures after the demise of supplementary feeding stations: consequences of the EU sanitary legislation*. European Journal of Wildlife Research 56 (4): 613–621. doi:10.1007/s10344-009-0358-0. (see pp. 154, 155).

Donohue, I., H. Hillebrand, J. M. Montoya, O. L. Petchey, S. L. Pimm, M. S. Fowler, K. Healy, et al. 2016. *Navigating the complexity of ecological stability*. Edited by F. Adler. Ecology Letters 19 (9): 1172–1185. doi:10.1111/ele.12648. (see pp. 51, 71).

Donohue, I., O. L. Petchey, J. M. Montoya, A. L. Jackson, L. McNally, M. Viana, K. Healy, M. Lurgi, N. E. O'Connor, and M. C. Emmerson. 2013. *On the dimensionality of ecological stability*. Edited by M. Gessner. Ecology Letters 16 (4): 421–429. doi:10.1111/ele.12086. (see p. 71).

Dougall, T. W., P. K. Holland, a. Mee, and D. W. Yalden. 2005. *Comparative population dynamics of Common Sandpipers Actitis hypoleucos: living at the edge*. Bird Study 52:80–87. (see pp. 164, 165, 173, 174, 175).

Douglass, D. H., and R. S. Knox. 2005. *Climate forcing by the volcanic eruption of Mount Pinatubo*. Geophysical Research Letters 32 (5): 1–5. doi:10.1029/2004GL022119. (see pp. 121, 134).

Drótos, G., T. Bódai, and T. Tél. 2016. *Quantifying nonergodicity in nonautonomous dissipative dynamical systems: An application to climate change*. Physical Review E 94 (2): 022214. doi:10.1103/PhysRevE.94.022214. (see p. 192).

Dunne, J. W. 1927. *An experiment with time*. London: Faber & Faber Ltd. (see p. 27).

Dunne, J. A., R. J. Williams, and N. D. Martinez. 2002. *Food-web structure and network theory: The role of connectance and size*. Proceedings of the National Academy of Sciences of the USA 99 (20): 12917–12922. doi:10.1073/pnas.192407699. (see p. 108).

Durant, J. M., T. Anker-Nilssen, D. Ø. Hjermann, and N. C. Stenseth. 2004. *Regime shifts in the breeding of an Atlantic puffin population*. Ecology Letters 7 (5): 388–394. doi:10.1111/j.1461-0248.2004.00588.x. (see p. 132).

Durbin, J., and S. J. Koopman. 2001. *Time Series Analysis by State Space Methods*. Oxford, UK: Oxford University Press. (see pp. 55, 71, 94).

Duriez, O., B. Eliotout, and F. Sarrazin. 2011. *Age identification of Eurasian Griffon Vultures Gyps fulvus in the field*. Ringing & Migration 26 (1): 24–30. doi:10.1080/03078698.2011.585912. (see p. 145).

Edwards, K. F. 2019. *Mixotrophy in nanoflagellates across environmental gradients in the ocean*. Proceedings of the National Academy of Sciences: 201814860. doi:10.1073/pnas.1814860116. (see p. 110).

Eilers, P. H. C., and B. D. Marx. 1996. *Flexible smoothing with B-splines and penalties*. Statistical Science 11 (2): 89–102. doi:10.1214/ss/1038425655. (see p. 124).

Elaydi, S. N. 2005. *An Introduction to Difference Equations*. Berlin, Heidelberg: Springer. (see pp. 71, 96, 125).

Ellegaard, M., and S. Ribeiro. 2018. *The long-term persistence of phytoplankton resting stages in aquatic 'seed banks'*. Biological Reviews 93 (1): 166–183. doi:10.1111/brv.12338. (see p. 85).

Elosegui, I. 1989. *Vautour fauve (Gyps fulvus), Gypaete barbu (Gypaetus barbatus), Percnoptere d'Egypte (Neophron percnopterus): Synthse bibliographique et recherches.* Acta Biol. Mont. 3. (see p. 145).

Enke, T. N., G. E. Leventhal, M. Metzger, J. T. Saavedra, and O. X. Cordero. 2018. *Microscale ecology regulates particulate organic matter turnover in model marine microbial communities*. Nature Communications 9 (1): 2743. doi:10.1038/s41467-018-05159-8. (see p. 110).

Esteban, F. J., J. A. Galadí, J. A. Langa, J. R. Portillo, and F. Soler-Toscano. 2018. *Informational structures: A dynamical system approach for integrated information*. Edited by V. K. Jirsa. PLOS Computational Biology 14 (9): e1006154. doi:10.1371/journal.pcbi.1006154. (see p. 193).

Fagan, Meir, Prendergast, Folarin, and Karieva. 2001. *Characterizing population vulnerability for 758 species*. Ecology Letters 4 (2): 132–138. doi:10.1046/j.1461-0248.2001.00206.x. (see p. 172).

Falkowski, P. G., R. T. Barber, and V. Smetacek. 1998. *Biogeochemical controls and feedbacks on ocean primary production*. Science 281:200–206. doi:10.1126/science.281.5374.200. (see pp. 64, 86).

Fargallo, J. A., F. Martínez, K. Wakamatsu, D. Serrano, and G. Blanco. 2018. *Sex-Dependent Expression and Fitness Consequences of Sunlight-Derived Color Phenotypes*. The American Naturalist 191 (6): 726–743. doi:10.1086/697218. (see pp. 145, 156).

Feng, J., J. M. Durant, L. C. Stige, D. O. Hessen, D. Ø. Hjermann, L. Zhu, M. Llope, and N. C. Stenseth. 2015. *Contrasting correlation patterns between environmental factors and chlorophyll levels in the global ocean*. Global Biogeochemical Cycles 29 (12): 2095–2107. doi:10.1002/2015GB005216. (see pp. 65, 86).

Fernández y Fernández-Arroyo, F. J. 1996. *Sobre Los Censos Realizados En El Refugio De Rapaces De Montejo (1975–1994)*. In Biología y Conservacion De Las Rapaces Mediterráneas, edited by J. M. J. Muntaner, 317–321. Madrid: SEO/BirdLife. (see p. 145).

Fernández-Bellon, D., A. Cortés-Avizanda, R. Arenas, and J. A. Donázar. 2016. *Density-dependent productivity in a colonial vulture at two spatial scales*. Ecology 97 (2): 406–416. doi:10.1890/15-0357.1. (see p. 157).

Fernández-Marín, X. 2016. *ggmcmc : Analysis of MCMC Samples and Bayesian Inference*. Journal of Statistical Software 70 (9). doi:10.18637/jss.v070.i09. (see pp. 103, 149).

Ferriere, R., and M. Gatto. 1995. *Lyapunov Exponents and the Mathematics of Invasion in Oscillatory or Chaotic Populations*. Theoretical Population Biology 48 (2): 126–171. doi:10.1006/tpbi.1995.1024. (see p. 168).

Field, C. B. 1998. *Primary Production of the Biosphere: Integrating Terrestrial and Oceanic Components*. Science 281 (5374): 237–240. doi:10.1126/science.281.5374.237. (see p. 86).

Flombaum, P., J. L. Gallegos, R. A. Gordillo, J. Rincón, L. L. Zabala, N. Jiao, D. M. Karl, et al. 2013. *Present and future global distributions of the marine Cyanobacteria Prochlorococcus and Synechococcus*. Proceedings of the National Academy of Sciences 110 (24): 9824–9829. doi:10.1073/pnas.1307701110. (see pp. 66, 84, 86, 191).

Flombaum, P., and A. C. Martiny. 2021. *Diverse but uncertain responses of picophytoplankton lineages to future climate change*. Limnology and Oceanography 66 (12): 4171–4181. doi:10.1002/lno.11951. (see p. 66).

Flombaum, P., W.-L. Wang, F. W. Primeau, and A. C. Martiny. 2020. *Global picophytoplankton niche partitioning predicts overall positive response to ocean warming*. Nature Geoscience 13 (2): 116–120. doi:10.1038/s41561-019-0524-2. (see p. 66).

Flynn, K. J., D. K. Stoecker, A. Mitra, J. A. Raven, P. M. Glibert, P. J. Hansen, E. Granéli, and J. M. Burkholder. 2013. *Misuse of the phytoplankton–zooplankton dichotomy: the need to assign organisms as mixotrophs within plankton functional types*. Journal of Plankton Research 35 (1): 3–11. doi:10.1093/plankt/fbs062. (see p. 91).

Folke, C., S. Carpenter, B. Walker, M. Scheffer, T. Elmqvist, L. Gunderson, and C. Holling. 2004. *Regime Shifts, Resilience, and Biodiversity in Ecosystem Management*. Annual Review of Ecology, Evolution, and Systematics 35 (1): 557–581. doi:10.1146/annurev.ecolsys.35.021103.105711. (see p. 138).

Follett, C. L., S. Dutkiewicz, F. Ribalet, E. Zakem, D. Caron, E. V. Armbrust, and M. J. Follows. 2022. *Trophic interactions with heterotrophic bacteria limit the range of Prochlorococcus*. Proceedings of the National Academy of Sciences 119 (2): e2110993118. doi:10.1073/pnas.2110993118. (see p. 84).

Fragoso, T. M., W. Bertoli, and F. Louzada. 2018. *Bayesian Model Averaging: A Systematic Review and Conceptual Classification*. International Statistical Review 86 (1): 1–28. doi:10.1111/insr.12243. (see p. 101).

Fraser, A. M. 2008. *Hidden Markov Models and Dynamical Systems*. 145. Society for Industrial / Applied Mathematics. doi:10.1137/1.9780898717747. (see p. 124).

Freedman, H. I., and P. Waltman. 1977. *Mathematical analysis of some three-species food-chain models*. Mathematical Biosciences 33 (3-4): 257–276. doi:10.1016/0025-5564(77)90142-0. (see p. 53).

Fretwell, S. D. 1972. *Populations in a seasonal environment*. Princeton, NJ.: Princeton University Press. (see pp. 23, 28).

Fukami, T., and M. Nakajima. 2011. *Community assembly: alternative stable states or alternative transient states?* Ecology Letters 14 (10): 973–984. doi:10.1111/j.1461-0248.2011.01663.x. (see p. 120).

Fuller, R. A., P. H. Warren, P. R. Armsworth, O. Barbosa, and K. J. Gaston. 2008. *Garden bird feeding predicts the structure of urban avian assemblages*. Diversity and Distributions 14 (1): 131–137. doi:10.1111/j.1472-4642.2007.00439.x. (see p. 142).

Gaillard, J.-M., and N. G. Yoccoz. 2003. *TEMPORAL VARIATION IN SURVIVAL OF MAMMALS: A CASE OF ENVIRONMENTAL CANALIZATION?* Ecology 84 (12): 3294–3306. doi:10.1890/02-0409. (see pp. 143, 162, 163, 174).

Gallinat, A. S., R. B. Primack, and D. L. Wagner. 2015. *Autumn, the neglected season in climate change research*. Trends in Ecology & Evolution 30 (3): 169–176. doi:10.1016/j.tree.2015.01.004. (see p. 192).

Ganter, B., and H. Boyd. 2000. *A tropical volcano, high predation pressure, and the breeding biology of Arctic waterbirds: A circumpolar review of breeding failure in the summer of 1992*. Arctic 53 (3): 289–305. doi:10.14430/arctic859. (see p. 135).

García-Callejas, D., R. Molowny-Horas, and M. B. Araújo. 2018. *Multiple interactions networks: towards more realistic descriptions of the web of life*. Oikos 127 (1): 5–22. doi:10.1111/oik.04428. (see p. 91).

Gaston, A. J., K. Woo, and J. M. Hipfner. 2003. *Trends in Forage Fish Populations in Northern Hudson Bay since 1981, as Determined from the Diet of Nestling Thick-billed Murres, ¡i¿Uria lomvia¡/i¿*. ARCTIC 56 (3): 227–233. doi:10.14430/arctic618. (see p. 134).

Gelfand, A. E., and A. F. M. Smith. 1990. *Sampling-Based Approaches to Calculating Marginal Densities*. Journal of the American Statistical Association 85 (410): 398. doi:10.2307/2289776. (see p. 74).

Gelman, A., J. B. Carlin, H. S. Stern, D. B. Dunson, A. Vehtari, and D. B. Rubin. 2014. *Bayesian Data Analysis*. 3rd. Chapman & Hall/CRC Press. doi:10.1007/s13398-014-0173-7.2. (see pp. 149, 150).

———. 2020. *Bayesian Data Analysis*. Chapman / Hall/CRC. (see pp. 72, 73, 74, 75, 99, 100, 102, 103).

Genin, A., B. Lazar, and S. Brenner. 1995. *Vertical mixing and coral death in the red sea following the eruption of Mount Pinatubo*. doi:10.1038/377507a0. (see pp. 121, 134).

George, E. I., and R. E. McCulloch. 1993. *Variable Selection via Gibbs Sampling*. Journal of the American Statistical Association 88 (423): 881–889. doi:10.1080/01621459.1993.10476353. (see pp. 100, 101, 149).

———. 1997. *Approaches for bayesian variable selection*. Statistica Sinica 7 (2): 339–373. (see p. 101).

Gerhard, M., C. Mori, and M. Striebel. 2021. *Nonrandom species loss in phytoplankton communities and its effect on ecosystem functioning*. Limnology and Oceanography 66 (3): 779–792. doi:10.1002/lno.11642. (see p. 107).

Geweke, J., and H. Tanizaki. 2001. *Bayesian estimation of state-space models using the Metropolis-Hastings algorithm within Gibbs sampling*. Computational Statistics and Data Analysis 37 (2): 151–170. doi:10.1016/S0167-9473(01)00009-3. (see p. 74).

Giere, R. N. 2006. *Scientific perspectivism*. Chicago, ILL.: The University of Chicago Press. (see p. 28).

Gill, J. A., K. Norris, P. M. Potts, T. G. Gunnarsson, P. W. Atkinson, and W. J. Sutherland. 2001. *The buffer effect and large-scale population regulation in migratory birds*. Nature 412 (6845): 436–438. doi:10.1038/35086568. (see pp. 173, 174).

Gillespie, J. H. 1977. *Natural Selection for Variances in Offspring Numbers: A New Evolutionary Principle*. The American Naturalist 111 (981): 1010–1014. doi:10.1086/283230. (see p. 162).

Gilljam, D. 2016. *Structure and Stability of Ecological Networks : The role of dynamic dimensionality and species variability in resource use*. 1735. Linköping University Electronic Press. doi:10.3384/diss.diva-123970. (see p. 97).

Gilpin, M. E. 1973. *Do Hares Eat Lynx?* The American Naturalist 107 (957): 727–730. doi:10.1086/282870. (see p. 166).

———. 1974. *A Liapunov function for competition communities*. Journal of Theoretical Biology 44 (1): 35–48. doi:10.1016/S0022-5193(74)80028-7. (see p. 37).

Godoy, O., I. Bartomeus, R. P. Rohr, and S. Saavedra. 2018. *Towards the Integration of Niche and Network Theories*. Trends in Ecology & Evolution 33 (4): 287–300. doi:10.1016/j.tree.2018.01.007. (see p. 91).

Godoy, O., L. Gómez-Aparicio, L. Matías, I. M. Pérez-Ramos, and E. Allan. 2020. *An excess of niche differences maximizes ecosystem functioning*. Nature Communications 11 (1): 4180. doi:10.1038/s41467-020-17960-5. (see p. 90).

Godoy, O., and J. M. Levine. 2014. *Phenology effects on invasion success: insights from coupling field experiments to coexistence theory*. Ecology 95 (3): 726–736. doi:10.1890/13-1157.1. (see p. 90).

Goh, B. S. 1977. *Global Stability in Many-Species Systems*. The American Naturalist 111 (977): 135–143. doi:10.2307/2678832. (see pp. 37, 54).

Goss-Custard, J., R. Stillman, A. West, R. Caldow, and S. McGrorty. 2002. *Carrying capacity in overwintering migratory birds*. Biological Conservation 105 (1): 27–41. doi:10.1016/S0006-3207(01)00175-6. (see p. 182).

Gould, S. J. 1970. *Dollo on Dollo's law: Irreversibility and the status of evolutionary laws*. Journal of the History of Biology 3 (2): 189–212. doi:10.1007/BF00137351. (see pp. 26, 27).

Grace, J. B., and K. M. Irvine. 2020. *Scientist's guide to developing explanatory statistical models using causal analysis principles*. Ecology, no. October: 0–2. doi:10.1002/ecy.2962. (see p. 75).

Grafen, A. 1999. *Formal Darwinism, the individual–as–maximizing–agent analogy and bet–hedging*. Proceedings of the Royal Society of London. Series B: Biological Sciences 266 (1421): 799–803. doi:10.1098/rspb.1999.0708. (see p. 163).

Grasman, R. P. P. P., H. L. J. v. d. Maas, and E.-J. Wagenmakers. 2009. *Fitting the Cusp Catastrophe in R : A cusp Package Primer*. Journal of Statistical Software 32 (8). doi:10.18637/jss.v032.i08. (see pp. 122, 126, 127, 128, 137).

Green, A. J., P. Alcorlo, E. T. Peeters, E. P. Morris, J. L. Espinar, M. A. Bravo-Utrera, J. Bustamante, et al. 2017. *Creating a safe operating space for wetlands in a changing climate*. Frontiers in Ecology and the Environment 15 (2): 99–107. doi:10.1002/fee.1459. (see pp. 121, 122, 135).

Green, R. E., M. A. Taggart, D. Das, D. J. Pain, C. Sashi Kumar, A. A. Cunningham, and R. Cuthbert. 2006. *Collapse of Asian vulture populations: risk of mortality from residues of the veterinary drug diclofenac in carcasses of treated cattle*. Journal of Applied Ecology 43 (5): 949–956. doi:10.1111/j.1365-2664.2006.01225.x. (see p. 157).

Green, T., P. R. Renne, and C. B. Keller. 2022. *Continental flood basalts drive Phanerozoic extinctions*. Proceedings of the National Academy of Sciences 119 (38): 1–9. doi:10.1073/pnas.2120441119. (see p. 121).

Griffiths, J. R., S. Hajdu, A. S. Downing, O. Hjerne, U. Larsson, and M. Winder. 2016. *Phytoplankton community interactions and environmental sensitivity in coastal and offshore habitats*. Oikos 125:1134–1143. doi:10.1111/oik.02405. (see p. 110).

Grønning, J., and T. Kiørboe. 2020. *Diatom defence: Grazer induction and cost of shell-thickening*. Edited by J. Cooke. Functional Ecology 34 (9): 1790–1801. doi:10.1111/1365-2435.13635. (see p. 110).

Gross, K., B. A. Craig, and W. D. Hutchinson. 2002. *Bayesian estimation of a demographic matrix model from stage- frequency data*. Ecology 83 (12): 3285–3298. doi:10.1890/0012-9658(2002)083[3285:BEOADM]2.0.CO;2. (see pp. 146, 155).

Gsell, A. S., U. Scharfenberger, D. Özkundakci, A. Walters, L.-A. Hansson, A. B. G. Janssen, P. Nõges, et al. 2016. *Evaluating early-warning indicators of critical transitions in natural aquatic ecosystems*. Proceedings of the National Academy of Sciences 113 (50): 201608242. doi:10.1073/pnas.1608242113. (see p. 120).

Gu, L., D. D. Baldocchi, S. C. Wofsy, J. William Munger, J. J. Michalsky, S. P. Urbanski, and T. A. Boden. 2003. *Response of a deciduous forest to the Mount Pinatubo eruption: Enhanced photosynthesis*. Science 299 (5615): 2035–2038. doi:10.1126/science.1078366. (see p. 121).

Gu, R., and Y. Shao. 2016. *How long the singular value decomposed entropy predicts the stock market?-Evidence from the Dow Jones Industrial Average Index*. Physica A: Statistical Mechanics and its Applications 453:150–161. doi:10.1016/j.physa.2016.02.030. (see p. 97).

Guillemain, M., N. Sadoul, and G. Simon. 2005. *European flyway permeability and abmigration in Teal Anas crecca, an analysis based on ringing recoveries*. Ibis 147 (4): 688–696. doi:10.1111/j.1474-919X.2005.00446.x. (see pp. 136, 137).

Guimarães, P. R. 2020. *The Structure of Ecological Networks Across Levels of Organization*. Annual Review of Ecology, Evolution, and Systematics 51 (1): 433–460. doi:10.1146/annurev-ecolsys-012220-120819. (see p. 25).

Gutenkunst, R. N., J. J. Waterfall, F. P. Casey, K. S. Brown, C. R. Myers, and J. P. Sethna. 2007. *Universally Sloppy Parameter Sensitivities in Systems Biology Models*. Edited by A. P. Arkin. PLoS Computational Biology 3 (10): e189. doi:10.1371/journal.pcbi.0030189. (see p. 102).

Hammouri, H., and S. Othman. 1992. *A remark on Lagrange stability of nonlinear systems stabilization.* Applied Mathematics Letters 5 (4): 35–39. (see p. 40).

Hampton, S. E., E. E. Holmes, L. P. Scheef, M. D. Scheuerell, S. L. Katz, D. E. Pendleton, and E. J. Ward. 2013. *Quantifying effects of abiotic and biotic drivers on community dynamics with multivariate autoregressive (MAR) models*. Ecology 94 (12): 2663–2669. doi:10.1890/13-1300.1. (see p. 56).

Hansen, J., A. Lacis, R. Ruedy, and M. Sato. 1992. *Potential climate impact of Mount Pinatubo eruption*. Geophysical Research Letters 19 (2): 215–218. doi:10.1029/91GL02788. (see p. 134).

Hastings, A. 2004. *Transients: the key to long-term ecological understanding?* Trends in Ecology & Evolution 19 (1): 39–45. doi:10.1016/j.tree.2003.09.007. (see pp. 37, 120).

Hastings, A., K. C. Abbott, K. Cuddington, T. Francis, G. Gellner, Y.-C. Lai, A. Morozov, S. Petrovskii, K. Scranton, and M. L. Zeeman. 2018. *Transient phenomena in ecology*. Science 361 (6406): eaat6412. doi:10.1126/science.aat6412. (see pp. 120, 193).

Hastings, A., K. C. Abbott, K. Cuddington, T. B. Francis, Y.-C. Lai, A. Morozov, S. Petrovskii, and M. L. Zeeman. 2021. *Effects of stochasticity on the length and behaviour of ecological transients*. Journal of The Royal Society Interface 18 (180): 20210257. doi:10.1098/rsif.2021.0257. (see p. 138).

He, D., and S. R. Biswas. 2019. *Negative relationship between interspecies spatial association and trait dissimilarity*. Oikos 128 (5): 659–667. doi:10.1111/oik.05876. (see p. 139).

Heino, M., J. Ripa, and V. Kaitala. 2000. *Extinction risk under coloured environmental noise*. Ecography 23 (2): 177–184. doi:10.1111/j.1600-0587.2000.tb00273.x. (see p. 183).

Henson, S. A., B. B. Cael, S. R. Allen, and S. Dutkiewicz. 2021. *Future phytoplankton diversity in a changing climate*. Nature Communications 12 (1): 5372. doi:10.1038/s41467-021-25699-w. (see p. 86).

Hess, S., W. Kuhnt, S. Hill, M. A. Kaminski, A. Holbourn, and M. De Leon. 2001. *Monitoring the recolonization of the Mt Pinatubo 1991 ash layer by benthic foraminifera*. Marine Micropaleontology 43 (1-2): 119–142. doi:10.1016/S0377-8398(01)00025-1. (see p. 134).

Hilborn, R. C. 2000. *Chaos and Nonlinear Dynamics*. Oxford, UK: Oxford University Press. doi:10.1093/acprof:oso/9780198507239.001.0001. (see pp. 165, 166, 167, 173, 178).

Hillebrand, H., I. Donohue, W. S. Harpole, D. Hodapp, M. Kucera, A. M. Lewandowska, J. Merder, J. M. Montoya, and J. A. Freund. 2020. *Thresholds for ecological responses to global change do not emerge from empirical data*. Nature Ecology & Evolution 4 (11): 1502–1509. doi:10.1038/s41559-020-1256-9. (see p. 121).

Hillebrand, H., C.-D. Dürselen, D. Kirschtel, U. Pollingher, and T. Zohary. 1999. *Biovolume Calculation for Pelagic and Benthic Microalgae*. Journal of Phycology 35 (2): 403–424. doi:10.1046/j.1529-8817.1999.3520403.x. (see p. 66).

Hillebrand, H., and B. Matthiessen. 2009. *Biodiversity in a complex world: Consolidation and progress in functional biodiversity research*. Ecology Letters 12 (12): 1405–1419. doi:10.1111/j.1461-0248.2009.01388.x. (see p. 64).

Hirsch, M. W., S. Smale, and R. L. Devaney. 2013. *Differential equations, dynamical systems, and an introduction to chaos*. 3rd Ed. San Diego, CA: Academic Press. (see pp. 34, 35, 36, 56).

Hofbauer, J., and S. J. Schreiber. 2022. *Permanence via invasion graphs: incorporating community assembly into modern coexistence theory*. Journal of Mathematical Biology 85 (5): 54. doi:10.1007/s00285-022-01815-2. (see p. 194).

Hofbauer, J., and K. Sigmund. 1998. *Evolutionary games and population dynamics.* Princeton, NJ.: Princeton University Press. (see pp. 51, 52, 53).

Holling, C. S. 1973. *Resilience and Stability of Ecological Systems*. Annual Review of Ecology and Systematics 4:1–23. doi:10.1146/annurev.es.04.110173.000245. (see p. 120).

———. 1983. *Surprise*. Options 4:16. (see p. 4).

Hooper, D. U., E. C. Adair, B. J. Cardinale, J. E. K. Byrnes, B. A. Hungate, K. L. Matulich, A. Gonzalez, J. E. Duffy, L. Gamfeldt, and M. I. O'Connor. 2012. *A global synthesis reveals biodiversity loss as a major driver of ecosystem change*. Nature 486 (7401): 105–108. doi:10.1038/nature11118. (see p. 62).

Horgan, J. 1995. *From Complexity to Perplexity*. Scientific American 272 (6): 104–109. doi:10.1038/scientificamerican0695-104. (see p. 24).

Horn, R. A., and C. R. Johnson. 2013. *Matrix Analysis*. 2nd Ed. Cambridge, UK: Cambridge University Press. (see p. 58).

Huang, A., and M. P. Wand. 2013. *Simple Marginally Noninformative Prior Distributions for Covariance Matrices*. Bayesian Analysis 8 (2): 439–452. doi:10.1214/13-BA815. (see pp. 73, 99).

Hurley, M. 1995. *Chain recurrence, semiflows, and gradients*. Journal of Dynamics and Differential Equations 7 (3): 437–456. doi:10.1007/BF02219371. (see p. 193).

Inchausti, P., and J. Halley. 2001. *Investigating long-term ecological variability using the Global Population Dynamics Database.* Science 293 (2001): 655–657. doi:10.1126/science.293.5530.655. (see p. 164).

Inchausti, P., and J. Halley. 2003. *On the relation between temporal variability and persistence time in animal populations*. Journal of Animal Ecology 72 (6): 899–908. doi:10.1046/j.1365-2656.2003.00767.x. (see pp. 165, 172).

International Wader Study Group. 2003. *Are waders world-wide in decline? Reviewing the evidence*. Wader Study Group Bulletin 101/102 (December): 1–8. (see pp. 164, 175).

IOCCG. 2009. *Partition of the Ocean into Ecological Provinces: Role of Ocean-Colour Radiometry.* Edited by M. Dowell and T. Platt. Dartmouth, CA: Reports of the International Ocean-Colour Coordinating Group, No. 9, IOCCG. (see p. 68).

———. 2020. *Synergy between Ocean Colour and Biogeochemical/Ecosystem Models*. (see p. 68).

Irigoien, X., J. Huisman, and R. P. Harris. 2004. *Global biodiversity patterns of marine phytoplankton and zooplankton*. Nature 429 (June): 863–867. doi:10.1038/nature02644.1.. (see p. 66).

Irwin, A. J., Z. V. Finkel, F. E. Müller-Karger, and L. Troccoli Ghinaglia. 2015. *Phytoplankton adapt to changing ocean environments*. Proceedings of the National Academy of Sciences 112 (18): 5762–5766. doi:10.1073/pnas.1414752112. (see pp. 86, 108).

Irwin, A. J., and M. J. Oliver. 2009. *Are ocean deserts getting larger?* Geophysical Research Letters 36 (18): 1–5. doi:10.1029/2009GL039883. (see p. 86).

IUCN. 2020. *IUCN Red List 2017-2020 Report*. Technical report. (see p. 176).

Ives, A. R. 1995. *Measuring Resilience in Stochastic Systems.* Ecological Monographs 65 (2): 217–233. (see p. 98).

Ives, A. R., and S. R. Carpenter. 2007. *Stability and Diversity of Ecosystems*. Science 317 (July): 58–62. doi:10.1126/science.1133258. (see pp. 62, 71).

Ives, A. R., B. Dennis, K. Cottingham, and S. Carpenter. 2003. *Estimating community stability and ecological interactions from time-series data*. Ecological Monographs 73 (2): 301–330. doi:10.1890/0012-9615. (see pp. 56, 57, 58, 59, 64, 71, 72, 98).

Ives, A. R., and J. B. Hughes. 2002. *General relationships between species diversity and stability in competitive systems.* The American naturalist 159 (4): 388–395. doi:10.1086/338994. (see p. 64).

Ives, A. R., J. L. Klug, and K. Gross. 2000. *Stability and species richness in complex communities*. Ecology Letters 3 (5): 399–411. doi:10.1046/j.1461-0248.2000.00144.x. (see p. 63).

Jenouvrier, S., C. Barbraud, B. Cazelles, and H. Weimerskirch. 2005. *Modelling population dynamics of seabirds: importance of the effects of climate fluctuations on breeding proportions*. Oikos 108 (3): 511–522. doi:10.1111/j.0030-1299.2005.13351.x. (see p. 163).

Jenouvrier, S., H. Weimerskirch, C. Barbraud, Y. H. Park, and B. Cazelles. 2005. *Evidence of a shift in the cyclicity of Antarctic seabird dynamics linked to climate*. Proceedings of the Royal Society B: Biological Sciences 272 (1566): 887–895. doi:10.1098/rspb.2004.2978. (see p. 132).

Jiang, Q., F. Jourdan, H. K. H. Olierook, R. E. Merle, J. Bourdet, D. Fougerouse, B. Godel, and A. T. Walker. 2022. *Volume and rate of volcanic CO 2 emissions governed the severity of past environmental crises*. Proceedings of the National Academy of Sciences 119 (31): 1–10. doi:10.1073/pnas.2202039119. (see p. 121).

Jochimsen, M. C., R. Kümmerlin, and D. Straile. 2013. *Compensatory dynamics and the stability of phytoplankton biomass during four decades of eutrophication and oligotrophication*. Ecology Letters 16 (1): 81–89. doi:10.1111/ele.12018. (see p. 86).

Jost, C., C. A. Lawrence, F. Campolongo, W. van de Bund, S. Hill, and D. L. DeAngelis. 2004. *The effects of mixotrophy on the stability and dynamics of a simple planktonic food web model*. Theoretical Population Biology 66 (1): 37–51. doi:10.1016/j.tpb.2004.02.001. (see p. 92).

Justus, J. 2008. *Ecological and Lyapunov Stability*. Philosophy of Science 75 (4): 421–436. doi:10.1086/595836. (see p. 37).

———. 2021. *The Philosophy of Ecology*. Cambridge University Press. doi:10.1017/9781139626941. (see p. 28).

Kahane, C. 1972. *Stability of solutions of linear systems with dominant main diagonal.* Proceedings of the American Mathematical Society 33 (1): 69–71. (see p. 40).

Kalita, P., J. A. Langa, and F. Soler-Toscano. 2019. *Informational Structures and Informational Fields as a Prototype for the Description of Postulates of the Integrated Information Theory*. Entropy 21 (5): 493. doi:10.3390/e21050493. (see p. 193).

Kass, R. E., and A. E. Raftery. 1995. *Bayes Factors*. Journal of the American Statistical Association 90 (430): 773–795. doi:10.1080/01621459.1995.10476572. (see pp. 101, 117).

Kéfi, S., V. Miele, E. A. Wieters, S. A. Navarrete, and E. L. Berlow. 2016. *How Structured Is the Entangled Bank? The Surprisingly Simple Organization of Multiplex Ecological Networks Leads to Increased Persistence and Resilience*. PLOS Biology 14 (8): e1002527. doi:10.1371/journal.pbio.1002527. (see p. 25).

Kenyon Ross, R., P. A. Smith, B. Campbell, C. A. Friis, and R. I. Guy Morrison. 2012. *Population Trends of Shorebirds in Southern Ontario, 1974–2009*. Waterbirds 35 (1): 15–24. doi:10.1675/063.035.0102. (see p. 164).

Kerner, E. H. 1959. *Further considerations on the statistical mechanics of biological associations*. The Bulletin of Mathematical Biophysics 21 (2): 217–255. doi:10.1007/BF02476361. (see p. 24).

———. 1962. *Gibbs Ensemble and Biological Ensemble*. Annals of the New York Academy of Sciences 96 (4): 975–984. doi:10.1111/j.1749-6632.1962.tb54115.x. (see p. 24).

Khodri, M., T. Izumo, J. Vialard, S. Janicot, C. Cassou, M. Lengaigne, J. Mignot, et al. 2017. *Tropical explosive volcanic eruptions can trigger El Niño by cooling tropical Africa*. Nature Communications 8 (1): 778. doi:10.1038/s41467-017-00755-6. (see p. 121).

King, R., B. J. T. Morgan, O. Gimenez, and S. P. Brooks. 2010. *Bayesian analysis for population ecology*. Boca Raton, FL: Chapman & Hall/CRC Press. (see pp. 55, 58, 69, 145, 148).

Kingsland, S. E. 1995. *Modeling Nature: Episodes in the History of Population Ecology*. Chicago, ILL.: The University of Chicago Press. (see pp. 28, 187).

Knowlton, N. 2004. *Multiple "stable" states and the conservation of marine ecosystems*. Progress in Oceanography 60 (2-4): 387–396. doi:10.1016/j.pocean.2004.02.011. (see p. 120).

Knudsen, M. F., B. H. Jacobsen, M.-S. Seidenkrantz, and J. Olsen. 2014. *Evidence for external forcing of the Atlantic Multidecadal Oscillation since termination of the Little Ice Age*. Nature Communications 5 (1): 3323. doi:10.1038/ncomms4323. (see p. 123).

Kondoh, M., and A. Mougi. 2015. *Interaction-type diversity hypothesis and interaction strength: the condition for the positive complexity-stability effect to arise*. Population Ecology 57 (1): 21–27. doi:10.1007/s10144-014-0475-9. (see p. 90).

Kortsch, S., R. Primicerio, M. Aschan, S. Lind, A. V. Dolgov, and B. Planque. 2019. *Food-web structure varies along environmental gradients in a high-latitude marine ecosystem*. Ecography 42 (2): 295–308. doi:10.1111/ecog.03443. (see p. 111).

Krakauer, N. Y., and J. T. Randerson. 2003. *Do volcanic eruptions enhance or diminish net primary production? Evidence from tree rings*. Global Biogeochemical Cycles 17 (4): n/a–n/a. doi:10.1029/2003GB002076. (see p. 134).

Kruk, C., E. Peeters, E. H. Van Nes, V. L. M. Huszar, L. S. Costa, and M. Scheffer. 2011. *Phytoplankton community composition can be predicted best in terms of morphological groups*. Limnology and Oceanography 56 (1): 110–118. doi:10.4319/lo.2011.56.1.0110. (see p. 108).

Kruk, C., V. L. M. Huszar, E. T. H. M. Peeters, S. Bonilla, L. Costa, M. LüRling, C. S. Reynolds, and M. Scheffer. 2010. *A morphological classification capturing functional variation in phytoplankton*. Freshwater Biology 55 (3): 614–627. doi:10.1111/j.1365-2427.2009.02298.x. (see p. 108).

Kuhnt, W., S. Hess, A. Holbourn, H. Paulsen, and B. Salomon. 2005. *The impact of the 1991 Mt. Pinatubo eruption on deep-sea foraminiferal communities: A model for the Cretaceous-Tertiary (K/T) boundary?* Palaeogeography, Palaeoclimatology, Palaeoecology 224 (1-3): 83–107. doi:10.1016/j.palaeo.2005.03.042. (see pp. 121, 134).

Kuiper, J. J., C. van Altena, P. C. de Ruiter, L. P. A. van Gerven, J. H. Janse, and W. M. Mooij. 2015. *Food-web stability signals critical transitions in temperate shallow lakes*. Nature Communications 6 (1): 7727. doi:10.1038/ncomms8727. (see p. 120).

Kunstler, G., D. Falster, D. A. Coomes, F. Hui, M. Kooyman Robert, D. C. Laughlin, L. Poorter, et al. 2016. *Plant functional traits have globally consistent effects on competition*. Nature 529 (7585): 1–15. doi:10.1038/nature16476. (see p. 90).

Labitzke, K., and M. P. McCormick. 1992. *Stratospheric temperature increases due to Pinatubo aerosols*. Geophysical Research Letters 19 (2): 207–210. doi:10.1029/91GL02940. (see pp. 121, 134).

Lack, D. 1969. *Population Changes in the Land Birds of a Small Island*. The Journal of Animal Ecology 38 (1): 211. doi:10.2307/2747. (see pp. 176, 177).

Ladyman, J. 1998. *What is structural realism?* Studies in History and Philosophy of Science Part A 29 (3): 409–424. doi:10.1016/S0039-3681(98)80129-5. (see p. 28).

Lagos, L., and F. Bárcena. 2015. *EU Sanitary Regulation on Livestock Disposal: Implications for the Diet of Wolves*. Environmental Management 56 (4): 890–902. doi:10.1007/s00267-015-0571-4. (see p. 154).

Lamb, J. S., and J. A. Roberts. 1998. *Time-reversal symmetry in dynamical systems: A survey*. Physica D: Nonlinear Phenomena 112 (1-2): 1–39. doi:10.1016/S0167-2789(97)00199-1. (see p. 26).

Lambertucci, S. A., A. Trejo, S. Di Martino, J. A. Sánchez-Zapata, J. A. Donázar, and F. Hiraldo. 2009. *Spatial and temporal patterns in the diet of the Andean condor: ecological replacement of native fauna by exotic species*. Animal Conservation 12 (4): 338–345. doi:10.1111/j.1469-1795.2009.00258.x. (see p. 142).

Lambertucci, S. A., J. Navarro, J. A. Sanchez Zapata, K. A. Hobson, P. A. E. Alarcón, G. Wiemeyer, G. Blanco, F. Hiraldo, and J. A. Donázar. 2018. *Tracking data and retrospective analyses of diet reveal the consequences of loss of marine subsidies for an obligate scavenger, the Andean condor*. Proceedings of the Royal Society B: Biological Sciences 285 (1879): 20180550. doi:10.1098/rspb.2018.0550. (see p. 142).

Lande, R., S. Engen, and B. E. Sæther. 2017. *Evolution of stochastic demography with life history tradeoffs in density-dependent age-structured populations*. Proceedings of the National Academy of Sciences of the United States of America 114 (44): 11582–11590. doi:10.1073/pnas.1710679114. (see p. 182).

Lande, R., S. Engen, and B.-E. Saether. 2003. *Stochastic Population Dynamics in Ecology and Conservation*. Oxford, UK: Oxford University Press. (see pp. 55, 162, 182).

Langa, J., J. Robinson, and A. Suárez. 2003. *Pullback permanence in a non-autonomous competitive Lotka–Volterra model*. Journal of Differential Equations 190 (1): 214–238. doi:10.1016/S0022-0396(02)00173-0. (see p. 192).

Lawton, J. H. 1999. *Are There General Laws in Ecology?* Oikos 84 (2): 177–192. doi:10.2307/3546712. (see p. 24).

Leathwick, J. R., J. Elith, and T. Hastie. 2006. *Comparative performance of generalized additive models and multivariate adaptive regression splines for statistical modelling of species distributions*. Ecological Modelling 199 (2): 188–196. doi:10.1016/j.ecolmodel.2006.05.022. (see p. 67).

Lefkovitch, L. P. 1965. *The Study of Population Growth in Organisms Grouped by Stages*. Biometrics 21 (1): 1. doi:10.2307/2528348. (see pp. 147, 180).

Lehman, C. L., and D. Tilman. 2000. *Biodiversity, Stability, and Productivity in Competitive Communities*. The American Naturalist 156 (5): 534–552. doi:10.1086/303402. (see pp. 63, 71).

Leles, S. G. 2019. *Accounting for mixotrophy within microbial food webs.* (see pp. 91, 92, 93, 108, 110).

Leles, S. G., J. Bruggeman, L. Polimene, J. Blackford, K. J. Flynn, and A. Mitra. 2021. *Differences in physiology explain succession of mixoplankton functional types and affect carbon fluxes in temperate seas*. Progress in Oceanography 190 (August 2020): 102481. doi:10.1016/j.pocean.2020.102481. (see pp. 91, 111).

Leles, S. G., L. Polimene, J. Bruggeman, J. Blackford, S. Ciavatta, A. Mitra, and K. J. Flynn. 2018. *Modelling mixotrophic functional diversity and implications for ecosystem function*. Edited by J. Dolan. Journal of Plankton Research 40 (6): 627–642. doi:10.1093/plankt/fby044. (see p. 93).

Levine, J. M., and J. HilleRisLambers. 2009. *The importance of niches for the maintenance of species diversity*. Nature 461 (7261): 254–257. doi:10.1038/nature08251. (see pp. 90, 107).

Levins, R. 1966. *The Strategy of Model Building in Population Biology*. American Scientist 54 (4): 421–431. (see pp. 28, 29, 187, 188).

———. 1968. *Evolution in Changing Environments*. Princeton, NJ.: Princeton University Press. (see pp. 28, 51, 94, 95, 96).

———. 1993. *A Response to Orzack and Sober: Formal Analysis and the Fluidity of Science*. The Quarterly Review of Biology 68 (4): 547–555. doi:10.1086/418302. (see pp. 29, 188).

———. 2007. *Strategies of abstraction*. Biology & Philosophy 21 (5): 741–755. doi:10.1007/s10539-006-9052-8. (see pp. 28, 187, 188).

Levins, R., and R. C. Lewontin. 1987. *The Dialectical Biologist*. Cambridge, MA: Harvard University Press. (see p. 28).

Lévy, M., O. Jahn, S. Dutkiewicz, M. J. Follows, and F. D'Ovidio. 2015. *The dynamical landscape of marine phytoplankton diversity*. Journal of the Royal Society Interface 12:20150481. doi:10.1098/rsif.2015.0481. (see p. 83).

Lewontin, R. C. 1966a. *On the Measurement of Relative Variability*. Systematic Biology 15 (2): 141–142. doi:10.2307/sysbio/15.2.141. (see p. 183).

Lewontin, R. C. 1966b. *Is Nature Probable or Capricious?* BioScience 16 (1): 25–27. doi:10.2307/1293548. (see pp. 26, 28).

———. 1969. *The meaning of stability*. In Diversity and stability in ecological systems, Brookhaven symposia in Biology 22, edited by G. M. Woodwell and H. H. Smith, 13–24. Springfield, VA: Brookhaven National Labratories, US Dept of Commerce. (see pp. 28, 51).

Lindström, Å., M. Green, M. Husby, J. A. Kålås, and A. Lehikoinen. 2015. *Large-Scale Monitoring of Waders on Their Boreal and Arctic Breeding Grounds in Northern Europe*. Ardea 103 (1): 3–15. doi:10.5253/arde.v103i1.a1. (see p. 164).

Litchman, E., and C. a. Klausmeier. 2008. *Trait-Based Community Ecology of Phytoplankton*. Annual Review of Ecology, Evolution, and Systematics 39 (1): 615–639. doi:10.1146/annurev.ecolsys.39.110707.173549. (see p. 69).

Litchman, E., C. A. Klausmeier, O. M. Schofield, and P. G. Falkowski. 2007. *The role of functional traits and trade-offs in structuring phytoplankton communities: Scaling from cellular to ecosystem level*. Ecology Letters 10 (12): 1170–1181. doi:10.1111/j.1461-0248.2007.01117.x. (see p. 110).

Llaneza, L., and J. V. López-Bao. 2015. *Indirect effects of changes in environmental and agricultural policies on the diet of wolves*. European Journal of Wildlife Research 61 (6): 895–902. doi:10.1007/s10344-015-0966-9. (see p. 154).

Lloyd, S. 2001. *Measures of complexity: a nonexhaustive list*. IEEE Control Systems 21 (4): 7–8. doi:10.1109/MCS.2001.939938. (see pp. 24, 97).

Loehle, C. 1989. *Catastrophe theory in ecology: a critical review and an example of the butterfly catastrophe*. Ecological Modelling 49 (1-2): 125–152. doi:10.1016/0304-3800(89)90047-1. (see p. 126).

Logofet, D. O. 1993. *Matrices and Graphs: stability problems in matematical ecology*. 308. Boca Raton, FL: CRC Press. (see pp. 51, 52, 53, 54, 55).

———. 2005. *Stronger-than-Lyapunov notions of matrix stability, or how "flowers" help solve problems in mathematical ecology*. Linear Algebra and Its Applications 398 (1-3): 75–100. doi:10.1016/j.laa.2003.04.001. (see pp. 51, 52, 53).

———. 2016. *Stability Versus Complexity*. In Reference Module in Earth Systems and Environmental Sciences. Amsterdam, NL: Elsevier Inc. doi:10.1016/B978-0-12-409548-9.09707-4. (see pp. 52, 64, 76, 86).

Longhurst, A. 2007. *Ecological Geography of the Sea.* 2nd. San Diego, CA: Academic Press. (see pp. 65, 70, 189).

López-Urrutia, Á., and X. A. G. Morán. 2015. *Temperature affects the size-structure of phytoplankton communities in the ocean*. Limnology and Oceanography 60 (3): 733–738. doi:10.1002/lno.10049. (see p. 83).

Loreau, M. 2010a. *From Populations to Ecosystems,* 320. Princeton, NJ.: Princeton University Press. doi:10.1111/j.1442-9993.2011.02326.x. (see pp. 64, 71, 76).

———. 2010b. *Linking biodiversity and ecosystems: towards a unifying ecological theory*. Philosophical Transactions of the Royal Society B: Biological Sciences 365:49–60. doi:10.1098/rstb.2009.0155. (see p. 62).

Lucht, W., I. C. Prentice, R. B. Myneni, S. Sitch, P. Friedlingstein, W. Cramer, P. Bousquet, W. Buermann, and B. Smith. 2002. *Climatic control of the high-latitude vegetation greening trend and Pinatubo effect*. Science 296 (5573): 1687–1689. doi:10.1126/science.1071828. (see pp. 121, 134).

LYAPUNOV, A. M. 1992. *The general problem of the stability of motion*. International Journal of Control 55 (3): 531–534. doi:10.1080/00207179208934253. (see pp. 34, 35).

MacArthur, R. 1970. *Species packing and competitive equilibrium for many species*. Theoretical Population Biology 1 (1): 1–11. doi:10.1016/0040-5809(70)90039-0. (see p. 37).

Macarthur, R. H., and R. Levins. 1967. *The Limiting Similarity, Convergence, and Divergence of Coexisting Species*. The American Naturalist 101 (921): 377–385. doi:10.1086/282505. arXiv:gr-qc/9809069v1. (see p. 91).

Machta, B. B., R. Chachra, M. K. Transtrum, and J. P. Sethna. 2013. *Parameter Space Compression Underlies Emergent Theories and Predictive Models*. Science 342 (6158): 604–607. doi:10.1126/science.1238723. (see p. 99).

Madsen, J., G. Cracknell, and T. Fox. 1999. *Goose Populations of the Western Palearctic: A Review of Status and Distribution.* Wageningen: Wetlands International & NERI. (see p. 137).

Makowski, D., M. Ben-Shachar, and D. Lüdecke. 2019. *bayestestR: Describing Effects and their Uncertainty, Existence and Significance within the Bayesian Framework*. Journal of Open Source Software 4 (40): 1541. doi:10.21105/joss.01541. (see pp. 103, 135).

Malisoff, M., and F. Mazenc. 2009. *Constructions of Strict Lyapunov Functions*. London, UK.: Springer-Verlag. doi:10.1017/CBO9781107415324.004. (see p. 35).

MAPAMA. 2018. *Informe epidemiológico final sobre las encefalopatías espongiformes transmisibles en España*. Technical report. Madrid: Subdirección General de Sanidad e Higiene Animal y Trazabilidad, Ministerio de Agricultura, Pesca y Alimentación. (see p. 151).

Marañón, E. 2015. *Cell Size as a Key Determinant of Phytoplankton Metabolism and Community Structure*. Annual Review of Marine Science 7 (1): 241–264. doi:10.1146/annurev-marine-010814-015955. (see pp. 67, 84).

Margalef, R. 1968. *Perspectives in ecological theory*. Chicago, ILL.: University of Chicago Press. (see pp. 25, 26, 28).

Margalida, A., G. Bogliani, C. G. R. Bowden, J. A. Donazar, F. Genero, M. Gilbert, W. B. Karesh, et al. 2014. *One Health approach to use of veterinary pharmaceuticals*. Science 346 (6215): 1296–1298. doi:10.1126/science.1260260. (see p. 154).

Margalida, A., M. À. Colomer, and D. Oro. 2014. *Man-induced activities modify demographic parameters in a long-lived species: effects of poisoning and health policies*. Ecological Applications 24 (3): 436–444. doi:10.1890/13-0414.1. (see p. 143).

Margalida, A., and M. À. Colomer. 2012. *Modelling the effects of sanitary policies on European vulture conservation*. Scientific Reports 2 (1): 753. doi:10.1038/srep00753. (see pp. 144, 155).

Margalida, A., J. A. Donázar, M. Carrete, and J. A. Sánchez-Zapata. 2010. *Sanitary versus environmental policies: fitting together two pieces of the puzzle of European vulture conservation*. Journal of Applied Ecology 47 (4): 931–935. doi:10.1111/j.1365-2664.2010.01835.x. (see pp. 143, 144, 155, 156).

Margalida, A., R. E. Green, F. Hiraldo, G. Blanco, J. A. Sánchez-Zapata, A. Santangeli, O. Duriez, and J. A. Donázar. 2021. *Ban veterinary use of diclofenac in Europe*. Edited by J. Sills. Science 372 (6543): 2–695. doi:10.1126/science.abj0131. (see p. 157).

Marín, C., and F. García. 2006. *Doñana, Water and Biosphere*. Madrid: Confederación Hidrográfica del Guadalquivir, Ministerio de Medio Ambiente, UNESCO-MaB & Junta de Andalucía. (see pp. 122, 135).

Markowitz, H. M. 1952. *Portfolio selection*. The journal of finance 7 (1): 77–91. doi:10.1111/j.1540-6261.1952.tb01525.x. (see p. 63).

Markowski, C. A., and E. P. Markowski. 1990. *Conditions for the Effectiveness of a Preliminary Test of Variance*. The American Statistician 44 (4): 322–326. doi:10.1080/00031305.1990.10475752. (see p. 183).

Maron, J. L., A. A. Agrawal, and D. W. Schemske. 2019. *Plant–herbivore coevolution and plant speciation*. Ecology 100 (7): e02704. doi:10.1002/ecy.2704. (see p. 91).

Marquet, P. A., A. P. Allen, J. H. Brown, J. A. Dunne, B. J. Enquist, J. F. Gillooly, P. A. Gowaty, et al. 2014. *On Theory in Ecology*. BioScience 64 (8): 701–710. doi:10.1093/biosci/biu098. (see pp. 23, 26).

Martinez, F., R. F. Rodriguez, and G. Blanco. 1997. *Effects of Monitoring Frequency on Estimates of Abundance, Age Distribution, and Productivity of Colonial Griffon Vultures*. Journal of Field Ornithology 68 (3): 392–399. (see p. 145).

Martínez, F., G. Blanco, and R. F. Rodríguez-Martínez. 1998. *Rate, timing and success of clutch replacement by colonial griffon vultures Gyps fulvus*. Ornis Fennica 75 (3): 145–148. (see p. 145).

Martínez-Abraín, A., G. Tavecchia, H. M. Regan, J. Jiménez, M. Surroca, and D. Oro. 2012. *Effects of wind farms and food scarcity on a large scavenging bird species following an epidemic of bovine spongiform encephalopathy*. Journal of Applied Ecology 49 (1): 109–117. doi:10.1111/j.1365-2664.2011.02080.x. (see pp. 154, 157).

Mateo-Tomás, P., and P. P. Olea. 2010. *When hunting benefits raptors: a case study of game species and vultures*. European Journal of Wildlife Research 56 (4): 519–528. doi:10.1007/s10344-009-0341-9. (see p. 142).

Mateo-Tomás, P., P. P. Olea, M. Moleón, J. Vicente, F. Botella, N. Selva, J. Viñuela, and J. A. Sánchez-Zapata. 2015. *From regional to global patterns in vertebrate scavenger communities subsidized by big game hunting*. Edited by D. M. Richardson. Diversity and Distributions 21 (8): 913–924. doi:10.1111/ddi.12330. (see pp. 142, 158).

Mateo-Tomás, P., P. P. Olea, J. V. López-Bao, P. González-Quirós, and P. Peón. 2019. *Different criteria for implementing sanitary regulations lead to disparate outcomes for scavenger conservation*. Edited by R. Fuller. Journal of Applied Ecology 56 (3): 500–508. doi:10.1111/1365-2664.13293. (see p. 158).

May, R. M. 1972. *Will a large complex system be stable?* Nature 238:413–414. (see pp. 62, 90).

———. 1973. *Stability and Complexity in Model Ecosystems*. Princeton, NJ.: Princeton University Press. (see pp. 24, 37, 62, 71).

———. 1977. *Thresholds and breakpoints in ecosystems with a multiplicity of stable states*. Nature 269 (5628): 471–477. doi:10.1038/269471a0. (see p. 120).

McCann, K. S. 2010. *Food Webs*. Princeton, NJ.: Princeton University Press. (see pp. 62, 107).

McCann, K. S. 2000. *The diversity-stability debate*. Nature 405 (May): 228–233. doi:10.1038/35012234. (see p. 62).

McClain, C. R. 2009. *A decade of satellite ocean color observations*. Annual Review of Marine Science 1:19–42. doi:10.1146/annurev.marine.010908.163650. (see p. 68).

McCormick, M. P., L. W. Thomason, and C. R. Trepte. 1995. *Atmospheric effects of the Mt Pinatubo eruption*. Nature 373 (6513): 399–404. doi:10.1038/373399a0. (see p. 121).

McGraw, J. B., and H. Caswell. 1996. *Estimation of Individual Fitness from Life-History Data*. The American Naturalist 147 (1): 47–64. doi:10.1086/285839. (see p. 168).

McManus, G. B., D. M. Schoener, and K. Haberlandt. 2012. *Chloroplast symbiosis in a marine ciliate: ecophysiology and the risks and rewards of hosting foreign organelles*. Frontiers in Microbiology 3 (SEP): 1–9. doi:10.3389/fmicb.2012.00321. (see pp. 91, 110).

McNaughton, S. J. 1977. *Diversity and stability of ecological communities: a comment on the role of empiricism in ecology*. The American Naturalist 111 (979): 515–525. (see p. 62).

Mesterton-Gibbons, M. 1993. *Why Demographic Elasticities Sum to One: A Postscript to De Kroon et al.* Ecology 74 (8): 2467–2468. doi:10.2307/1939599. (see p. 181).

Middleton, A. D. 1934. *Periodic Fluctuations in British Game Populations*. The Journal of Animal Ecology 3 (2): 231. doi:10.2307/1146. (see pp. 176, 177).

Miele, V., C. Guill, R. Ramos-Jiliberto, and S. Kéfi. 2019. *Non-trophic interactions strengthen the diversity—functioning relationship in an ecological bioenergetic network model*. Edited by J. Grilli. PLOS Computational Biology 15 (8): e1007269. doi:10.1371/journal.pcbi.1007269. (see p. 90).

Mierczynski, J., and S. J. Schreiber. 2002. *Kolmogorov vector fields with robustly permanent subsystems*. Journal of Mathematical Analysis and Applications 267:329–337. doi:10.1006/jmaa.2001.7776. (see p. 51).

Millán, L., M. L. Santee, A. Lambert, N. J. Livesey, F. Werner, M. J. Schwartz, H. C. Pumphrey, et al. 2022. *The Hunga Tonga-Hunga Ha'apai Hydration of the Stratosphere*. Geophysical Research Letters 49 (13): 1–10. doi:10.1029/2022GL099381. (see p. 121).

Mitchell, C., A. D. Fox, J. Harradine, and I. Clausager. 2008. *Measures of annual breeding success amongst Eurasian Wigeon Anas penelope*. Bird Study 55 (1): 43–51. doi:10.1080/00063650809461503. (see p. 135).

Mitra, A., K. J. Flynn, J. M. Burkholder, T. Berge, A. Calbet, J. A. Raven, E. Granéli, et al. 2014. *The role of mixotrophic protists in the biological carbon pump*. Biogeosciences 11 (4): 995–1005. doi:10.5194/bg-11-995-2014. (see p. 92).

Mitra, A., K. J. Flynn, U. Tillmann, J. A. Raven, D. Caron, D. K. Stoecker, F. Not, et al. 2016. *Defining Planktonic Protist Functional Groups on Mechanisms for Energy and Nutrient Acquisition: Incorporation of Diverse Mixotrophic Strategies*. Protist 167 (2): 106–120. doi:10.1016/j.protis.2016.01.003. (see pp. 91, 92, 110).

Moeller, H. V., E. Peltomaa, M. D. Johnson, and M. G. Neubert. 2016. *Acquired phototrophy stabilises coexistence and shapes intrinsic dynamics of an intraguild predator and its prey*. Edited by J. Drake. Ecology Letters 19 (4): 393–402. doi:10.1111/ele.12572. (see p. 92).

Moleón, M., J. A. Sánchez-Zapata, A. Margalida, M. Carrete, N. Owen-Smith, and J. A. Donázar. 2014. *Humans and Scavengers: The Evolution of Interactions and Ecosystem Services*. BioScience 64 (5): 394–403. doi:10.1093/biosci/biu034. (see pp. 142, 157).

Moleón, M., J. A. Sánchez-Zapata, N. Selva, J. A. Donázar, and N. Owen-Smith. 2014. *Inter-specific interactions linking predation and scavenging in terrestrial vertebrate assemblages*. Biological Reviews 89 (4): 1042–1054. doi:10.1111/brv.12097. (see pp. 143, 144, 157).

Monsalve-Bravo, G. M., B. A. J. Lawson, C. Drovandi, K. Burrage, K. S. Brown, C. M. Baker, S. A. Vollert, K. Mengersen, E. McDonald-Madden, and M. P. Adams. 2022. *Analysis of sloppiness in model simulations: Unveiling parameter uncertainty when mathematical models are fitted to data*. Science Advances 8 (38). doi:10.1126/sciadv.abm5952. (see p. 102).

Montoya, J. M., and R. V. Solé. 2002. *Small world patterns in food webs*. Journal of Theoretical Biology 214 (3): 405–412. doi:10.1006/jtbi.2001.2460. (see p. 25).

Montoya, J. M., I. Donohue, and S. L. Pimm. 2018. *Planetary Boundaries for Biodiversity: Implausible Science, Pernicious Policies*. Trends in Ecology & Evolution 33 (2): 71–73. doi:10.1016/j.tree.2017.10.004. (see p. 120).

Montoya, J. M., M. A. Rodríguez, and B. A. Hawkins. 2003. *Food web complexity and higher-level ecosystem services*. Ecology Letters 6 (7): 587–593. doi:10.1046/j.1461-0248.2003.00469.x. (see p. 109).

Moosmann, M., M. Cuenca-Cambronero, S. De Lisle, R. Greenway, C. M. Hudson, M. D. Lürig, and B. Matthews. 2021. *On the evolution of trophic position*. Edited by F. Adler. Ecology Letters 24 (12): 2549–2562. doi:10.1111/ele.13888. (see p. 108).

Morales-Reyes, Z., J. M. Pérez-García, M. Moleón, F. Botella, M. Carrete, J. A. Donázar, A. Cortés-Avizanda, et al. 2017. *Evaluation of the network of protection areas for the feeding of scavengers in Spain: from biodiversity conservation to greenhouse gas emission savings*. Edited by M.-A. Villard. Journal of Applied Ecology 54 (4): 1120–1129. doi:10.1111/1365-2664.12833. (see p. 158).

Morales-Reyes, Z., J. M. Pérez-García, M. Moleón, F. Botella, M. Carrete, C. Lazcano, R. Moreno-Opo, A. Margalida, J. A. Donázar, and J. A. Sánchez-Zapata. 2015. *Supplanting ecosystem services provided by scavengers raises greenhouse gas emissions*. Scientific Reports 5 (1): 7811. doi:10.1038/srep07811. (see pp. 143, 144).

Moran, A. G., L. Alonso-sa, E. Nogueira, H. W. Ducklow, N. Gonza, A. Calvo-dı, N. Arandia-gorostidi, et al. 2015. *More , smaller bacteria in response to ocean ' s warming ?* Proceedings of the Royal Society B: Biological Sciences 282:1–9. doi:http://dx.doi.org/10.1098/rspb.2015.0371. (see pp. 66, 84).

Morán, X. A. G., J. M. Gasol, M. C. Pernice, J. F. Mangot, R. Massana, E. Lara, D. Vaqué, and C. M. Duarte. 2017. *Temperature regulation of marine heterotrophic prokaryotes increases latitudinally as a breach between bottom-up and top-down controls*. Global Change Biology, no. April: 3956–3964. doi:10.1111/gcb.13730. (see p. 76).

Morris, D. W., and P. Lundberg. 2011. *Pillars of Evolution: Fundamental principles of the eco-evolutionary process*. Oxford, UK: Oxford University Press. doi:10.1093/acprof:oso/9780198568797.001.0001. (see p. 192).

Morris, W. F., and D. F. Doak. 2002. *Quantitative conservation biology: theory and practice of population viability analysis*. Sunderland, MA: Sinauer Associates. (see pp. 181, 182).

Mougi, A., and M. Kondoh. 2012. *Diversity of Interaction Types and Ecological Community Stability*. Science 337 (6092): 349–351. doi:10.1126/science.1220529. (see pp. 90, 91).

Mutshinda, C. M., Z. V. Finkel, C. E. Widdicombe, and A. J. Irwin. 2016. *Ecological equivalence of species within phytoplankton functional groups*. Functional Ecology 30:1714–1722. doi:10.1111/1365-2435.12641. (see p. 69).

Mutshinda, C. M., R. B. O'Hara, and I. P. Woiwod. 2009. *What drives community dynamics?* Proceedings of the Royal Society B: Biological Sciences 276 (1669): 2923–2929. doi:10.1098/rspb.2009.0523. (see pp. 94, 95, 125).

Mutshinda, C. M., R. B. O'Hara, and I. P. Woiwod. 2011. *A multispecies perspective on ecological impacts of climatic forcing*. Journal of Animal Ecology 80 (1): 101–107. doi:10.1111/j.1365-2656.2010.01743.x. (see pp. 94, 95, 99, 100, 101, 125, 147, 149).

Naeem, S., and S. Li. 1997. *Biodiversity enhances ecosystem reliability.* Nature 390 (December): 507–510. (see pp. 63, 64, 85).

Nash, K. L., C. Cvitanovic, E. A. Fulton, B. S. Halpern, E. J. Milner-Gulland, R. A. Watson, and J. L. Blanchard. 2017. *Planetary boundaries for a blue planet*. Nature Ecology & Evolution 1 (11): 1625–1634. doi:10.1038/s41559-017-0319-z. (see p. 120).

Navarro, G., P. Almaraz, I. Caballero, Á. Vázquez, and I. E. Huertas. 2017. *Reproduction of Spatio-Temporal Patterns of Major Mediterranean Phytoplankton Groups from Remote Sensing OC-CCI Data*. Frontiers in Marine Science 4 (August): 246. doi:10.3389/fmars.2017.00246. (see p. 68).

Navarro, G., and J. Ruiz. 2013. *Hysteresis conditions the vertical position of deep chlorophyll maximum in the temperate ocean*. Global Biogeochemical Cycles 27 (4): 1013–1022. doi:10.1002/gbc.20093. (see p. 85).

Neubert, M. G., and H. Caswell. 1997. *Alternatives To Resilience for Measuring the Responses of Ecological Systems To Perturbations*. Ecology 78 (3): 653–665. doi:10.1890/0012-9658(1997)078[0653:ATRFMT]2.0.CO;2. (see pp. 37, 38).

Norris, K., P. W. Atkinson, and J. A. Gill. 2004. *Climate change and coastal waterbird populations - past declines and future impacts*. Ibis 146 (SUPPL.1): 82–89. doi:10.1111/j.1474-919X.2004.00331.x. (see pp. 164, 174).

Northrup, J. M., and M. S. Boyce. 2012. *Mad cow policy and management of grizzly bear incidents*. Wildlife Society Bulletin 36 (3): 499–505. doi:10.1002/wsb.167. (see p. 154).

Norton, D. E. 1995. *The fundamental theorem of dynamical systems*. Commentationes Mathematicae Universitatis Carolinae 36 (3): 585–597. (see p. 193).

Novak, M., J. D. Yeakel, A. E. Noble, D. F. Doak, M. Emmerson, J. A. Estes, U. Jacob, M. T. Tinker, and J. T. Wootton. 2016. *Characterizing Species Interactions to Understand Press Perturbations: What Is the Community Matrix?* Annual Review of Ecology, Evolution, and Systematics 47 (1): 409–432. doi:10.1146/annurev-ecolsys-032416-010215. (see pp. 51, 94, 95, 96).

Ogada, D. L., F. Keesing, and M. Z. Virani. 2012. *Dropping dead: causes and consequences of vulture population declines worldwide*. Annals of the New York Academy of Sciences 1249 (1): 57–71. doi:10.1111/j.1749-6632.2011.06293.x. (see p. 143).

Olea, P. P., and P. Mateo-Tomás. 2009. *The role of traditional farming practices in ecosystem conservation: The case of transhumance and vultures*. Biological Conservation 142 (8): 1844–1853. doi:10.1016/j.biocon.2009.03.024. (see p. 143).

Oppenheimer, C. 2003. *Climatic, environmental and human consequences of the largest known historic eruption: Tambora volcano (Indonesia) 1815*. Progress in Physical Geography: Earth and Environment 27 (2): 230–259. doi:10.1191/0309133303pp379ra. (see p. 121).

Oro, D. 2020. *Perturbation, Behavioural Feedbacks, and Population Dynamics in Social Animals*. Oxford University Press. doi:10.1093/oso/9780198849834.001.0001. (see pp. 25, 138).

Oro, D., and L. Freixas. 2021. *Flickering body temperature anticipates criticality in hibernation dynamics*. Royal Society Open Science 8 (1): 201571. doi:10.1098/rsos.201571. (see p. 138).

Oro, D., M. Genovart, G. Tavecchia, M. S. Fowler, and A. Martínez-Abraín. 2013. *Ecological and evolutionary implications of food subsidies from humans*. Edited by B. Worm. Ecology Letters 16 (12): 1501–1514. doi:10.1111/ele.12187. (see pp. 142, 154).

Orzack, S. H., and E. Sober. 1993. *A Critical Assessment of Levins's The Strategy of Model Building in Population Biology (1966)*. The Quarterly Review of Biology 68 (4): 533–546. doi:10.1086/418301. (see pp. 29, 188).

Orzack, S. H., and S. Tuljapurkar. 2001. *Reproductive Effort in Variable Environments, or Environmental Variation Is for the Birds*. Ecology 82 (9): 2659. doi:10.2307/2679944. (see p. 163).

Osipov, S., G. Stenchikov, K. Tsigaridis, A. N. LeGrande, S. E. Bauer, M. Fnais, and J. Lelieveld. 2021. *The Toba supervolcano eruption caused severe tropical stratospheric ozone depletion*. Communications Earth & Environment 2 (1): 71. doi:10.1038/s43247-021-00141-7. (see p. 121).

Osland, M. J., L. C. Feher, G. H. Anderson, W. C. Vervaeke, K. W. Krauss, K. R. Whelan, K. M. Balentine, G. Tiling-Range, T. J. Smith, and D. R. Cahoon. 2020. *A Tropical Cyclone-Induced Ecological Regime Shift: Mangrove Forest Conversion to Mudflat in Everglades National Park (Florida, USA)*. Wetlands 40 (5): 1445–1458. doi:10.1007/s13157-020-01291-8. (see p. 121).

Ostfeld, R. S., and F. Keesing. 2000. *Ostfeld_and_Keesing_2000_TREE_15_232-237.* 15 (6): 232–237. (see p. 154).

Otterå, O. H., M. Bentsen, H. Drange, and L. Suo. 2010. *External forcing as a metronome for Atlantic multidecadal variability*. Nature Geoscience 3 (10): 688–694. doi:10.1038/ngeo955. (see p. 123).

Ovaskainen, O., G. Tikhonov, D. Dunson, V. Grøtan, S. Engen, B.-e. Sæther, and N. Abrego. 2017. *How are species interactions structured in species-rich communities? A new method for analysing time-series data*. Proceedings of the Royal Society B: Biological Sciences 284 (1855): 20170768. doi:10.1098/rspb.2017.0768. (see pp. 56, 57).

Paleczny, M., E. Hammill, V. Karpouzi, and D. Pauly. 2015. *Population Trend of the World's Monitored Seabirds, 1950-2010*. Edited by M. Krkosek. PLOS ONE 10 (6): e0129342. doi:10.1371/journal.pone.0129342. (see p. 164).

Palis, J., and W. de Melo. 1982. *Geometric Theory of Dynamical Systems*. New York, NY: Springer US. doi:10.1007/978-1-4612-5703-5. (see p. 43).

Parejo, M., J. G. Navedo, J. S. Gutiérrez, J. M. Abad-Gómez, A. Villegas, C. Corbacho, J. M. Sánchez-Guzmán, and J. A. Masero. 2015. *Geographical origin of dabbling ducks wintering in Iberia: sex differences and implications for pair formation*. Edited by J. Reneerkens. Ibis 157 (3): 536–544. doi:10.1111/ibi.12256. (see p. 137).

Parra, J., and J. L. Tellería. 2004. *The increase in the Spanish population of Griffon Vulture Gyps fulvus during 1989–1999: effects of food and nest site availability*. Bird Conservation International 14 (01): 33–41. doi:10.1017/S0959270904000048. (see p. 156).

Pásztor, L., Z. Botta-Dukát, G. Magyar, T. Czárán, and G. Meszéna. 2016. *Theory-Based Ecology*. Oxford, UK: Oxford University Press. doi:10.1093/acprof:oso/9780199577859.001.0001. (see pp. 23, 26, 97).

Payo-Payo, A., M. Genovart, A. Bertolero, R. Pradel, and D. Oro. 2016. *Consecutive cohort effects driven by density-dependence and climate influence early-life survival in a long-lived bird*. Proceedings of the Royal Society B: Biological Sciences 283 (1829): 20153042. doi:10.1098/rspb.2015.3042. (see p. 156).

Peach, W., P. Thompson, and J. Coulson. 1994. *Annual and Long-Term Variation in the Survival Rates of British Lapwings Vanellus vanellus*. The Journal of Animal Ecology 63 (1): 60. doi:10.2307/5583. (see pp. 164, 173, 174, 175).

Peig, J., and A. J. Green. 2009. *New perspectives for estimating body condition from mass/length data: the scaled mass index as an alternative method*. Oikos 118 (12): 1883–1891. doi:10.1111/j.1600-0706.2009.17643.x. (see p. 165).

Peixoto, M. M. 1959. *On Structural Stability*. The Annals of Mathematics 69 (1): 199. doi:10.2307/1970100. (see pp. 43, 45).

Peixoto, M. M., and C. C. Pugh. 1968. *Structurally Stable Systems on Open Manifolds are Never Dense*. The Annals of Mathematics 87 (3): 423. doi:10.2307/1970713. (see p. 46).

Petraitis, P. 2013. *Multiple Stable States in Natural Ecosystems*. Oxford, UK: Oxford University Press. doi:10.1093/acprof:osobl/9780199569342.001.0001. (see pp. 120, 190).

Pfister, C. A. 1998. *Patterns of variance in stage-structured populations: Evolutionary predictions and ecological implications*. Proceedings of the National Academy of Sciences 95 (1): 213–218. doi:10.1073/pnas.95.1.213. (see pp. 143, 144, 156, 163, 174).

Piironen, J., and A. Vehtari. 2017. *Sparsity information and regularization in the horseshoe and other shrinkage priors*. Electronic Journal of Statistics 11 (2): 5018–5051. doi:10.1214/17-EJS1337SI. (see pp. 99, 100).

Pimm, S. L. 1984. *The complexity and stability of ecosystems*. Nature 307 (26): 321–326. doi:10.1038/315635c0. (see pp. 62, 71, 172).

———. 1991. *The Balance of Nature? Ecological Issues in the Conservation of Species and Communities*. Chicago, ILL.: The University of Chicago Press. (see p. 187).

Pimm, S. L., and A. Redfearn. 1988. *The variability of population densities*. Nature 334 (6183): 613–614. doi:10.1038/334613a0. (see pp. 165, 173).

Pitelka, F. A. 1974. *Intellectual Censorship in Ecology*. Ecology 55 (5): 925–926. doi:10.2307/1940345. (see p. 187).

Plummer, M. 2003. *JAGS: A program for analysis of Bayesian graphical models using Gibbs sampling*. In Proceedings of the 3rd International Workshop on Distributed Statistical Computing, March, 20–30. doi:10.1.1.13.3406. (see pp. 74, 99, 102, 149).

Portillo, J. R., F. Soler-Toscano, and J. A. Langa. 2022. *Global structural stability and the role of cooperation in mutualistic systems*. Edited by P. M. Rodriguez. PLOS ONE 17 (4): e0267404. doi:10.1371/journal.pone.0267404. (see p. 193).

Post, E. 2013. *Ecology of Climate Change: The Importance of Biotic Interactions*. Princeton, NJ.: Princeton University Press. (see p. 120).

———. 2019. *Time in Ecology: A Theoretical Framework*. Princeton, NJ.: Princeton University Press. doi:10.2307/j.ctv3s8sns. (see pp. 26, 27).

Poston, T., and I. Stewart. 1979. *Catastrophe Theory and Its Applications*. (see p. 122).

Prigogine, I. 1978. *Time, Structure, and Fluctuations*. Science 201 (4358): 777–785. doi:10.1126/science.201.4358.777. (see pp. 25, 191).

———. 1980. *From Being to Becoming. Time and complexity in the physical sciences*. New York, NY: W. H. Freeman / Company. (see pp. 26, 191, 194).

Prinzing, A., M. Brändle, R. Pfeifer, and R. Brandl. 2002. *Does sexual selection influence population trends in European birds?* Evolutionary Ecology Research 4 (1): 49–60. (see p. 173).

Promislow, D. E., R. Montgomerie, and T. E. Martin. 1992. *Mortality costs of sexual dimorphism in birds*. Proceedings of the Royal Society of London. Series B: Biological Sciences 250 (1328): 143–150. doi:10.1098/rspb.1992.0142. (see p. 172).

Prys-Jones, R. P., L. G. Underhill, and R. J. Waters. 1994. *Index Numbers for Waterbird Populations. II. Coastal Wintering Waders in the United Kingdom, 1970/71-1990/91*. The Journal of Applied Ecology 31 (3): 481. doi:10.2307/2404444. (see pp. 176, 179).

Ptacnik, R., A. G. Solimini, T. Andersen, T. Tamminen, P. Brettum, L. Lepisto, E. Willen, and S. Rekolainen. 2008. *Diversity predicts stability and resource use efficiency in natural phytoplankton communities*. Proceedings of the National Academy of Sciences of the USA 105 (13): 5134–5138. doi:10.1073/pnas.0708328105. (see p. 85).

Purvis, A., J. L. Gittleman, G. Cowlishaw, and G. M. Mace. 2000. *Predicting extinction risk in declining species*. Proceedings of the Royal Society of London. Series B: Biological Sciences 267 (1456): 1947–1952. doi:10.1098/rspb.2000.1234. (see p. 177).

Putman, R. J., and B. W. Staines. 2004. *Supplementary winter feeding of wild red deer Cervus elaphus in Europe and North America: justifications, feeding practice and effectiveness*. Mammal Review 34 (4): 285–306. doi:10.1111/j.1365-2907.2004.00044.x. (see p. 142).

Ranta, E., M. S. Fowler, and V. Kaitala. 2008. *Population synchrony in small-world networks*. Proceedings of the Royal Society B: Biological Sciences 275 (1633): 435–442. doi:10.1098/rspb.2007.1546. (see p. 25).

Ranta, E., P. Lundberg, and V. Kaitala. 2006. *Ecology of Populations*. Cambridge, UK: Cambridge University Press. (see pp. 25, 95, 96, 125).

Ratikainen, I. I., and H. Kokko. 2019. *The coevolution of lifespan and reversible plasticity*. Nature Communications 10 (1): 538. doi:10.1038/s41467-019-08502-9. (see p. 27).

RCoreTeam. 2021. *R: A Language and Environment for Statistical Computing*. Vienna, Austria. (see pp. 75, 103, 149, 179).

Rehfisch, M., G. Austin, M. Armitage, P. Atkinson, S. Holloway, A. Musgrove, and M. Pollitt. 2003. *Numbers of wintering waterbirds in Great Britain and the Isle of Man (1994/1995–1998/1999): II. Coastal waders (Charadrii)*. Biological Conservation 112 (3): 329–341. doi:10.1016/S0006-3207(02)00330-0. (see pp. 164, 173).

Reiners, W. A., and J. A. Lockwood. 2009. *Philosophical Foundations for the Practices of Ecology*. Cambridge, UK: Cambridge University Press. (see pp. 23, 28).

Reiners, W. A., J. A. Lockwood, D. S. Reiners, and S. D. Prager. 2017. *100 Years of Ecology: What Are Our Concepts and Are They Useful?* Ecological Monographs 87 (2): 260–277. doi:10.1002/ecm.1243. (see p. 23).

Rendón, M., A. Green, E. Aguilera, and P. Almaraz. 2008. *Status, distribution and long-term changes in the waterbird community wintering in Doñana, south–west Spain*. Biological Conservation 141 (5): 1371–1388. doi:10.1016/j.biocon.2008.03.006. (see pp. 121, 122, 135).

Reygondeau, G., A. Longhurst, E. Martinez, G. Beaugrand, D. Antoine, and O. Maury. 2013. *Dynamic biogeochemical provinces in the global ocean*. Global Biogeochemical Cycles 27 (4): 1046–1058. doi:10.1002/gbc.20089. (see p. 65).

Reynolds, C. S. 2006. *The Ecology of Phytoplankton*. Cambridge: Cambridge University Press. (see pp. 70, 111).

Ribando, J. M. 2006. *Measuring Solid Angles Beyond Dimension Three*. Discrete & Computational Geometry 36 (3): 479–487. doi:10.1007/s00454-006-1253-4. (see pp. 54, 55).

Ridgill, S., and A. Fox. 1990. *Cold weather movements of waterfowl in Western Europe*. Technical report. Slimbridge, UK.: IWRB Special Publ. 13. (see p. 136).

Righetti, D., M. Vogt, N. Gruber, A. Psomas, and N. E. Zimmermann. 2019. *Global pattern of phytoplankton diversity driven by temperature and environmental variability*. Science Advances 5 (5): eaau6253. doi:10.1126/sciadv.aau6253. (see pp. 75, 83, 84, 85).

Righetti, D., M. Vogt, N. E. Zimmermann, M. D. Guiry, and N. Gruber. 2020. *PhytoBase: A global synthesis of open-ocean phytoplankton occurrences*. Earth System Science Data 12 (2): 907–933. doi:10.5194/essd-12-907-2020. (see p. 84).

Roberts, A. 1974. *The stability of a feasible random ecosystem*. Nature 251:607–608. doi:10.1016/0025-5564(75)90030-9. (see pp. 62, 90, 96).

Robertson, G. J., and F. Cooke. 1999. *Winter Philopatry in Migratory Waterfowl*. The Auk 116 (1): 20–34. doi:10.2307/4089450. (see pp. 136, 137).

Robinson, C. 1974. *Structural stability of vector fields.* The Annals of Mathematics 99 (1): 154–175. (see p. 44).

Robock, A. 2000. *Volcanic eruptions and climate*. Reviews of Geophysics (Dordrecht) 38 (2): 191–219. doi:10.1029/1998RG000054. (see p. 134).

———. 2002. *The Climatic Aftermath*. Science 295 (5558): 1242–1244. doi:10.1126/science.1069903. (see pp. 121, 134).

Rocha, J. C., G. Peterson, Ö. Bodin, and S. Levin. 2018. *Cascading regime shifts within and across scales*. Science 362 (6421): 1379–1383. doi:10.1126/science.aat7850. (see p. 120).

Rocha, J. C., G. D. Peterson, and R. Biggs. 2015. *Regime shifts in the anthropocene: Drivers, risks, and resilience*. PLoS ONE 10 (8): 10–12. doi:10.1371/journal.pone.0134639. (see p. 120).

Rockström, J., W. Steffen, K. Noone, Å. Persson, F. S. Chapin, E. F. Lambin, T. M. Lenton, et al. 2009. *A safe operating space for humanity*. Nature 461 (7263): 472–475. doi:10.1038/461472a. (see p. 120).

Rodó, X., and M. Á. Rodríguez-Arias. 2006. *A new method to detect transitory signatures and local time/space variability structures in the climate system: The scale-dependent correlation analysis*. Climate Dynamics 27 (5): 441–458. doi:10.1007/s00382-005-0106-4. (see pp. 123, 129).

Rodríguez-Arias, M. À., and X. Rodó. 2004. *A primer on the study of transitory dynamics in ecological series using the scale-dependent correlation analysis*. Oecologia 138 (4): 485–504. doi:10.1007/s00442-003-1464-4. (see pp. 123, 129).

Rodríguez-Ramos, T., E. Marañón, and P. Cermeño. 2015. *Marine nano- and microphytoplankton diversity: redrawing global patterns from sampling-standardized data*. Global Ecology and Biogeography 24 (5): 527–538. doi:10.1111/geb.12274. (see pp. 66, 83).

Roff, D. A. 2002. *Life history evolution.* Sunderland, MA: Sinauer Associattes. (see p. 143).

Rohr, R. P., S. Saavedra, and J. Bascompte. 2014. *On the structural stability of mutualistic systems*. Science 345 (6195): 1253497. doi:10.1126/science.1253497. (see pp. 55, 62, 86, 91).

Roomen, M. van, K. Laursen, C. van Turnhout, E. van Winden, J. Blew, K. Eskildsen, K. Günther, et al. 2012. *Signals from the Wadden sea: Population declines dominate among waterbirds depending on intertidal mudflats*. Ocean & Coastal Management 68:79–88. doi:10.1016/j.ocecoaman.2012.04.004. (see p. 164).

Rosen, R. 2012. *Anticipatory Systems*. Vol. 1. IFSR International Series on Systems Science and Engineering. New York, NY: Springer New York. doi:10.1007/978-1-4614-1269-4. (see p. 28).

Rotella, J. J., W. A. Link, T. Chambert, G. E. Stauffer, and R. A. Garrott. 2012. *Evaluating the demographic buffering hypothesis with vital rates estimated for Weddell seals from 30 years of mark-recapture data*. Journal of Animal Ecology 81 (1): 162–173. doi:10.1111/j.1365-2656.2011.01902.x. (see p. 143).

Royama, T. 1977. *Population Persistence and Density Dependence*. Ecological Monographs 47 (1): 1–35. doi:10.2307/1942222. (see p. 178).

———. 1992. *Analytical Population Dynamics*. London, UK.: Chapman & Hall. (see pp. 166, 170, 177, 178, 179).

Rudnick, D. L., and R. E. Davis. 2003. *Red noise and regime shifts*. Deep-Sea Research Part I: Oceanographic Research Papers 50 (6): 691–699. doi:10.1016/S0967-0637(03)00053-0. (see p. 120).

Rzevski, G., and P. Skobelev. 2014. *Managing Complexity*. Boston, MA: WIT Press. (see pp. 24, 189).

Saavedra, S., R. P. Rohr, J. Bascompte, O. Godoy, N. J. B. Kraft, and J. M. Levine. 2017. *A structural approach for understanding multispecies coexistence*. Ecological Monographs 87 (3): 470–486. doi:10.1002/ecm.1263. (see pp. 53, 54, 55, 56, 60).

Sadler, J. P., and J. P. Grattan. 1999. *Volcanoes as agents of past environmental change*. Global and Planetary Change 21 (1-3): 181–196. doi:10.1016/S0921-8181(99)00014-4. (see p. 121).

Sæther, B.-E., T. Coulson, V. Grøtan, S. Engen, R. Altwegg, K. B. Armitage, C. Barbraud, et al. 2013. *How Life History Influences Population Dynamics in Fluctuating Environments*. The American Naturalist 182 (6): 743–759. doi:10.1086/673497. (see pp. 156, 162).

Sæther, B.-E., S. Engen, and E. Matthysen. 2002. *Demographic Characteristics and Population Dynamical Patterns of Solitary Birds*. Science 295 (5562): 2070–2073. doi:10.1126/science.1068766. (see pp. 165, 166, 167).

Sæther, B.-E., T. H. Ringsby, E. Røskaft, B.-E. Saether, and E. Roskaft. 1996. *Life History Variation, Population Processes and Priorities in Species Conservation: Towards a Reunion of Research Paradigms*. Oikos 77 (2): 217. doi:10.2307/3546060. (see pp. 162, 164).

Sæther, B.-E., S. Engen, A. Pape Møller, H. Weimerskirch, M. E. Visser, W. Fiedler, and E. Matthysen. 2004. *Life-History Variation Predicts the Effects of Demographic Stochasticity on Avian Population Dynamics*. The American Naturalist 164 (6): 793–802. doi:10.1086/425371. (see p. 167).

Saether, B.-E., and O. Bakke. 2000. *Avian life history variation and contribution of demographic traits to the population growth rate*. Ecology 81 (3): 642–653. doi:10.1890/0012-9658(2000)081[0642:ALHVAC]2.0.CO;2. (see pp. 143, 156, 157, 162, 163, 174, 179).

Safriel, U. N., M. P. Harris, M. D. L. Brooke, and C. K. Britton. 1984. *Survival of Breeding Oystercatchers Haematopus ostralegus*. The Journal of Animal Ecology 53 (3): 867. doi:10.2307/4664. (see pp. 176, 177).

Sal, S., Á. López-Urrutia, X. Irigoien, D. S. Harbour, and R. P. Harris. 2013. *Marine microplankton diversity database*. Ecology 94 (7): 1658. doi:10.1890/13-0236.1. (see pp. 66, 67, 76, 77).

Sanz-Aguilar, A., A. Cortés-Avizanda, D. Serrano, G. Blanco, O. Ceballos, J. M. Grande, J. L. Tella, and J. A. Donázar. 2017. *Sex- and age-dependent patterns of survival and breeding success in a long-lived endangered avian scavenger*. Scientific Reports 7 (1): 40204. doi:10.1038/srep40204. (see p. 157).

Scheffer, M. 2009. *Critical Transitions in Nature and Society*. Princeton, NJ.: Princeton University Press. (see pp. 25, 120, 121, 126, 138, 139, 190).

Scheffer, M., S. Barrett, S. R. Carpenter, C. Folke, A. J. Green, M. Holmgren, T. P. Hughes, et al. 2015. *Creating a safe operating space for iconic ecosystems*. Science 347 (6228): 1317–1319. doi:10.1126/science.aaa3769. (see pp. 121, 122).

Schindler, D. E., J. B. Armstrong, and T. E. Reed. 2015. *The portfolio concept in ecology and evolution*. Frontiers in Ecology and the Environment 13 (5): 257–263. doi:10.1890/140275. (see p. 63).

Schmoker, C., S. Hernández-León, and A. Calbet. 2013. *Microzooplankton grazing in the oceans: impacts, data variability, knowledge gaps and future directions*. Journal of Plankton Research 35 (4): 691–706. doi:10.1093/plankt/fbt023. (see p. 109).

Schoener, T. W., and D. A. Spiller. 2006. *Nonsynchronous recovery of community characteristics in island spiders after a catastrophic hurricane*. Proceedings of the National Academy of Sciences 103 (7): 2220–2225. doi:10.1073/pnas.0510355103. (see p. 121).

Schreiber, S. J. 2000. *Criteria for Cr Robust Permanence*. Journal of Differential Equations 162 (2): 400–426. doi:10.1006/jdeq.1999.3719. (see p. 53).

Schuster, P., K. Sigmund, and R. Wolff. 1979. *On ω- limits for competition between three species.* SIAM Journal on Applied Mathematics 37 (1): 49–54. (see p. 53).

Seger, J., and H. J. Brockmann. 1987. *Bet-Hedging*. In Encyclopedia of Entomology, 4:297–297. Dordrecht: Kluwer Academic Publishers. doi:10.1007/0-306-48380-7{_}461. (see p. 162).

Segura, A. M., D. Calliari, B. L. Lan, H. Fort, C. E. Widdicombe, R. Harmer, and M. Arim. 2017. *Community fluctuations and local extinction in a planktonic food web*. Ecology Letters 20:471–476. doi:10.1111/ele.12749. (see p. 107).

Segura, A. M., C. Kruk, D. Calliari, F. García-Rodriguez, D. Conde, C. E. Widdicombe, and H. Fort. 2013. *Competition Drives Clumpy Species Coexistence in Estuarine Phytoplankton*. Scientific Reports 3 (1): 1037. doi:10.1038/srep01037. (see p. 107).

Selaković, S., T. Säterberg, and H. Heesterbeek. 2022. *Ecological impact of changes in intrinsic growth rates of species at different trophic levels*. Oikos 2022 (4). doi:10.1111/oik.08712. (see p. 107).

Selosse, M.-A., M. Charpin, and F. Not. 2017. *Mixotrophy everywhere on land and in water: the grand écart hypothesis*. Edited by P. Jeyasingh. Ecology Letters 20 (2): 246–263. doi:10.1111/ele.12714. (see p. 91).

Serrano, D., A. Margalida, J. M. Pérez-García, J. Juste, J. Traba, F. Valera, M. Carrete, et al. 2020. *Renewables in Spain threaten biodiversity*. Edited by J. Sills. Science 370 (6522): 1282–1283. doi:10.1126/science.abf6509. (see p. 158).

Sguotti, C., S. A. Otto, X. Cormon, K. M. Werner, E. Deyle, G. Sugihara, and C. Möllmann. 2020. *Non-linearity in stock–recruitment relationships of Atlantic cod: insights from a multi-model approach*. Edited by G. Griffith. ICES Journal of Marine Science 77 (4): 1492–1502. doi:10.1093/icesjms/fsz113. (see p. 126).

Sguotti, C., S. A. Otto, R. Frelat, T. J. Langbehn, M. P. Ryberg, M. Lindegren, J. M. Durant, N. Chr. Stenseth, and C. Möllmann. 2019. *Catastrophic dynamics limit Atlantic cod recovery*. Proceedings of the Royal Society B: Biological Sciences 286 (1898): 20182877. doi:10.1098/rspb.2018.2877. (see pp. 25, 126).

Shoemaker, L. G., L. L. Sullivan, I. Donohue, J. S. Cabral, R. J. Williams, M. M. Mayfield, J. M. Chase, et al. 2019. *Integrating the underlying structure of stochasticity into community ecology*. Ecology: ecy.2922. doi:10.1002/ecy.2922. (see p. 90).

Siegel, D. A., M. J. Behrenfeld, S. Maritorena, C. R. McClain, D. Antoine, S. W. Bailey, P. S. Bontempi, et al. 2013. *Regional to global assessments of phytoplankton dynamics from the SeaWiFS mission*. Remote Sensing of Environment 135:77–91. doi:10.1016/j.rse.2013.03.025. (see pp. 64, 68, 87).

Sinha, S. 2005. *Complexity vs. stability in small-world networks*. Physica A: Statistical Mechanics and its Applications 346 (1-2): 147–153. doi:10.1016/j.physa.2004.08.062. (see p. 108).

Slatkin, M. 1974. *Hedging one's evolutionary bets*. Nature 250 (5469): 704–705. doi:10.1038/250704b0. (see p. 162).

Smale, S. 1966. *Structurally Stable Systems are not Dense*. American Journal of Mathematics 88 (2): 491. doi:10.2307/2373203. (see p. 46).

———. 1967. *Differentiable dynamical systems*. Bulletin of the American Mathematical Society 73 (6): 747–817. doi:10.1090/S0002-9904-1967-11798-1. (see p. 43).

———. 1969. *What is Global Analysis?* The American Mathematical Monthly 76 (1): 4–9. (see p. 45).

Smith, D. M., B. B. Booth, N. J. Dunstone, R. Eade, L. Hermanson, G. S. Jones, A. A. Scaife, K. L. Sheen, and V. Thompson. 2016. *Role of volcanic and anthropogenic aerosols in the recent global surface warming slowdown*. Nature Climate Change 6 (10): 936–940. doi:10.1038/nclimate3058. (see p. 134).

Smith, S. L., S. M. Vallina, and A. Merico. 2016. *Functional diversity mediates an emergent trade-off in the response of phytoplankton communities to rare versus frequent disturbances*. Scientific Reports 6:34170. doi:10.1038/srep34170. (see pp. 67, 84).

Smyth, T. J., J. R. Fishwick, L. AL-Moosawi, D. G. Cummings, C. Harris, V. Kitidis, A. Rees, V. Martinez-Vicente, and E. M. S. Woodward. 2010. *A broad spatio-temporal view of the Western English Channel observatory*. Journal of Plankton Research 32 (5): 585–601. doi:10.1093/plankt/fbp128. (see pp. 92, 93).

Snyder, R. E. 2010. *What makes ecological systems reactive?* Theoretical Population Biology 77 (4): 243–249. doi:10.1016/j.tpb.2010.03.004. (see p. 98).

Soden, B. J., R. T. Wetherald, G. L. Stenchikov, and A. Robock. 2002. *Global cooling after the eruption of Mount Pinatubo: a test oc climate feedback by water vapour*. Science 296 (26 April): 727–730. (see p. 121).

Solé, R. V., and J. Bascompte. 2006. *Self-organization in complex ecosystems*. Princeton, NJ.: Princeton University Press. (see p. 25).

Soler-Toscano, F., J. A. Galadí, A. Escrichs, Y. Sanz Perl, A. López-González, J. D. Sitt, J. Annen, et al. 2022. *What lies underneath: Precise classification of brain states using time-dependent topological structure of dynamics*. Edited by D. Scheinost. PLOS Computational Biology 18 (9): e1010412. doi:10.1371/journal.pcbi.1010412. (see p. 193).

Soler-Toscano, F., H. Zenil, J.-P. Delahaye, and N. Gauvrit. 2014. *Calculating Kolmogorov Complexity from the Output Frequency Distributions of Small Turing Machines*. Edited by M. Dehmer. PLoS ONE 9 (5): e96223. doi:10.1371/journal.pone.0096223. (see p. 97).

Sommer, U., and A. Lewandowska. 2011. *Climate change and the phytoplankton spring bloom: Warming and overwintering zooplankton have similar effects on phytoplankton*. Global Change Biology 17 (1): 154–162. doi:10.1111/j.1365-2486.2010.02182.x. (see p. 111).

Sommeria-Klein, G., R. Watteaux, F. M. Ibarbalz, J. J. Pierella Karlusich, D. Iudicone, C. Bowler, and H. Morlon. 2021. *Global drivers of eukaryotic plankton biogeography in the sunlit ocean*. Science 374 (6567): 594–599. doi:10.1126/science.abb3717. (see pp. 83, 84).

Song, C., S. Von Ahn, R. P. Rohr, and S. Saavedra. 2020. *Towards a Probabilistic Understanding About the Context-Dependency of Species Interactions*. Trends in Ecology & Evolution. doi:10.1016/j.tree.2019.12.011. (see p. 91).

Sorci, G., A. P. Møller, and J. Clobert. 1998. *Plumage dichromatism of birds predicts introduction success in New Zealand*. Journal of Animal Ecology 67 (2): 263–269. doi:10.1046/j.1365-2656.1998.00199.x. (see p. 172).

Stearns, S. C., and T. J. Kawecki. 1994. *Fitness Sensitivity and the Canalization of Life-History Traits*. Evolution 48 (5): 1438. doi:10.2307/2410238. (see pp. 156, 174).

Steele, J. H. 1996. *Regime shifts in fisheries management*. Fisheries Research 25 (95): 19–23. doi:10.1016/0165-7836(95)00440-8. (see p. 120).

Steffen, W., K. Richardson, J. Rockström, S. E. Cornell, I. Fetzer, E. M. Bennett, R. Biggs, et al. 2015. *Planetary boundaries: Guiding human development on a changing planet*. Science 347 (6223). doi:10.1126/science.1259855. (see p. 120).

Steinacher, M., F. Joos, T. L. Frölicher, L. Bopp, P. Cadule, S. C. Doney, M. Gehlen, B. Schneider, and J. Segschneider. 2009. *Projected 21st century decrease in marine productivity: a multi-model analysis*. Biogeosciences Discussions 6:7933–7981. doi:10.5194/bgd-6-7933-2009. (see p. 86).

Steiner, C. F., Z. T. Long, J. A. Krumins, and P. J. Morin. 2005. *Temporal stability of aquatic food webs: Partitioning the effects of species diversity, species composition and enrichment*. Ecology Letters 8 (8): 819–828. doi:10.1111/j.1461-0248.2005.00785.x. (see p. 64).

Stelzer, J. A. A., J. P. Mesman, R. Adrian, and B. W. Ibelings. 2021. *Early warning signals of regime shifts for aquatic systems: Can experiments help to bridge the gap between theory and real-world application?* Ecological Complexity 47:100944. doi:10.1016/j.ecocom.2021.100944. (see p. 120).

Stewart, I. 1988. *Yin—yang and the art of noise*. Nature 335 (6189): 394–394. doi:10.1038/335394a0. (see p. 29).

Stoecker, D. K., P. J. Hansen, D. A. Caron, and A. Mitra. 2016. *Mixotrophy in the Marine Plankton*. Annual Review of Marine Science 9 (June): 010816–060617. doi:10.1146/annurev-marine-010816-060617. (see pp. 91, 108, 109, 111).

Strydom, T., G. V. Dalla Riva, and T. Poisot. 2021. *SVD Entropy Reveals the High Complexity of Ecological Networks*. Frontiers in Ecology and Evolution 9 (June): 1–10. doi:10.3389/fevo.2021.623141. (see p. 97).

Suding, K. N., K. L. Gross, and G. R. Houseman. 2004. *Alternative states and positive feedbacks in restoration ecology*. Trends in Ecology & Evolution 19 (1): 46–53. doi:10.1016/j.tree.2003.10.005. (see pp. 120, 139).

Sultan, S. E. 2015. *Organism and Environment: Ecological Development, Niche Construction, and Adaptation*. Oxford, UK: Oxford University Press. (see p. 26).

Summers, R. W., and M. Nicoll. 2004. *Geographical variation in the breeding biology of the Purple Sandpiper Calidris maritima*. Ibis 146 (2): 303–313. doi:10.1111/j.1474-919X.2004.00260.x. (see p. 165).

Svanbäck, R., and D. I. Bolnick. 2007. *Intraspecific competition drives increased resource use diversity within a natural population*. Proceedings of the Royal Society B: Biological Sciences 274 (1611): 839–844. doi:10.1098/rspb.2006.0198. (see pp. 108, 110).

Svanbäck, R., P. Eklöv, R. Fransson, and K. Holmgren. 2008. *Intraspecific competition drives multiple species resource polymorphism in fish communities*. Oikos 117 (1): 114–124. doi:10.1111/j.2007.0030-1299.16267.x. (see p. 110).

Svirezhev, Y. M., and D. O. Logofet. 1983. *Stability of Biological Communities*. Moscow: Mir Publishers. (see pp. 37, 40, 51, 52, 53, 54, 55).

Szekely, T., and Z. Bamberger. 1992. *Predation of Waders (Charadrii) on Prey Populations: An Exclosure Experiment*. The Journal of Animal Ecology 61 (2): 447. doi:10.2307/5335. (see p. 182).

Takeuchi, Y. 1996. *Global Dynamical Porperties of Lotka-Volterra Systems*. Singapore: World Scientific. (see pp. 37, 51, 52, 53, 96, 194).

Tanaka, Y. 1996. *Sexual Selection Enhances Population Extinction in a Changing Environment*. Journal of Theoretical Biology 180 (3): 197–206. doi:10.1006/jtbi.1996.0096. (see p. 172).

Tang, S., and S. Allesina. 2014. *Reactivity and stability of large ecosystems*. Frontiers in Ecology and Evolution 2 (June): 1–8. doi:10.3389/fevo.2014.00021. (see p. 85).

Tarran, G. A., and J. T. Bruun. 2015. *Nanoplankton and picoplankton in the Western English Channel: abundance and seasonality from 2007–2013*. Progress in Oceanography 137:446–455. doi:10.1016/j.pocean.2015.04.024. (see pp. 92, 93).

Taylor, P. J. 1988. *The construction and turnover of complex community models having Generalized Lotka-Volterra dynamics*. Journal of Theoretical Biology 135 (4): 569–588. doi:10.1016/S0022-5193(88)80276-5. (see p. 193).

Tella, J. L. 2001. *Action is needed now, or BSE crisis could wipe out endangered birds of prey*. Nature 410 (6827): 408–408. doi:10.1038/35068717. (see p. 144).

Thom, R. 1975. *Structural stability and morphogenesis*. Reading, USA: W. A. Benjamin, Inc. (see pp. 29, 126, 127).

———. 1977. *Structural Stability, Catastrophe Theory, and Applied Mathematics*. SIAM Review 19 (2): 189–201. doi:10.1137/1019036. (see p. 126).

Thomas, M. K., C. T. Kremer, C. A. Klausmeier, and E. Litchman. 2012. *A global pattern of thermal adaptation in marine phytoplankton.* Science 338 (6110): 1085–1088. doi:10.1126/science.1224836. (see pp. 76, 83).

Thompson, D. B. A., P. S. Thompson, and D. Nethersole-Thompson. 1986. *Timing of Breeding and Breeding Performance in a Population of Greenshanks (Tringa nebularia)*. The Journal of Animal Ecology 55 (1): 181. doi:10.2307/4701. (see p. 176).

Thompson, J. N. 2013. *Relentless Evolution*. Chicago, ILL.: The University of Chicago Press. (see p. 26).

Thompson, P. L., L. M. Guzman, L. De Meester, Z. Horváth, R. Ptacnik, B. Vanschoenwinkel, D. S. Viana, and J. M. Chase. 2020. *A process-based metacommunity framework linking local and regional scale community ecology*. Edited by V. Calcagno. Ecology Letters: ele.13568. doi:10.1111/ele.13568. (see p. 90).

Thornton, K. W., and R. J. Mulholland. 1974. *Lagrange Stability and Ecological Systems*. Journal of Theoretical Biology 45:473–485. (see pp. 39, 40).

Tilman, D., P. B. Reich, and F. Isbell. 2012. *Biodiversity impacts ecosystem productivity as much as resources, disturbance, or herbivory*. Proceedings of the National Academy of Sciences of the USA 109 (26): 10394–10397. doi:10.1073/pnas.1208240109. (see p. 62).

Tilman, D. 1987. *The importance of the mechanisms of interspeccific competition.* The American Naturalist 129 (5): 769–774. (see p. 107).

———. 2001. *Functional diversity*. 3:109–121. doi:http://dx.doi.org/10.1016/B0-12-226865-2/00132-2. (see pp. 63, 64).

Tilman, D., P. B. Reich, and J. M. H. Knops. 2006. *Biodiversity and ecosystem stability in a decade-long grassland experiment.* Nature 441 (7093): 629–632. doi:10.1038/nature04742. (see p. 64).

Tittensor, D. P., C. Novaglio, C. S. Harrison, R. F. Heneghan, N. Barrier, D. Bianchi, L. Bopp, et al. 2021. *Next-generation ensemble projections reveal higher climate risks for marine ecosystems*. Nature Climate Change 11 (11): 973–981. doi:10.1038/s41558-021-01173-9. (see p. 86).

Tobias, J. A., C. Sheard, A. L. Pigot, A. J. M. Devenish, J. Yang, F. Sayol, M. H. C. Neate-Clegg, et al. 2022. *AVONET: morphological, ecological and geographical data for all birds*. Edited by T. Coulson. Ecology Letters 25 (3): 581–597. doi:10.1111/ele.13898. (see p. 177).

Torrence, C., and G. P. Compo. 1998. *A Practical Guide to Wavelet Analysis*. Bulletin of the American Meteorological Society 79 (1): 61–78. doi:10.1175/1520-0477(1998)079<0061:APGTWA>2.0.CO;2. (see pp. 123, 129).

Trefethen, L. N., and M. Embree. 2005. *Spectra and Pseudospectra: the behavior of nonnormal matrices and operators*. Princeton, NJ.: Princeton University Press. (see pp. 48, 97).

Trenberth, K. E., and A. Dai. 2007. *Effects of Mount Pinatubo volcanic eruption on the hydrological cycle as an analog of geoengineering*. Geophysical Research Letters 34 (15): 1–5. doi:10.1029/2007GL030524. (see pp. 121, 135).

TSAY, R. S. 1986. *Nonlinearity tests for time series*. Biometrika 73 (2): 461–466. doi:10.1093/biomet/73.2.461. (see p. 178).

Tuljapurkar, S. 1990. *Population Dynamics in Variable Environments*. Vol. 85. Lecture Notes in Biomathematics. Berlin, Heidelberg: Springer Berlin Heidelberg. doi:10.1007/978-3-642-51652-8. (see pp. 167, 169, 180).

Tuljapurkar, S. D. 1982. *Population dynamics in variable environments. III. Evolutionary dynamics of r-selection*. Theoretical Population Biology 21 (1): 141–165. doi:10.1016/0040-5809(82)90010-7. (see pp. 167, 169, 171, 174, 180).

Turchin, P. 2003. *Complex Population Dynamics: A Theoretical/Empirical Synthesis*. Monographs. Princeton, NJ.: Princeton University Press. (see pp. 162, 163, 165, 166, 167).

Vallina, S. M., M. J. Follows, S. Dutkiewicz, J. M. Montoya, P. Cermeño, and M. Loreau. 2014. *Global relationship between phytoplankton diversity and productivity in the ocean*. Nature Communications 5:4299. doi:10.1038/ncomms5299. (see pp. 75, 83).

Van Valen, L. 1973a. *A New Evolutionary Law*. Evolutionary Theory 1:1–30. (see p. 28).

———. 1973b. *Pattern and the balance of nature*. Evolutionary Theory 1:31–49. (see p. 28).

———. 1975. *Some aspects of mathematical ecology*. Evolutionary Theory 1:91–96. (see p. 28).

———. 1976. *Energy and Evolution*. Evolutionary Theory 1 (7): 179–229. (see pp. 26, 28, 197).

———. 2003. *Fitness - scalar or vector?* Evolutionary Theory 12:155–157. (see p. 26).

Vázquez-Loureiro, D., V. Gonçalves, A. Sáez, A. Hernández, P. M. Raposeiro, S. Giralt, M. J. Rubio-Inglés, V. Rull, and R. Bao. 2019. *Diatom-inferred ecological responses of an oceanic lake system to volcanism and anthropogenic perturbations since 1290 CE*. Palaeogeography, Palaeoclimatology, Palaeoecology 534 (July): 109285. doi:10.1016/j.palaeo.2019.109285. (see p. 121).

Vellend, M. 2016. *The Theory of Ecological Communities*. Princeton, NJ.: Princeton University Press. (see pp. 23, 26, 120).

Villaverde, A. F. 2019. *Observability and Structural Identifiability of Nonlinear Biological Systems*. Complexity 2019:1–12. doi:10.1155/2019/8497093. (see p. 102).

Visintini, N., and P. Flombaum. 2022. *Picophytoplankton phenology in the global ocean assessed by quantitative niche models*. Marine Biology 169 (7): 93. doi:10.1007/s00227-022-04080-5. (see p. 84).

Visintini, N., A. C. Martiny, and P. Flombaum. 2021. *Prochlorococcus , Synechococcus , and picoeukaryotic phytoplankton abundances in the global ocean*. Limnology and Oceanography Letters 6 (4): 207–215. doi:10.1002/lol2.10188. (see pp. 76, 77, 84).

VLIZ. 2009. *Longhurst Biogeographical Provinces*. (see p. 66).

Ward, B. A., and M. J. Follows. 2016. *Marine mixotrophy increases trophic transfer efficiency, mean organism size, and vertical carbon flux*. Proceedings of the National Academy of Sciences 113 (11): 2958–2963. doi:10.1073/pnas.1517118113. (see p. 92).

Ward, E. J., S. C. Anderson, M. E. Hunsicker, and M. A. Litzow. 2022. *Smoothed dynamic factor analysis for identifying trends in multivariate time series*. Methods in Ecology and Evolution 13 (4): 908–918. doi:10.1111/2041-210X.13788. (see pp. 121, 123, 124, 132).

Watts, K., R. C. Whytock, K. J. Park, E. Fuentes-Montemayor, N. A. Macgregor, S. Duffield, and P. J. K. McGowan. 2020. *Ecological time lags and the journey towards conservation success*. Nature Ecology & Evolution 4 (3): 304–311. doi:10.1038/s41559-019-1087-8. (see p. 138).

Weithoff, G. 2003. *The concepts of 'plant functional types' and 'functional diversity' in lake phytoplankton - A new understanding of phytoplankton ecology?* Freshwater Biology 48 (9): 1669–1675. doi:10.1046/j.1365-2427.2003.01116.x. (see p. 84).

Wennerberg, L., M. Klaassen, and Å. Lindström. 2002. *Geographical variation and population structure in the White-rumped Sandpiper Calidris fuscicollis as shown by morphology, mitochondrial DNA and carbon isotope ratios*. Oecologia 131 (3): 380–390. doi:10.1007/s00442-002-0890-z. (see p. 165).

West, M., and J. Harrison. 1997. *Bayesian Forecasting and Dynamic Models*. 2nd. New York, NY: Springer-Verlag. doi:10.1007/978-0-387-98135-2. (see p. 71).

WetlandsInternational. 2012. *Waterbird Population Estimates, Fifth Edition. Summary Report.* Edited by WetlandsInternational. Wagenigen: WetlandInternational. (see pp. 164, 175).

Widdicombe, C. E., D. Eloire, D. Harbour, R. P. Harris, and P. J. Somerfield. 2010. *Long-term phytoplankton community dynamics in the Western English Channel*. Journal of Plankton Research 32 (5): 643–655. doi:10.1093/plankt/fbp127. (see p. 93).

Wielgus, J., M. Gonzalez-Suarez, D. Aurioles-Gamboa, and L. R. Gerber. 2008. *A noninvasive demographic assessment of sea lions based on stage-specific abundances*. Ecological Applications 18 (5): 1287–1296. doi:10.1890/07-0892.1. (see p. 146).

Wilken, S., J. Huisman, S. Naus-Wiezer, and E. Van Donk. 2013. *Mixotrophic organisms become more heterotrophic with rising temperature*. Edited by G. Fussmann. Ecology Letters 16 (2): 225–233. doi:10.1111/ele.12033. (see p. 92).

Williams, G. C. 1992. *Natural Selection: Domains, Levels, and Challenges*. Oxford, UK: Oxford University Press. (see pp. 26, 27).

Williams, J. W., A. Ordonez, and J. C. Svenning. 2021. *A unifying framework for studying and managing climate-driven rates of ecological change*. Nature Ecology and Evolution 5 (1): 17–26. doi:10.1038/s41559-020-01344-5. (see p. 138).

Williamson, M. 1983. *The Land-Bird Community of Skokholm: Ordination and Turnover*. Oikos 41 (3): 378. doi:10.2307/3544096. (see pp. 176, 177, 179).

Wilson, W. G., and P. Lundberg. 2004. *Biodiversity and the Lotka-Volterra theory of species interactions: Open systems and the distribution of logarithmic densities*. Proceedings of the Royal Society B: Biological Sciences 271 (1551): 1977–1984. doi:10.1098/rspb.2004.2809. (see p. 164).

Wimsatt, W. C. 2007. *Re-Engineering Philosophy for Limited Beings: Piecewise Approximations to Reality*. Cambridge, MA: Harvard University Press. (see pp. 28, 187, 188).

Wolkowicz, H., and G. P. H. Styan. 1980. *Bounds for eigenvalues using traces*. Linear Algebra and Its Applications 29:471–506. doi:10.1016/0024-3795(80)90258-X. (see pp. 37, 38).

Womack, T. M., J. S. Crampton, M. J. Hannah, and K. S. Collins. 2021. *A positive relationship between functional redundancy and temperature in Cenozoic marine ecosystems*. Science 373 (6558): 1027–1029. doi:10.1126/science.abf8732. (see p. 84).

Wood, S. N. 1997. *Inverse Problems and Structured-Population Dynamics*. In Structured-Population Models in Marine, Terrestrial, and Freshwater Systems, 555–586. Boston, MA: Springer US. doi:10.1007/978-1-4615-5973-3{_}19. (see p. 146).

———. 1994. *Obtaining Birth and Mortality Patterns From Structured Population Trajectories*. Ecological Monographs 64 (1): 23–44. doi:10.2307/2937054. (see pp. 146, 155).

Wood, S. N. 2006. *Generalized Additive Models: An Introduction with R*. Boca Raton, FL: Chapman & Hall/CRC Press. (see p. 67).

Worden, A. Z., M. J. Follows, S. J. Giovannoni, S. Wilken, A. E. Zimmerman, and P. J. Keeling. 2015. *Rethinking the marine carbon cycle: Factoring in the multifarious lifestyles of microbes*. Science 347 (6223). doi:10.1126/science.1257594. (see p. 91).

Yachi, S., and M. Loreau. 1999. *Biodiversity and ecosystem productivity in a fluctuating environment: the insurance hypothesis.* Proceedings of the National Academy of Sciences of the USA 96 (4): 1463–1468. doi:10.1073/pnas.96.4.1463. (see pp. 63, 64, 85).

Yang, Q., M. S. Fowler, A. L. Jackson, and I. Donohue. 2019. *The predictability of ecological stability in a noisy world*. Nature Ecology & Evolution 3 (2): 251–259. doi:10.1038/s41559-018-0794-x. (see p. 120).

Yao, F., and I. Hoteit. 2018. *Rapid Red Sea Deep Water renewals caused by volcanic eruptions and the North Atlantic Oscillation*. Science Advances 4 (6): eaar5637. doi:10.1126/sciadv.aar5637. (see p. 134).

Yletyinen, J., Ö. Bodin, B. Weigel, M. C. Nordström, E. Bonsdorff, and T. Blenckner. 2016. *Regime shifts in marine communities: a complex systems perspective on food web dynamics*. Proceedings of the Royal Society B: Biological Sciences 283 (1825): 20152569. doi:10.1098/rspb.2015.2569. (see p. 120).

Yodzis, P. 1980. *The connectance of real ecosystems*. Nature 284 (5756): 544–545. doi:10.1038/284544a0. (see p. 62).

Yosef, R. 2001. *Wader ringing at Eilat , Israel.* WSG Bulletin 96:86–87. (see pp. 176, 177).

Zeeman, E. C. 1988. *On the Classification of Dynamical Systems*. Bulletin of the London Mathematical Society 20 (6): 545–557. doi:10.1112/blms/20.6.545. (see p. 126).

Zeppilli, D., A. Pusceddu, F. Trincardi, and R. Danovaro. 2016. *Seafloor heterogeneity influences the biodiversity–ecosystem functioning relationships in the deep sea*. Scientific Reports 6 (April): 26352. doi:10.1038/srep26352. (see p. 64).

Zhong, D., L. Listmann, M.-E. Santelia, and C.-E. Schaum. 2020. *Functional redundancy in natural pico-phytoplankton communities depends on temperature and biogeography*. Biology Letters 16 (8): 20200330. doi:10.1098/rsbl.2020.0330. (see pp. 83, 84).

Zuberogoitia, I., J. A. González-Oreja, J. E. Martínez, J. Zabala, I. Gómez, and P. López-López. 2013. *Foraging movements of Eurasian griffon vultures (Gyps fulvus): Implications for supplementary feeding management*. European Journal of Wildlife Research 59 (3): 421–429. doi:10.1007/s10344-012-0687-2. (see p. 145).